MONASH University

Implementation of antibody microarrays for the determination and meta-analysis of host signalling dynamics during intracellular Apicomplexan infection

Jack David Adderley

Bbiotech (Hons.)

A thesis submitted as a requirement for the degree of Doctor of Philosophy at Monash University in 2019

Department of Microbiology

Biomedicine Discovery Institute, Monash University

Australia

Table of Contents

Copyright notice

Abstract

Apicomplexan parasites are a diverse phylum of organisms with widespread clinical relevance for human as well as cattle and livestock. All apicomplexan parasites develop within a host cell and therefore must adapt to changes in host cell signalling pathways. Indeed some parasites have also been shown to utilise these pathways to their benefit. To better understand which host signalling pathways are implicated during Apicomplexan infection, we implemented an approach based on a microarray of >900 antibodies directed against human signalling proteins. >50% of these antibodies are phosphorylation-specific and hence allow the determination of the activation status of kinases and other signalling proteins. Through the utilisation of this microarray system, we could compare the effects that several Apicomplexan parasites had on their respective host cells. Furthermore, we were able to directly compare the perturbation of host cell signalling across different Apicomplexan parasites. The parasites explored in this study were; *Plasmodium falciparum* the pathogen responses for the most deadly form of malaria, *Plasmodium knowlesi* a significant cause of malaria in Southeast Asia, *Babesia bovis*, a commercially relevant pathogen of cattle and *Toxoplasma gondii* a highly prevalent pathogen of all warn blood animals.

We completed a total of ten arrays on *P. falciparum* across distinct stages of the parasites asexual development revealing a dynamic modulation of host cell pathways during infection. Two of the most significant changes seen across *P. falciparum* development were for the receptor tyrosine kinase, c-MET and the mitogen-activated 3 kinase (B-Raf) which were further explored. We showed that compounds that are highly selective against c-MET and B-Raf have sub-micromolar IC_{50}s on parasite proliferation, with a time-course analysis revealing a clear trophozoite killing effect. Furthermore, we demonstrated that one of the c-MET inhibitors used (PHA-665752) reduced parasite burden of *P. berghei in vivo*. Taken together, these observations strongly suggest that host erythrocyte c-Met and B-Raf and their downstream pathways play a crucial role in parasite proliferation and survival and open the way to host-directed strategies in antimalarial drug discovery and development.

The studies conducted on *P. knowlesi*, *B. bovis* and *T. gondii* widened our application of the antibody microarray system and illustrated that these parasites caused unique perturbation of their host cells signalling pathways. Overall this study has illustrated that antibody microarrays are effective tools for determining how phosphorylation of host signalling molecules changes during intracellular parasitic infections. The signalling molecules identified and highlighted

throughout this work provide dozens of new hypotheses on how host cell signalling is manipulated by intracellular parasitic infection.

Declaration

This thesis contains no material which has been accepted for the award of any other degree or diploma at any university or equivalent institution and that, to the best of my knowledge and belief, this thesis contains no material previously published or written by another person, except where due reference is made in the test of the thesis.

Jack David Adderley

Department of Microbiology

Biomedicine discovery institute, Monash University

Australia

Thesis including published works declaration

I hereby declare that this thesis contains no material which has been accepted for the award of any other degree or diploma at any university or equivalent institution and that, to the best of my knowledge and belief, this thesis contains no material previously published or written by another person, except where due reference is made in the text of the thesis.

This thesis includes one original paper submitted to a peer-reviewed journal. The core theme of the thesis is host cell signalling during infection with Apicomplexan parasites. The ideas, development and writing up of all this paper were the principal responsibility of myself, the student, working within the Microbiology department at Monash University under the supervision of Christian Doerig and Simona John von Freyend.

In the case of Chapter 3.2, my contribution to the work involved the following:

Thesis Chapter	Publication Title	Status	Nature and % of student contribution	Co-author name(s) Nature and % of Co-author's contribution*	Co-author(s), Monash student
3.2	Signalome-wide assessment of erythrocyte response to *Plasmodium falciparum* infection reveals novel targets for host-directed antimalarial intervention	*Submitted*	***1)*** *Jack D. Adderley 65%. Concept and experimental design, Primary data collection and writing the first draft and editing*	***2)*** *Simona John von Freyend. input into manuscript 7%* ***3)*** *Sarah A. Jackson input into manuscript 3%* ***4)*** *Megan J. Bird, input into manuscript 1%* ***5)*** *Amy L. Burns, input into manuscript 2%* ***6)*** *Burcu Anar, input into manuscript 2%* ***7)*** *Tom Metcalf, input into manuscript 2%* ***8)*** *Jean-Philippe, input into manuscript 1% Semblat* ***9)*** *Oliver Billker, input into manuscript 2%* ***10)*** *Danny W. Wilson, input into manuscript 5%* ***11)*** *Christian Doerig input into manuscript 10%*	*2 - N* *3 - Y* *4 - N* *5 - N* *6 - N* *7 - N* *8 - N* *9 - N* *10 – N* *11 – N*

I have renumbered sections of the submitted paper in order to generate a consistent presentation within the thesis.

The undersigned hereby certify that the above declaration correctly reflects the nature and extent of the student's and co-authors' contributions to this work. In instances where I am not the responsible author, I have consulted with the responsible author to agree on the respective contributions of the authors.

Acknowledgements

I want to thank the School of Biomedical Sciences at the Biomedicine Discovery Institute located at Monash University for providing me with the financial support to undertake my doctoral studies over the past three years. This financial support was critical and enabled me to focus exclusively on my studies without seeking employment externally, and for that, I am grateful.

Next, I would like to give a special thanks to my PhD supervisors and mentors, Professor Christian Doerig and Dr Simona John von Freyend, for believing and enabling me to undertake a PhD under their guidance. To Christian, for providing a level of enthusiasm to my work that I did not think was possible, and for his guidance and immeasurable knowledge on all things cell signalling. To Simona, for our 'quick' impromptu catch-ups and experiment planning/brainstorming sessions that would somehow envelop a whole day, and for putting up with my incredibly stubborn outlook, and having the patience to talk me into a different opinion. Together, I could not have asked for a better pair of supervisors.

The completion of my PhD would not have been possible without the support of many individuals from within the Microbiology department at Monash University, and specifically within the Doerig and Garcia-Bustos, and Cooke groups. The members of these groups have made the many years of this PhD immeasurably more enjoyable. In particular, I would like to acknowledge Dr Mitchell Batty, Dr William Poole and Sarah Jackson, whose friendship I value deeply and will not forget in the years to come. I would also like to thank the many collaborators of this work particularly Dr Danny Wilson, Dr Giel van Dooren, Associate Professor Alex Maier, Professor Robin Gasser and Professor Oliver Bilker for their assistance and guidance in this study.

Last but not least, I would like to thank Liriye for her love and support through my studies and my family, particularly my parents Patrick and Cathy for their patience and understanding as well as their encouragement through this endeavour, enabling me to get where I am today.

List of Figures

List of Tables

List of abbreviations

%CFC	Percentage change from the control
µl	Microliters
µl	Micrograms
ACT	Artemisinin combinational therapy
AGC	PKA, PKG and PKC
AKT	Protein kinase B
AMPK	AMP-activated protein kinase
aPK	Atypical protein kinases
ATP	Adenosine triphosphate
BAD	Bcl-2 associated death promoter
Bcl-2	B-cell lymphoma 2
BFU-e	Burst forming unit-erythroid
BSA	Bovine serum albumin
BTK	Bruton's tyrosine kinase
Ca^{2+}	Calcium
CAK	CDK-activating kinase
CAMK	Calcium/calmodulin-dependent kinases
c-CBL	Casitas B-lineage lymphoma
CDPA	Citrate phosphate dextrose adenine
CFU-e	Colony-forming unit-erythroid
CGMC	CDK, MAPK, GSK, DYRK and CLK families
CK1	Casein kinase 1
CK2	Casein kinase 2
c-MET	The hepatocyte growth factor receptor
CT	Congenital toxoplasmosis
ddH_2O	Double deionised water
DDR2	Discoidin domain-containing receptor 2
DTT	Dithiothreitol
EphA3	Ephrin type-A receptor 3 precursor
ePK	Eukaryotic protein kinases
ER-Alpha	Estrogen-receptor alpha
ERK1/2	Mitogen-activated kinase 3 and 4
eryptosis	Erythrocytic cell death
FGFR3	Fibroblast growth factor receptor 3
FGFR4	Fibroblast growth factor receptor 4
FLT1	Fms-related tyrosine kinase 1
FRS2	Fibroblast growth factor receptor substrate 2
FRS3	Fibroblast receptor substrate 2
g	Gravity units
G proteins	Heterotrimeric guanine nucleotide-binding regulatory proteins
Gab1	GRB2-associated protein 1

GPCR	The G-coupled protein receptors
Grb2	The receptor-bound protein 2
HCMV	Human cytomegalovirus
HCV	Hepatitis C virus
HDT	Host-targeted therapy
HGF	Hepatocyte growth factor
HIV	Human Immune Deficiency Virus
hpi	Hrs post invasions
hrs	Hours
ICK	Intestinal cell (MAK-like) kinase
IFN-γ	Interferon-gamma
IGF	Insulin-like growth factor
IGFR	Insulin-like growth factor receptor
IRS1	Insulin receptor substrate 1
ITSN2	Intersectin-2
IU	International units
JAK	Janus kinase
JNK1	C-Jun N-terminal kinases
K13	*Kelch* gene on chromosome 13
kg	Kilogram
LATS1	Large tumour suppressor kinase
Lck	Lymphocyte-specific protein tyrosine kinase
LIMK1	LIM domain kinase 1
LKB1	Liver kinase B1
M	Molar
MAP3K	MAP kinase kinase kinase
MAP3K5	Mitogen-activated protein kinase kinase kinase 5
MAPK	Mitogen-activated protein kinase
MAPK11	Mitogen-activated protein kinase 11
MAPK1K	MAP kinase kinase
MEK1/2	Mitogen-activated kinase kinase 1 and 2
MEK3	Mitogen-activated kinase kinase 3
mg	Milligrams
ml	Millilitre
MOI	Multiple of infection
MOK	MAPK/MAK/MRK overlapping kinase
mTOR	Mammalian target of rapamycin
Myt1	Myelin transcription factor 1
NEK9	“Never in mitosis gene a related kinase” 9
nM	Nanomolar
NTCB	2-Nitro-5-thiocyanobenzoic acid
nTK	Non-receptor tyrosine kinase
ºC	Degrees Celcius
OPK	“Other” or “orphan” protein kinases
p70 S6K	Ribosomal protein S6 kinase beta-1
PAK	P21-activated kinase

PBK	Lymphokine-activated killer T-cell-originated protein kinase
PBS	Phosphate buffered saline
PDGFRα	Platelet-derived growth factor receptor alpha
PDK1	Phosphoinositide-dependent kinase 1
PfMAP1	P. falciparum MAP1
PfMAP2	P. falciparum MAP2
PGK1	Phosphoglycerate kinase 1
PI3K	Phosphoinositide 3-kinase
PK	Protein kinase
PKA	Protein Kinase A
PKC	Protein kinase C
PPIC	Phosphatase and protease inhbitory cocktail
PTB	Phosphotyrosine binding domain
Rb	Retinoblastoma
RCK	V-ros cross-hybridising kinase
RGC	Receptor guanylyl cyclases
RMPI	Roswell Park Memorial Institute
Ron	Macrophage-stimulating protein receptor
ROPK	Rhoptry kinases
RPM	Revolutions per minute
RSK1	Ribosomal S6 kinase 1
rTK	Receptor TK
SCF	Stem cell factor
SMG1	PI-3kinase-related kinase
Sos	Son of sevenless
STAT	Signal transducer and activator of transcription proteins
STE	Homologues STE7/11/20
STK	Serine/threonine-specific protein kinases
Syk	Spleen tyrosine kinase
TBST	Tris-buffered saline with 0.05% Tween
TCEP	Tris 2-carboxyethyl phosphine
TK	Tyrosine-specific protein kinases
TKL	Tyrosine kinase-like kinases
Trk	The neurotrophin receptor
V	Volts
v/v	Volume per volume
VEGF	Vascular endothelial growth factor
VEGFR2	Vascular endothelial growth factor receptor 2
VRAP	VEGF receptor-associated protein
w/v	Weight per volume
Wee1	Mitosis inhibitor protein kinase 1
WHO	World Health Organisation
WNK1	Lysine deficient protein kinase 1
μM	Micromolar

Chapter 1 – Introduction

1.1 Apicomplexan parasites

The phylum Apicomplexa is a unique group of single-celled obligate intracellular organisms, which are often considered parasitic to the host cell (Figure 1.1). A hallmark of Apicomplexan organisms is their complex life cycle, usually involving multiple host species and cell types. Most of the life cycle is spent in a haploid state, though many Apicomplexan organisms also have a sexual stage, during which male and female gametes merge into a diploid zygote [1]. All Apicomplexans are obligate intracellular organisms, meaning they require a host cell for successful development, and to ultimately proliferate. Therefore these organisms must manipulate the host cell to survive and develop, and one way this occurs is through the host's intracellular signalling pathways. Dependence on host signalling provides a unique opportunity to develop therapeutics that target the host rather than the pathogen directly.

Manipulation of host cell signalling by most Apicomplexan organisms is poorly understood. However, *Toxoplasma gondii*, a globally distributed pathogen of warm-blooded animals, is known to manipulate host signalling pathways during infection [2]. For *Plasmodium*, development within hepatocytes has been reported to involve manipulation of several host pathways; however, only a few studies have investigated host signalling molecules during the later erythrocytic stage of development [3-7]. Conversely, *Babesia bovis*, a tick-borne pathogen of cattle, has no reported host signalling interactions. In this thesis, I aimed to determine the global changes in host signalling during erythrocyte infection with *Plasmodium falciparum* and *Plasmodium knowlesi*, two of the causative organisms of human malaria, as well as infection with *B. bovis*. Also, we sought to confirm and further identify global changes in host signalling pathways during *T. gondii* infection. The Apicomplexans, *P. falciparum*, *P. knowlesi*, *B. bovis* and *T. gondii* (highlighted blue in Figure 1.1) are therefore the focus of this thesis, as they represent phylogenetically distinct parasites that are amenable to *in vitro* culture.

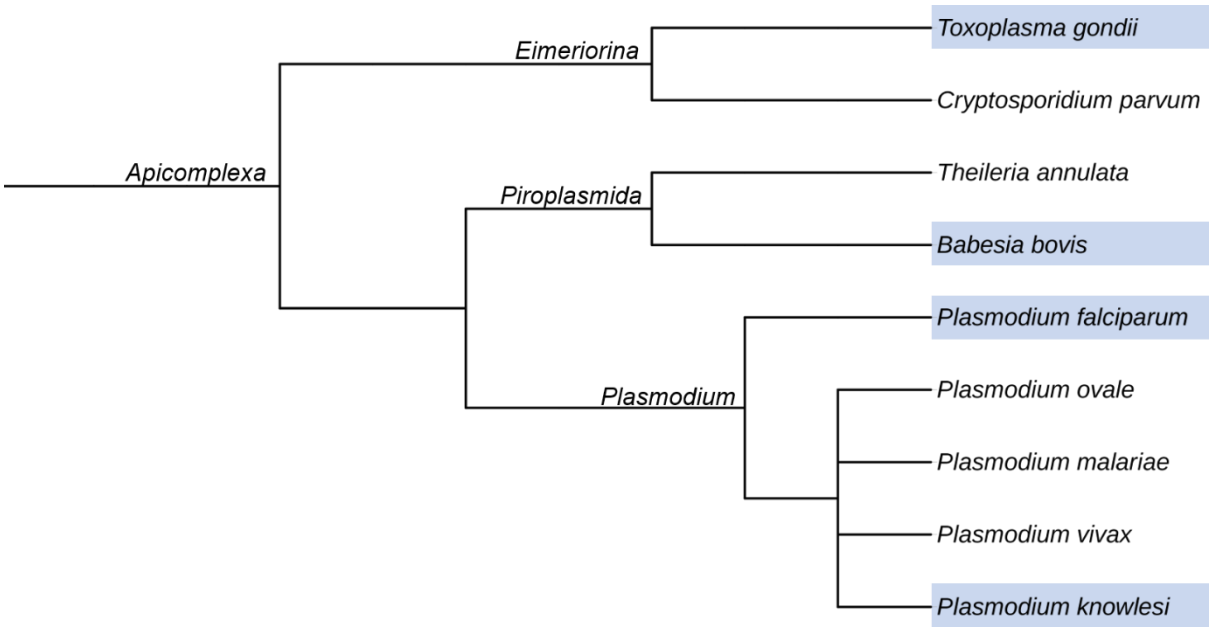

Figure 1.1 – Phylogenetic tree of Apicomplexan parasites investigated in this thesis.
Representative Apicomplexan parasites including members of the *Eimeriorina*, *Piroplasmida*, and *Plasmodium*, suborder, order, and genus respectively. Highlighted in blue are the parasites relevant to this thesis, which will be discussed in greater detail. Schematic representation of the Apicomplexan phylogenetic tree, not to scale. Generated using phyloT (phylot.biobyte.de).

1.1.1 Malaria and its causative organism *Plasmodium spp*.

Human malaria is caused by infection with one of five species of eukaryotic parasites of the genus *Plasmodium*. These include *Plasmodium falciparum*, *Plasmodium vivax*, *Plasmodium knowlesi*, *Plasmodium ovale*, and *Plasmodium malariae*. Of the five species, *P. falciparum* accounts for the majority of malaria cases and deaths [8]. The most widespread is *P. vivax*, which is also the most common cause of malaria in South America [8]. Until the early 2000s, *P. knowlesi* was considered to cause simian malaria exclusively [9]. Today it is thought that *P. knowlesi* has been a human pathogen in Southeast Asia for some time [9], but was previously misdiagnosed as *P. malariae* due to the inability to distinguish these two parasites by microscopy, the primary method of diagnosis at the time. Southeast Asia is still making progress towards the elimination of *P. falciparum* and *P. vivax*; however, the prevalence of *P. knowlesi* is of increasing concern [8-10]. Many regions of Malaysia have reported that *P. knowlesi* is the most prevalent local cause of malaria, which suggests a re-evaluation of control and elimination procedures may be warranted [9, 11].

From the years 2000 - 2015, global human cases of malaria, when accounting for population growth during this time, decreased by 37% [12]. During this time the death toll of malaria also reduced by 48%, to an estimated 435,000 in 2017 [8, 12]. These reductions were made possible through initiatives such as Roll Back Malaria and international aid, in the form of insecticide-treated bed net distribution and deployment of the highly effective front line treatment of malaria, artemisinin combinational therapy (ACT) [13, 14]. Unfortunately, progress towards malaria elimination has stalled in recent years [15]. In 2017 there was an estimated 219 million cases of malaria, an increase of 3 million cases from 2016 [8].

In addition to the direct effect on public health and the health programs maintained by affected societies, the impact of malaria on economic development is often overlooked. Malaria alone has been estimated to cost an endemic country up to 1.3% of its economic growth rate per year [16]. When a region is also heavily affected by other high burden diseases such as the Human Immune Deficiency Virus (HIV), a country's ability to grow becomes compromised, reducing sources of internal funding for these diseases [17]. There are many contributing factors for this loss of growth, which include a reduced capacity for productivity due to sick individuals, and the high costs of effective treatments. The current front-line treatment for malaria, ACT, has been an effective treatment since deployment. However, one of the key components of this therapy, artemisinin, is under threat of drug resistance. Prevalence of artemisinin resistance is on the rise in Thailand and is spreading to neighbouring countries [18, 19].

1.1.1.1 Antimalarials, drug resistance and the current antimalarial emergency

The evolutionary arms race between drug treatment of pathogens and drug resistance is an ever-escalating battle. In recent years this has become a larger issue as the development of new drug treatments is lagging behind the rate at which pathogens acquire resistance [20]. This same arms race also affects the treatment of malaria and has now led to the precarious position, where the last resistance-free treatment is becoming less effective [21]. Antimalarials have been utilised since the 17th century with the discovery of quinine, which was isolated from the bark of cinchona trees [22]. Quinine saw widespread use up until the discovery of chloroquine, after which it was quickly retired due to a list of adverse side effects [22, 23]. Chloroquine was extensively used in the 1940s and during World War II [22, 24] before compounds such as sulphadoxine, pyrimethamine, and mefloquine were developed [21]. Since 2006 the treatment guidelines outlined by the World Health Organisation (WHO) suggest *P. falciparum* infection should be treated with ACTs [8, 25]. Artemisinin is a fast-acting sesquiterpene lactone, able to rapidly reduce parasite burden in the host. Due to the relatively short half-life of Artemisinin

(2 - 5 hours), it requires combination with a longer-lasting antimalarial compound to ensure complete parasite clearance [26, 27]. The implementation of ACT was additionally designed to help slow, if not stop the possibility of drug resistance [21]. However, the emergence of artemisinin resistance was first documented in 2008 on the Thailand-Cambodia border and appeared as delayed parasite clearance following the first three days of ACT treatment [28, 29]. There is also some speculation that resistance may have first appeared as early as 2001 when artemisinin was used as a monotherapy [30]. Resistance to artemisinin has been associated with mutations to the propeller domain of the *kelch* gene on chromosome 13 (K13). K13 is part of a large family of kelch proteins, whose propeller domain assists with multiple protein-protein interactions and oxidative stress responses [31]. The commonly identified mutations associated with K13 artemisinin resistance are; mutation from Tyr position 493 to His (Tyr493His), Gln539Thr, Ile543Thr, and Cys580Tyr [32].

The development of resistance to several other antimalarials also occurred in the Thai-Cambodia region before global dissemination: chloroquine resistance (1950s) [33], sulphadoxine/pyrimethamine resistance (1960s) [34], and mefloquine resistance (1980s) [35]. This raises fears that the recent resistance to artemisinin may spread globally in the future [21]. Parasite proliferation during drug treatment is how antimalarial resistance usually presents. However, in the case of artemisinin resistance, parasites enter a state of dormancy during ring stage development and become active again following artemisinin clearance from the host [36, 37]. By itself, artemisinin resistance does not lead to treatment failure, as the partner drugs used in the therapy are able to clear the infection. However, a study in Vietnam found that increasing levels of resistance to the partner drug, such as piperaquine, resulted in treatment failure rising from 0% in 2012 to 26% in 2015 [38]. Artemisinin resistance was first documented in 2008 in Thailand and has since spread to Vietnam, Bangladesh, China, and India [38-41]. Artemisinin resistance mutations have also been detected in Africa. These mutations are believed to have originated locally, however, unlike the resistant mutants present in Southeast Asia, the mutants seen in Africa appear to be under less pressure from evolutionary selection, suggesting there are other factors involved in the emergence and spread of antimalarial resistance, aside from parasite mutation as ACTs are used globally [42]. These unknown factors raise fears that resistance could rapidly emerge due to the natural existence of these mutations in the parasite populations in Africa today [43].

Ultimately a vaccine against malaria would be the desired goal, though there are no long-term efficacious vaccines yet available. GlaxoSmith Kline and the PATH's Malaria Vaccine Initiative developed the currently available malaria vaccine, RTS,S/AS01. This vaccine uses a four-dose immunisation scheme, which showed efficacy ranging from 30 - 55% that sharply declined over time [44, 45]. Without an efficacious vaccine, there is a heavy reliance on the ACTs, which now show increased levels of treatment failure in some regions [38]. Also, insecticide-treated bed nets which were pivotal in the reduction of global malaria cases in the early 2000s are becoming less effective due to insecticide resistance and persistent issues with miss-use [46-48]. There are presently fifteen antimalarial agents in clinical development, which includes: Artefenomel (synthetic endoperoxide), KAF156 (imidazolopiperazines), Cipargamin (spiroindolone), Fosmidomycin (antibiotic), DSM2655 (dihydroorotate dehydrogenase inhibitor), AQ-13 (Modified 4- aminoquinoline), Methylene blue (Phenothiazine derivative), Sevuparin (anti-adhesive polysaccharide), and MMV 390048 (Aminopyridine), all of which are in phase 2 trials [49]. However, *P. falciparum* has already shown the capacity to develop resistance to many of the parent compounds (artemisinin and chloroquine) of these derivatives. Moving forward, there is a need for new antimalarial compounds that are not derived from previously utilised drugs to reduce the risk of resistance in the future.

1.1.1.2 The life cycle of *Plasmodium spp*.

The five species of *Plasmodium* infectious to humans follow the same general lifecycle, though the maturation times of the parasites vary between the species. The following description of the parasite's lifecycle relates to *P. falciparum*, with notable differences for *P. knowlesi* stated throughout the text (Fig. 1.2).

During a blood meal, an infected female *Anopheles* mosquito will release *P. falciparum* sporozoites from the salivary gland into the host's skin. These sporozoites traverse into the circulatory system, where they are passively carried to the liver, and invade hepatocytes [50]. Within a hepatocyte, a single parasite develops into thousands of merozoites, which - as shown for *P. falciparum* - are packaged into merosomes, hepatocyte membrane-derived vesicles, and migrate into the bloodstream [51, 52]. Once released from the merosomes, the merozoites rapidly bind and invade host erythrocytes, initiating the erythrocytic cycle. Up until this point, the human host shows no observable symptoms of malaria, however as the erythrocytic cycle progresses, the clinical symptoms associated with malaria, such as fever, malaise, and anemia, begin to develop. If not treated early, these symptoms rapidly progress into a life-threatening condition in children and malaria naïve individuals [53].

Erythrocytic cycle – Asexual development

Plasmodium invasion of an erythrocyte is a rapid event occurring in less than 90 seconds [54]. Invasion results in the formation of a double-membraned parasitophorous vacuole, which the parasite resides in throughout asexual development [55]. During the initial 20 hours of red blood cell infection, the parasites appear as ring-like structures that, when stained with an adequate dye such as Giemsa, are observable with a light microscope [56, 57]. During this "ring stage", the parasite is metabolically less active compared to later stages of the life cycle [58]. From approximately 20 hours post-infection, the parasite becomes more metabolically active and is now referred to as a trophozoite [58, 59]. At this stage, the parasite begins to digest haemoglobin for essential amino acids [59]. By the completion of the asexual life cycle, the parasite will have consumed 65 – 80% of the erythrocyte's total haemoglobin [59, 60]. The trophozoite stage is also notable for its asynchronous 3 – 4 rounds of DNA synthesis [61]. Completion of DNA synthesis occurs at approximately thirty-six hours post-infection, where the nuclei begin to separate in a process called schizogony, forming a segmented schizont [62]. This process results in the assembly of daughter merozoites, on average 16 merozoites for *P. falciparum* and 10 for *P. knowlesi* [63]. Forty-eight hours post erythrocyte infection the merozoites have completed maturation and are released through the rupture of the erythrocyte

membrane [64]. Free merozoites bind to and invade circulating erythrocytes, perpetuating the infection. In the other species of *Plasmodium*, infectious to humans this cycle is complete in; 24 hours (*P. knowlesi)*, 48 hours (*P. vivax*) 50 hours (*P. ovale*) and 72 hours (*P. malariae*) [65].

Erythrocytic cycle – Sexual development

Parasites need to undergo at least one round of the asexual erythrocytic cycle before sexual development is possible [66]. Sexual development by gametocytogenesis results in either one male or female gametocyte per infected erythrocyte. The exact mechanism that determines commitment to gametocytogenesis remains unknown; however, it is known to occur in the preceding asexual cycle [67, 68] and involves epigenetic control of expression the transcription factor, Api2-G [69]. Factors such as endoplasmic reticulum/metabolic stress, pressure from the host immune response and treatment with chloroquine have all been shown to influence this process [67, 68, 70]. Merozoites that are committed to undergo gametocytogenesis invade a host erythrocyte and form a ring-stage parasite as per the asexual cycle. After 24 – 30 hours post-invasion, the committed parasite becomes identifiable as a stage I gametocyte [71, 72]. Over the next eight days, (*P. falciparum*; two days for *P. knowlesi*) gametocytes develop within their host erythrocyte, differentiating into either a male or female gametocyte and transitioning from stage I through to stage V [65, 71]. Stage V gametocytes are the only stage of parasite capable of sexual reproduction [73]. During a blood meal these stage V gametocytes can be ingested by the female *Anopheles* mosquito where they undergo gametogenesis followed by fertilisation in the midgut. Zygotes develop into motile ookinetes that cross the midgut epithelium and mature into oocysts, in which sporogony occurs. The newly formed sporozoites then migrate through the mosquito into its salivary glands in preparation for infection of a human host [74].

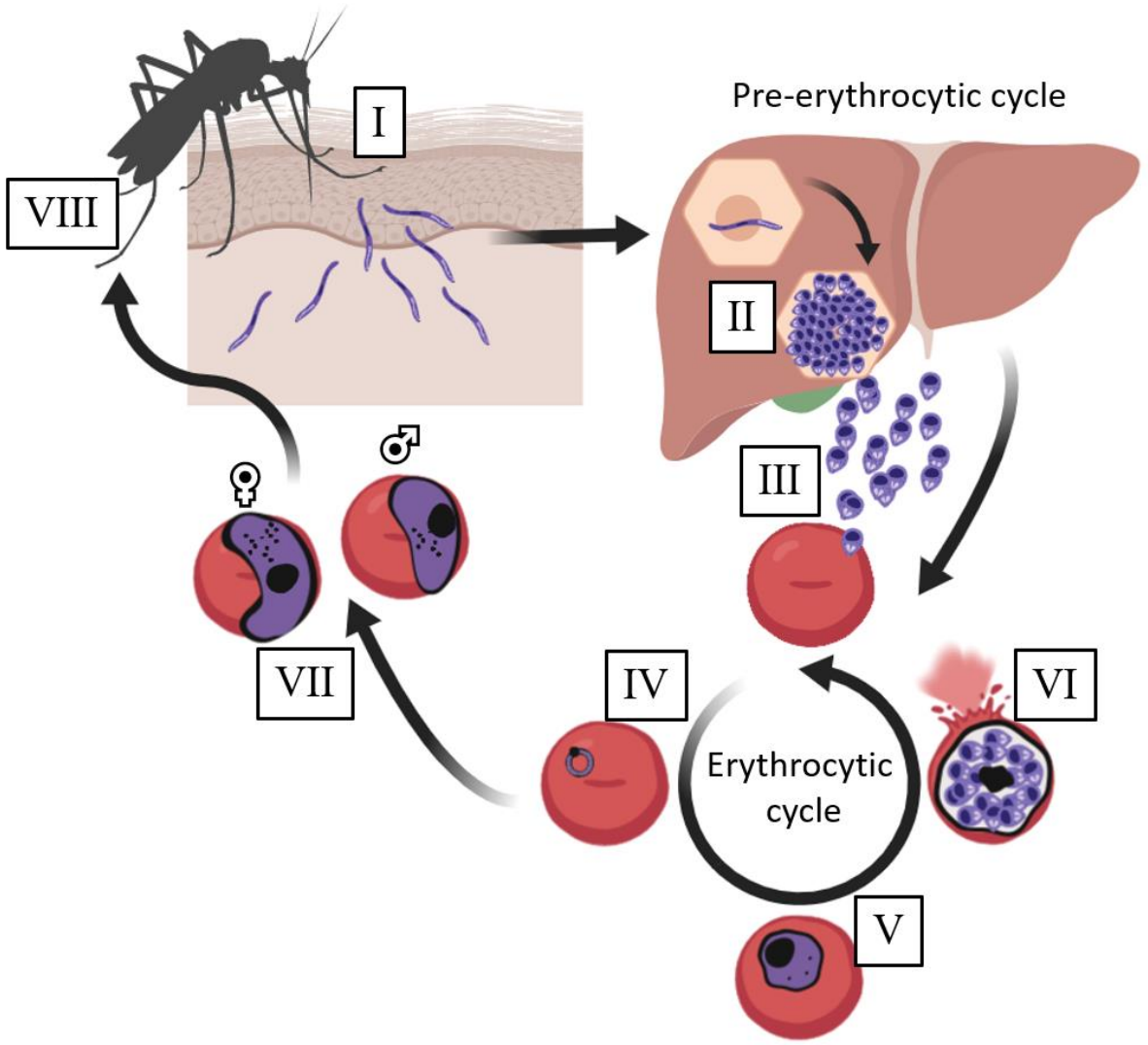

Figure 1.2 – The life cycle of *Plasmodium falciparum*.

An *Anopheles* mosquito infected with *P. falciparum* releases sporozoites into a human host during a blood meal (I). The infectious sporozoites move from the inoculation site through the bloodstream to the liver before differentiation and development into merozoites, known as the pre-erythrocytic stage (II). Mature merozoites are released into the bloodstream and infect circulating erythrocytes (III). Following infection, the parasite initially present as a ring-like structure (IV) before development into trophozoites (V) and finally multi-nucleated schizonts (VI). Mature schizonts rupture to release the contained daughter merozoites (VI). Gametocytogenesis can occur following a single erythrocytic cycle. Merozoites that are committed to gametocytogenesis infect circulating erythrocytes, initially appearing as ring-stage parasites (IV). Following this, the committed parasites undergo sexual development into stage V male and female gametocytes (VII). These gametocytes when consumed by a mosquito during a blood meal undergo sexual replication in the midgut before differentiating into sporozoites, enabling transmission back into a human host (VIII). (Created using BioRender).

1.1.2 Toxoplasmosis and the causative organism *Toxoplasma gondii*

1.1.2.1 Overview

Toxoplasma gondii, the causative organism of Toxoplasmosis, can infect virtually all warm-blooded animals and is prevalent worldwide. The exact global prevalence of *T. gondii* infection in humans is unknown, but is estimated at 30%, and has been reported to be as high as 83% in some countries in South America [75, 76]. Although *T. gondii* undergoes sexual replication, greater than 95% of all strains isolated in North America and Europe are from three distinct clonal lineages, Type I, II and III. [77]. In South America, there is a greater level of genetic diversity seen in the *T. gondii* population, which is believed to account for the higher level of *T. gondii* prevalence in this region [77, 78]. The Type I-III strains have emerged from a single paternal line within the last 10,000 years [79], with the success of these strains being due to their increased level of direct oral infectivity, enabling these parasites to bypass sexual replication more easily [79, 80] (Figure 1.3 (V); a full description of the *T. gondii* lifecycle is reviewed in the following section).

The most virulent of these clonal strains is Type I, which is also the main cause of severe disease in immunocompromised individuals [81, 82]. In most circumstances, initial infection is asymptomatic, but can also present as a mild flu-like illness. However, regardless of clinical presentation, all cases will develop into a chronic asymptomatic infection that persists for the life of the host [83]. Interestingly, chronic *T. gondii* infection is associated with several psychiatric disorders, including schizophrenia, bipolar illness, higher rates of suicide, and memory impairment [84-89]. One of the largest risks *T. gondii* poses to healthy individuals is during pregnancy, during which a *de novo* infection causes congenital toxoplasmosis (CT) that often results in miscarriage or stillbirth. In 2012 a systematic review by the WHO indicated that CT occurs at a rate of 1.5 cases per 1000 live births [90]. While some babies survive until full term, there is a multitude of developmental defects including blindness, epilepsy and developmental disabilities, which manifest in early childhood [83].

In immunocompromised individuals, toxoplasmosis is a serious disease that can be fatal if left untreated. Unlike the mild illness observed in healthy individuals, primary infection in the immunocompromised can spread to multiple organs, which results in many life-threatening systemic diseases, including encephalitis [91]. Additionally, during the reactivation of dormant *T. gondii* infection, individuals who become immunocompromised through infection with the human immunodeficiency virus (HIV), commonly develop encephalitis [92]. Treatment of *T.*

gondii infection is possible with pyrimethamine and sulfadiazine, however, due to the long 6-week treatment required there is a high rate of toxic side effects, which also present dangers during pregnancy [80]. Additionally, there is no treatment currently available, which can eliminate chronic *T. gondii* infection.

1.1.2.2 The life cycle of *T. gondii*

The life cycle of *T. gondii* (Figure 1.3) spans between an intermediate host (warm-blooded animal) and a definitive host (domestic or wild cats) [91]. The life cycle begins as an infected cat sheds *T. gondii* oocysts into the environment, where they remain until ingestion by an intermediate host. Following ingestion, *T. gondii* oocysts release sporozoites, which penetrate the host's intestinal epithelium. Sporozoites then differentiate into tachyzoites by rapidly replicating through endodyogeny, which is a unique form of asexual development whereby two daughter cells develop inside the mother cell [93]. Following replication, tachyzoites can subsequently penetrate deeper into the host tissue, where they disseminate and replicate in any cell type [91]. The fast replicating tachyzoites convert into bradyzoites as early as seven days post-infection and begin to form tissue cysts [91]. Bradyzoites form predominately in the host brain and muscle cells and remain as a chronic infection throughout the life of the host [94]. If another intermediate host consumes an infected intermediate host, the bradyzoites infect the intestinal cells of this new host where they re-differentiate into tachyzoites [91]. Only ingestion of bradyzoites by the definitive feline host allows progression of the life cycle through its sexual stages in the intestinal cells of the cat [95]. Following sexual development, the infected cat begins to shed *T. gondii* oocysts into the environment, which can remain infectious for up to 18 months [96].

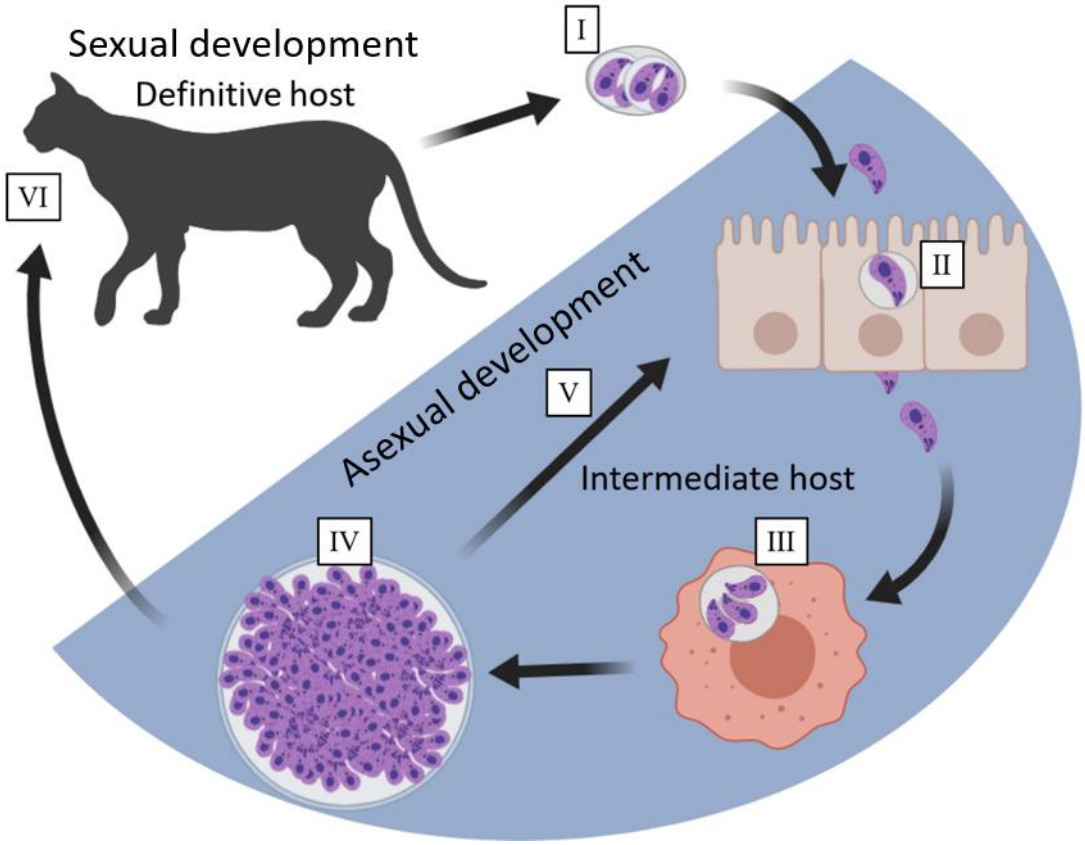

Figure 1.3 – The life cycle of *Toxoplasma gondii*.

The infected cat sheds *T. gondii* oocysts into the environment (I). Following ingestion by an intermediate host, *T. gondii* oocysts release sporozoites infecting the host intestinal epithelium. Intracellular sporozoites differentiate into tachyzoites (II), which can infect all other nucleated host cells (III). Tachyzoites convert to bradyzoites forming tissue cysts (IV). Ingestion of bradyzoites by another intermediate host results in infection of host intestinal epithelium and differentiation back into tachyzoites (V). Ingestion of bradyzoites by a definitive host enables sexual replication of the parasite in the host's intestinal cells (VI). (Created using BioRender).

1.1.3 Babesiosis and the causative organism *Babesia spp.*

1.1.3.1 Overview

Babesia spp. are a genus of tick-borne Apicomplexan protozoa which cause babesiosis in many mammals. The clinical symptoms associated with babesiosis are similar to those seen with malaria, notably fever, fatigue and anaemia [97]. The most common cause of human babesiosis, *Babesia microti,* is becoming increasingly important as disease prevalence specifically in North America appears to be on the rise [98]. In addition to its incidence in humans, babesiosis represents one of the most important tick-borne diseases in cattle [99]. The most important species that cause babesiosis in cattle are *Babesia bovis*, *Babesia bigemina* and *Babesia divergens,* which are also arguably the most studied of the genus [100]. These pathogens are distributed across the world, and are therefore, a heavy burden on the cattle industry in many developed and developing economies [101]. The direct effect of babesiosis on cattle farms is the loss of meat/beef production; however, the indirect costs of babesiosis are often overlooked and include expenses of vaccination, treatment of infected animals, disease prevention and detection, as well as vector control [101].

Similar to naïve infections of malaria in humans, cows transported from *Babesia* free regions into an endemic region have a higher risk of acquiring a severe and often fatal infection [102, 103]. Consequently, farmers in endemic areas are unwilling to import purebred animals, which produce better yields, as many die from infection in the first few weeks. This further impedes the development of cattle farming in poorer regions of the world [101]. At present, there is a vaccine for *B. bovis* available, which has been shown to provide immunity for greater than three years [104]. This is a live-attenuated vaccine, which requires cryopreservation for storage to maintain the viability of the attenuated parasites. While effective, the use of a live-attenuated vaccine has the risk of parasites reverting to the pathogenic form and causing an outbreak in a *Babesia* free region [105]. This, along with the high costs of vaccine production, are less than ideal. No alternative vaccines are currently available, and vector control interventions have become problematic due to insecticide resistance [106]. A new vaccine, better treatment or prevention of infection is of high interest to the cattle industry. Additionally, success with the bovine forms of *Babesia* may provide a gateway to combat the emerging prevalence seen in the human forms of the disease.

1.1.3.2 The life cycle of *B. bovis*

The lifecycle of *B. bovis* (Figure 1.4) begins with an infected *Rhipicephalus annulatus* tick that releases sporozoites during a bovine blood meal. *B. bovis* sporozoites traverse into the circulatory system where they differentiate into merozoites before invading host erythrocytes [101]. Within the erythrocyte, merozoites first appear as a ring-like structure, which develops into a trophozoite [106]. *B. bovis* trophozoites undergo binary fission and then lyse the host erythrocyte to release two daughter merozoites, which can infect other circulating erythrocytes. Alternatively, some trophozoites undergo one round of asexual development, before developing into what are considered pre-gametocytes [107, 108]. Transmission of *B. bovis* infected erythrocytes to the *R. annulatus* tick occurs during a blood meal of infected cattle. Digestion by the tick causes lysis of the ingested infected erythrocytes, killing all but the pre-gametocyte forms of the parasites [109]. Following release from the host erythrocyte, pre-gametocytes mature in the tick midgut [109]. The mature male and female gametocytes fuse into a zygote, proliferate, and then spread throughout the tick, including the ovaries and eggs in the females [110]. Interestingly, adult ticks that consume infected erythrocytes do not re-transmit parasites back into a bovine host [111]. Instead, the female tick now carries *B. bovis* infected eggs [111]. As these eggs develop from larvae, nymph to an adult, they can transmit the infectious form of *B. bovis* into a bovine host, completing the lifecycle [111].

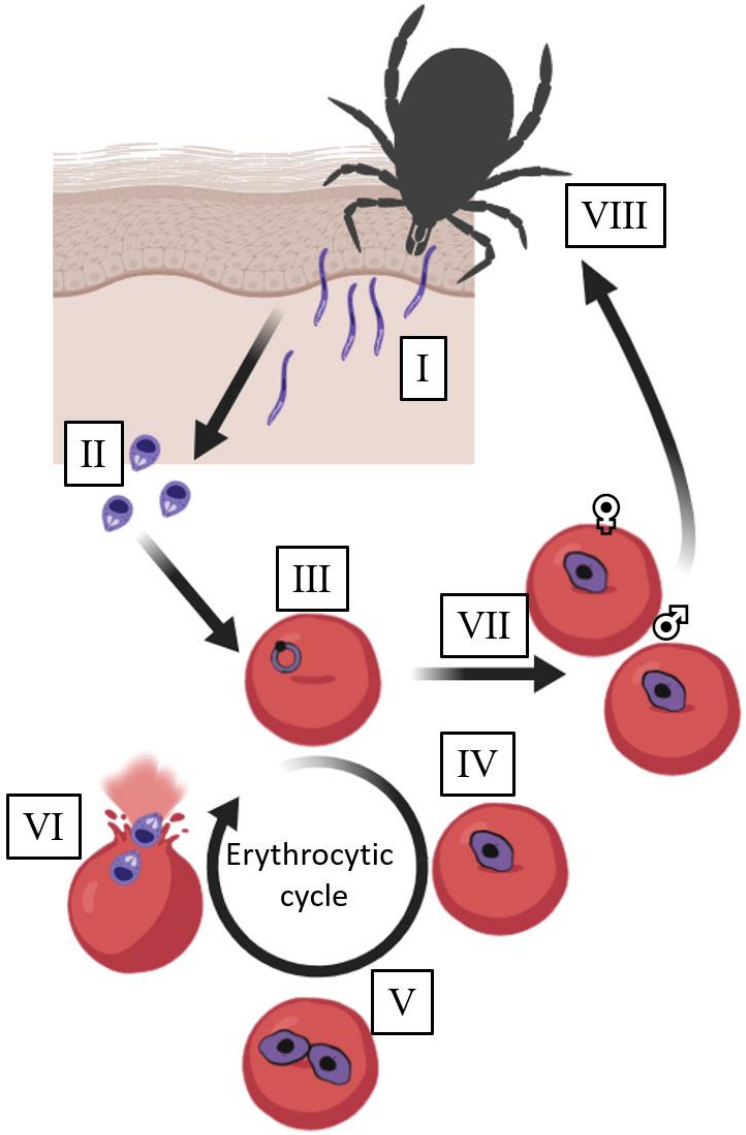

Figure 1.4 – The life cycle of *Babesia bovis*.

An infected *Rhipicephalus annulatus* tick releases sporozoites during a blood meal (I). The *B. bovis* sporozoites traverse into the circulatory system where they mature to merozoites (II), invade host erythrocytes (III) and then undergo maturation to trophozoites (IV). *B. bovis* trophozoites undergo binary fission (V) and lyse the host erythrocyte to release two daughter merozoites, which go on to infect other erythrocytes (VI). The parasites can also develop into pre-gametocytes within the erythrocyte (VII). Once ingested by a tick, the male and female gametes mature and undergo sexual reproduction, and infect the eggs of female ticks. While these eggs mature, *B. bovis* differentiates into sporozoites, which are deposited into a bovine host during a blood meal. (VIII). (Created using BioRender).

1.2. Protein kinases

1.2.1 Overview

Kinases are a large and diverse family of signalling proteins that play a crucial role in regulating intra- and extracellular processes [112-114]. Kinases transfer the gamma phosphate of adenosine triphosphate (ATP) onto hydroxyl groups of amino acids (protein kinases), lipids (lipid kinases), or carbohydrates (metabolic kinases) [115]. In eukaryotic cells, there are two primary types of protein kinases, named after the amino acids they phosphorylate: tyrosine-specific protein kinases (TK) and serine/threonine-specific protein kinases (STK). Both TKs and STKs contain a common catalytic domain comprised of approximately 290 residues, typically spanning the N and C terminal lobes of the protein [116, 117]. Figure 1.5 illustrates the structure of a typical protein kinase, (P. *falciparum* casein kinase 1, PfCK1), with the N and C terminal lobes represented. Notably, the ATP binding site and substrate binding pocket are both located between the terminal lobes of the protein (Figure 1.5b). Protein kinases are in an active conformation when there is compression of the helical component of the C-terminal lobe to the N-terminal lobe. This exposes the ATP binding pocket of the kinase, which provides ATP access and enables substrate phosphorylation. When the protein kinase is in an inactive conformation, the ATP binding pocket is blocked by the N and C-terminal lobes, which thereby inhibits enzymatic function [117]. The dynamics of kinase activation and inactivation, together with the activity of protein phosphatases that remove the phosphate groups from the substrate proteins, enable finely tuned control of many cellular functions and play a key role in regulating metabolism, transcription and translation, protein transport and cell division/growth [116, 118].

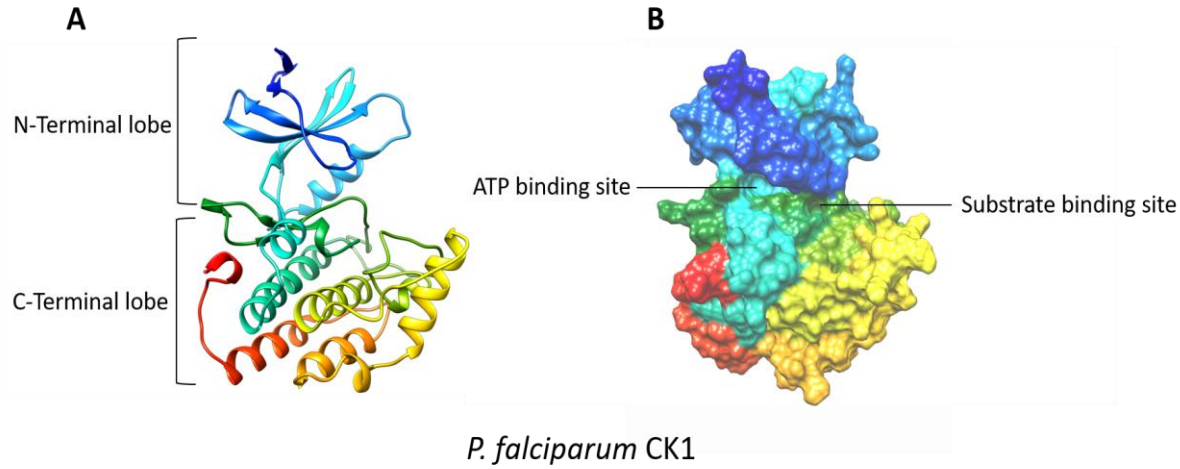

Figure 1.5 – Protein kinase structure of *P. falciparum* CK1 (PfCK1).

a) Ribbon structure of PfCK1 indicating the N-terminal lobe (upper) and C-terminal lobe (lower). **b)** Surface-fill model which illustrates the location of the ATP binding site, and substrate binding sites for the kinase. The structures presented here were generated by Dr Mitchell Batty from Monash University, Australia.

Phosphorylation can modulate the affinity of protein-protein interactions, which regulates protein binding and the formation of protein complexes [119]. Protein kinases are often members of these complexes which enable kinases to act as substrates for other protein kinases and thus foster the formation of an interconnected web of signal transductions. One example of a serine/threonine protein kinase cascade is the mitogen-activated protein kinase (MAPK) pathways, which consist of three sequential kinases. Firstly a MAP kinase kinase kinase (MAP3K) phosphorylates and thereby activates a MAP kinase kinase (MAP2K), which then activates a MAP kinase by phosphorylation [120]. These three-tiered cascades are utilised by many different cell types and regulate a range of signalling processes, including proliferation, apoptosis, mitosis, and differentiation [121, 122]. Phosphorylation can also affect the localisation of proteins, including protein kinases. This is the case for one example of the MAPK pathway; B-Raf (MAP3K), MEK1/2 (MAP2K) and ERK1/2 (MAPK). Activation of B-Raf generally results in the phosphorylation of ERK1/2. This phosphorylation primes ERK1/2 for phosphorylation by casein kinase 2 (CK2), which enables importin 7 to bind and transport ERK1/2 from the cytosol of the cell into the nucleus [123]. Interestingly, there is a growing body of evidence which suggests that B-Raf, which usually localises within the cytoplasm of the cell and is activated by Ras at the plasma membrane, has a function within the nucleus and other compartments of eukaryotic cells [124-126]. The substrates of B-Raf under these circumstances are not well understood; however, B-Raf is suspected of being the cause of sustained ERK1/2 phosphorylation, despite its nuclear localisation [124].

1.2.1.1 Human protein kinase families

The human genome encodes approximately 518 different protein kinases, representing 1.7 - 2% of all encoded genes [116, 117]. While this represents a small percentage of genes, over 50% of all proteins are phosphorylated, with over 200,000 known phosphorylation sites detected in the human proteome [127-129]. The high level of phosphorylation is made possible by the ability of each kinase to phosphorylate multiple proteins at different phosphorylation sites. In healthy eukaryotic cells, the ratio of phosphorylated serine to phosphorylated threonine to phosphorylated tyrosine (pSer:pThr:pTyr) = 1000:100:1 [130]. This ratio can, in part, be explained by the number of members in each group of kinases. The TKs contain approximately 90 members that fall within two distinct groups, the receptor TKs (rTKs) and the non-receptor (nTKs). The STKs are a much larger group of kinases (approximately 400 members), which also have more diverse functions than TKs [131]. Most of these members are further divided into seven groups listed in Table 1; briefly they are the TKL (Tyrosine kinase-like kinases), CMGC (CDK, MAPK, GSK, DYRK and CLK families) AGC (PKA, PKG and PKC), CAMK (calcium/calmodulin-dependent kinases), the STE (homologues STE7/11/20), RGC (receptor guanylyl cyclases) and CK1 (casein kinase 1) families. A few STKs do not fit into these groups but still conform to the primary structure of eukaryotic protein kinases (ePKs), known as OPK ("other" protein kinases). Finally, there is one last group of kinases known as the atypical protein kinases (aPK), which exhibit little to no sequence similarity to ePKs, despite retaining catalytic kinase activity [132, 133].

Table 1.1 – Eukaryotic protein kinases groups

Group abbreviation	Complete name
TK	Tyrosine kinases
TKL	Tyrosine kinase-like kinases
CMGC	Cyclin-dependent kinases (CDK), mitogen-activated kinases (MAPK), glycogen synthase kinases (GSK), dual-specificity tyrosine regulated kinases (DYRK) and the CDK-like kinases (CLK)
AGC	Cyclic-adenosine-monophosphate-dependent kinases (PKA), cyclic-guanosine-monophosphate-dependent protein kinase (PKG) and protein kinases C (PKC)
CAMK	Calcium/Calmodulin-dependent kinases
STE	Sterile (STE) 7, 11 and 20 yeast homologues
RGC	Receptor guanylyl cyclases
CK1	Casein kinase 1
OPK	Other protein kinases

1.2.3 Apicomplexan Kinases

Kinases expressed in Apicomplexan parasites are generally very distinct from those found in the host organism [134]. Additionally, the kinomes of Apicomplexan parasites have been considerably reduced throughout their evolution, making them amongst the smallest kinome in Eukaryotes [135]. The Apicomplexan kinome contains 65 distinct orthologous groups with approximately 75% of the kinases being specific to Apicomplexan parasites [135]. Not only does the kinome size differ between Apicomplexans and other Eukaryotes, but also the kinome composition when categorised into major groups, as illustrated in Figure 1.6.

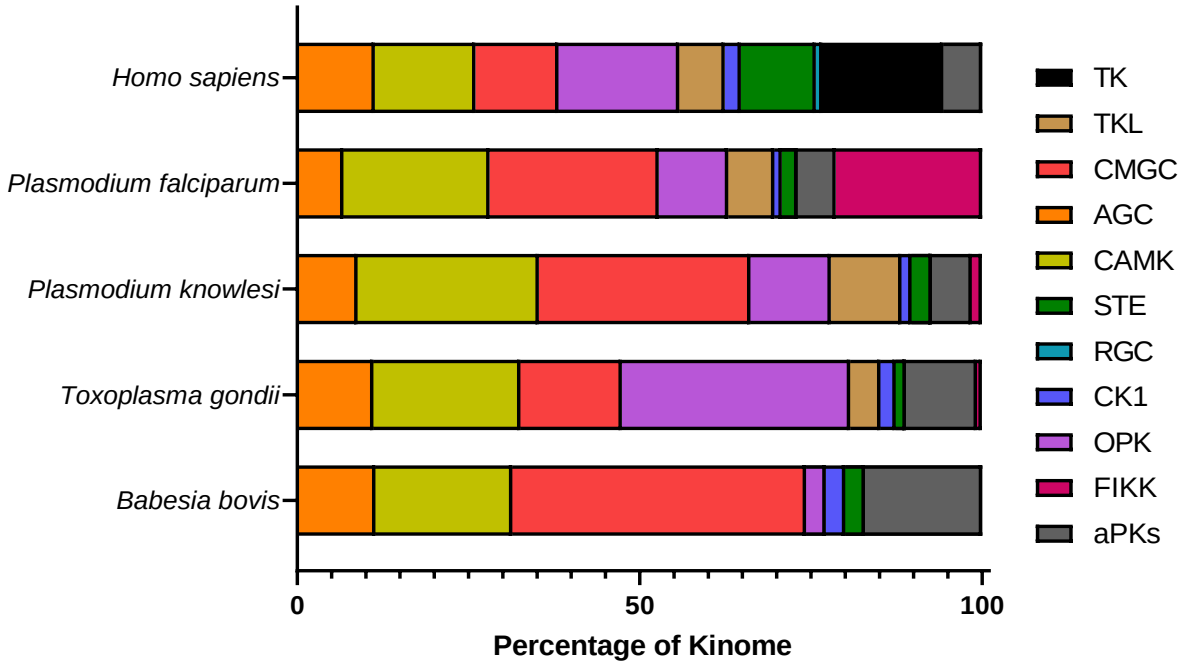

Figure 1.6 – Kinome composition of Apicomplexan parasites compared to *Homo sapiens*.
Comparison of the following kinomes; *Homo sapiens, P. falciparum, P. knowlesi, T. gondii* and *B. bovis*. Kinase families included are TK, TKL, CMGC, AGC, CAMK, STE, RGC, CK1, OPK (contains *T. gondii* ROPK kinases) FIKK and aPKs. Values for each kinase family represented as a percentage of the total organisms kinome, created using (GraphPad Prism 8) [132, 135, 136].

In a study by Miranda-Saavedra *et al.* the kinomes of 12 Apicomplexan parasites were compared, which revealed a set of 20 protein kinases conserved across the studied parasites, including *P. falciparum*, *P. knowlesi*, *T. gondii* and *B. bovis* [135]. Interestingly, there are only 35 kinases encoded by *B. bovis*, which makes the 20 conserved kinases the majority of this parasite's kinome [135]. *Apicomplexan* parasites contained all of the ePK groups, with the exception of the RGC and the TKs [135]. Of the ePKs groups, the CMGC sub-group is the most abundant one, which is found across all *Apicomplexan* parasites. Furthermore, approximately 70% of these CMGC sub-group kinases are alveolate-specific and are not found in higher-order organisms [135]. The second-largest ePK group is the CAMK sub-group that contains calcium signalling kinases, which are crucial for parasite development [135, 137]. In addition to this, *T. gondii* also encodes 44 serine/threonine kinases which form a unique group that is absent from other *Apicomplexan* parasites. These kinases are the rhoptry kinases (ROPK) represented in Figure 1.6 as part of the OPK sub-group. This family of kinases have a typical serine-threonine protein kinase structure, with the addition of ROPK specific sequences [138]. The function of the ROPK proteins are not fully understood; however, many are associated with virulence, chronic infection and host cell signalling manipulation [138, 139].

1.2.3.1 *Plasmodium falciparum* kinome

Several genome-wide studies have determined that there are 86 - 99 putative protein kinases encoded by *P. falciparum* [135, 140, 141]. Most recently, Miranda-Saavedra *et al*. proposed there are a total of 89 protein kinases encoded by *P. falciparum* [135]. Of these, 65 were related to typical ePKs, five were related to aPKs, and the remaining 19 belong to an *Apicomplexan*-specific group known as the FIKK kinases [135, 140, 142]. The FIKK kinases are represented in most *Apicomplexan* parasites, although *P. falciparum* encodes by far the most members of this family (Figure 1.6). Ward *et al.* suggested that the FIKK kinase group has undergone a recent substantial expansion within *P. falciparum*, noting that seven of the FIKKs are located on chromosome 9 in a region involved in antigenic variation, and are therefore likely to undergo mutation events [143]. The exact function of many of the FIKK kinases are not well understood; however, many are thought to be exported into the cytoplasm of human host erythrocytes during blood-stage development [144-146].

Of the ePKs in *P. falciparum*, 36 have been shown to have a critical role during asexual parasite development within erythrocytes, while a further 26 were non-essential in blood stages [147]. Notably, several members of the MAPK pathway are missing from the *P. falciparum* kinome [140]. The three-tiered MAPK cascade is a highly conserved pathway in most eukaryotic organisms; however, it is incomplete in several Apicomplexan species [148, 149]. *P. falciparum* encodes two homologues to human MAPKs known as *P. falciparum* MAP1 (PfMAP1) and (PfMAP2), though there are no homologues to human MAP3K or MAP2Ks [140]. This incomplete MAPK cascade is highly unusual and could suggest that the parasitic nature of Apicomplexans has made encoding their own complete MAPK pathway redundant [4]. Interestingly, PfMAP1 shows the highest homology to human ERK7/8, which can be activated without MAP2Ks [143]. Therefore, this could indicate the parasite has developed to utilise an atypical MAPK pathway.

1.2.1.2 Protein kinases as drug targets

The first protein kinase inhibitor was developed in the 1980s and showed inhibitory activity against cyclic-nucleotide-dependent protein kinases and protein kinase C (PKC) [150]. From this initial discovery, a compound known as HA1077 (Fasudil) completed clinical trials and was approved for use in Japan in 1995 [151]. HA1077 was a Type I ATP competitive inhibitor that targeted a number of protein kinases, although there was some doubt regarding its specificity [151, 152]. Today it is clear that protein kinases are exceedingly druggable targets. By 2019, 48 small molecule kinase inhibitors had successfully received FDA approval for use for the treatment of various cancers, rheumatoid arthritis, myelofibrosis and glaucoma [153]. Many of these compounds are classed as either Type I or Type II inhibitors. Type I inhibitors bind the ATP-binding pocket of the target protein in an active conformation, whereas Type II inhibitors bind in the hinge of the ATP pocket to stabilise the inactive conformation of the protein [154]. Consequently, many Type I and II inhibitors, such as HA1077, suffer from lack of selectivity as they can affect kinases that are structurally similar to the target enzyme often resulting in undesirable side effects.

The MAPK pathway was identified as a druggable target for anti-cancer treatments and has been the focus of drug discovery for more than 30 years [155, 156] In 2012, a compound known as Trametinib was approved for use by the FDA for the treatment of B-Raf-mutant melanoma [157]. Trametinib is unique in that it was the first Type III inhibitor to be approved for human use. Unlike the Type I and II inhibitors, Type III inhibitors bind to an adjacent allosteric site that does not overlap with the ATP binding pocket/hinge region of the target protein [154]. The major benefit of Type III inhibitors is the added selectivity to the target protein as allosteric sites are generally unique. Although allosteric inhibitors are the ultimate goal, many Type I and II inhibitors have a place in the treatment of disease, despite the possible off-target effects.

Kinase inhibitors have been primarily explored for the treatment of cancer, though recently using kinase inhibitors for the treatment of infectious diseases has begun to gain traction [158]. Parasite-encoded protein kinases have been proposed as attractive potential targets for selective intervention [159], including the cGMP-dependent protein kinase produced by *Plasmodium*, and the calcium-dependent protein kinase 1 in *Toxoplasma* [160, 161]. Another approach hypothesises infectious diseases could be treated by targeting the host rather than the pathogen directly (host-targeted therapy, HDT) [162]. In terms of *Plasmodium* infection, both the host erythrocyte and hepatocyte protein kinases are being explored for their potential as targets of antimalarial interventions [4, 163, 164]. A major benefit of HDT is that pathogens cannot escape through the selection of mutated target under drug pressure, which removes an important possible avenue of resistance development. Additionally, targeting host kinases for anti-infectious therapies could allow for the repurposing of drugs developed for other diseases such as cancer. This could significantly reduce the time to market and cost of development of these compounds as anti-infectious therapies.

1.2.2 Erythrocyte differentiation and development

1.2.2.1 Reticulocyte development and signalling

The differentiation and development of mature erythrocytes from hematopoietic stem cells is a complex process that involves multiple steps, as depicted in Figure 1.7. In humans, the first erythroid committed cell is the burst forming unit-erythroid (BFU-e). The BFU-e further differentiates into colony-forming unit-erythroid (CFU-e), then into several erythroblast forms [165]. In the final stages of erythroblast development, the nucleus is ejected to form a denucleated cell known as a reticulocyte. The development of reticulocytes from hematopoietic stem cells is a highly regulated process that utilises many aspects of human signalling including MAPK, phosphoinositide 3-kinase (PI3K) / Protein kinase B (AKT), Janus kinase (JAK)/ signal transducer and activator of transcription proteins (STAT) [165-170]. Other molecules such as the insulin-like growth factor (IGF), as well as the receptor c-Kit and its ligand stem cell factor (SCF), have been shown to also play a role in erythroid cell proliferation [171-175]. In adults, reticulocytes leave the bone marrow to circulate in the bloodstream for approximately one week while they mature into erythrocytes [165]. The week-long maturation from reticulocyte to erythrocyte is notable for its substantial mRNA translation, the ejection of the mitochondria and, as translation concludes, the ejection of the translation machinery.

mRNA translation in reticulocytes primarily generates the α and β subunits of haemoglobin. In fact, up to a third of the total haemoglobin of mature erythrocytes is translated during reticulocyte development [176, 177]. The large amounts of haemoglobin transcripts in reticulocytes presented a unique challenge to the identification of the reticulocyte transcriptome. However, using a microarray approach, Goh *et al.* mitigated the haemoglobin transcript issue and identified mRNA transcripts for a large set of proteins present in adult reticulocytes [178]. Included in the top 100 most abundant transcripts was the mitogen-activated kinase kinase 3 (MEK3) [178]. MEK3 belongs to the second tier of the MAPK pathway and phosphorylates the MAPK p38 in response to cell stress [179]. Signalling pathways involving MEK3 generally result in apoptotic signalling or cell growth inhibition [180].

In addition to the transcriptome, the reticulocyte proteome has been shown to contain many kinase signalling elements, including multiple members of the three tiers of the MAPK pathway [181]. However, as is the case with the transcriptome, proteomic analysis of reticulocytes is significantly obstructed by the large amount of haemoglobin present. Consequently, kinases, due to their already low levels of abundance in endogenous conditions, are often undetected [182].

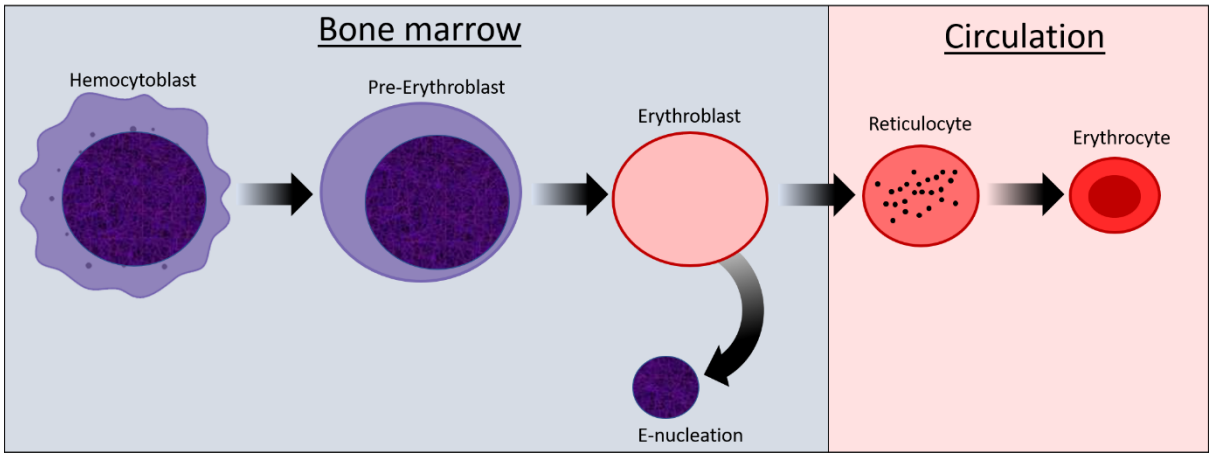

Figure 1.7 – Overview of erythroid development from hemocytoblast to mature erythrocyte.
Hemocytoblasts rapidly differentiate into pre-erythroblasts, which then undergo a series of modifications, including the production of haemoglobin. Erythroblast development ends with the ejection of the cell's nucleus and the cell entering circulation, forming a reticulocyte. During circulation reticulocytes further differentiate into mature erythrocytes.

1.2.2.2 Protein kinase signalling in erythrocytes

Upon maturation, erythrocytes survive in the blood for an average of 115 days and lack organelles, including the nucleus, ribosomes and mitochondria [183]. Despite the absence of organelles, kinase signalling pathways including PI3K/AKT, MAPK and JAK-STAT pathways are still present, yet their functions in erythrocytes are not well characterised [184, 185]. One of the few pathways that have been established in erythrocytes is calcium (Ca^{2+}) signalling. Ca^{2+} is universally used to regulate a vast array of cellular events, such as metabolism, structure and cell volume [186]. In erythrocytes, Ca^{2+} levels are relatively low compared to blood plasma levels; therefore the import of Ca^{2+} into the cell can be used to initiate multiple signalling pathways, including erythrocytic aging and clearance, and oxygen transport and delivery [187-189]. PKC is a family of enzymes which respond to a diverse array of external stimuli. Activation of PKC requires Ca^{2+}, diacylglycerol or a phospholipid. Active PKC enables a variety of downstream effectors, including changes to energy homeostasis, increased Ca^{2+} transport, proliferation and apoptosis [190]. In erythrocytes, PKC has a role in eryptosis and affects cellular volume following glucose starvation [191]. Klarl *et al.* demonstrated that during glucose starvation PKC increases Ca^{2+} influx into erythrocytes, where it initiates phosphatidylserine exposure on the erythrocyte surface [191], one of the hallmarks of eryptosis. The MAPK p38 has also been demonstrated to trigger Ca^{2+} entry into the cell, following hyperosmotic shock; however, the upstream signalling pathway remains unknown [192].

Increased Ca^{2+} also activates the liver kinase B1 (LKB1) and in turn, activates AMP-activated protein kinase (AMPK) by phosphorylation [193]. AMPK plays a central role in the regulation of cellular energy consumption by controlling ATP usage. Studies in mice determined that erythrocytes which lack AMPK have increased levels of oxidative stress and shorter erythrocyte life spans due to premature eryptosis [194, 195]. In addition, a large pharmacological study indicated that the signalling molecules CK2, ALK, VEGFR-2 and the PI3K/AKT and JAK-STAT pathways were all involved in erythrocyte shrinkage and vesicle formation, which accelerates the aging process of erythrocytes [185, 196]; however, these results are yet to be supported by biochemical means.

1.3. Host-Parasite interactions during intracellular Apicomplexan infection

The following section summarises the known host cell signalling elements that are effected during intracellular infection with the Apicomplexan parasites. This section covers *P. falciparum* and *T. gondii* exclusively, as nothing is known about host cell signalling during the intracellular infection of *P. knowlesi* and *B. bovis.*

1.3.1 Hepatocyte signalling during infection with *Plasmodium*

Hepatocytes are the first cell type of the human host that get infected with *Plasmodium spp*. Within hepatocytes a single sporozoite will develop into tens of thousands of merozoites. This process takes approximately a week, depending on the species of *Plasmodium* [51]. During this time significant changes within the host cell occur, including parasite manipulation of host cell signalling to aid parasite proliferation or to subvert host apoptosis or evade the host immune system. The following section details many of the human kinases that are known to be manipulated during *Plasmodium* hepatocyte development.

1.3.1.1 AMP-activated protein kinase (AMPK)

Intracellular pathogens dramatically increase host cell energy demands, and it is therefore unsurprising that such pathogens can interfere with the major energy regulator of eukaryotic cells, AMPK. *Plasmodium spp.* suppresses AMPK during development within hepatocytes [197]. This process was shown to be important for parasite survival, as treatment with an AMPK agonist reduced liver-stage burden in a murine model of malaria [197]. Chemical activation of AMPK has also been demonstrated to suppress the proliferation of other intracellular pathogens, including *Trypanosoma cruzi* [198], the hepatitis C virus [199], and Rift valley fever virus [200]. In most circumstances, suppression of AMPK activity should inherently make pathogen development more difficult, as AMPK activation increases glucose uptake, the rate of glycolysis, and the breakdown of fatty acids in the host cell, all of which provide more energy to the host cell and therefore, the intracellular pathogen [201]. However, fatty acid synthesis is also suppressed when AMPK is activated; hence, AMPK activation in HCV infected cells causes a reduction in lipids [199-201]. Therefore, HCV and other select pathogens may rely on the host cell for fatty acid synthesis, thereby requiring AMPK suppression, despite the disadvantages stated above. Notably, there are a larger number of other pathogens that use AMPK activation to their advantage, including the Human cytomegalovirus [202], *Leishmania infantum* [203], Simian virus 40 [204], *Escherichia coli* [205] and *Mycobacterium tuberculosis* [206].

1.3.1.2 The hepatocyte growth factor receptor (c-MET)

The hepatocyte growth factor receptor (c-MET) is a key receptor tyrosine kinase that influences cellular proliferation, motility, migration and invasion [207]. C-MET is activated through the binding of the hepatocyte growth factor (HGF), which results in the dimerisation and trans-phosphorylation of the receptor [208]. Activation of c-MET enables multiple downstream signalling events, often including the MAPK and Akt/PI3K pathways discussed in the previous sections. The deletion of c-MET expression in mice did not alter hepatocyte function under standard physiological conditions; however, these hepatocytes were more vulnerable to apoptosis, and the liver displayed delayed healing following injury [209]. Therefore c-MET may not be essential for cell survival, but still plays an important role in response to injury, and potentially infection. Indeed, *P. berghei* [210, 211] and numerous other pathogens, including *Helicobacter pylori* [212] *Listeria monocytogenes* [213] and Hepatitis B virus [214], can manipulate c-MET signalling. *Plasmodium* sporozoites migrate through several hepatocytes before invading a terminal cell for subsequent development [215]. This migration process wounds hepatocytes and results in the release of HGF, which can then bind to c-MET on neighbouring cells, increasing their susceptibility to *Plasmodium* infection [210]. There is also evidence that c-MET signalling through the anti-apoptotic Akt/PI3K pathway promotes parasite survival within hepatocytes [211]. These studies were performed with a commonly used mouse model of malaria, *P. berghei*. However, the phosphorylation of c-MET was more recently compared among hepatocytes infected with different *Plasmodium spp.* and was significantly higher for *P. berghei* than *P. falciparum* [216]. This illustrated that while there are many similarities between the species, there can be a wide variation in how the parasite modulates and interacts with host cells.

1.3.1.2 p53 and the B-cell lymphoma 2 (Bcl-2) family of proteins

For successful development within hepatocytes, *Plasmodium* is required to prevent host cell apoptosis. There are numerous ways the host cell can regulate apoptosis due to stress or infection, among them, are the pro-death proteins p53 and the B-cell lymphoma 2 (Bcl-2) family of proteins. p53 is a DNA binding protein that regulates transcription, promotes cell cycle arrest, and initiates apoptosis [217]. Kaushansky *et al.* demonstrated that stabilising hepatocyte p53 with Nutlin-3 reduce *P. berghei* liver-stage burden in infected mice [218]. This study also identified increased phosphorylation levels of Retinoblastoma (Rb), the mammalian target of rapamycin (mTOR), both of which are involved in pro-proliferation signalling and Akt, involved in anti-apoptotic signalling, suggesting a network of changes occur to host cell signalling during *Plasmodium* liver-stage development.

The Bcl-2 family of proteins function together to regulate apoptosis in nucleated cells and are often referred to as the gatekeepers of apoptosis. This family of proteins is divided into three distinct groups, the anti-apoptotic proteins (which includes the first protein identified in this family, Bcl-2), the pro-apoptotic pore-forming proteins and the pro-apoptotic Bcl-2 homolog 3 (BH3)-only proteins [219]. The function of this anti-apoptotic protein group is to bind to and inhibit the pro-apoptotic group proteins through sequestration [219]. Inhibition of the anti-apoptotic proteins (Bcl-2), stops the sequestration of the pro-apoptotic proteins, resulting in the formation of pores in the mitochondrial outer membrane, irreversibly releasing the intermembrane space proteins, leading to apoptosis [219]. Treatment of *P. yoelii* infected mice with a Bcl-2 inhibitor (ABT-737) reduces parasite liver-stage burden, demonstrating that *P. yoelii* is unable to resist host cell apoptosis when the anti-apoptotic mitochondrial proteins are inhibited [3].

1.3.2 Erythrocyte signalling during infection with *Plasmodium*

The asexual blood stage of *Plasmodium* development is responsible for the clinical symptoms of malaria. Consequently, blood-stage development of *Plasmodium* is the ideal point to target for anti-malarial intervention. Several studies have found elements of nucleated host cell signalling present in erythrocytes, which are also manipulated during *Plasmodium* infection of these cells. However, the extent of erythrocytic signalling during *Plasmodium* infection is largely unknown. The few pathways that have been identified are described here.

1.3.2.1 Activation of host p21-activated kinase (PAK) and MAP2K (MEK)

The human MAPK pathway, and more specifically the mitogen-activated kinase kinase (MEK) as well as one of its activators, the p21-activated kinase (PAK), are implicated during infection with several intracellular pathogens [220, 221]. Erythrocyte infection with *P. falciparum* results in high levels of MEK1 phosphorylation at residue Ser298, promoting homodimerisation and thus enabling trans-auto-phosphorylation of the kinase on its activation loop [4]. Presently the only known activator of MEK1 at Ser298 is PAK1, and indeed PAK activation was detected in infected erythrocytes, and the enzyme was confirmed to be the activator of MEK1 during *P. falciparum* infection [4, 222]. Activation of MEK1 usually results in the subsequent activation of the mitogen-activated kinase 3/mitogen activated kinase 1 (ERK1/2). However, during *P. falciparum* infection, ERK1/2 activation was minimal, suggesting that MEK1 activates a non-conventional substrate, potentially encoded by the parasite [4]. Pharmacological studies determined that inhibition of host PAK or MEK affected parasites during trophozoite/early schizont formation [4]. Through analysis of the *P. falciparum* kinome, it was determined that there are no obvious orthologues to either PAK or MEK encoded by the parasite; however, there are two MAPK homologues [140, 223]. Whether these MAPKs orthologues are the target of human MEK1 during infection remains to be shown.

1.3.2.2 Phospholipid-dependent protein kinase C (PKC)

During *P. falciparum* development in erythrocytes, PKC activity has been observed, and following depletion of host PKC parasites exhibited a significant growth defect [5]. A later study further explored the role of erythrocyte PKC during infection and determined that *Plasmodium* infection of erythrocytes depleted of two PKC isoforms (PKCα and PKCβ) resulted in the accumulation of schizonts with failure to egress after 60 hours post-invasion [224]. Interestingly, merozoites mechanically released from these schizonts were able to invade erythrocytes and continue development, indicating that human PKC plays a critical role in

parasite egress from the host cell, but not daughter merozoite viability [224]. Host PKC also has an important role in the invasion and successful infection of the mosquito vector [225]. This suggests that there may be a much larger role for PKC throughout the parasite's entire lifecycle.

1.3.2.3 Band 3 phosphorylation by the Spleen tyrosine kinase (Syk)

Band 3 is a membrane-spanning protein with a key role in erythrocyte stability. Band 3 gives erythrocytes stability by anchoring spectrin and actin to the cell membrane. Additionally, Band 3 functions as a docking site for many signalling molecules [226, 227]. Using chemical inhibition, the human Spleen tyrosine kinase (Syk), a membrane-associated kinase, was shown to phosphorylate Band 3 during *P. falciparum* infection [6, 228, 229]. Interestingly, in a similar manner to PKC depletion, inhibition of Syk activity stops parasite egress [6]. Whether PKC and Syk function through a shared mechanism during infection is unknown.

1.3.2.4 Heterotrimeric guanine nucleotide-binding regulatory proteins (G proteins)

Heterotrimeric guanine nucleotide-binding regulatory proteins (G proteins) and their receptors, the G-coupled protein receptors (GPCR) regulate cellular signalling and processes such as transcription, motility and secretion in nucleated cells [230]. However, the biology of heterotrimeric G proteins and their receptors in mature erythrocytes is poorly understood. Inhibition of one of the G proteins present in erythrocytes, Gas, was demonstrated to block *P. falciparum* infection [231]. A later study identified that G proteins are also required for successful parasite asexual development [232]. During infection Gas and its GPCR, the β2-adrenergic receptor, are internalised and associate with the parasites' vacuole [231]. In nucleated cells, G proteins are known to aid in the rapid reorganisation of the cytoskeleton. G protein signalling may be used by the parasite to establish itself inside the host cell, as *P. falciparum* is known to dramatically reorganisation the infected erythrocytes membrane proteins and is therefore required to modulate host cytoskeleton-associated proteins to achieve this [232, 233].

1.3.3 Host cell signalling during infection with *Toxoplasma gondii*

Toxoplasma is a well-known manipulator of host cell signalling. Many host cell pathways are modulated through secreted ROP serine/threonine protein kinases. The best understood of these secreted proteins is ROP16, which localises to the host cell nucleus during infection. In the host cell nucleus ROP16 is involved in tyrosine phosphorylation-dependent activation of host STAT3/6 by the tyrosine kinase JAK [234, 235]. In this instance, STAT3/6 activation is sustained longer than in uninfected cells, which has been associated with the activity of ROP16 [235, 236]. This is thought to be a key survival mechanism for *T. gondii*, as continued STAT3/6 signalling prevents the host cell from targeting the parasite for autophagy [237].

One pathway affected by *T. gondii*, specifically during macrophage infection is that leading to the release of interferon-gamma (IFN-γ). IFN-γ is a powerful cytokine involved in the hosts' immune response and stimulates *T. gondii* to develop into its latent form (bradyzoites) [94]. When infecting macrophages, *T. gondii* manipulates the intracellular signalling triggered by the IFN-γ receptor through the downstream JAK-STAT pathway. Once IFN-γ is bound to its receptor, JAK is recruited and phosphorylated, which in turn enables phosphorylation of STAT1 [238]. Normally STAT1 translocates to the host cell nucleus where it influences transcription of genes involved in intracellular pathogen control [239]. Using an unclear mechanism, *T. gondii* manipulates host cell STAT1-directed transcription [238]. Consequently, the infected cell is non-responsive to this cytokine, which enables a higher rate of parasite survival. The kinetoplastid parasite *Leishmania donovani* similarly infects host cell macrophages and manipulates host cell IFN-γ signalling through the JAK-STAT1 pathway [240], illustrating convergent evolution of mechanisms in phylogenetically unrelated parasites to fight innate host cell defences.

In 2013 Moser *et al.*, completed an siRNA knockdown screen of 18,200 human genes during infection with *T. gondii* [241]. This group determined that many host proteins expressed during *T. gondii* infection affect parasite growth [241]. Knockdown of hepatocyte PI-3 kinase-related kinase (SMG1), mitogen-activated protein kinase kinase kinase 5 (MAP3K5) and the mitogen-activated protein kinase 11 (MAPK11) all resulted in a reduction of *T. gondii* growth by approximately 50%, indicating that the parasite requires these host cell kinases for optimal growth. Conversely, knock-down of a number of host proteins increased the growth of the parasite, indicating that these proteins may form part of the host's defence mechanism. Among these were CDK9, the fibroblast growth factor receptor 4 (FGFR4), PI3K, fms-related tyrosine kinase 1 (FLT1), "never in mitosis gene a related kinase" 9 (NEK9), RAF1 and PAK4. This suggests that cells infected with *T. gondii* actively suppress parasite growth, by a number of different signalling pathways. Further exploration of the kinases that resulted in increased parasite growth has not been published; however, these kinases may provide critical understanding of previously unknown host-parasite interactions.

1.8 Aims

Much remains to be known about the influence of parasitic infection on host signalling and the potential of host kinases as targets for host-directed anti-parasitic therapies. **We hypothesise** (i) that the few reported host kinase pathways that are activated during Apicomplexan infection represent only the tip of the iceberg in terms of host cell signalling during infection, and (ii) that at least some of the host cell kinases that are activated by infection represent potential targets for therapeutic intervention. We designed this study to address this hypothesis, with an aim to generate a comprehensive global host phospho-signalling picture during infection with several intracellular Apicomplexan parasites, namely *Plasmodium falciparum*, *Plasmodium knowlesi*, *Babesia bovis* and *Toxoplasma gondii*. To achieve this, we used antibody microarrays, where many of the antibodies are phosphorylation-specific, and target human signalling molecules. This allowed us to generate a large data set of global signalling changes during infection with these parasites. In addition, we closely monitored *Plasmodium falciparum* erythrocytic development to determine if any human kinases undergo dynamic changes in phosphorylation during the development of the parasite through stages of sexual and asexual development (Chapter 3). We were also able to successfully apply the antibody microarray approach to study how the host cells signalling is modulated during infection with *P. knowlesi*, *B. bovis* and *T. gondii* and compare the effects on host cell signalling across Apicomplexan infection (Chapter 4). Through the evaluation of the antibody signals and comprehensive characterise of the similarities and differences in host signalling, we were able to identify and further explore several host kinases for further validation including c-MET and B-Raf (Chapter 3) as well as FRS2 (Chapter 4). Furthermore, we explored the effects of inhibiting host B-Raf and c-MET on *P. falciparum* asexual development and determined a parasiticidal effect of asexual growth (Chapter 3). Thus, the specific aims of this study were:

Aim 1 – To generate a comprehensive phospho-signalling derived map of host erythrocyte signalling during the development of the malaria parasite *Plasmodium falciparum*, using antibody microarrays, and to identify small molecular inhibitors of some of the hit kinases that display parasiticidal potency

Aim 2 – To apply the antibody microarray approach from Aim 1 to other *Apicomplexan* parasites. Namely, *Plasmodium knowlesi*, *Babesia bovis* and *Toxoplasma gondii*.

Chapter 2 – Materials and methods

2.1 *P. falciparum* cell culture

2.1.1 Cell culture media

Roswell Park Memorial Institute (RPMI) media 1640-HEPES powder (Gilco) was reconstituted in water (Baxter) with the addition of 50 mg/ml hypoxanthine (Sigma) and 10 mg/ml gentamycin (Pfizer). The pH was adjusted to 6.74, and the solution was filtered through a 0.2 µM pore filter (Merck). This mix is referred to as incomplete RPMI and stored at 4ºC until required. Complete RPMI was prepared before use with the incomplete RPMI plus the addition of 0.22% w/v sodium bicarbonate (Sigma) and 0.5%w/v Albumax II (Gibco) and stored at room temperature (RT).

2.1.2 Human erythrocyte preparation

Purified red blood cells (O+) supplemented with the anticoagulant citrate phosphate dextrose adenine (CDPA) were provided by the Australia Red Cross Service and stored at 4ºC. Packed erythrocytes (approximately 15 ml) were prepared weekly by centrifugation at 5 minutes at 1500*g* for 5 minutes at RT. The clear supernatant containing the CDPA was removed by aspiration, before resuspension of the packed erythrocytes in 30 ml of incomplete RPMI. Erythrocytes were centrifuged at 1500*g* for 5 minutes at RT. Incomplete RPMI was removed by aspiration following resuspension of the erythrocytes in an equal volume of complete RPMI and stored at 4ºC.

2.1.3 *P. falciparum* cell culture

Wild-type (clone 3D7) [242] *P. falciparum* were cultured in 10 ml, or 30 ml petri dishes (Sarstedt) in human erythrocytes prepared as per 2.1.2 at a concentration of 4% haematocrit. Parasites were cultured using complete RPMI prepared as per 2.1.1. Parasite cultures were incubated at 37ºC under 1% O_2 and 5% CO_2 (Balance N_2), in a sealed Perspex box (Labquip technologies). To measure the parasitemia (% infected cells) of a cell culture and morphologically determine the parasite developmental stages, 5 µl of parasite culture was prepared as a thin blood smear on a glass slide. Glass slides were dried for 30 seconds, fixed in 100% methanol (chem-supply) for 20 seconds and stained in 10% (v/v) Giemsa solution (Merck) for 2 minutes. Analysis of thin blood smears was conducted by bifocal microscopy

with a 100x oil immersion lens of a Leica DME microscope. Parasitemia was determined by counting a total of 500 cells using multiple fields of view. Parasite cultures were maintained at 2 - 5% parasitemia, unless required at a higher percentage for synchronisation. Parasitemia was maintained between these values with dilutions of 1 in 10 twice a week (Monday and Wednesday) and a 1 in 20 dilutions on Friday.

2.1.4 Uninfected erythrocyte culture

Erythrocytes prepared as per 2.1.2 were co-cultured alongside infected cells as a control for both the Kineus microarrays and for Western blot analysis. Cultures of uninfected erythrocytes were kept at a haematocrit of 4% using complete RPMI. They were incubated alongside infected samples at 37ºC under 1% O_2 and 5% CO_2 (Balance N_2), in a sealed Perspex box (Labquip technologies).

2.1.5 Cryopreservation of cell culture

Cell cultures were harvested via centrifugation for 5 minutes at 650*g*. Generally, this was conducted on >30ml of cell culture when >10% of the culture contained parasites at the ring stage of development. Complete RPMI was removed through aspiration, followed by resuspension of the cell pellet in 2x the pellet volume of freezing solution (8% v/v glycerol, 3% w/v D-sorbitol [Sigma], 0.65% w/v NaCl in double deionised water [ddH_2O]). Cells were mixed gently and 1 ml aliquots transferred to cryopreservation tubes (Thermo Fisher) which were stored at -80ºC, these frozen samples are now referred to as parasite stabilates.

2.1.6 Thawing of parasite stabilates

When required, parasite stabilates prepared as described in section 2.1.4 were thawed to room temperature and transferred to a 50 ml centrifuge tube (Corning). 200 µl of thawing solution one (12% w/v NaCl resuspended in phosphate-buffered saline [PBS]), and filter sterilised using a 0.2 µM filter (PALL life sciences) was added dropwise followed by gentle mixing. 10 ml of thawing solution two (1.6% w/v NaCl in PBS, filter-sterilised as per solution one) was added dropwise while swirling, followed by thawing solution three (0.9% NaCl /w/v and 0.2% w/v glucose in PBS, filter sterilised as per solution one) in a similar manner. Thawed cultures were centrifuged at 650*g* for 5 minutes, followed by aspiration of the thawing solutions. Cell pellets were washed with 30 ml of incomplete RPMI then resuspended in 10 ml of complete RMPI with 4% haematocrit (2.1.2).

2.1.7 Parasite synchronisation

2.1.7.1 Sorbitol synchronisation

Ring stage parasite synchronisation (0 – 24 hours post erythrocyte invasion) was achieved by treating parasite cultures with pre-heated (37 ºC) 5% w/v D-Sorbitol prepared in PBS and sterilised using a 0.2 µm filter (PALL life sciences). 5% w/v Sorbitol is known to result in the lysis of late-stage parasites (trophozoite and schizonts) in cell culture while leaving the ring stage parasite viable [243]. Cultures were harvested by centrifugation at 650*g* for 5 minutes and the supernatant removed by aspiration. 5% w/v D-Sorbitol at 37ºC was added to cell pellet at 10 ml / 1.2 ml of cell pellet before mixing and incubation at 37ºC for 15 minutes. Treated cells were sedimented by centrifugation at 650*g* for 5 minutes. The supernatant was removed by aspiration, and the cell pellet was washed in incomplete RPMI at 30 ml / 1.2 ml cell pellet. Lastly, the cell pellet was resuspended in the same amount of complete RPMI that the cells began in before sorbitol treatment. Sorbitol treatment was usually repeated at 48 - hour intervals to ensure continued synchronisation, and to increase the percentage of synchronised parasites.

2.1.7.2 Heparin synchronisation

Heparin treatment of parasite cultures was utilised to block merozoite invasion of new erythrocytes, as heparin blocks critical receptor-ligand interactions between the merozoite and erythrocyte [244]. Heparin (Pfizer) was added to a culture of schizonts at 15 international units (UI) per ml of culture. The culture was maintained and incubated as per 2.1.3 until the desired level of segmented schizont were about to rupture. When deemed ready to remove, the culture was centrifuged at 650*g* for 5 minutes before supernatant removal by aspiration. The cell pellet was washed once in incomplete RPMI (30 ml / 1.2 ml of cell pellet), before resuspension in complete RPMI (30 ml / 1.2 ml of cell pellet).

2.1.7.3 Parasite synchronisation into 0 – 4 - hour or 0 – 8 - hour development window

A 0 – 4 - hour development window was used for the asexual *P. falciparum* trophozoite and schizont stage samples analysed on the Kinexus arrays. A 0 – 4-hour development window was created utilising both sorbitol and heparin protocols of 2.1.6.1 and 2.1.6.2. Initially, the cell culture was sorbitol on Day 1, then again on Day 3 at midday. Cultures were further treated with sorbitol on Day 3 at midnight. Day 4 at midday heparin is added to the cultures and left on for approximately 16 hours (4 am Day 5), before being washed from the cultures allowing merozoite invasion of erythrocytes. Day 5 at 8 am cultures were treated with sorbitol, stopping

further schizont rupture, and merozoite invasion of erythrocytes. Following the final sorbitol, the parasites were left to mature to the desired time point.

To create the 8 - hour development window used in the *P. falciparum* ring stage array, the final Day 5 sorbitol was delayed by 4 hours.

2.1.8 *In vitro* IC_{50} determination of various compounds on *P. falciparum* asexual growth

To determine the susceptibility of *P. falciparum* to various human kinase inhibitors, a modified SYBR green fluorescence-based DNA quantification assay was utilised [245]. 10 ml of parasite culture was prepared at 0.25% parasitemia, with a 2% haematocrit per compound. 150 µl of culture was added to 22 wells on a 96 well plate. To the first well, an additional 150 µl of culture was added, with the tested compound at a final concentration of 50 µM. This first well was mixed and used to perform a serial 1: 2 dilution across the plate, resulting in drug concentrations from 50 µM to 0.002 µM. The last three wells contained the controls for this assay, non-treated parasites (positive growth control), a DMSO control (positive growth control, mock-treated), as well as artemisinin and chloroquine (50 µM of each, negative growth control). An equivalent amount of DMSO which was present in the 50 µM drug test well was added to the positive growth control. From each of the serial dilution and control wells, 50 µl was transferred into two new wells in the 96 well plate. The plate was then incubated as per 2.1.3 for 72 hours, at 48 hours the Perspex box was re-gassed with the mix in 2.1.3. After 72 hours, the plate was wrapped in parafilm to seal the edges and placed at -80°C for a minimum of 12 hours.

The plate was thawed at RT for 2 hours to facilitate cell lysis. The quantity of DNA was determined and used as a proxy for parasite proliferation in each well. DNA quantification was achieved by incubating each well with 1x SYBR gold buffer (20 mM Tris-HCl [pH 7.5], 5mM EDTA [pH 8] 0.0008% w/v saponin, 0.08% Triton-X100, 1x SYBR Gold [10,000 x concentrate, Life technologies]) for 1 hour in the dark. Fluorescence of SYBR Gold was measured using a Tecan M 200 plate reader (excitation 495 nm, emission 537 nm, gain set to optimal). For each plate, the mean of the technical triplicates was determined along with the percentage growth inhibition for the compound, using the below formula:

$$\left(1 - \frac{mean\ of\ the\ triplicates - \text{negative growth control}}{non-treated\ positive\ growth\ control - negative\ growth\ control}\right) * 100$$

The data points were transferred from excel in GraphPad Prism 8 and transformed using x = Log(x), followed by analysis with log(inhibitor) vs. response with a variable slope and four parameters. The IC_{50} of each compound tested was the average of three biological replicates, unless otherwise stated. Error bars used were the standard error of the mean.

2.1.9 Parasite purification and lysis

2.1.9.1 Magnet purification of late-stage parasite

Late-stage *P. falciparum* (trophozoites and schizonts) can be purified from ring-stage parasites and uRBCs using a strong magnet. This is possible due to the digestion of host erythrocyte hemoglobin, as the parasite produces hemozoin from heme. Hemozoin is magnetic due to the electron state of Iron in this form. Cultures designated for late-stage parasite enrichment were harvested by centrifugation at 650*g* for 5 minutes. The supernatant was discarded, and the cell pellet was re-suspended in the same volume with fresh complete RPMI. A super MACS® cell separation column (Miltenyi Biotec) was used with a SuperMACS magnet as per the manufacturer's instructions, using complete RPMI as a buffer.

Following the collection of the parasites within the magnet, the column was removed from the magnet and turned upside down. The syringe was removed and the stop-clock set to the column and the syringe plunger (used to fill the column with buffer). The syringe plunger was replaced with a filled 50 ml plunger containing complete RPMI. Using only gravity, the 50ml plunger containing complete RPMI was let to flow through the magnet backwards, where the flow-through, containing the magnet purified parasites was collected. Flow-through containing magnet purified parasites was centrifuged at 650*g* for 5 minutes. Samples were either harvested for Western blot analysis (Section 2.2.5) / Kinexus microarray analysis (Section 2.2.1) or returned to culture, without the addition of fresh uninfected erythrocytes. If enriched parasites were to be re-cultured, parasite pellet was resuspended in the same volume of media the cells were in before enrichment.

If parasites were to be analysed Kinexus microarray or Western blot, the pellet was resuspended in 1 ml of incomplete RPMI. 5 µl of parasites was taken and diluted 1:500. 10 µl of the diluted sample was placed on a haemocytometer, counted and processed using the formula: dilution used x chamber factor (10,000) x cell count within the five by five grid of the haemocytometer. This gave an approximation of the cell number in the sample, which was used to estimate the loading of the Kinexus microarray (2.2.1).

2.1.9.2 Whole-cell lysis of infected and uninfected erythrocytes

Parasites used for Western blot analysis were washed in 1 ml of 1 x PBS supplemented 1 x Protease inhibitory cocktail (EDTA free) (Roche), 300 mM benzamidine, 200 mM phenylmethylsulfonyl fluoride, 500 mM sodium fluoride, 100 mM sodium orthovanadate and 500 mM β-glycerophosphate (PPIC) three times. The supernatant was removed, and the pellet lysed using 80µl of Mammalian protein extraction reagent (M-PER, Pierce) supplemented with PPIC per 10^8 cells and vortexed in 1-minute intervals for 5 minutes. The sample was sonicated in a water bath for 3 minutes before centrifugation at 22,000g for 30 minutes at 4ºC. Following centrifugation, the supernatant was extracted and placed into a new tube. Samples were then nickel resin-treated (see 2.2.3) before being treated with 4 x Laemmli loading buffer (Bio-Rad) including 200mM dithiothreitol (DTT). Samples were heated to 70ºC for 10 minutes before analysis by Western blot (Section 2.2.5).

Uninfected erythrocytes used in Western blot analysis were prepared in the same manner as infected cells.

2.1.9.2 Saponin lysis of *P. falciparum* for antibody microarray analysis

To determine which of the signals on the antibody microarray cross-reacted with parasite proteins, a sample of magnet enriched (see 2.1.8.1) trophozoites and schizonts, which were sorbitol synchronised (see 2.1.6.1) was prepared. Following sorbitol synchronisation cell culture was left for 24 hours to mature to the late stages of development (24 - 48 hours). Cell culture was harvested by centrifugation by at 650*g* for 5 minutes and magnet enriched (see 2.1.8.1). After enrichment, the parasites were washed four times in 1ml of PBS supplemented with PPIC. Following the final wash, the supernatant was discarded and the parasite pellet resuspended in 160 µl of 0.15% w/v saponin (prepared in 1 x PBS, with PPIC), per 30ml petri dish of parasites harvested with a parasitemia of 5% before magnet enrichment. The sample was incubated for 10 minutes at 4°C, with brief vortexing before centrifugation at 650*g* for 5 minutes at 4°C. The supernatant was transferred to a new tube and centrifuged at 22,000*g* for 30 minutes at 4°C. The supernatant was then removed, careful not to disturb any residual pellet. This sample is the saponin supernatant, which will be used in the Kinexus array.

The first pellet following saponin treatment was resuspended in 1ml fresh 0.15% w/v saponin (prepared in 1 x PBS, with PPIC) and incubated for 10 minutes at 4°C. The supernatant was removed and discarded. Saponin lysis was repeated a further two times to ensure all of the host erythrocytes had lysed. This repeatedly lysed pellet is the saponin pellet used in the Kinexus array. Following the final saponin lysis, the pellet was washed three times with 1 ml of 1 x PBS including PPIC. The PBS was removed after the final wash, and the pellet was lysed in 200µl of Kinexus' lysis buffer including protease inhibitors and DTT (see 2.2.1). This sample is the saponin pellet, which will be used in the Kinexus array.

Samples used in the Kinexus array analysis (2.2.1) were loaded according to equal cell numbers. For the saponin lysed samples, this was not possible. Instead, the saponin supernatant and saponin pellet were both loaded at a concentration of 2 mg/ml. Due to a large discrepancy in protein mass between the supernatant vs the pellet, the pellet fraction was loaded with 20x more parasite material than would normally be present in the 2mg/ml of host erythrocyte supernatant it was compared to.

2.2 Biochemistry methods

2.2.1 Sample preparation for Kinexus KAM-900P antibody arrays

The antibody microarrays used in this thesis were the KAM-900P arrays produced by Kinexus. *P. falciparum* asexual samples were prepared as per 2.1.8.1 using the synchronisation techniques covered in 2.1.6. In these arrays, the control for comparative purposes were co-cultured uninfected erythrocytes prepared as per 2.1.4. The samples used for the arrays conducted on *P. falciparum* gametocytes vs co-cultured uninfected erythrocytes, *P. knowlesi* vs uninfected human reticulocytes, *B. bovis* vs uninfected bovine erythrocytes, *T. gondii* vs uninfected human foreskin fibroblasts were all produced by the following collaborators: *P. falciparum* gametocytes, Alex Maier (Australian National University) *P. knowlesi*, Danny Wilson (Adelaide University), *B. bovis*, Brian Cooke (Monash University) and *T. gondii*, Giel Van Dooren (Australian National University). The control and parasite samples were harvested by centrifugation at 650*g* for 5 minutes. Samples were washed three times in ice-cold PBS to remove as much of the culture media and serum. Following the final wash, the PBS was removed, and the samples were lysed in 200µl of Kinexus' lysis buffer, including protease inhibitors and DTT. Lysates were passed through a 26-gauge needle several times (human foreskin fibroblasts were instead sonicated for 5 minutes using 1-minute pulses), until the sample was no longer viscous, before centrifugation at 22,000g for 30 minutes at 4ºC. The resultant supernatant for each sample was transferred into a new 1.5 ml microcentrifuge tube. The concentration of each sample was measured using Bradford assay reagent, compared to Bovine serum albumin (BSA) protein concentration standards. Samples were diluted down to approximately 2mg / ml (each sample pair, uninfected and infected were kept at equal cell numbers). Approximately, 100µg of the protein (adjusted to cell number) of each sample was separated and used for analysis. The saponin lysates were kept at exactly 2mg / ml, and therefore contained 100µg of protein.s

To each sample, 2 µl of Tris(2-carboxyethyl)phosphine (TCEP) was added to reduce proteins. Each sample was vortexed and briefly centrifuged (1000*g*, 15 seconds) before incubation at 37ºC for 30 minutes. Following incubation 3 µl of 2-nitro-5-thiocyanobenzoic acid (NTCB) was added to cyanidate and digest the proteins. Each sample was vortexed and briefly centrifuged before incubation at 37ºC for 30 minutes. At the end of incubation, each sample was briefly centrifuged and transferred into a new tube containing the Kinex 543 dye. Each

tube was vortexed for 1 minute and briefly centrifuged before incubation in the dark for 1 hour at room temperature. Each tube was vortexed and briefly centrifuged every 15 minutes.

Kinexus provided micro spin G-25 columns containing resin for excess dye absorption and coagulated protein binding. The caps of these tubes were loosened, and bottom closures were removed. Each tube was placed inside another microfuge tube to collect flow through. Each tube was centrifugation at 750*g* for 2 minutes, removing the storage buffer from the resin. The columns were washed once using 400 µl of water (MilliQ, Merck) and centrifuged at 750*g* for 2 minutes. The collection tubes were discarded and replaced with a new tube. The dye labelled samples (pink in colour) were briefly centrifuged and added drop-wise to the top of the micro spin columns into the centre of the resin. The columns containing the dye labelled samples were left for 5 minutes in the dark to allow the sample to flow through the resin. The columns with collection tubes attached were centrifuged at 750*g* for 2 minutes. 10 µl of PBS was added to the resin before the columns were centrifuged again. The total flow-through was collected for each sample and columns discarded. These samples are now ready to be loaded onto the array.

The antibody array was stored at -20ºC in a vacuum-sealed bag until samples are prepared. Antibody array was left to thaw at room temperature for 20 minutes before removal from the vacuum bag. This was critical to ensure no condensation build-up on the surface of the array. Once opened the array was incubated for 1 hour at room temperature with 20 ml of 1x Blocking buffer (diluted from the solution provided by Kinexus) inside its 40 ml housing tube. Following blocking the microarray was washed three times with 1x Incubation buffer (diluted from the solution provided by Kinexus) for 2 minutes, each wash was completed on a platform shaker. The microarray was washed finally in water (MilliQ) and dried using an N_2 gas line. The adhesive incubation chamber (Provided by Kinexus) was stuck onto the dry microarray, surrounding the two regions which contained the antibodies. The samples prepared earlier were diluted to 400 µl using Sample dilutent (94.4%v/v 1x Incubation buffer, 5%v/v 1x Blocking buffer, 0.6%v/v HCl [1 M stock]), before loading on to the respective chambers of the microarray. The microarray was covered and left to incubate with the samples for 2 hours while rotating slowly on a platform shaker. Following incubation, the samples were shaken off and the chamber adhesive removed, before quickly washing the array with water (MilliQ) and storing the array in the 40 ml tube provided.

Four separate wash buffers were diluted from solutions provided by Kinexus; these were wash buffer denoted; L, M, N and O. Each wash buffer was diluted to 20 ml. The microarray was washed with each wash buffer sequentially for 5 minutes, 2 minutes, 2 minutes and 2 minutes respectively, while on a platform shaker. Following the final wash, the microarray was further washed using water (MilliQ) until the glass slide appeared clear. The microarray was removed from the 40 ml tube and dried using an N_2 gas line. The dried microarray was returned to the 40 ml tube (once both were dry) and gassed again using N_2 and sealed. The 40 ml tube containing the microarray was wrapped in parafilm and then in foil to seal and protect the microarray from light. The microarray was sent back to the Kinexus facility where they scanned the array and provided the results in an excel spreadsheet.

Eight arrays were performed using asexual stage *P. falciparum*. These compared a co-cultured uninfected erythrocyte control with parasites at the ring 4 – 12 hrs (33% parasitemia, n=3), trophozoite 24 – 28 hrs (magnet purified, n=3) and schizont 44 - 48 hrs (magnet purified, n=2) stage of development. The final array compared purified parasites lysed with saponin. For *P. knowlesi* one array was performed, which compared co-cultured uninfected reticulocytes (70% enriched) with reticulocytes infected with *P. knowlesi* schizonts 24 - 28 hrs (10% parasitemia). For *B. bovis* one array was performed, which compared co-cultured uninfected bovine erythrocytes with a mixed population *B. bovis* infected erythrocytes (50% parasitemia). Lastly, for *T. gondii* one array was performed, which compared uninfected human foreskin fibroblasts with fibroblasts infected with *T. gondii* at a multiple of infection (MOI) of 5:1.

2.2.3 Removal of haemoglobin from protein lysates

Haemoglobin commonly results in undesirable SDS-PAGE migration of proteins in a lysate. Also, haemoglobin binds to most antibodies used for Western blot analysis, often masking the desired proteins signal. This is the result of the large abundance of haemoglobin present in erythrocytes, and consequently why it was removed from the samples analysed by Western blots in this thesis. Haemoglobin can be removed from a lysate using nickel affinity resin (Talon), as the protein binds efficiently to these beads.

Approximately 10x cell pellet volume (before lysis) is required to extract the majority of the haemoglobin present in uninfected erythrocytes. Haemoglobin is digested by the parasites. Therefore, samples containing late trophozoites and schizonts required only 5x cell pellet volume of resin. Required Talon resin was collected from the stock bottle and briefly centrifuged (2 minutes, 500*g*). The resin storage buffer was removed and discarded, and resin

resuspended in 1x PBS, in a 1:1 resin to PBS ratio. The resin was briefly centrifuged, and PBS wash removed. The resin was split into three microfuge tubes, and the lysate was equally added to all. Resin and lysate were mixed by pipetting up and down and incubated on a rotating wheel for 2 minutes at room temperature. Following incubation, the samples were centrifuged at 2500*g* for 1 minute to pellet the resin. The supernatant was extracted from the beads and pooled into a single tube. The sample was further centrifuged at 22,0000*g* for 1 minute to ensure no resin is present. Samples were treatment with Lamemmli loading buffer (see 2.1.9.2).

2.2.4 Sodium dodecyl sulphate-polyacrylamide gel electrophoresis (SDS-PAGE) and transfer to nitrocellulose membrane

4-12% Bis-Tris protein gels, 1.0 mm, 12 wells (NuPAGE Novex) were used for sample separation before transfer and detection via Western immunoblotting. The gels were run in a ThermoFisher Scientific Bolt Mini gel tank using 1x Running buffer (5% [v/v] 20x Bolt MOPS SDS-page running buffer [Novex] in dH_2O) at 165V for 55 minutes, or until desired protein ladder separation was achieved. Gels were removed from gel tanks and transferred to a nitrocellulose membrane (Bio-Rad) by wet transfer in a Bio-Rad Mini Protean^{TM} electrophoresis cell using 1x Transfer buffer (20% [v/v] Methanol, 100mM and Glycine 25mM Tris in dH_2O). Gels were left to transfer for 1.5 hrs at 100V, on ice. Following transfer membranes were analysed via Western blot analysis (see 2.2.5).

2.2.5 Western blot analysis

Membranes were blocked for 1 hour at RT with 15 ml of 5% skim milk (Diploma) in Tween-20 Tris-buffered saline (0.5M Tris, 1.5M NaCl, dissolved in dH_2O, 0.1% [w/v] Tween 20 [Astral Scientific], pH 7.5, TBST). Membranes were rinsed twice with 10 ml of TBST and incubated in the primary antibody. Primary antibodies, dilution and incubation times and secondary antibody are listed in Table 2.1. All primary antibodies were diluted in 5% BSA in TBST and incubated a rotating platform shaker. Following incubation, membranes were washed three times in 20 ml of TBST using a platform shaker at 130 revolutions per minute (RPM). Membranes were incubated in an appropriate secondary antibody (see Table 2.1) diluted in 5% skim milk in TBST and incubated for 1 hour at room temperature on a roller mixer, speed setting 6 (Ratex). Following secondary incubation, membranes were washed five times in 20 ml of TBST using a platform shaker at 130 RPM. The membrane was let drip dry over a paper towel for 20 seconds before incubation with ECL Prime Western immunoblotting

detection reagents (Amersham GE healthcare). 500 ul of Component A and B were mixed and applied to the membrane for 3 minutes. Luminescence was detected on a Bio-Rad Chemidoc XRS+ using Image Lab version v6.0.1 as per the manufacturer's instructions. When required densitometry analysis was also conducted in Image Lab using volume tools and the adjusted volume value.

Table 2.1 – Antibodies used in Western blot studies

Antibody	**Company**	**Dilution**	**Incubation time**	**Secondary used**
Pan-c-Met	D1C2 (CST)#8198	1:500	3 hrs Room temperature	Anti-Rabbit
Phospho (Y1234+Y1235) c-Met	D26 (CST)#3077	1:1000	Overnight 4ºC	Anti-Rabbit
Pan-B-Raf	OTI4B2 (Bio-Rad)	1:1000	Overnight 4ºC	Anti-Mouse
Phospho (S729) B-Raf	PK535 (Kinexus)	1:500	Overnight 4ºC	Anti-Rabbit
Phospho (Y196) FRS2	(CST)#3864	1:1000	Overnight 4ºC	Anti-Rabbit
Pan-FRS2	A-5 (Santa cruz) sc-17841	1:500	Overnight 4ºC	Anti-Rabbit

2.3 Flow cytometry analysis of *P falciparum* growth following inhibitor treatment

Highly synchronous cultures (2.1.7.3) at 2% haematocrit treated with DMSO (vehicle), Crizotinib, PHA-665752, SB-590885 or artemisinin at 5x the IC_{50} values determined (2.1.8), and were monitored at 12-hr time intervals over two full asexual intra-erythrocytic cycles (84 hrs) by flow cytometry. Live parasitaemia was measured by a bi-colour flow cytometry staining protocol using 2 μM Hoechst-33342 staining for 8 minutes and 75 nM MitoTracker Orange for 25 minutes. Staining was completed in v-bottom plates with two washes in complete RPMI using a centrifuge (200*g* for 3 min). Stained cells were then transferred to polypropylene tubes and diluted one in four in complete RPMI. Cells were then immediately analysed on an LSR BD Fortessa with the laser UV379 and filter 450/50 for Hoechst-33242 staining, and laser YG585 with filter 585/15 for MitoTracker Orange staining. The flow rate was maintained at <10 000 events/second, and voltages were kept consistent at 320 V and 450 V for Hoechst-33342 and MitoTracker Orange staining respectively. Biological replicates (n=5) were normalised to a 2% total parasitemia value at the first time point (0 – 4 hrs post-invasion). Total parasitemia was defined as the total events of quadrant 1 (Hoechst-33342 positive and MitoTracker Orange negative cells, dead parasites) and quadrant 2 (Hoechst-33342 and MitoTracker Orange positive cells, live parasites). The live parasitemia value (quadrant 2) were graphed over the total 84 hrs of drug treatment. Chapter 3 – Host erythrocyte phospho-signalling during intracellular infection with *Plasmodium falciparum.*

Chapter 3 – Host erythrocyte phospho-signalling during intracellular infection with *Plasmodium falciparum*

3.1 Introduction

Intracellular signalling through kinases is undoubtedly pivotal to cellular and organism survival. As discussed in Chapter 1, it is well known that *P. falciparum* and all Apicomplexan parasites encode a variety of kinases for a diverse set of functions, which in some instances are specific to the species. Often overlooked during *P. falciparum* infection is the role of signalling in the host cell, and how it responds to or is manipulated by intracellular infection. During *P. berghei* liver stage development, transcriptional profiling of the host cell has outlined numerous changes in host protein expression [246]. Studies on phosphorylation of Bcl-2, p53, AMPK, and c-MET have indicated that these molecules all play roles during murine *Plasmodium* liver stage development (see Chapter 1.3.1) [3, 197, 211, 218]. There is, however, little data on how signalling in host erythrocytes changes during infection with *Plasmodium* blood stages. The signalling proteins PAK, MEK, BAD, PKC and syk have been identified as important for *P. falciparum* blood-stage development [4, 5, 224, 228, 229]. These are valuable enzyme-specific data; however, a global, system-wide analysis of erythrocyte signalling during *P. falciparum* infection had not yet been completed. We aimed at filling this gap by generating a comprehensive map of phosphorylation/activation status of a wide range of host erythrocyte signalling proteins over the course of *P. falciparum* development, by using commercially available antibody microarrays.

The antibody microarrays used in this study are developed by Kinexus Bioinformatics Co. and contain pan- and phosphorylation-specific antibodies directed against 363 human signalling molecules, most of which are kinases. Figure 1.8 represents the process by which two samples are prepared before incubation on the antibody microarray. In brief, two samples (uninfected and infected) are collected, lysed and cleaved into fragmented proteins using tris 2-carboxyethyl phosphine (TCEP) and 2-nitro-5-thiocyanobenzoic acid, (NTCB). These samples are then directly labelled with a fluorescence dye, before incubation on the microarray. The array is scanned, which produces qualitative, as well as quantitative data. Each of the antibodies

on these arrays is present in technical duplicate, which provides reliability, and an associated error for each of the signals. Using the signal intensity and the percentage change from the control (%CFC), the fold change can be determined, and further investigated.

Kinexus' antibody microarrays have primarily been used to study cancers and to determine drug targets of new inhibitors [247, 248]. Recently, Kinexus' antibody microarrays have successfully identified host signalling changes during infection with some intracellular pathogens [249-251]. Currently, no global host signalling arrays, which investigate phosphorylation have been completed on Apicomplexan parasites. We use this antibody microarray approach to distinguish the differences in host protein phosphorylation during infected with a variety of Apicomplexan parasites. As discussed in Chapter 1, during the erythrocytic cycle of *P. falciparum*, several distinct stages of parasite development can be identified, namely ring, trophozoite and schizont stages for asexual development, and male and female gametocyte stages for sexual development. Through *in vitro* continuous culture, it is possible to synchronise parasites and isolate these distinct forms of parasite development. Using techniques described in Chapter 2.1, we were able to purify protein extracts of highly synchronised parasites, which were analysed on an antibody microarray and compared to control extracts from uninfected erythrocytes. This Chapter discusses data from these experiments and identifies the most prominent and reliable host signalling changes that occur during infection. Several of these key human kinases are shown to have an essential role in parasite blood-stage development. These datasets, including the results of the extensive comparative bioinformatic analysis, are presented in Chapter 3.2 as a paper draft currently under review at *Nature - Microbiology*, titled 'Signalome-wide assessment of erythrocyte response to *Plasmodium falciparum* infection uncovers novel targets for host-directed antimalarial intervention'. This paper is integrated into the below text to enable more consistent flow through this Chapter. Chapter 3.3 presents the datasets obtained through the analysis of stage IV *P. falciparum* gametocytes.

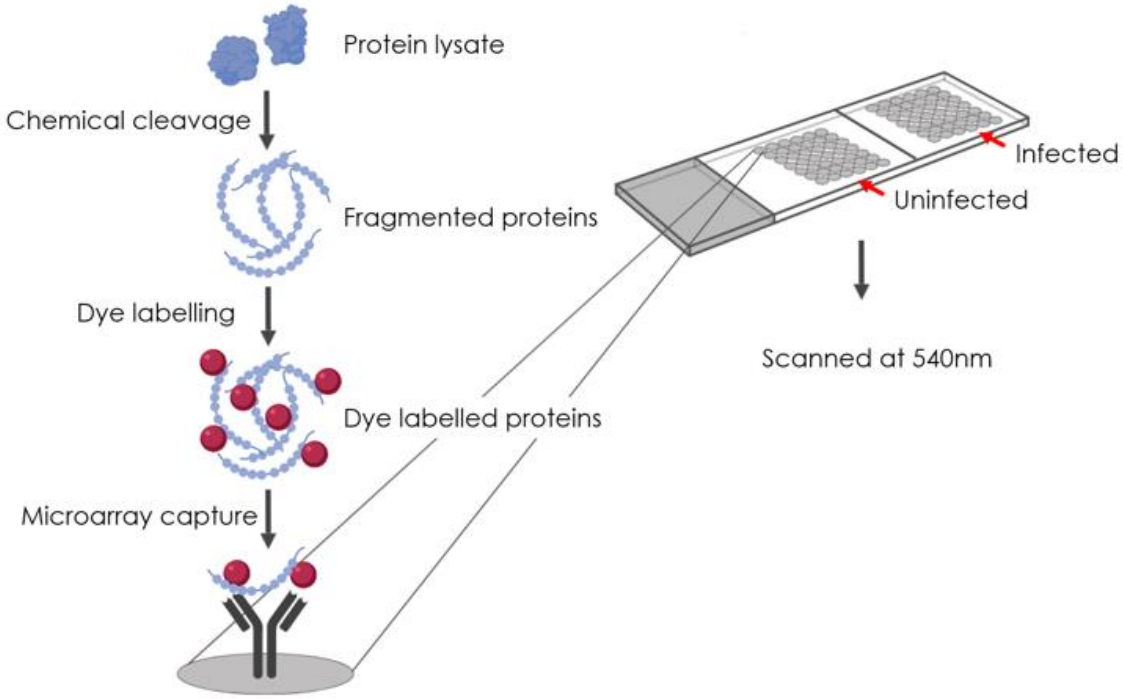

Figure 3.1 – Schematic of sample preparation and procedure for Kinexus array experiments.

Lysates are fragmented using tris 2-carboxyethyl phosphine (TCEP) and 2-nitro-5-thiocyanobenzoic acid, (NTCB) before labelling with a fluorescent dye. The dye labelled samples are incubated on the array before scanning at 540nm to determine protein signal intensity for each sample, before comparison to determine the percentage change from the control, or uninfected sample (%CFC). Created using BioRender.

3.2 Paper: Signalome-wide assessment of erythrocyte response to *Plasmodium* reveals novel targets for host-directed antimalarial intervention

Jack D. Adderley[1], Simona John von Freyend[2], Sarah A. Jackson[2], Megan J. Bird[2], Amy L. Burns[3], Burcu Anar[4], Tom Metcalf[4], Jean-Philippe Semblat[5], Oliver Billker[4,6], Danny W. Wilson[3,7], Christian Doerig[1]

[1]Centre for Chronic Infectious and Inflammation Disease, Biomedical Sciences Cluster, School of Health and Biomedical Sciences, RMIT University, Bundoora VIC 3083, Australia

[2]Infection and Immunity Program, Biomedicine Discovery Institute and Department of Microbiology, Monash University, Clayton VIC 3800, Australia

[3]Research Centre for Infectious Diseases, School of Biological Sciences, University of Adelaide, Adelaide SA 5005, Australia

[4]Wellcome Trust Sanger Institute, Hinxton, Cambridgeshire, CB10 1SA, United Kingdom.

[5]Institut National de la Transfusion Sanguine, Inserm UMR S1134, 75015 Paris, France

[6]Molecular Infection Medicine Sweden (MIMS), Department of Molecular Biology, Umeå University, Umeå, SE-901 87, Sweden.

[7]Burnet Institute, Melbourne, Victoria, Australia 3004

3.2.1 Abstract

Intracellular pathogens are known to mobilise host signalling pathways to manipulate gene expression in their host cell to promote their own survival. Surprisingly, evidence is emerging that specific signal transduction elements are activated in a-nucleated erythrocytes in response to infection with malaria parasites, but the extent of this phenomenon remains unknown. Here, we fill this knowledge gap by providing a comprehensive and dynamic assessment of host erythrocyte signalling during the course of infection with *Plasmodium falciparum*. We used an antibody microarray that comprises 878 antibodies directed against human signalling proteins, >600 of which are phospho-specific, to interrogate the status of host erythrocyte signalling pathways at three stages of parasite development during the asexual cycle. This confirmed the pre-existing fragmentary data on the activation of a PAK-MEK pathway, and revealed the modulation of a large number of additional signalling elements during infection.

We focussed on the receptor tyrosine kinase c-MET, also known as the hepatocyte growth factor receptor, and the MAP kinase pathway component B-Raf that is reported to lie downstream of c-MET in a number of cell types. Array data validated by Western blotting revealed that activation sites of MET are phosphorylated in trophozoite-infected erythrocytes, and we show that treatment of parasite cultures with selective inhibitors of human c-MET or B-Raf kinase activity have high potency (in the low nM range) against *in vitro* proliferation of both *P. falciparum* and the phylogenetically distant species *P. knowlesi*. Additionally, a c-MET inhibitor impaired *in vivo* proliferation of the rodent malaria parasite *P. berghei* in mice.

Overall, we provide a comprehensive dataset on the modulation of host erythrocyte signalling during infection with malaria parasites, as well as a proof of concept that human signalling kinases identified as activated by malaria infection represent attractive targets for antimalarial intervention.

3.2.2 Introduction

Malaria, caused by infection of mosquito-borne apicomplexan parasites in the genus *Plasmodium*, remains one of the most devastating infectious diseases globally. Among the six species that infect humans, *P. falciparum* is the most virulent and is responsible for the majority of malaria-related deaths. The remaining human malaria species *P. vivax, P. ovale, P. malariae* and two zoonotic species, *P. knowlesi* and *P. simium* [252, 253], are major contributors to global malaria morbidity and must be considered in the context of new treatment strategies for malaria. Recent years have seen a 50% drop in malaria-related mortality, yet the disease still kills an estimated 445,000 people every year, mostly young children in sub-Saharan Africa [15]. Progress towards malaria elimination and ultimately eradication has stagnated, and the emergence of parasites resistant to the most recently deployed global front-line treatment, artemisinin-combination therapies (ACT) [15, 254], is a major concern. It remains critical to develop novel antimalarial drugs with untapped modes of action.

Protein kinases (PKs) are core components of signalling pathways in eukaryotic cells. Phosphorylation of the target protein can lead to conformational changes and generate or mask binding motifs, and thus can affect its activity, binding properties, stability or subcellular localisation. PK activity can be regulated positively or negatively by phosphorylation of specific amino acids, or by binding to specific activator or inhibitor proteins. Activation leads to a conformational change making the active site accessible to ATP and the substrate protein. PKs are eminently druggable targets, as illustrated by the fact that > 48 small molecule kinase inhibitors have reached the market, largely in the context of cancer chemotherapy [153, 255]. The kinomes of apicomplexan parasites and humans are quite divergent owing to the large phylogenetic distance between these organisms [143], and parasite-encoded PKs have been proposed as attractive potential targets for selective intervention [159]. Host-directed therapy (HDT) is another avenue that is currently gaining traction to combat infectious diseases generally [162]. We and others [163, 164] have proposed that host erythrocyte (and hepatocyte) PKs represent excellent potential targets for antimalarial intervention. Many anti-infective drugs are rendered ineffective by the selection of mutations in their pathogen-encoded targets, which explains the rapid emergence of resistance across essentially all pathogen taxons. Targeting host enzymes would deprive the pathogen of this most direct pathway to resistance. Furthermore, repurposing anti-cancer kinase inhibitors as agents against infectious diseases would greatly alleviate the lack of resources that severely affects anti-infective drug development.

Malaria pathology is caused by the blood stage of the parasite lifecycle. Blood stage malaria begins with the infection of erythrocytes by *Plasmodium* merozoites, followed by rapid growth and asexual multiplication. Newly formed merozoites are then released into the bloodstream and invade erythrocytes to begin the next replication cycle (~48 hrs for *P. falciparum*). Several human signalling molecules of the host erythrocyte have been implicated in parasite survival during infection. These include G-coupled protein receptors [231, 232, 256], the protein kinases MEK (MAP/ERK kinase) [4], PAK (p21-activated kinase) [4], PKC [5], and peroxiredoxin [7, 257, 258]. In our study of the erythrocyte PAK-MEK pathway [4], we showed that host MEK1 is phosphorylated on residue Ser298 in infected erythrocytes. pSer298 is known to cause activation of the enzyme through stimulating trans-auto-phosphorylation on its activation loop. The only PK known to phosphorylate MEK1 on Ser298 is PAK1 [222], and indeed we showed that the latter enzyme is also activated in infected erythrocytes [4]. PAK isoforms are notorious for having a multitude of substrates [259] and serve as a node to integrate signals from a number of upstream receptors and transmit these signals to several downstream effector pathways (including the mitogen-activated protein kinase pathway [MAPK] that includes the aforementioned MEK). We, therefore, hypothesised that our description of the PAK-MEK pathway addresses but a minute fraction of the signalling events that may be modulated by infection. Here, in order to comprehensively assess the host erythrocyte signalling response to infection, we use a microarray of antibodies designed to recognise human signalling proteins and their phosphorylation status. Comparison of the signals obtained from extracts of uninfected erythrocytes with those obtained from erythrocytes infected with *P. falciparum* at three main developmental stages of the replication cycle (rings, trophozoites and schizonts) allowed us to generate a comprehensive and dynamic picture of the modulation of host erythrocyte signalling by infection. This identified several host kinases as potential targets for HDT; on this basis, we further demonstrate that selective inhibitors against human c-MET and B-Raf display high potency against *P. falciparum* and *P. knowlesi in vitro*, and show that a c-MET inhibitor has *in vivo* activity against *P. berghei* in a murine model of malaria.

3.2.3 Results and Discussion

Kinexus antibody microarray analysis. To investigate dynamic changes in host erythrocyte signalling during *P. falciparum* asexual proliferation, we employed an antibody microarray developed by Kinexus (Vancouver, Canada). The array consists of 878 unique antibodies, 265 of which are pan-specific, i.e. recognise both the phosphorylated and unphosphorylated forms of the target protein; the remaining 613 antibodies are phosphorylation-specific, recognising signalling molecules only if their activating or inhibitory phosphorylation sites are modified by the addition of a phosphate group. Some of the most important and well-known signalling molecules, such as members of the Mitogen-activated protein kinase (MAPK) pathways or the PKC isoforms, are detected by multiple antibodies aimed at various phosphorylation sites within the same protein. The array thus provides a comprehensive picture as to how signalling mediated by these molecules changes during infection. Each array device comprises two identical chambers, each carrying two spots for each of the 878 antibodies, thus delivering each read-out in duplicate. Two sample lysates are labelled with protein-binding fluorescent dye [e.g. from *Plasmodium*-infected (iRBC) and non-infected (uRBC) red blood cells] and compared on each device, one sample per chamber. Binding of proteins to the antibodies on the array is quantitated through the measurement of the signal intensity.

Signal robustness and overall changes in phosphosignalling in response to infection.

To evaluate the reproducibility and robustness of the approach, we used four uninfected erythrocyte (uRBC) samples from different blood donors. In view of the absence of gene expression in erythrocytes, we focused our analysis on the phosphorylation-specific antibodies. The mean signal intensity across these four samples for each phospho-specific antibody on the array was determined (the entire datasets are available in Supplemental Dataset 1), and the standard deviation from this mean was calculated for all data points for each of the four uRBC samples (Fig. 3.2). Despite some variation, none of the standard deviations exceeded 2, illustrating that sample-to-sample variation was minimal. To assess the impact of infection on host cell signalling, whole-cell protein extracts were obtained from synchronised *P. falciparum* cultures at three time windows during the erythrocytic cycle: 4-12 hrs post-invasion (hpi) (rings, n=3), 24-28 hpi (trophozoites, n=3) and 44-48 hpi (segmented schizonts, n=2). Each of these extracts were loaded onto a separate antibody array and compared to the mean of the four uRBC lysates (see above). In stark contrast to the minimal variation between the uRBC samples, analysis of the iRBC extracts showed that 6% (ring-stage), 23% (trophozoite-stage)

and 12% (schizont stage) of the phospho-specific antibody intensities differed by more than 2 standard deviations from the uRBC mean. The datasets for each of the three developmental stages showed no internal variation greater than 2 standard deviations (Supplemental Figure 1), highlighting the robustness and reliability of the approach (Fig. 3.2; the complete datasets are available as a collection of Excel spreadsheets in Supplemental Dataset 1). Overall, this implies (i) that there is little variation between biological replicates of uRBCs, attesting to the reliability of the system, and (ii) that infection with *P. falciparum* causes significant variation in the signals yielded by phospho-specific antibodies, suggesting a strong impact of infection on phosphosignalling of the infected cell.

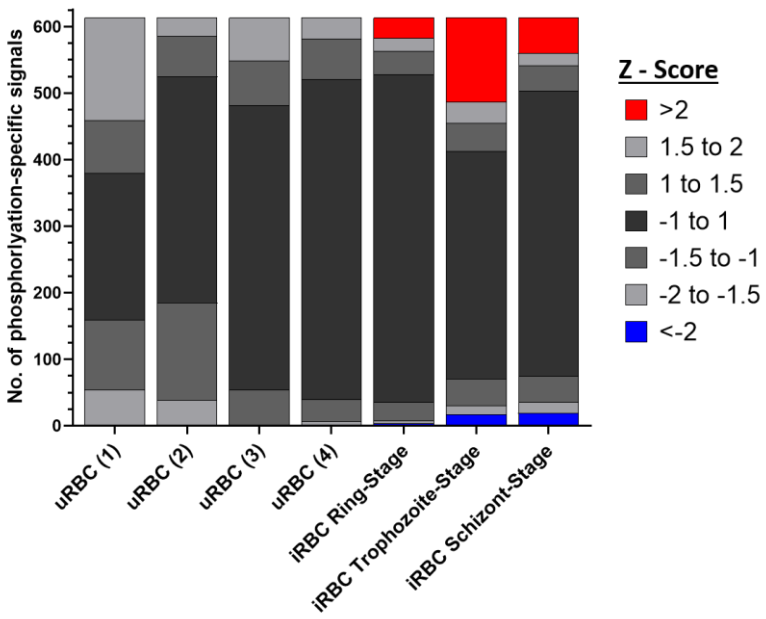

Figure 3.2 – Distribution of Z-scores for each sample.

All microarray signals from each sample (four from uRBCs and the mean signal for each iRBC harbouring parasites at the ring (n=3), trophozoite (n=3) and schizont stage (n=2)) were compared to the uninfected erythrocyte mean value for each signal, and the Z-score determined for each phosphorylation-specific signal. The Z-score is defined as the number of standard deviations from the uRBC mean for each sample; a positive or negative value indicates the direction of the signal (increase or decrease, respectively) from the uRBC mean. No signals from the uRBC samples (n=4) had associated Z-scores above 2 or below -2, while the three iRBC time points showed clear variations from uRBCs.

Data filtering- removal of cross-reacting antibodies. To address the issue of possible cross-reactivity of the antibodies with parasite-derived proteins, we compared signals from purified unsynchronised parasites (pellet obtained by saponin lysis followed by centrifugation) with those of the purified erythrocyte cytoplasm (saponin supernatant). Saponin disrupts the erythrocyte membrane, thereby releasing erythrocyte cytoplasmic proteins and exported parasite proteins, while the parasite and insoluble erythrocytic material can be pelleted [260]. The array was loaded with 20x more (protein mass) pellet material than supernatant material, to confer high stringency with respect to cross-reactivity. A heatmap of the results is shown in Supplemental Figure 2a, and the full dataset is presented in Supplemental Dataset 2. Antibodies showing a fold change > 1.5 between the erythrocyte cytoplasm (saponin supernatant) and the parasite extract (saponin pellet), amounting to 224 signals (37%) of the phospho-specific antibodies, were withdrawn from further analysis (Supplemental Figure 2 and Supplemental Dataset 2). This level of cross-reactivity is not surprising, as many signalling proteins display conservation between *Homo sapiens* and *P. falciparum,* especially in their regulatory sites [143]. Many of these cross-reactive antibodies may recognise parasite-encoded orthologues of the human target proteins and thus prove to be useful tools to study *P. falciparum* signal transduction; however, this lies outside of the scope of the present study.

Data filtering - removal of low-signal antibodies. Some antibodies showed a weak fluorescence signal, likely due to the low abundance of the target protein. The antibodies yielding a signal intensity below a fluorescence reading of 1000 units in both the erythrocyte control and parasite-infected samples were removed from further analysis, as recommended by Kinexus (Supplemental Dataset 1). This included 26 signals from the ring array, and 41 and 48 signals from the trophozoite and schizont arrays, respectively.

Broad analysis of the post-filtering iRBC dataset

Following low and cross-reactive signal removal, 1 of the ring stage signals, 29 of the trophozoite stage and 17 of the schizont stage signals had fold changes differences above 2 or below 0.5 from the uRBC signals, revealing dynamic changes in the phosphorylation of host signalling proteins during *P. falciparum* asexual development (Fig. 3.3a: heatmap of all retained signals; Fig 3.3b: distribution of increased and decreased signals at the three development stages). There were few changes in ring-infected cells; the effect on host cell signalling was considerable at later stages. The majority of changes in trophozoite- and schizont-infected cells (80% and 65%, respectively) are increases in phosphorylation. A dot

plot for each of the three life stages (Fig. 3.3c) further illustrates this trend and highlights the strongest individual changes.

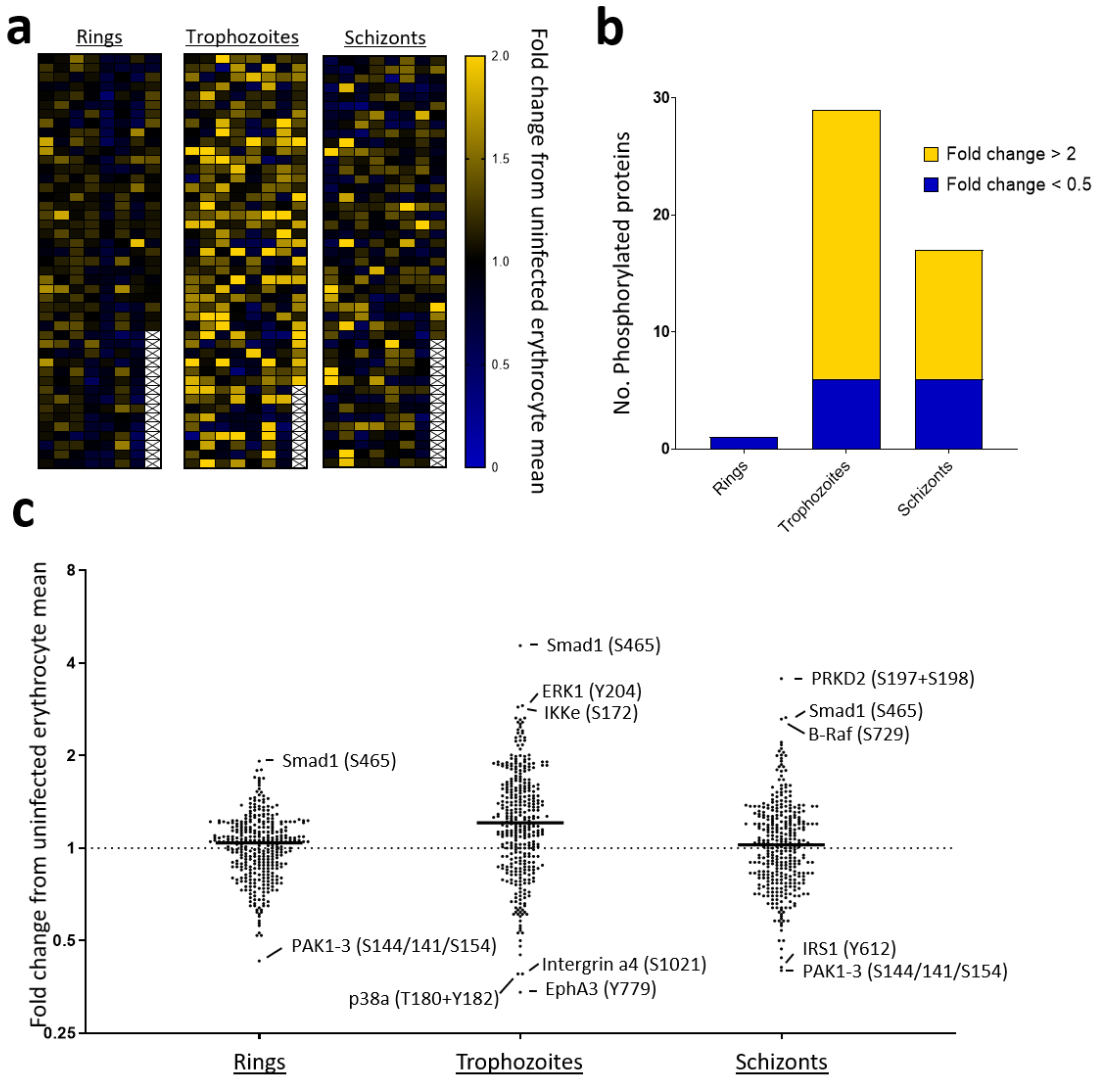

Figure 3.3 – Microarray data for the ring, trophozoite and schizont stages.

a) Heat map of phosphospecific antibody array data for ring- trophozoite- and schizont-infected cells after removal of cross-reactive and weak signals. **b)** Phosphorylation-specific signals (post-filtering) ranked according to fold change. Yellow represents changes with a fold change greater than 2; blue represents changes with a fold change less than 0.5. Full datasets are presented in Supplemental Dataset 1 and 2. **c)** Dot plot highlighting differences in phosphosite signals represented as fold change. Strong changes are listed with their associated phosphorylation site.

Shortlisting of high-confidence changes in phosphosignalling. Following low and cross-reactive signal removal (Figure 3.3), there remain 345, 351 and 346 reliable signals on the phosphorylation/activation status of human signalling proteins during erythrocyte infection with ring, trophozoite and schizont stages, respectively. Of the remaining signals, 16 (ring stage), 102 (trophozoite stage) and 35 (schizont stage) were significantly different ($p<0.5$, unpaired t-test) from the uninfected erythrocyte signals. Figure 3.4 lists the most noteworthy changes observed from this analysis (the full list of the significant changes is available in Supplemental Dataset 3).

PKCδ phosphorylated on T507 appears significantly more phosphorylated at both the trophozoite and schizont stages, a critical phosphorylation site within the activation loop of the kinase (Supplementary Figure 3) [261]. Similarly, PKCθ also has several phosphorylation sites which were significantly increased at the trophozoite and schizont stages (S695 and Y545). The phosphorylation site Y545 is within the activation loop of PKCθ, while S695 is present on the hydrophobic motif and required for optimal kinase activity [262, 263]. These data are consistent with previous reports that host cell PKC activity is detectable during schizont development (30-40 hrs post-invasion) with limited activity before 25 hrs [224, 264], and considerably refine these previous findings, by providing information on the dynamic phosphorylation changes that occur on specific residues of the various PKC isoforms during parasite development.

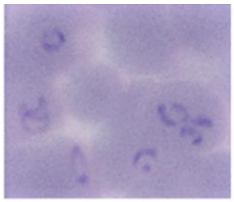

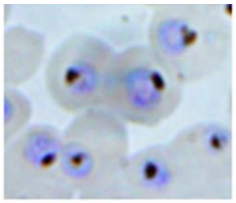

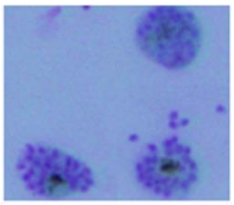

Rings

Protein	Phospho Site (Human)	Fold change	p value
FAK	Y397	1.80	0.043
DDR1	Y796+Y797	1.69	0.027
B-Raf	S729	1.69	0.029
SCYL1	S754	1.63	0.045
PTEN	S380+T382+T383	1.43	0.042
HSP90AB1	Y484	1.38	0.044
DDR2	Y736	1.34	0.044
CHK1	S317	1.30	0.019
JAK2	Y570	1.20	0.044
Rac1/cdc42	S71	0.65	0.010
RSK1/2	S380/S386	0.64	0.006
Tau	S713	0.58	0.050
Paxillin 1	Y31	0.56	0.012
Tau	S713	0.53	0.011
p38a MAPK	T180+Y182	0.52	0.045
Rb	S780	0.52	0.029

Trophozoites

Protein	Phospho Site (Human)	Fold change	p value
Smad1	S465	4.56	0.0003
IKKe	S172	2.88	0.007
InsR	Y1189	2.65	0.005
SCYL1	S754	2.65	0.0002
B-Raf	S729	2.53	0.020
PTEN	S380+T382+T383	2.17	0.001
RET	Y905	2.00	0.013
PKCd	T507	1.96	0.004
PKCq	S695	1.90	0.006
ERK2	T185+Y187	1.85	0.001
PKCq	Y545	1.80	0.013
MET	T1241	1.72	0.023
DDR2	Y736	1.65	0.008
PKCq	S695	1.59	0.040
DDR2	Y740	1.55	0.002
MET	Y1234+Y1235	1.52	0.025
DDR1	Y796+Y797	1.51	0.022
MET	S1236	1.38	0.035
Paxillin 1	Y31	0.62	0.021
PTEN	S380+T382+S385	0.53	0.008
Tau	S713	0.50	0.006
p38a MAPK	T180+Y182	0.39	0.014

Schizonts

Protein	Phospho Site (Human)	Fold change	p value
PRKD2	S197+S198	3.56	0.005
Smad1	S465	2.66	0.008
B-Raf	S729	2.63	0.002
ERK1	Y204	2.11	0.037
EIF2AK3	T982	2.07	0.005
PKCd	T507	2.05	0.005
DDR2	Y736	2.01	0.001
IKKe	S172	2.00	0.034
InsR	Y1189	1.92	0.032
SCYL1	S754	1.84	0.040
PTEN	S380+T382+T383	1.80	0.012
DDR2	Y740	1.79	0.001
PKCq	S695	1.43	0.044
ERK2	T185+Y187	1.42	0.033
SMG1	T3550	0.67	0.006
ABL1	Y469	0.64	0.025
CLK1	S337	0.63	0.042
Paxillin 1	Y31	0.57	0.026
Tau	S713	0.50	0.012
ErbB3	Y1328	0.50	0.046

Figure 3.4 – Shortlist of the highest confidence signals for rings, trophozoites and schizonts.

Increases in phosphosite occupancy are marked in yellow; decreases are marked in blue. All values listed are the fold change from the uRBC control mean (n=4); the corresponding p-value for each signal is also listed. Each signal has a p-value <0.05, as determined through an unpaired t-test. All listed signals passed stringent parasite cross-reactivity and signal intensity filters (see text for details and Figure 3.3).

MAP-Kinase signalling in infected erythrocytes – B-Raf, MEK and ERK. The canonical MAPK pathway is a highly conserved, three-tiered cascade, in which a MAP kinase kinase kinase (MAP3K, or MEKK for MAP/ERK kinase kinase) phosphorylates and thereby activates a MAP2K (or MEK), which in turn phosphorylates and activates a MAP kinase. A well-understood MAPK pathway involves Raf, MEK and ERK. Both Raf isoforms are activated by Ras-GTPase binding, which enables phosphorylation of T598 and S601 (on B-Raf) and S338 and Y340 (on C-Raf) [265-267]. This results in the full activation of Raf, enabling downstream phosphorylation of MEK and consequently ERK1/2. *P. falciparum* has no homologues for either Ras, Raf or MEK, but expresses two MAPKs, either of which is a close homologue of ERK1/2 [268]. Figure 3.5 lists the phosphorylation sites detected on the array that are relevant to canonical MAPK pathways (Fig. 3.5a) and indicates the activating phosphorylation sites for each of the three kinases involved (Fig. 3.5b). The activating Ras-induced phosphorylation sites on B-Raf (T598 and S601) and C-Raf (S338 and Y340) are not represented in the array. Phosphorylation of B-Raf on S446 and S447 is increased by a fold change of 1.79 at the ring stage, but decreases back to levels that are similar to those in uninfected cells in trophozoites and schizonts. S446+S447 plays a role in priming B-Raf for activation by Ras [267, 269]. In some cell lines, B-Raf S446 is constitutively phosphorylated, but this remains to be shown in cells of the erythropoietic lineage [267, 269-271]. B-Raf phosphorylation on S729 increases at all three life cycle stages. The largest fold change (>2.63) was recorded in the schizont-infected cells (Fig 3, Fig. 4a). Phosphorylation of B-Raf on S729 is the result of AMP-activated protein kinase (AMPK) activity, which is itself triggered by energy stress, and promotes association with the scaffolding protein 14-3-3 and C-Raf, enabling downstream MAPK signalling; interestingly, increased phosphorylation for C-Raf is also observed at this stage [272]. Of the two AMPK antibodies on the array, one was discounted due to cross-reactivity with a parasite protein, while the other (AMPKa2 S377) indicates a slight increase (1.17 fold change) in phosphorylation at the trophozoite time point (Supplemental Dataset 1). Antibodies against C-Raf S296 and (S301+T303) yielded a consistent fold change of >1.2 for all three parasite stages. Phosphorylation of C-Raf on S296 and S301 is thought to be mediated by ERK1/2; although a functional role of these phosphorylation sites is debated. Hekman *et al.* suggested these sites are involved in a negative feedback loop of ERK1/2, consistent with the activity of the MAPK pathway we see here (see below for further discussion) [273].

The B-Raf substrates MEK1/2 showed increased phosphorylation on several residues, primarily at the schizont time point (Fig. 3.5a). MEK1/2 phosphorylation of S298 (resulting from p21-activated kinase [PAK] phosphorylation) during late stages of *P. falciparum* infection has previously been ascertained by Western blot analysis [4], aligning with the 1.51-fold increase of pS298 at the schizont stage observed in the array experiment. Other phospho-sites such as T386, T292 and S222 (MEK1) and T394 (MEK2) also show a signal increase in the presence of ring-stage *P. falciparum*. MEK1 T386 and T292 and MEK2 T394 are involved in negative feedback loops [274-276], while the activation loop phosphosites for MEK1 and MEK2 are S218+S222 and S222+S226, respectively [277, 278]. All the MEK1/2 phospho-specific antibodies, as well as the ERK1 (Y204) antibody, showed some cross-reactivity with parasite protein (underlined in Fig. 3.5a), which makes the overall MEK1/2 data difficult to interpret (Fig. 3.5a).

ERK1 and ERK2 are phosphorylated by MEK1/2 (on T202- 204 for ERK1, on T185 -Y187 for ERK2), and these residues are the only known targets of MEK1 activity [279, 280]. ERK2 is slightly more phosphorylated in ring-infected cells than in uninfected erythrocytes (fold change = 1.09); at the trophozoite stage it has increased further (fold change = 1.85), and at the schizont stage ERK2 phosphorylation is still elevated (fold change = 1.42). The array results for the ERK1 activation sites (T202 and Y204) at the ring-stage of *P. falciparum* development are however difficult to interpret as these signals indicate increases as well as decreases. ERK1 T207 is a known autophosphorylation regulatory site and showed a fold change value of 1.25 in the presence of trophozoites-, suggesting that regulation of ERK1 activity occurs during infection [281]. Overall, the data points to a clear activation of B-Raf throughout asexual development, with fragmented downstream activation of both MEK1/2 and ERK1/2, which could be indicative of negative feedback. Following the identification of the MAPK pathway activation, we focused our attention on signalling components that lie upstream of the MAPK pathway and found that the receptor tyrosine kinase c-MET, which is known to signal to MAPK pathways in other systems [207], was clearly activated by infection (Figure 3.4, trophozoite time point).

a

Protein	Phospho Site (Human)	uRBC Error (%)	Ring stage Fold change	Ring stage Error (%)	Trophozoite stage Fold change	Trophozoite stage Error (%)	Schizont stage Fold change	Schizont stage Error (%)
B-Raf	S446+S447	10	1.79	125	0.94	39	1.07	74
	S729	22	1.69*	39	2.53*	33	2.63*	11
	Pan-specific	25	1.66*	64	2.36*	30	2.26*	1
C-Raf	S296	10	1.20	34	1.25	7	1.20	11
	Pan-specific	29	1.17	36	1.26	10	0.99	10
	Pan-specific	46	1.67	10	2.92*	6	2.54*	9
MEK1	S298	11	1.24	5	0.84	7	1.35	11
	T292	3	1.17	4	0.79	3	1.27	9
	T386	4	1.05	12	0.82	9	1.05	13
	T386	10	1.13	7	0.83	8	1.04	8
	Pan-specific	9	0.90	10	0.81	11	0.57	8
	Pan-specific	23	1.09	14	1.33*	5	1.07	20
MEK1/2	S218+S222	17	0.90	23	1.09	18	1.45	16
MEK2	T394	11	1.01	12	0.70	5	0.85	5
	T394	10	1.11	7	0.75	18	1.15	8
	Pan-specific	17	0.86	5	0.83	10	0.70	3
ERK1	T202	16	0.88	19	0.78	40	1.04	36
	T207	21	1.04	10	1.25	34	0.72	28
	Y204	10	0.90	25	0.83	16	0.67	19
	Y204	19	1.44	32	2.91	19	2.11*	31
	Pan-specific	20	1.01	10	0.87	7	0.98	10
	Pan-specific	13	1.05	15	1.07	14	0.82	12
ERK2	T185+Y187	14	1.09	13	1.85*	6	1.42*	14
	Pan-specific	10	1.17	4	1.25	9	1.01	14

* p<0.05

b

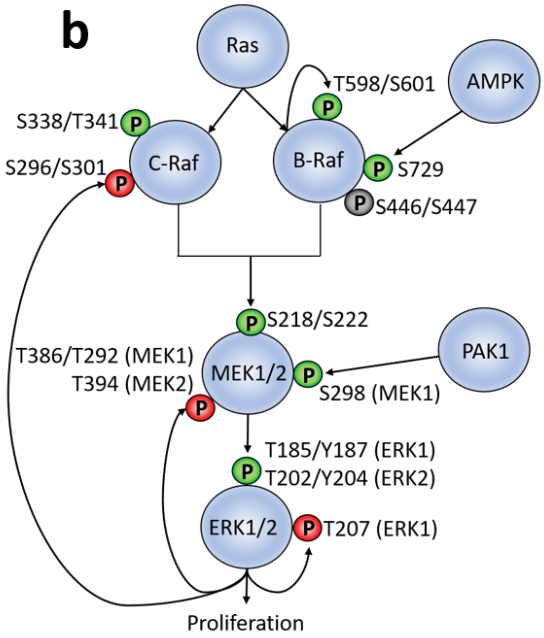

Figure 3.5 – Activation of a MAPK pathway in infected erythrocytes.

a) Summary table of the MAPK pathway components and phosphorylation sites covered by the antibody microarray, including RAF, MEK1/2 and ERK1/2 with the fold change from the uninfected erythrocyte control signal for each of the three time points (erythrocytes in the presence of rings, trophozoites and schizonts) shown. Signals which were significantly different during infection are marked by * ($p<0.05$, unpaired t-test). Phosphosites

underlined in the table were flagged as potentially cross-reactive with parasite material in Fig. 2, but are included here for completeness **b)** Schematic representation of the MAPK pathway with the relevant phosphorylation sites present in the array data set covered in **a**. Green 'P' represents phosphorylation sites associated with the activity of the respective kinase, while the red 'P's represent negative feedback phosphorylation sites. The grey 'P' represents a known priming site on B-Raf.

c-MET signalling in infected erythrocytes. C-MET is expressed in many cells of mesenchymal origins [282, 283], and its activation occurs through the binding of hepatocyte growth factor (HGF) to the extracellular domain, prompting homodimerization and trans-autophosphorylation and activation [208]. C-MET controls several key downstream pathways including (but not limited to) the MAPK pathway (proliferation, motility and cell cycle progression) and the phosphatidylinositol 3-kinase (PI3K)/AKT pathway (cell survival) [207]. There is no homologue of c-MET (or any member of the Tyrosine kinase group) in *P. falciparum* [143].

The array contained a total of eight phospho-specific antibodies targeting c-MET, 7 of which passed cross-reactive and low-intensity signal thresholds (Fig. 3.6a). There was no noteworthy change in the phosphorylation of any of these residues at the ring stage. In contrast, five out of the seven sites show an increase in phosphorylation in the presence of trophozoites (fold change >1.38, Fig. 3.6a). The signals from two antibodies against c-Met phosphorylation sites decreased at the trophozoite stage. One of these is directed against Y1230+Y1234+Y1235; this antibody is affected by high error between duplicates (848% at the trophozoite stage) and was deemed unreliable. The other antibody recognises Y1230 and is the only reliable c-MET antibody to show a decrease of phosphorylation at the trophozoite stage. At the schizont stage, most sites were slightly higher than the uninfected control. Two unique pan-specific c-MET antibodies were also present on the array. Across the three-time points, both pan-specific antibodies showed slight decreases, indicating that the level of c-MET remained relatively constant as expected (Fig 3.6a).

Y1230, Y1234 and Y1235 lie within the c-MET catalytic domain and are phosphorylated in response to binding of HGF, activating the kinase [284]. Antibodies against S975 and T1349+T1356 were not present on the array, or flagged as a low-intensity signal and removed from analysis, respectively. Western blot analysis using the Y1234 + Y1235 antibody and a pan-MET antibody as the loading control confirmed that c-MET is indeed highly phosphorylated in the catalytic domain during trophozoite infection (Fig. 3.6c).

Phosphorylation of c-MET Y1003 peaks at the trophozoite stage, which in nucleated cells signals for the recruitment of c-CBL (casitas B-lineage lymphoma) protein. Recruitment of c-CBL promotes ubiquitination and degradation of c-MET via the 26S proteasome [285, 286]. The activity of the 20S proteasome has been previously reported in mature erythrocytes; in contrast, no 26S activity was observed in these cells [287]. The absence of 26S proteasomal activity in erythrocytes could explain why c-MET protein maintains a steady-state level throughout blood stage parasite development (Fig. 3.6a), despite Y1003 phosphorylation.

a

Phospho Site (Human)	uRBC Error (%)	Ring stage Fold change	Ring stage Error (%)	Trophozoite stage Fold change	Trophozoite stage Error (%)	Schizont stage Fold change	Schizont stage Error (%)
Y1003	11	0.97	13	1.54	5	1.19	8
S1236	14	1.13	6	1.38 *	1	1.06	2
T1241	16	1.06	9	1.72 *	7	1.19	8
Y1234+Y1235	9	1.28	15	1.52 *	6	1.20	5
Y1234+Y1235+S1236	24	0.99	15	1.46	5	0.83	18
Y1230+Y1234+Y1235	26	0.77	954	0.74	848	1.04	7
Y1230	10	0.97	17	0.89	5	1.24	15
Pan-specific	9	0.88	16	0.66 *	3	0.94	10
Pan-specific	7	0.88	8	0.83	7	0.87	16

* p<0.05

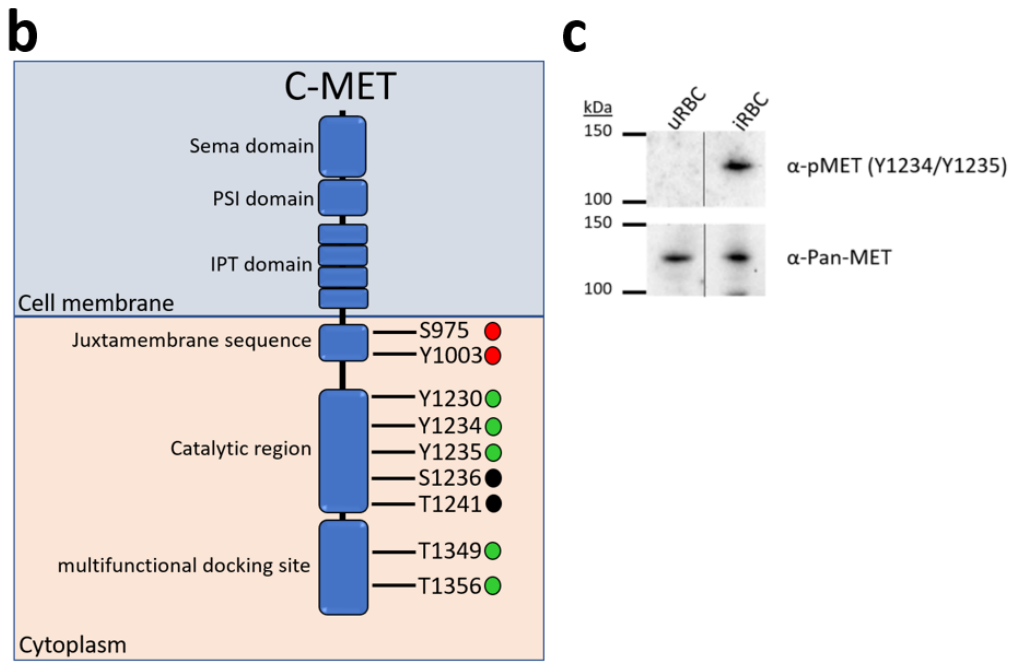

Figure 3.6 – Activation of c-MET in infected erythrocytes.

a) c-MET phosphorylation sites covered by the antibody microarray, with the fold change from uRBC control values for the three-time points (ring, trophozoite and schizont). Signals which were significantly different during infection are marked by * ($p<0.05$, unpaired t-test). **b)** Schematic of the c-MET protein. The juxtamembrane sequence contains both S975 and Y1003, which represent c-CBL binding sites that target the receptor for degradation (red circles) [288, 289]. The catalytic domain contains Y1230, Y1234, Y1235, S1236 and T1241. All activating tyrosine phosphorylations (green circles) occur through receptor homodimerisation [207, 208, 210]. The function of S1236 and T1241 (black circles) is uncharacterised. The multifunctional docking site contains two phosphosites, T1349 and T1356, which aid in the binding of adapter molecules such as grb2 and GAB1 [208]. **c)** Western blot validation of c-MET phosphorylation during trophozoite development. A phospho-specific antibody to c-MET (Y1234+Y1235) detected phosphorylated c-MET in the infected erythrocyte sample (upper panel). A pan-MET antibody detected MET in both the uninfected and infected erythrocyte samples (lower panel).

Small-molecule inhibitors of host kinases identified with the array impair parasite proliferation. We previously published that U0126, a highly selective allosteric inhibitor of MEK1/2, as well as other structurally distinct selective inhibitors of these kinases, display low µM potency against *P. falciparum in vitro* [4]. The findings reported here that several additional human kinases such as c-MET and B-Raf are activated by infection raises the question whether their inhibition would likewise impair parasite proliferation. Several selective inhibitors of c-MET and B-Raf have emerged from the cancer drug discovery pipeline, allowing us to measure the IC_{50} values in parasite proliferation assays of the following inhibitors: Crizotinib (an inhibitor of c-Met and of the related receptor tyrosine kinase ALK [anaplastic lymphoma kinase]); PHA-665752 (a c-MET-selective inhibitor), SB-590885 (a B-Raf selective inhibitor) and Sorafenib (a B-Raf inhibitor which also targets C-Raf, albeit with a 10-fold lower potency) [290] (Fig. 3.7b&c). Despite the absence of B-Raf, c-MET and ALK homologues in the *Plasmodium* kinome, all these inhibitors displayed low nano- to micromolar IC_{50} values against both *P. falciparum* and *P. knowlesi* blood-stage parasite growth (Fig. 3.7a). While we cannot at this stage exclude off-target effects against *Plasmodium* proteins, this, together with the fact that the kinomes of malaria parasites do not include any receptor tyrosine kinase or B-Raf homologues [135], strongly suggests that inhibition of host erythrocyte c-MET, ALK or B-Raf impairs blood-stage parasite proliferation across different human pathogenic *Plasmodium* spp. This in turn suggests that activation of these human kinases by malaria parasites may play an important role in their survival inside erythrocytes.

To determine at which point in the asexual cycle the parasite is susceptible to c-MET and B-Raf inhibition, cultures of *P. falciparum* were highly synchronised to a 0 – 4 hrs post-invasion window of development. Cultures were treated with 5x IC_{50} of SB-590885, Crizotinib, PHA-665752, the frontline antimalarial Artemisinin, or with the merozoite invasion inhibitor heparin. Parasites were monitored via flow cytometry every 12 hr over 84 hrs. The normalised live parasitemia detected for each time point was determined through co-staining with Hoechst 33342 (DNA stain) and Mito-tracker Orange (mitochondrial potential stain). The average values of the biological replicates are represented graphically in Fig. 3.7d. Treatment with Artemisinin resulted in a reduction in live parasitemia at 12-16hpi, indicative of ring stage parasite death. Treatment with heparin caused a drop in live parasitemia post 48hpi, as expected for an invasion inhibitor.

In contrast, the first notable reduction in parasitemia observed after treatment with Crizotinib, PHA-665752 or SB-590885 occurs 24-28hpi. This indicated that all three human kinase inhibitors exert their largest effect on parasite survival at a time that is consistent with the activation time of their target kinases, as revealed by the microarray analysis. Notably, all compounds except heparin resulted in a live parasitemia below 0.2% by 84-88hpi, with SB-590885 and Crizotinib reducing live parasitemia to <0.1%. For an initial assessment of the *in vivo* efficacy of the c-MET inhibitor PHA-665752, we treated mice infected with the rodent malaria parasite *Plasmodium berghei*. A treatment regime and formulation that was previously used to control tumour growth in mice with the same inhibitor [291] led to a marked reduction in parasite proliferation *in vivo* (Fig. 3.7e).

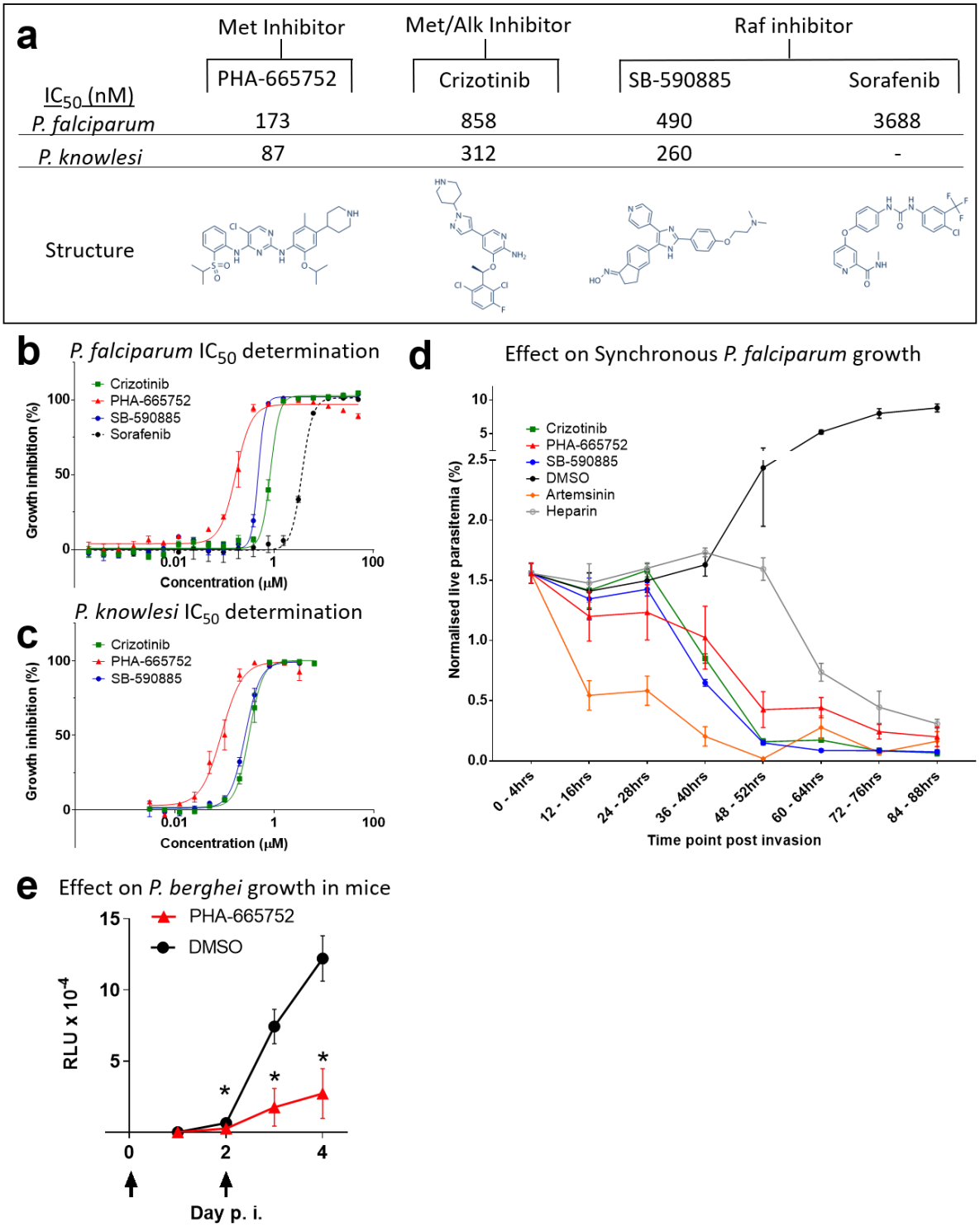

Figure 3.7 – IC_{50} and phenotypic effect of human kinase inhibitors on *P. falciparum* and *P. knowlesi* blood stage development.

a) IC_{50} values of the human kinase inhibitors Crizotinib (MET/ALK inhibitor), PHA-665752 (Met inhibitor), SB-590885 (B-Raf inhibitor) and Sorafenib (B-Raf inhibitor, *P. falciparum* only) on asynchronous *P. falciparum* and ring stage *P. knowlesi* asexual growth. **b)** Growth inhibition curve for asynchronous *P. falciparum*, IC_{50} measured after 72 hrs of compound exposure, n=3, n=2 for sorafenib. **c)** Growth inhibition curve for *P. knowlesi*, IC_{50}s measured after 50 hrs of compound exposure, n=3. **d)** Effect of treatment with 5x the IC_{50} value of the compounds

Crizotinib, PHA-665752, SB-590885, Artemisinin, DMSO (equivalent volume of DMSO in Crizotinib sample) and heparin (15 □l/ml) on highly synchronous (4-hr window) *P. falciparum* cultures over 88 hrs (n=5). The Y-axis represents the normalised live parasitemia values for each time point. Normalisation was achieved by setting the starting total parasitemia at 2% to allow for direct comparison between each biological replicate. All error bars are the standard error of the mean (SEM). **e)** Effect of treating mice with PHA-665752 on the growth of *P. berghei*. Graph shows relative luminescence units (RLU) in the blood of BALB/c mice infected with parasites constitutively expressing firefly luciferase and treated or not with PHA-665752 at 25 mg/kg at the times indicated by arrows. * = $p < 0.001$ by two-tailed *T*-test; n = 7 mice per treatment group.

3.2.4 Concluding remarks

The antibody microarray analysis generated a large number of testable hypotheses on the involvement of host erythrocyte signalling proteins in the process of infection by the human malaria parasite *P. falciparum*. We achieved Western blot validation for three of the host kinases (MEK1 [15], c-Met [this study] and B-Raf [Supplementary Figure 4]) that the array data suggest are activated by infection. In the other infection systems that we characterised through this approach (hepatocyte/hepatitis C virus [250] and mosquito cells/*Wolbachia* endosymbiont [249]) the functional relevance of the most interesting array hits was established through siRNA campaigns. In the erythrocyte/*Plasmodium* system where siRNA-based knock-down of host genes is not feasible, we propose that similar Western blot validation should be undertaken as the first step in further work on any of the numerous enzyme/pathways identified as hits in the array.

The need for further validation notwithstanding, the extent of host erythrocyte signalling modulation by *Plasmodium* infection is surprising. The array data are consistent with earlier observations implicating some of the host cell signalling pathways in the infection process, and allowing a significantly deeper and more specific understanding of the mobilisation of such pathways (for example, see above the section pertaining to PKC isoforms).

A major long-term objective of this research is the identification of antimalarial compounds with untapped modes of action. It is a clear possibility that part of the signalling response of the erythrocyte to infection may be directed towards activating innate immune defence mechanisms, and thus downregulating such responses would be undesirable. However, based on the notion that at least some of the signalling events triggered in the host cell by infection are required by the parasite for its survival, we tested highly selective inhibitors against some of the activated kinases and showed that some of these compounds have high potency (in the low nM range) in *in vitro* culture systems. The nanomolar activity against both *P. falciparum*

and the phylogenetically distant *P. knowlesi* for c-Met and B-Raf inhibitors indicate that the reliance on the activation of host erythrocyte pathways spans various *Plasmodium* species. Importantly, the drastically impaired proliferation of *P. berghei* in a murine malaria model treated with the c-Met inhibitor PHA-665752 shows that targeting host kinases to control malaria infection *in vivo* is achievable, strengthening the case for kinase-focussed host-targeted intervention.

Major attractive features of targeting host-cell kinases as a strategy to develop novel antimalarials are threefold: First is the effectiveness of specific inhibitors across phylogenetically distant *Plasmodium* species, illustrated by the facts (i) that inhibitors against three host cell kinases activated by infection (MEK1, c-Met and B-Raf) display similar *in vitro* potency on *P. falciparum* and *P. knowlesi*, and (ii) that MEK and c-Met inhibitors also have activity against the *P. berghei* rodent malaria parasite *ex vivo* (MEK [4]) and *in vivo* (c-MET). A second tremendous advantage of this strategy is that the most parsimonious pathway to resistance, i.e. the selection under drug pressure of genotypes encoding a mutated target with decreased susceptibility, is not possible if the target is encoded by the host. Third, large kinase-directed compound libraries are available from the intensive efforts made over the past two decades in the context of cancer chemotherapy (including inhibitors of many of the kinases identified in this study as being activated in infected erythrocytes), providing a unique repository of potential antimalarials. These can now be exploited as a basis for fundamental research into host-parasite interactions, and as leads for the development of novel antimalarials with untapped modes of actions.

3.2.5 Methods

Plasmodium spp. culture and life stage synchronisation

Human erythrocytes were supplied by the Australian Red Cross. *P. falciparum* (clone 3D7) and *P. knowlesi* (YH1) were grown in human erythrocytes as previously described [242, 292-294]. *P. falciparum* synchronisation (4-hr window) was achieved using 5% w/v Sorbitol as well as 150 µl/10ml culture of heparin [295]. Both techniques were utilised for the trophozoite and schizont stages, whereas an 8-hr synchronisation window was achieved through sorbitol alone for the ring stage. Purification of *P. falciparum* trophozoite and schizont-infected cells was achieved using a super-MACS column [296]. *P. knowlesi* cultures for *in vitro* assays were partially synchronised (~12-hr age range) using heparin [293].

IC_{50} determination

P. falciparum – The IC_{50} values of Crizotinib, PHA-665752, SB590885, Sorafenib and Artemisinin were determined with asynchronous cultures with a starting parasitemia of 0.25% in 2% haematocrit. Cultures were incubated with the compounds for 72 hrs before adding SYBR-gold nucleic acid stain (1:10000 dilution) (ThermoFisher Scientific) modified from [297] substituting SYBR-green for SYBR-gold. Plates were incubated with SYBR-gold for 1 hr in the dark prior to reading fluorescence on a Tecan plate reader (I-control software), and the inhibitory IC_{50} determined using GraphPad PRISM (GraphPad software).

P. knowlesi – *P. knowlesi* growth inhibition assays using ring stage parasites were set up at 1% parasitaemia and 1% haematocrit in 96-well round-bottom plates at a final volume of 45 µL as described [298, 299]. A 10x final concentration of drug and controls was added to make the final volume to 50 µL and the drug assay cultured for 50 hrs until parasites reached late trophozoites in the next growth cycle. Assays were stained with 10 µg/mL ethidium bromide (EtBr, Bio-Rad) for 1hr and washed prior to flow cytometry (Becton Dickinson LSR) assessment of parasitaemia with gating as per established protocols [300]. Parasitaemia counts were quantitated using FlowJo software (Tree Star) and the inhibitory IC_{50} determined using GraphPad PRISM (GraphPad Software).

Kinexus antibody microarray preparation

The Kinex 900P array kits were purchased from Kinexus. Protein extracts were prepared as per the manufacturer's instruction. Each array was, unless otherwise specified, loaded with protein extracts normalized to equivalent cell number. Array scanning was conducted by the manufacturer at their facility. Arrays were loaded with protein extracts of rings 4-12 hrs (approximately 33% parasitemia) (n=3), trophozoites 24-28 hrs (magnet purified)(n=3) and schizonts 44-48 hrs (magnet purified) (n=2). In order to identify phosphosites of malaria proteins cross-reactive to the array, saponin pellets and supernatants of magnet purified, saponin lysed trophozoites/schizonts were compared. Saponin pellet samples were loaded at 2 mg/ml on the array, 20x more pellet material than is present in 2 mg/ml of equivalent saponin supernatant material.

Western blotting

Western blot analysis of infected and uninfected erythrocytic material performed on protein extracts prepared by resuspending cells in M-PER mammalian protein extraction reagent (Pierce) supplemented with 1x protease inhibitory cocktail (EDTA free) (Roche), 300 mM benzamidine, 200 mM phenylmethylsulfonyl fluoride, 500 mM sodium fluoride, 100 mM sodium orthovanadate and 500 mM β-glycerophosphate. Lysates were cleared by centrifugation (10,000 g for 15 mins at 4°C); samples were boiled in Laemmli reducing sample buffer before separation on 4-12% Tris/Bis gradient SDS-PAGE gels (Invitrogen). After electrophoresis, proteins were transferred to nitrocellulose membrane (Amersham) previously blocked (1-hr room temperature) with 5% Skim milk (Diploma) in Tris-buffered saline containing 0.05% Tween 20 (TBST). Immunoblotting was performed using the following antibodies; phosphorylated c-MET (Y1234/Y1235; D26, Cell Signalling Technologies) at 1:500 dilution; pan c-MET (D1C2, Cell Signalling Technologies) at 1:500 dilution. All primary antibodies incubated overnight at 4°C. Anti-Rabbit/Mouse-horseradish peroxidase-conjugated secondary antibody was used for all experiments at 1:5000 dilution (Monoclonal antibody facility Monash University Clayton, Vic, Australia).

Time-dependent inhibitor treatment of parasites monitored via flow cytometry

Highly synchronous cultures (0 - 4 hrs post-invasion) at 2% haematocrit treated with DMSO (vehicle), Crizotinib, PHA-665752, SB-590885 or artemisinin at 5x the IC_{50} values were monitored at 12-hr time intervals over two full asexual intra-erythrocytic cycles (84 hrs) by flow cytometry. Live parasitaemia was quantitated by a dual-colour flow cytometry staining protocol using 2 μM Hoechst-33342 staining for 8 minutes and 75 nM MitoTracker Orange for 25 minutes. Staining was completed in v-bottom plates with two washes in complete RPMI. Stained cells were transferred to polypropylene tubes and diluted one in four in complete RPMI. Cells were then immediately analysed on an LSR BDFortessa^{TM} with the laser UV379 and filter 450/50 for Hoechst-33242 staining, and laser YG585 with filter 585/15 for MitoTracker Orange staining. Flow rate was maintained at <10 000 events/second, and voltages were kept consistent at 320 V and 450 V for Hoechst-33342 and MitoTracker Orange staining respectively. Biological replicates (n=5) were normalised to a 2% total parasitemia value at the first-time point (0 – 4 hrs post invasion). A full description of this method will be published elsewhere.

P. berghei in vivo drug treatment assay

Assays were performed as described [301], using the reporter parasite line PbGFPLuc$_{con}$ (RMgm-29 in the rodent malaria genetic modification database, http://www.pberghei.eu/index.php?rmgm=29), which expresses a GFP-firefly luciferase fusion protein under the control of the constitutive *eef1a* promoter [302]. Briefly, seven female, 10-week-old BALB/c mice per treatment group were infected by i.v. inoculation with 10^6 infected erythrocytes. Treatment with PHA-665752 or solvent control was 3hr thereafter and on day 2 post infection by i.p. injection of 25 mg/kg/day of PHA-665752. The drug was prepared fresh by diluting a stock of 50 mg PHA-665752 in 0.5 ml DMSO (w/v) in water (1:40, v/v). The same drug formulation and treatment regime had proved effective in controlling carcinoma growth [291].

Data Availability Statement

All raw data pertaining to this study are available in Supplemental Datasets 1 to 3.

Acknowledgements

We thank Dr Kylie Quinn for lending her Flow Cytometry expertise and the staff of Monash FlowCore Facility, in particular Andrew Fryga and Adam Dinsdale, for their continued experimental assistance. We also thank Prof Roger Daly, Dr. Teresa Carvalho, A/Prof Jose Garcia-Bustos and Prof Brian Cooke for fruitful discussions. This work was supported by the Australian Government National Health and Medical Research Council (Project Grants APP1082619 [CD] and APP1143974 [DW]), Australian Research Council PhD Scholarship (AB) and internal support from Monash University and the University of Adelaide, including a Beacon Fellowship (DW).

3.2.6 Supplementary Figures and Datasets

Supplementary Dataset 1 to 3 have been made available via dropbox due to their size - https://www.dropbox.com/sh/0zklb3n5teh63wr/AAC-tEaydkWGvY98MTVvdfcLa?dl=0

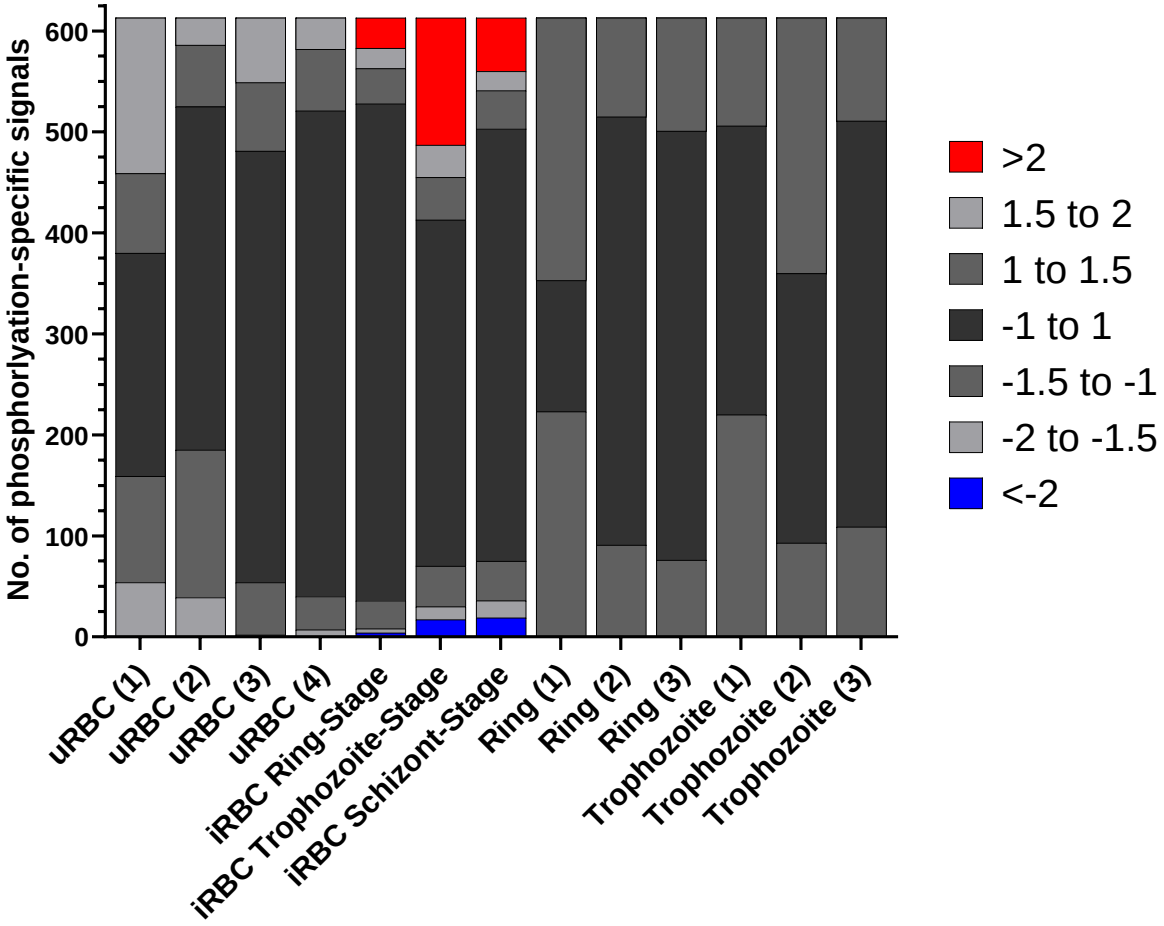

Supplementary Figure 1 – Distribution of Z-scores for each sample. All microarray signals from each sample (four from uRBCs and the mean signal for each iRBC harbouring parasites at the ring (n=3), trophozoite (n=3) and schizont stage (n=2)) were compared to the uninfected erythrocyte mean for each signal and internally for each of the iRBC stages, and the Z-score determined for each phosphorylation-specific signal. The Z-score is defined as the number of standard deviations from the uRBC mean for each sample; a positive or negative value indicates the direction of the signal (increase or decrease, respectively) from the uRBC, or iRBC stage mean. No signals from the uRBC samples (n=4) had associated Z-scores above 2 or below -2, while the three iRBC time points showed clear variations from uRBCs. Internally the iRBC samples also showed low variation as there were no Z-scores above 2 or below -2 from the iRBC stage mean. Schizont stage Z-scores not determined as n=2.

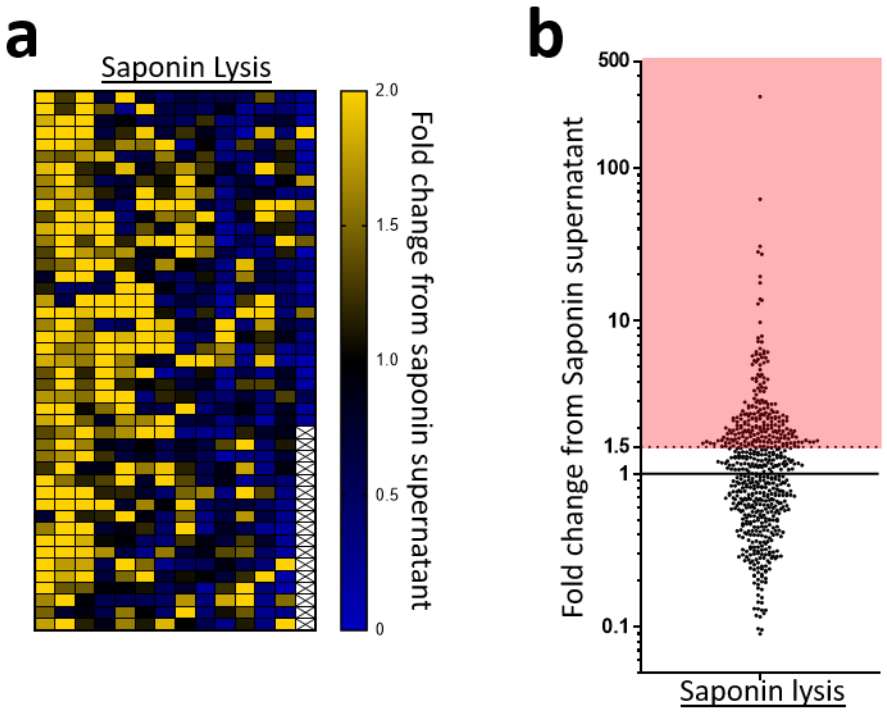

Supplementary Figure 2 – Summary information for the saponin lysis comparison array. a) Heatmap of the 613 phosphorylation-specific signals on the antibody microarray. Each pixel represents a single antibody, were the colour represents the fold change difference between the saponin supernatant (erythrocyte cytoplasm) and the saponin pellet (parasite material). Yellow pixels indicate that the signal was stronger in the saponin pellet material, indicating likely cross-reactivity of the corresponding antibody. **b)** Dot plot of the phosphorylation-specific signals on the saponin lysis comparison array, the red region indicates the signals removed due to potential cross-reactivity (signals above a fold change of 1.5).

		uRBC	Ring stage		Trophozoite stage		Schizont stage	
Protein	Phospho Site (Human)	Error (%)	Fold change	Error (%)	Fold change	Error (%)	Fold change	Error (%)
PKCd	Y313	18	0.89	11	0.86	6	1.46	2
	Y313	6	0.90	12	0.82	10	1.37	7
	Y313	5	0.88	6	1.19	17	1.20	12
	S645	8	0.79	18	1.11	10	1.17	11
	S664	28	0.68	16	0.55	65	0.93	26
	T507	9	1.05	12	1.96*	9	2.05*	20
	Pan-specific	16	0.91	15	1.59	14	1.53*	13
PKCq	S676	25	0.73	8	0.87	8	0.80	15
	S695	30	1.00	23	1.90*	29	1.43*	21
	S695	15	0.86	13	1.59*	5	1.49	12
	Y545	5	1.08	6	1.80*	11	1.47	3

* p<0.05

Supplementary Figure 3 - Summary of the antibody microarray signals for the PKC isoforms delta and gamma and theta, that were not flagged as cross-reactivity or low signal intensity. Fold change indicates the fold change from the uRBC control, yellow = increase, blue = decrease. * indicates which of the fold changes were noted as significant changes ($p<0.05$, unpaired t-test).

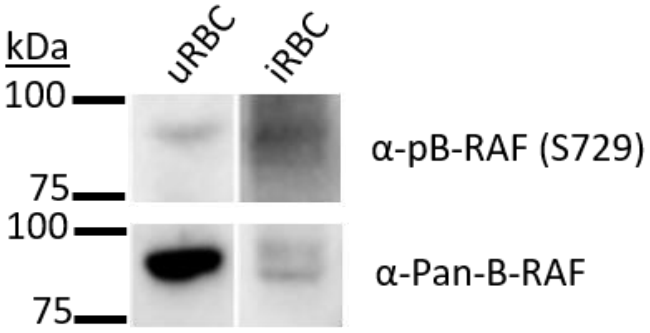

Supplementary Figure 4 - Western blot validation of B-Raf phosphorylation during trophozoite development. A phospho-specific antibody to B-Raf (S729) detected phosphorylated B-Raf in the infected erythrocyte sample (upper panel). A pan-Braf antibody detected B-Raf in both the uninfected and infected erythrocyte samples (lower panel).

3.3 Human erythrocyte signalling during intracellular infection with *P. falciparum* gametocytes

To extend and complement the data of host-signalling during the asexual development of *P. falciparum* (Chapter 3.2), we completed two further array analyses on erythrocytes harbouring the sexual stages of *P. falciparum* development. We aimed at (i) comparing gametocyte-infected to uninfected erythrocytes and (ii) comparing erythrocytes infected with males versus females gametocytes, to identify possible sex-dependent differences in host erythrocyte signalling. Previous studies with *P. berghei* have illustrated that transcription varies quite significantly between gametocyte types [303]. Therefore, we hypothesised that though we expect that some aspects of host signalling would be similar between male- and female-infected erythrocytes, there would also be pathways or phosphorylation that would be unique to either population [303-305].

The arrays completed on *P. falciparum* gametocytes compared uninfected erythrocytes to purified erythrocytes harbouring stage IV male and female *P. falciparum* gametocytes; male and female gametocytes were analysed separately. We used Stage IV gametocytes as they are the most mature form of gametocytes that are not highly sensitive to temperature fluctuations [304, 306]. The mosquito-infective stage V gametocytes are highly sensitive to reductions in temperature, as these trigger gamete development within the mosquito [304]. Handling stage V gametocytes could have thus resulted in the activation of pathways linked to the initiation of sexual development, which would have confounded our analysis.

Development of synchronised gametocytes is a difficult endeavour, which produces relatively small yields. To generate the material required to complete an antibody microarray on male and female gametocytes, we collaborated with Associate Professor Alex Maier at the Australian National University in Canberra, Australia, as his lab has expertise in generating and purifying gametocytes in the required numbers. I travelled to Canberra to perform the array analysis on the samples prepared by A/Prof Maier and his team. To allow direct comparison across the sexual and asexual datasets, we will compare here the uninfected erythrocyte mean from Chapter 3.2 (n=3) to the gametocyte stages. Note Chapter 3.2 has been updated to contain four biological replicates of uninfected erythrocytes, as well as biological replicates for all of the asexual time points tested. The analyses presented here in Chapter 3.3, as well as Chapter 4, were performed prior to the completion of these biological replicates.

Mature human erythrocytes are e-nucleated and consequently unable to express proteins during infection with *P. falciparum*. Therefore, we focused our gametocyte analysis not on protein levels, but on the 613 different phosphorylation-specific antibodies present on the array, represented as a heatmap here (Figure 3.8). Each phosphorylation-specific signal on the array is represented by a pixel, with the colour representing the change during infection (yellow = increase, blue = decrease). As stated above, we compared the uninfected erythrocyte mean signal (n=3) to the signals from the samples of purified male and female gametocytes. Both heatmaps of the gametocyte data illustrate that there are numerous changes to host signalling protein phosphorylation during parasite sexual development. Notably, the changes observed here are comparable to the asexual stages of parasite development discussed in Chapter 3.2. Between the two gametocyte samples, it is also apparent that there are more yellow pixels in the sample of female gametocytes, which indicates higher overall levels of phosphorylation.

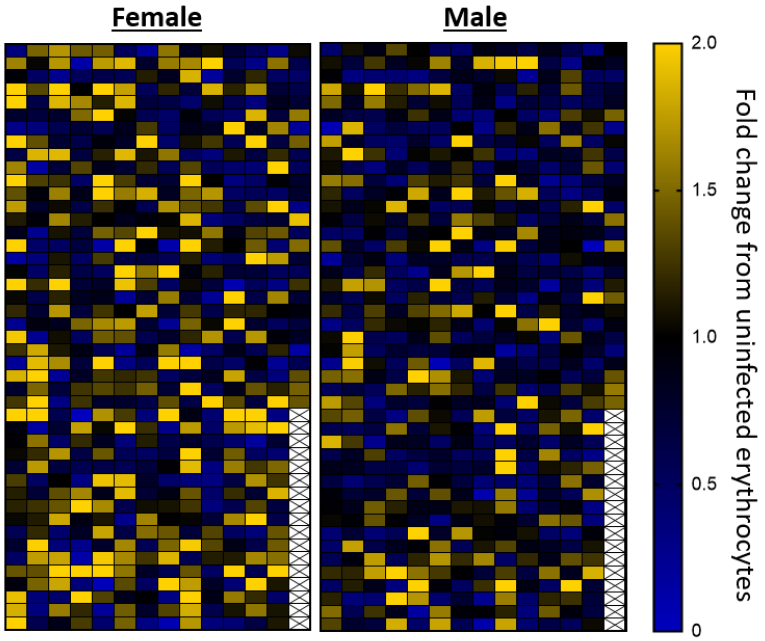

Figure 3.8 – Heatmap of antibody microarray data representing the changes in erythrocyte phosphorylation during infection with *P. falciparum* gametocytes.

Data compare lysates of uninfected human erythrocytes with lysates of human erythrocytes harbouring stage IV female (left) and male (right) gametocytes. Each pixel represents the fold change recorded from the uninfected erythrocyte mean value (n=3) compared to the mean of the technical duplicate antibodies in the male and female infected erythrocyte samples (n=1), respectively. Colourisation represents the following; Blue pixels indicate a fold change of less than one from the control; yellow pixels indicate a fold change greater than one in comparison to the uninfected erythrocyte control.

In line with the analysis of asexual stage signals discussed in section 3.2, we removed signals from the gametocyte datasets that were shown to cross-react with parasite proteins, as well as signals that were of low signal intensity, as they were highly variable and unreliable (for further explanation of the signal removal process see section 3.2). One limitation of applying the cross-reactivity (saponin array) from section 3.2 is that it was performed on the asexual stages of *P. falciparum* development. Consequently, proteins specific to male or female gametocytes could potentially cross-react with the antibodies on this array. Therefore, some of the signals which were not flagged as cross-reactive could still be so. A microarray comparing purified gametocytes against the infected host cell could eliminate this problem; however, completion of such an array was cost-prohibitive at the time of this study. The complete list of signals, along with the signals flagged as cross-reactive and those with low-intensity are available in Appendix 1.

The criteria mentioned above reduced the 613 initial signals to 342 (male) and 350 (female), listed in Figure 3.9b. We have represented the remaining signals as a dot plot, noting the several signals outside the main signal concentration around a fold change of 1. These signals were for the male gametocytes; intestinal cell kinase (ICK) (Tyr159), protein-tyrosine phosphatase 1D (PTP1D) (S580), Tau (S713) and MET (Y1230+Y1234+Y1235) and for the female gametocytes; mothers against decapentaplegic homologs 1 (Smad1) (S465), retinoblastoma-associated protein 1 (RB) (S780) PAK1/2/3 (S144/S141/S154), ICK (Y159) and Paxillin 1 (Y31). C-MET was covered in detail in section 3.2 due to increased phosphorylation on several sites, particularly at the trophozoite stage of development. C-MET will be further discussed in the context of gametocyte development later in this section. Decreased phosphorylation of Tau is noteworthy in the context of all Apicomplexan parasites used in this study; discussion of Tau phosphorylation will be covered in Chapter 4.4.5. ICK is a MAP-like kinase, which belongs to the *v-ros* cross-hybridising kinase (RCK) serine-threonine kinases. ICK is ubiquitously expressed in nucleated cells and has a role in promoting G1 cell cycle proliferation [307, 308]. Phosphorylation of Tyr159 is a marker of basal ICK activity achieved through autophosphorylation [308, 309]. Rb is involved in the checkpoint between G1 and S-phase, often referred to as tumour suppressor protein [310]. The phosphorylation site Ser780 is associated with activation and belongs to the highly phosphorylated region of the protein. There are a number of proteins, including Aurora B and p38 MAPK that can phosphorylate, and activate Rb at this site [311, 312].

Representing the data as a dot plot (Figure 3.9a) also enables us to put into perspective the largest fold changes observed, and provide visualisation of the global signal distribution and median (median noted in red). Interestingly, the median of the two datasets is quite different (male = 0.97, female = 1.205), despite these parasites being at equal stages of development. This could suggest a larger role for host cell signalling in female gametocytes. We also compared the number of signals above a fold change of 2 or below 0.5 from the uninfected control. For male gametocytes, there was a total of 57 signals that met this criterion, of which 22 had fold changes above 2. For the female gametocytes, there were a total of 81 signals that met our criteria, of which 44 had fold changes above 2. Compared to the asexual stages, the female gametocyte dataset has 38% more signals in these categories. This further indicates that of the arrays completed on *P. falciparum*, stage IV female gametocyte resulted in the highest level of perturbation to the host erythrocyte phosphorylation signalling.

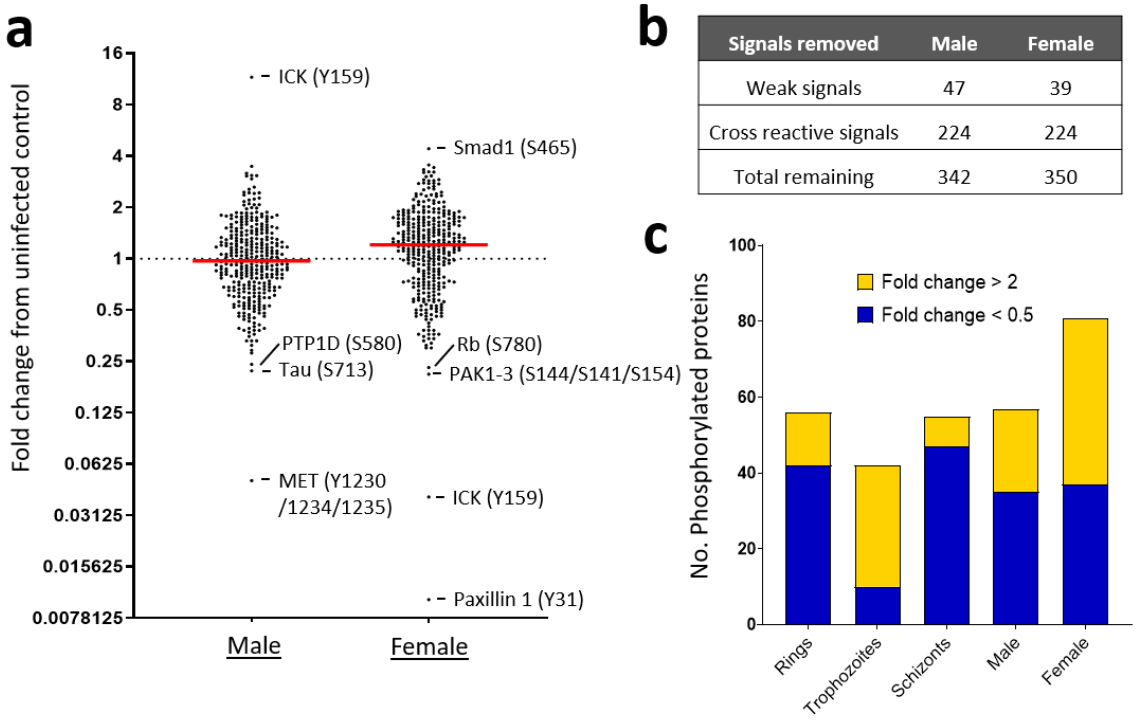

Figure 3.9 – **Gametocyte signal distribution following the identification of (i) cross-reactive antibodies and (ii) low-intensity signals.**

a) dot plot of phosphorylation-specific signals for the male and female gametocyte datasets, following removal of cross-reactive and low-intensity signals. Median signal for each dataset is represented in red (male = 0.97, female = 1.205). Outliers are listed with their associated phosphorylation site. **b)** A summary table indicating the numbers of antibodies removed from analysis due to cross-reactivity with parasite proteins, or signals which were below an intensity threshold of 1000-fluorescence units in both the erythrocyte control and parasite-infected samples. **c)** the remaining phosphorylation-specific signals ranked according to fold change. Included here is the asexual stage dataset for comparison. Yellow represents changes with a fold change greater than 2; blue represents changes with a fold change less than 0.5.

3.3.1 Identification of the most significant changes in erythrocyte signalling during infection with male and female gametocytes

The remaining 342 (male) and 350 (female) phosphorylation-specific signals from the male and female gametocytes analysis were further assessed to determine which signals were significantly different from the uninfected erythrocyte control. We designated all signals outside two standard deviations from the erythrocyte mean as significant (p=0.05). For the female gametocyte dataset, this identified 139 signals, which made up approximately 40% of the remaining signals at this stage of the analysis. Due to the large number of signals that were noted as significant, we further shortlisted signals that had fold changes above 2 or below 0.5 as these represent the largest changes in the dataset. From this list, we further filtered out all signals based on the associated error value from the technical duplicates (each antibody is represented twice on each chamber of the array). We removed all signals which had associated error values above 25% in either the infected or uninfected sample. This reduced the listed signals to 32 (female gametocytes) and 19 (male gametocytes) (Table 3.1). The complete list of signals identified as significantly different from the uninfected erythrocyte control are available in Appendix 2. Interestingly, there are numerous signals present in both of the shortlisted tables, which indicated that there are a number of similarities in host erythrocyte signalling during male and female gametocyte infection (noted by the red arrows). In fact, a comparison of the complete list of significant changes during gametocyte development identified 67 signals present in both tables. This represented approximately 50% of all signals in the female gametocyte table and 70% of the signals in the male gametocyte table, many of which had very similar fold change values. This further illustrates that there are numerous similarities in erythrocyte signalling during infection with gametocytes regardless of sex.

Female

Protein	Phospho Site (Human)	Fold change
Smad1	S465	4.41
B-Raf	S729	3.54
JAK3	Y980+Y981	3.42
ErbB3	Y1289	3.32
GSK3a	T19+S21	3.23
IRAK4	T345+S346	3.22
IKKe	S172	3.20
NDR1	S281+T282	3.06
EGFR	Y869	2.90
GIT1	Y545	2.87
MEK5	S311	2.86
IR	Y1189	2.78
LOK	S191	2.77
ERK1	Y204	2.76
ERK2	T185+Y187	2.74
ACK1	Y284	2.65
EIF2AK3	T982	2.60
FLT3	Y842	2.56
EphA1	Y781	2.45
FAK	Y397	2.40
PAK4	S474	2.39
PDK1	S241	2.37
GSK3a	S278+Y279	2.33
Aurora B	S227	2.32
TNK1	Y277	2.19
LTK	Y672	2.15
p38a MAPK	T180+Y182	2.14
YSK1	T174	2.07
PDLIM5	Y251	2.04
DDR2	Y736	2.02
p38b MAPK	T180+Y182	2.01
PKCd	S664	0.36

Male

Protein	Phospho Site (Human)	Fold change
ErbB3	Y1289	3.48
IRAK4	T345+S346	3.17
CDK2	T160	3.08
B-Raf	S729	3.07
ACK1	Y284	3.05
IKKa	T179+S180	2.94
MKK3	S218	2.55
LOK	S191	2.45
CDKL5	Y171	2.43
GIT1	Y545	2.43
Smad1	S465	2.36
PECAM-1	Y713	2.27
PGK1	Y196	2.24
ErbB2	Y1248	2.21
EIF2AK3	T982	2.07
GSK3a	T19+S21	2.07
Aurora B	S227	2.06
Paxillin 1	Y31	0.33
MET	Y1230+Y1234+Y1235	0.05

Table 3.1 – Shortlist of the highest confidence signals for male and female gametocytes.

Increases marked in yellow, decreases are marked in blue. All values listed are the fold change from the uninfected erythrocyte control mean (n=3). The red arrows indicate signals which are present in both lists. Each signal was outside two standard deviations of the uninfected erythrocyte mean. Each signal listed has a duplicate error value below 25% from the infected erythrocyte signal and below 25% from the mean error of the uninfected erythrocyte control, and the signals listed were not flagged as cross-reactive or low intensity.

The high level of similarity observed between the significant signals of the male and female gametocyte datasets further prompted us to compare these signals to the list of significant signals from the asexual analysis in section 3.2 (full signals lists available in Supplementary Figure 4 and Appendix 2). This comparison netted 11 different proteins, which included the previously discussed, B-Raf and ERK2 of the MAPK pathway as well as Tau, mentioned earlier in this section (Table 3.2). The only other proteins to show consistent phosphorylation across all five of the *P. falciparum* datasets were the epithelial discoidin domain-containing receptor 1 and 2 (DDR1/2). DDR1/2 are RTKs; however, they are not activated by growth factors like the rest of this family; instead, they are activated through the binding of collagen [313]. Interestingly, again, unlike other RTKs that activate in minutes following ligand binding, collagen-binding to DDR1/2 results in maximal activation hours after initial stimulation [313]. This, in part, could be due to the requirement of DDR1/2 to be phosphorylated in the intracellular domain by Src [314]. Src is responsible for the phosphorylation of DDR1/2 at Y736 and Y740 following receptor-ligand binding, which enables autophosphorylation of DDR2 across multiple tyrosine residues [314]. Two other phosphorylation sites for DDR1 were listed in Table 3.2 (Y796+Y797), and are believed to be involved in Src activation [315]. DDR1/2 are expressed across most cell types with functions and downstream signalling found to be tissue-specific [313]. Generally, the functions of DDR1/2 in adults cells are not well characterised; however, it is believed that they have roles in tissue homeostasis and regeneration [316]. To date, no proteomics-based analysis has identified DDR1/2 in erythrocytes. Therefore the role and function of these RTKs in erythrocytes is unknown. Interestingly, c-MET activity has been suggested to cause the phosphorylation of DDR; however, further validation of this interaction is required [317].

		uRBC	Ring		Trophozoite		Schizont		Female		Male	
Protein	Phospho Site (Human)	Error%	Fold change	%Error	Fold change	%Error	Fold change	%Error	Fold change	%Error	Fold change	%Error
AcCoA carboxylase	S80	7	1.43	9	1.22	6.2	0.54	4	1.56	9	1.65	1
B-Raf	S729	27	2.20	96	2.57	12.9	2.39	15	3.54	5	3.07	13
CHK1	S317	23	1.36	8	1.23	0.4	0.60	12	1.39	12	1.29	5
DDR1	Y796+Y797	12	2.27	8	N/S		N/S		1.85	14	1.46	27
DDR2	Y736	14	1.59	11	N/S		1.68	29	2.02	12	N/S	
DDR2	Y740	9	1.38	18	1.45	17.0	1.79	22	1.91	3	N/S	
ERK2	T185+Y187	16	1.27	12	2.18	3.3	1.61	5	2.74	2	1.99	2
Huntingtin	S421	27	1.27	17	0.86	23.1	0.59	9	1.21	2	0.77	6
KHS1	S174	30	0.85	6	1.15	5.6	0.55	1	1.53	12	1.25	3
LMR2	S1450	8	0.82	23	1.62	19.0	0.71	3	1.58	5	1.47	0
MAPKAPK2	T222	16	1.29	8	1.98	12.4	0.40	9	2.40	6	1.80	29
PIK3R2	Y464	9	1.28	2	1.16	14.7	0.63	3	1.11	10	0.53	5
Tau	S713	81	0.32	53	0.73	0.2	0.70	2	0.33	51	0.39	45

Table 3.2 – List of significant signals common to all five *P. falciparum* array datasets.

Increases marked in yellow, decreases are marked in blue. All values listed are the fold change from the uninfected erythrocyte control mean (n=3). Each signal was outside two standard deviations of the uninfected erythrocyte mean and had a duplicate error value below 25% from the infected erythrocyte signal and below 25% from the mean error of the uninfected erythrocyte control. The signals listed were; not flagged as cross-reactive or low intensity.

C-Met phosphorylation during *P. falciparum* sexual development

The prominence of the RTK c-MET during *P. falciparum* asexual development indicated further comparison to the sexual stages of the parasite was warranted. Interestingly c-MET was present in Figure 3.8 and Table 3.3; however, in both circumstances, it was observed to be phosphorylated significantly less on Y1230+Y1234+Y1235 in erythrocytes infected male gametocytes, compared to uninfected erythrocytes. This was contrary to what was seen for the asexual stages of *P. falciparum* development, as higher levels of phosphorylation were observed at this site (section 3.2). We compiled the c-MET signals for the female and male gametocyte datasets, in a similar manner to Figure 3.5 in Section 3.2 (Table 3.3). Overall c-Met appears to be more phosphorylated in both the female and male gametocytes; however, one of the triplicate phosphorylation recognising antibodies (Y1230+Y1234+Y1235) indicated lower levels of phosphorylation in both samples. The signal for this site, in the female dataset could be the result of the high duplicate error (1515%) associated with this signal; yet, this is not the case for the male dataset. As this site is the only inconsistency in the overall phosphorylation status of c-MET in both the male and female datasets, this antibody may not have performed as expected in these arrays. Further verification of this antibody in the uninfected erythrocyte replicate performed at the time of the gametocyte arrays also noted the duplicate error of 1592%. Together this indicates a technical issue with the duplicate spots for

the MET (Y1230+Y1234+Y1235) antibody on this particular array (such error was not observed in the experiments on asexual parasites). Note high levels of error were not detected for the other c-MET listed signals, suggesting these antibodies were unaffected. We looked further into this uninfected erythrocyte signal set to identify other antibodies that did not perform well. This identified four other signals not flagged as cross-reactive or of low signal intensity, which had duplicate error values over 100%. These signals were ICK Y159 (8041% error), FRS2 Y348 (1643% error), EGFR T693 (367% error) and MYOD S200 (159% error). This antibody spot problem, therefore, explains the inconsistency seen on Y1230+Y1234+Y1235. Excluding this signal, c-MET does appear to be more phosphorylated during sexual stages of parasite development tested here. However, whether c-MET phosphorylation is elevated through the earlier I-III stages of gametocyte development remains to be shown.

	uRBC mean	Female		Male	
Phospho Site (Human)	%Error	Fold change	%Error	Fold change	%Error
S1236	17	1.51*	21	1.65*	16
T1241	15	1.85*	7	1.16	16
Y1003	11	1.28	30	0.99	6
Y1230	6	1.19	14	1.68*	12
Y1230+Y1234+Y1235	25	0.31	1515	0.05*	8
Y1234+Y1235	9	1.38	12	1.37	8
Y1234+Y1235+S1236	24	1.74*	11	1.17	3
Pan-specific	9	0.92	3	1.18	2
Pan-specific	7	0.96	1	1.05	10

* Signals outside of 2x standard deviation of uRBC mean

Table 3.3 – Phosphorylation status of c-MET during male and female gametocyte development.

Increases marked in yellow, decreases are marked in blue. All values listed are the fold change from the uninfected erythrocyte control mean (n=3). Signals marked by * were outside two standard deviations of the uninfected erythrocyte mean (p=0.5). The signals listed were; not flagged as cross-reactive or low intensity.

MAPK pathway phosphorylation during *P. falciparum* sexual development

The traditional MAPK pathway (RAF, MEK1/2 and ERK1/2) was discussed in section 3.2 of this chapter, due to the increased level of phosphorylation seen across the three tiers of the pathway. Briefly, section 3.2 noted increased levels of phosphorylation at all three tiers of the pathway during ring stage development, while the trophozoite stage displayed only increased phosphorylation of B-Raf at S729 and ERK at T185+Y187, and the schizont stage showed increased phosphorylation of B-Raf at S729, MEK1 on multiple sites and ERK at T185+Y187. This was in line with a previous study which demonstrated MEK1/2 activity in the later stages of *P. falciparum* asexual development [4]. Together the activity of the MAPK pathway at ring stage development, then again later at the schizont stage of development may reflect two independent roles of this pathway during *P. falciparum* asexual development.

To assess the relevance of this MAPK pathway during Stage IV gametocyte development, we isolated these signals from the dataset (Table 3.4). At the first tier of this MAPK pathway (B-Raf/C-Raf), we only observed an increase in phosphorylation of B-Raf at S729 (fold changes >3), which was consistent for erythrocytes infected with both the male and female gametocytes. The S446+S447 phosphorylation site of B-Raf, which was prominent in the ring stage data, displayed a reduction in phosphorylation in both male and female gametocyte datasets here. We also noted that similarly to the asexual stages, there was an increased signal for the pan-specific B-Raf antibody (fold changes >2.5). As discussed in section 3.2, the fluctuations of the B-Raf pan-specific signal cannot be due to increased expression of B-Raf, as erythrocytes do not expression proteins. Therefore, as this signal was not flagged as cross-reactive to parasite material, the abundance change detected here could be due to differential extractability, possibly as a result of differential localisation or recruitment to subcellular structures (and hence differential extractability) in infected versus non-infected cells. The female gametocyte data also indicated a slight increase in phosphorylation for S296 of C-Raf (fold change = 1.32), which was not reflected in the male gametocyte data. Together, the Raf data here most closely resembles what was observed in the trophozoite/schizont stages of asexual development, suggesting a conserved signalling function for B-Raf across the entirety of blood-stage development.

The second tier of this MAPK pathway (MEK1/2) was notably phosphorylated during asexual development with rings and schizont stage parasites. Interestingly, all of the phosphorylation sites listed in Table 3.4 indicate lower levels of phosphorylation during parasite sexual development. This was similar to what was observed for trophozoites in section 3.2 and illustrates that although B-Raf is phosphorylated, its activity is not resulting in downstream MEK1/2 phosphorylation at these time points. The final tier of this MAPK pathway is ERK1/2, which shows increased phosphorylation of several residues in Table 3.4. Most notable of these is the phosphorylation of ERK2 at T185+Y187 with fold changes of 2.74 and 1.99 recorded for the female and male gametocyte infected cells, respectively. These sites are phosphorylated by MEK1/2 activity resulting in ERK2 activation, indicating that although MEK1/2 is not phosphorylated and activated in the stage IV gametocyte samples, it is likely they were active earlier during parasite development, or are activated only within a very brief window within stage IV development [279, 280]. This is similar to what was observed for asexual development as the T185+Y187 site was more phosphorylated at the trophozoite stage, despite no increased MEK1 phosphorylation. The ring stage of asexual development did, however, show increased MEK1/2 activity and therefore, may also be the activator of ERK2 in gametocytes. The array results for the ERK1 activation sites (T202 and Y204) are however difficult to interpret as these signals indicate increases as well as decreases on the same phosphorylation sites. This phenomenon was also recorded for the ring and trophozoite stages of *P. falciparum* asexual development and may be due to negative feedback loops phosphorylated earlier during infection.

The sustained B-Raf phosphorylation at S729 throughout infection, without consistent MEK1/2 downstream activity, illustrates that B-Raf may have multiple functions during parasite development, one of which appears to be active throughout infection. As discussed in section 3.2, the B-Raf selective inhibitor SB-590885 was able to inhibit asexual parasite development potently. Despite not being tested here, the activity of the kinase observed through the microarray analysis of sexual development does suggest the SB-590885 might also be effective on stage IV of the parasite sexual development.

		uRBC mean	Female		Male	
Protein	Phospho Site (Human)	%Error	Fold change	%Error	Fold change	%Error
B-Raf	S446+S447	8	0.87	3	0.57	27
	S729	27	3.54*	5	3.07*	13
	Pan-specific	33	2.57*	13	2.93*	2
C-Raf	S296	6	1.32	17	0.92	11
	Pan-specific	32	0.79	11	0.82	9
	Pan-specific	57	1.33	6	0.64	50
MEK1	S298	11	0.74	19	0.54	8
	T292	2	0.78	10	0.67	9
	T386	5	0.55	4	0.48	5
	T386	9	0.73	2	0.68	1
	Pan-specific	9	0.93	3	0.71	3
	Pan-specific	18	2.08*	12	1.71*	2
MEK1/2	S218+S222	18	0.52	3	0.38	20
MEK2	T394	13	0.45	16	0.38	7
	T394	10	0.50	1	0.29	24
	Pan-specific	21	0.83	7	0.49	3
ERK1	T202	15	0.82	6	0.81	21
	T207	20	1.32	15	0.97	9
	Y204	9	0.58	29	0.67	3
	Y204	17	2.76*	9	1.43	11
	Pan-specific	13	1.37	11	1.76	13
	Pan-specific	12	1.22	2	1.24	1
ERK2	T185+Y187	16	2.74*	2	1.99*	2
	Pan-specific	8	1.35	4	0.96	0

* Signals outside of 2x standard deviation of uRBC mean

Table 3.4 – Phosphorylation status of the MAPK pathway during infection with *P. falciparum* stage IV gametocytes.

Increases marked in yellow, decreases are marked in blue. All values listed are the fold change from the uninfected erythrocyte control mean (n=3). Signals marked by * were outside two standard deviations of the uninfected erythrocyte mean (p=0.5). Signals flagged as cross-reactive to *P. falciparum* asexual stages are underlined. The signals listed were; not flagged as cross-reactive or low intensity, unless otherwise stated.

3.3.2 Differences between host cell signalling during male and female gametocyte infection

As we hypothesised, many significant phosphorylation changes observed on the host erythrocyte signalling molecules are consistent between male and female gametocytes. However, as noted in Table 3.1, there appeared to be a number of phosphorylation changes specific to either the male or female gametocyte sets. To ascertain which signals from the two datasets were the most different, we directly compared them, without the intermediate uninfected erythrocytes. This emphasised the differences more dramatically; however, it did mean we were no longer working with the uninfected erythrocyte mean (n=3). Consequently, we could not determine the significance of each signal, as n=1 for both gametocyte arrays.

Similar to the previous sections, this dataset first had the low-intensity and potentially cross-reactive signals removed (see Chapter 3.2 for more detail on this process). There were a total of 348 signals that passed the above criteria, which were split into two sets; signals which were higher during infection with female gametocytes (Figure 3.10a, left dot plot) and those that were higher during infection with male gametocytes (Figure 3.10a, right dot plot). Four signals are highlighted in Figure 3.10 as they were outside the general signal distribution. These signals were; Met phosphorylated on Y1230+Y1234+Y1235, which was higher in the female gametocyte datasets, and the following phosphorylation sites which were more highly phosphorylated in the male gametocyte dataset; ICK Y159, Paxillin Y31 and FRS2 Y348. All four of these phosphorylation sites were noted in Figure 3.9a in the direct comparison to uninfected erythrocytes. Furthermore, Paxillin and MET were also listed in Table 3.1, which contained the most significant differences between gametocytes and uninfected erythrocytes (see section 3.2.1). The high level of phosphorylation in the female gametocyte dataset is also reflected in the medians, which were 1.34- and 1.17-fold change for females and males, respectively. Additionally, 68% of the signals were higher during infection with female gametocytes, consistent with the previous discussions and observations (Figure 3.9a and Table 3.1).

We further filtered out signals that had folds changes less than two, to highlight the largest differences in the datasets. This identified sixteen signals in the female gametocyte data and three signals for the male dataset (Figure 3.10b). The three signals higher in male gametocytes were phosphorylation sites of ICK Y159, Paxillin 1 Y31 and FRS2 Y348. Of these three signals FRS2 had an associated error value of 1532% indicating this fold change is unreliable (Figure 3.10, coloured red), and was also flagged due to high signal error on the uninfected erythrocyte replicate (conducted at the time of the gametocyte arrays) detected an error of 1643%, which could be the reason for the difference detected here. The full list of signals from this uninfected erythrocyte replicates are available in Appendix 3. The uninfected erythrocyte signal also flagged high error (8041%) for the ICK Y159 phosphorylation and suggested there may have been an issue with this antibody duplicate. The final signal listed that was higher for male gametocytes was for Paxillin 1 Y31. This signal was not flagged as problematic in the uninfected erythrocyte control (Appendix 3), though it did have a 299% duplicate error for the female gametocyte signal (Figure 3.10b). However, the fold change difference was 22, which cannot be explained by this error value. Paxillin is a focal adhesion adapter protein, which functions as a scaffold for recruitment of several kinases including FAK, Src and Abl to the plasma membrane [318]. Paxillin enables integrin-dependent activation of the MAPK pathway through the kinases mentioned above and also has a role in actin reorganisation through PAK interactions [318]. Phosphorylation of Paxillin at Y31 is the result of combined FAK and Src activity, which creates docking sites for Crk adapter proteins, required for MAPK activation [319]. Though Y31 is more phosphorylated in erythrocytes infected with male gametocytes compared to females, the overall level of phosphorylation is much lower than in uninfected erythrocytes. In fact, both of the Paxillin phosphorylation signals on the antibody microarray indicated reduced levels of phosphorylation across all of the *P. falciparum* arrays completed (Appendix 1 and Supplementary Figure 1). This suggests that, although higher levels of Paxillin was observed in male gametocytes compared to females, it is unlikely to be recruiting Crk adapter proteins during infection.

Of the sixteen signals listed in Figure 3.10b, which were higher in female gametocytes compared to males, MET phosphorylation at Y1230+Y1234+Y1235 had the largest fold change. This particular signal had an associated error value of 1515%, and as previously discussed in section 3.3.1 was also flagged for error in the uninfected erythrocyte control and therefore was not considered further. The next largest fold change in the female gametocyte table is for p38α MAPK phosphorylated at T180+Y182 (fold change of 2.79). p38a MAPK belongs to the same family of kinases as ERK1/2 described in the previous sections. However, activation of p38a MAPK by phosphorylation of T180+Y182 is the result of MEK3/4/6 (MKK3/4/6), instead of MEK1/2 [320, 321]. The T180+Y182 phosphorylation was also higher in erythrocytes infected with female gametocytes compared to uninfected erythrocytes. The p38 family of MAPK contains multiple members, of which three were present on the microarray and had signals not flagged as cross-reactive or of low intensity (Table 3.5). Table 3.5 also contains upstream activators of p38 (MEK3/4). Activation of MEK3/4 is achieved by a range of upstream MAP3Ks including; MLK1-4, Tpl-2, DLK, TAO1/2, TAK1 and ASK1/2 [118]. MLK3, TAO1/2, TAK1 and ASK1 are present on the microarray; however, most signals were flagged as cross-reactive or weak. Consequently, it is difficult to determine which may be involved during infection. The p38 isoforms α, β and δ, share the same T180+Y182 phosphorylation and activation site. Erythrocyte infection with female gametocytes compared to males and uninfected erythrocytes have higher levels of p38 phosphorylation at the T180+Y182 site. Additionally, phosphorylation of MEK3 at S218 and MEK4 at S257, indicative of MEK activity, are phosphorylated higher in erythrocytes infected female gametocytes, this is also true for MEK3 during infection with male gametocytes (Table 3.5) [322, 323]. Together these results indicate that during female gametocyte development, MEK3/4 are activated through phosphorylation of S218 and S257 by an unknown kinase, which in turn enables MKK3/4 to phosphorylate p38 MAPK on Thr180+Tyr182 for an unknown function. Activated p38 results in numerous downstream signalling events inside the cytoplasm were it acts on metabolism and cytoskeleton reorganisation, or in the nucleus where it acts on transcription factors [324]. In erythrocytes, p38 has been demonstrated to trigger Ca^{2+} entry into the cell, following hyperosmotic shock; however, the upstream signalling pathway remains unknown [192].

a

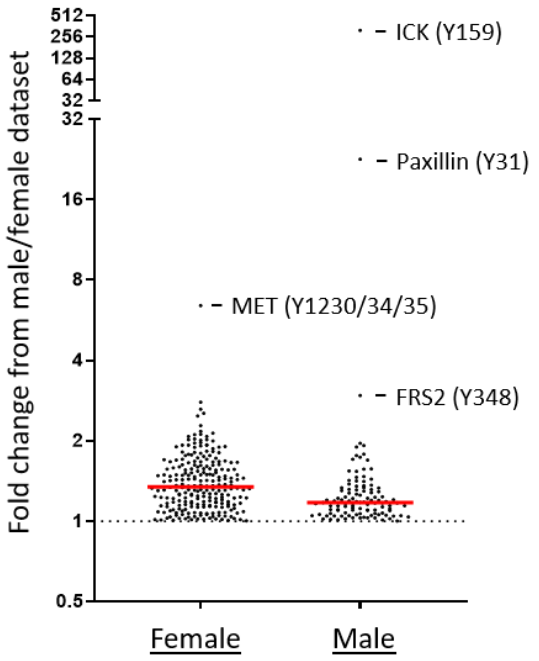

b

Higher in Female

Protein	Phospho Site (Human)	%Error (Male)	%Error (Female)	Fold change
MET	Y1230+Y1234+Y1235	8	1515	6.41
p38a MAPK	T180+Y182	11	2	2.79
PAK4	S474	4	17	2.63
IR	Y1189	9	25	2.53
snRNP 70	Y126	7	15	2.48
FLT3	Y842	13	5	2.28
NDR1	S281+T282	15	22	2.17
JNK1	Y185	17	4	2.14
PIK3R2	Y464	5	10	2.12
EGFR	Y869	18	10	2.11
HGK	T187	43	9	2.08
SgK269	Y635	9	6	2.08
Tau	S713	85	17	2.03
SOX9	S181	16	9	2.02
ITSN2	Y968	12	9	2.02
VEGFR3	Y1068	2	10	2.01

Higher in Male

Protein	Phospho Site (Human)	%Error (Male)	%Error (Female)	Fold change
ICK	Y159	33	49	315.17
Paxillin 1	Y31	21	299	22.66
FRS2	Y348	22	1532	2.96

Figure 3.10 – **Direct comparison of the male and female gametocyte datasets.**

a) Dot plot representing the fold change of the signals which were higher in the female gametocyte dataset (left) and signals which were higher in the male gametocyte dataset (right). Signals represented here were not flagged as cross-reactive to parasite proteins or of low signal intensity. Median fold change values represented in red, 1.34 (females) 1.17 (males). **b)** tables of the signals with fold changes values greater than 2 for the data represented in A (higher in female gametocytes [left], higher in male gametocytes [right]). Fold changes values greater than 3 are coloured gold, while error values with percentages above 1000% are coloured red as they are highly unreliable.

		uRBC mean	Female		Male	
Protein	Phospho Site (Human)	%Error	Fold change	%Error	Fold change	%Error
p38α MAPK	T180+Y182	12	0.68	26	0.82	8
		17	1.18	3	0.79	2
		22	2.14*	2	0.77	11
p38β MAPK	T180+Y182	21	2.01*	17	1.24	34
	Pan-specific	8	1.28	10	0.52	17
	Pan-specific	18	0.78	57	0.58	40
p38δ MAPK	Y182	34	1.93*	49	1.45*	16
	Pan-specific	5	1.06	18	0.82	7
MEK3	S218	16	1.63	14	2.55	8
	Y230	8	1.15	22	1.01	4
	Pan-specific	13	1.35	0	1.23	41
	Pan-specific	5	2.75*	27	1.49	14
	Pan-specific	12	0.45	6	0.62	12
MEK4	S257	11	1.55	7	0.93	16
	S80	16	1.13	5	0.68	10
	Pan-specific	36	0.73	5	0.44*	26
	Pan-specific	12	0.94	9	0.86	4

* Signals outside of 2x standard deviation of uRBC mean

Table 3.5 – MEK3/4 and p38α/β/δ MAPK signalling during erythrocyte infection with male and female gametocytes.

Increases marked in yellow, decreases are marked in blue. All values listed are the fold change from the uninfected erythrocyte control mean (n=3). Signals marked by * were outside two standard deviations of the uninfected erythrocyte mean (p=0.5). None of the listed signals were flagged as cross-reactive or of low signal intensity.

3.4 Concluding remarks

This chapter sought to address the first aim of this thesis which was '*to generate a comprehensive phospho-signalling derived map of host erythrocyte signalling during the development of the malaria parasite Plasmodium falciparum, using antibody microarrays.'* Through the utilisation of the Kinexus KAM900P arrays, we determined that the signalling in the host erythrocyte changes dynamically as the parasite develops, with a general trend of high levels of phosphorylation observed during trophozoite development, and large reductions in phosphorylation seen by the schizont stage. Additionally, preliminary arrays on Stage IV male and female gametocytes were completed, despite the challenges faced with sample generation. These arrays illustrated that during the same time frame of development, the sex of the harboured parasite has in many instances, a unique effect on the signalling of the host cell.

We were able to determine the most reliable signals on the array through three different measures. The first was to determine signals that were not cross-reactive to suspected parasite-encoded proteins. This was achieved via the completion of an array on saponin lysed parasites which compared the saponin supernatant (host erythrocyte cytoplasm) with the saponin pellet (parasite material). Though not a perfect purification system, it enabled us to approach the array data critically. The second approach used was to flag signals of low signal intensity, as these signals were more variable and often associated with higher levels of error and therefore less reliable. The final method used the biological replicates for the uninfected erythrocyte samples (n=3) to determine which of the phosphorylation-specific signals on the array were significantly different during infection (Chapter 3.3). A number of signals were identified and highlighted using the above three signal filtering systems. These signals were highlighted and explored in more detail in Chapter 3.2 and 3.3. Generating enough material for Western blot analysis of Stage IV male and female gametocytes is a difficult feat. Consequently, the validation of studies in this Chapter focused primarily on the asexual cycle; however, validation of the results obtained for gametocyte arrays are underway in Alex Maier's laboratory.

In Chapter 3.2 (*P. falciparum* asexual development) two of the most distinct signalling differences were the host kinases c-MET, as well as B-Raf, with c-MET phosphorylation validated through Western blot. Moreover, inhibition studies, using highly specific compounds against c-MET and B-Raf at submicromolar concentration resulted in parasite death. Through a time-course analysis on highly synchronised parasites, we were able to determine that c-MET and B-Raf phosphorylation, coincided with parasite death following treatment. Additionally,

the c-MET inhibitor PHA-665752 was further shown to significantly reduce the *P. berghei* burden in the murine model of malaria. This provides a clear example of how targeting the host is a potentially viable strategy for the treatment of infectious diseases. With the success of this array system, we sought to employ them in an effort to understand host signalling in other Apicomplexan parasites (Aim 2). These arrays, as well as further comparative analysis, are covered in Chapter 4.

Chapter 4 – Host cell phospho-signalling during intracellular infection with *Plasmodium knowlesi*, *Babesia bovis* and *Toxoplasma gondii*.

4.1 Introduction

Chapter 3 describes the use of antibody microarrays to identify human erythrocyte signalling molecules that are pivotal for *P. falciparum* erythrocytic development. In chapter 4, the antibody microarrays were employed to investigate host cell signalling during infection with other intracellular Apicomplexan parasites. We selected three Apicomplexan species for this study on the grounds of clinical relevance, accessibility, capacity for continuous cell culture and the ability to produce enough material to perform the antibody microarray analysis. Section 4.2 investigates signalling during human reticulocyte infection with *P. knowlesi* and compares signalling in uninfected human erythrocytes and reticulocytes. Section 4.3 details signalling in bovine erythrocyte infection with *B. bovis*, while section 4.4 covers host signalling during human foreskin fibroblast infection with *T. gondii*. Comparative analysis and the commonalities in host signalling during infection are covered in these subsequent sections.

4.2 Human reticulocyte signalling during infection with *Plasmodium knowlesi*

Plasmodium knowlesi, originally considered an exclusive parasite of macaques in South East Asia, is now known to be a zoonotic human parasite, with infection reported throughout Asia [325]. In Malaysia, from 2006-2008, a district hospital recorded rates of severe malaria caused by *P. knowlesi* infection to be higher than infection with *P. falciparum* [326]. This led to increased research into *P. knowlesi* biology and the development of continuous cell culture in human erythrocytes and reticulocytes [327]. The asexual development of *P. knowlesi* is overall similar to *P. falciparum*; however, the lifecycle is completed in approximately 28 hours [328]. To capitalise on the *in vitro* cell culture capacity of *P. knowlesi*, we completed an antibody microarray, which compared uninfected human reticulocytes with those infected with *P. knowlesi.* However, harvesting, purifying and infecting human reticulocytes produces very small yields as a consequence of the low abundance of reticulocytes in human blood (0.5-2.5%) [329]. We overcame this obstacle through collaboration with Dr Danny Wilson at the University of Adelaide, Australia, as he has extensive experience with reticulocyte and *P. knowlesi* culture. Dr Wilson was able to prepare samples of enriched human reticulocytes (70%) and infected one of the samples with *P. knowlesi*, achieving 10% parasitemia. These parasites were predominantly at the schizont stage of development (22 – 26 hours post-invasion). Once the samples were generated, they were snap-frozen and shipped to our laboratory, where we processed the samples, incubated them on the array and completed the antibody microarray analysis. We used a single antibody microarray, where we compared human reticulocytes to human reticulocytes infected with *P. knowlesi* at the schizont stage of development, where the reticulocytes used in both samples came from the same pool of donors.

Reticulocytes are unable to alter transcription, similar to mature erythrocytes; therefore, we focused our analysis on the microarray phospho-specific antibodies, which provided information about changes in host signalling protein phosphorylation during infection. The antibody microarray used here contained 613 different phosphorylation-specific antibodies, represented in Figure 4.1a as a heatmap. Each phosphorylation-specific signal on the array is represented by a pixel, with the colour representing the change during infection (yellow = increase, blue = decrease). Figure 4.1a illustrates that there is little change in overall host phosphorylation during *P. knowlesi* schizont stage development in comparison to uninfected reticulocytes. This is further confirmed by the dot plot in Figure 4.1b (left) where each dot represents one of the aforementioned phosphorylation-specific signals. In this dot plot, the red

line indicates the median signal, which has a fold change of 1.026. In comparison, for the array completed on *P. falciparum* schizonts, the median was 0.76.

The signals displayed in Figure 4.1a/b were processed in the same manner as the datasets obtained in Chapter 3.2 and 3.3 by taking into consideration potential cross-reactivity and the signal strength for each antibody (see Chapter 3.2 for a full description of the filtering parameters). This removed a total of 301 signals from the analysis, which equated to approximately 50% on the phosphorylation-specific signals on the array. The remaining 312 signals were further explored and are referred to as the trimmed data-set. The trimmed dataset illustrates that the overall signal distribution following signal clean-up remains relatively the same, with the median fold change of 0.992 (Figure 4.1b – Trimmed). Note, the signal clean-up did not significantly change the distribution of the data ($p = 0.176$, Mann-Whitney statistical test). Interestingly, Figure 4.1a/b illustrated that there appeared to be very few signals with fold changes above 2 or below 0.5 during *P. knowlesi* infection of reticulocytes. To quantify this, we counted these signals and presented them in a histogram (Figure 4.1c). There were only six signals with fold changes above 2 or below 0.5 for the *P. knowlesi* dataset, which is far less than what was recorded for each of the *P. falciparum* asexual stages (56 signals for the ring stage dataset, 42 trophozoite stage and 55 schizont stage) covered in Chapter 3.2 (Figure 4.1c). We had hypothesised that the *P. knowlesi* dataset would resemble the data distribution of *P. falciparum* schizonts, as this represents the equivalent parasite developmental stage. However, we observed only a few large changes in the levels of phosphorylated host signalling proteins during *P. knowlesi* infection. Why the *P. knowlesi* dataset is so different is not clear, although there are a few considerations that may have influenced this result. 1) That the infected culture contained 10% *P. knowlesi* infected cells; therefore, there were predominately uninfected reticulocytes in this sample, which may have had a dampening effect of the signals recorded. 2) That we are looking at a phylogenetically distant species of *Plasmodium*, which for the comparison completed here, was infecting a more metabolically active host cell type (reticulocyte compared to erythrocyte).

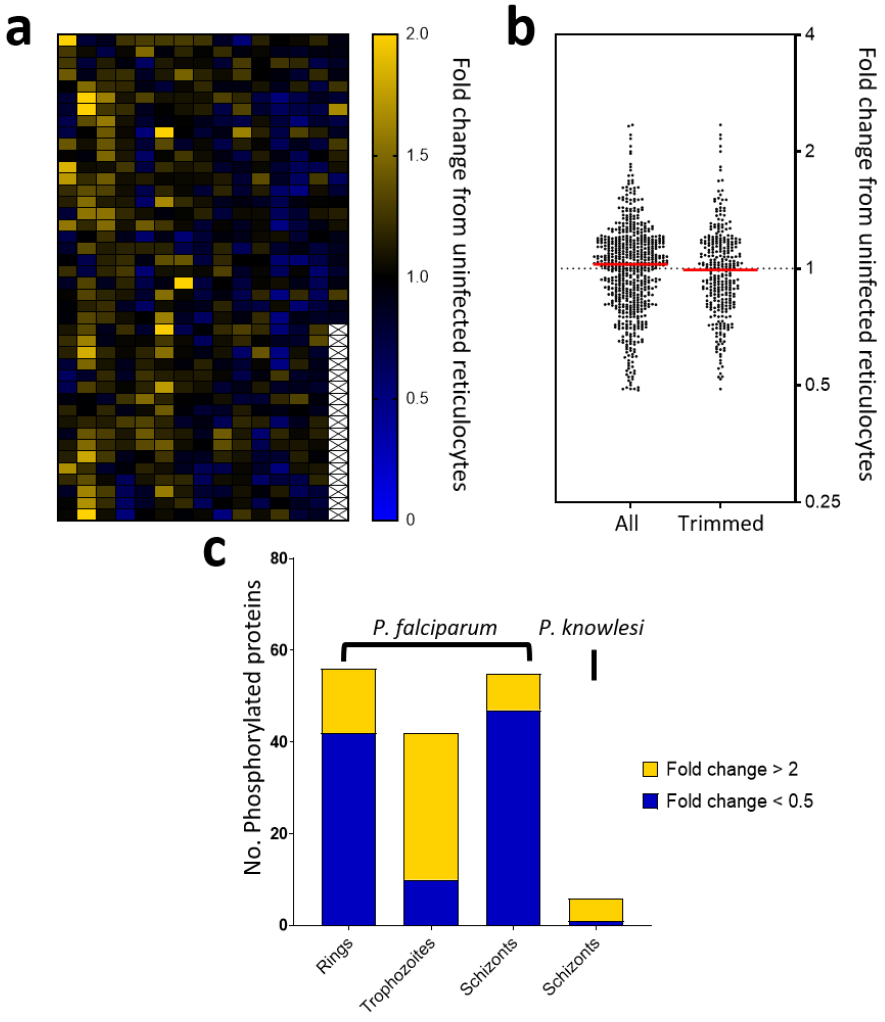

Figure 4.1 – (i) Kinexus KAM900 antibody microarray data for comparing human reticulocytes to those infected with *P. knowlesi*, (ii) removal of cross-reactive and low-intensity signals.

a) Heatmap of antibody microarray data representing the changes in reticulocyte phosphorylation during infection with *P. knowlesi* schizonts (24 – 28 hours post-invasion). Each square represents the fold change in signal for one antibody on the array. The colour represents the change in abundance compared to the uninfected reticulocyte control. Blue squares indicate that the level of a specific phosphorylated kinase has decreased, yellow indicates an increase. **b)** Dot plot of reticulocyte signalling protein phosphorylation during infection *P. knowlesi* in comparison to uninfected reticulocytes. Left, (all) 613 phosphorylation-specific signals, Right (Trimmed) signals remaining following cross-reactive and low-intensity signal removal. The median fold change is represented in red (1.026 and 0.992, respectively) ($p = 0.176$, Mann-Whitney statistical test). Y-axis represented in a Log2 scale. **c)** The remaining phosphorylation-specific signals (trimmed dataset) ranked according to fold change. Yellow represents changes with a fold change greater than 2; blue represents changes below a fold change of 0.5. The full dataset is presented in Appendix 4.

4.2.1 Shortlisting of the most reliable signals on the *P. knowlesi* array

To filter the *P. knowlesi* trimmed data-set of 312 signals into a list of the most promising leads, we further took into consideration the error between the duplicate antibodies present in each panel of the array. This enabled us to determine if the fold change during infection was the result of the internal signal error and hence to directly assess the reliability of each signal on the array. In Chapter 3.2, we had three biological replicates for uninfected erythrocytes, which allowed us to determine the standard deviation between these samples. Using the standard deviation approach, we were able to determine which phosphorylation-specific signals were significantly different from the uninfected mean following *P. falciparum* infection. In this experiment, we used human reticulocytes instead of erythrocytes. Consequently, we cannot use the erythrocyte signal mean and standard deviation employed in Chapter 3. Instead, we developed a stringent system for assessing the error on the duplicate signals within each panel of this array. We defined four different categories based on the total error for each fold change recorded, where the total error is the sum of the duplicate error values for the uninfected and infected samples. We then compared the total error to the percentage change recorded for each signal during infection (converted from fold change). This category system is designed to determine which of the signals on the array have the lowest total signal error as a percentage of the signal change during infection. Below we have outlined the criteria for each of the four categories used;

- **Category 1** – error of uninfected reticulocyte signal + error of infected reticulocyte signal (total error) > 10% of signal change observed.
- **Category 2** – total error > 25% of signal change observed.
- **Category 3** – total error > 50% of signal change observed.
- **Category 4** – total error ≤ 50% of signal change observed.

The signals ranked as Category 1 are the most reliable signals on the array as the total error makes up less than 10% of the signal change during infection. Category 2 signals are still very reliable at >25%; however, Category 3 >50% and Category 4 <50% are less reliable, were the change during infection could be attributed to signal error. This system is highly effective at determining signals, which have high reliability, and can easily be applied to subsequent array datasets. However, this system does under-represent reductions in phosphorylation levels, as the system is based on the percentage change, which can range from -100% to infinity. Therefore an increase of 100% during infection (fold change 2) is the equivalent of -50% (fold change 0.5), as the error is recorded as a percentage of the signal, it more heavily affects the results of signals, which decrease during infection.

Table 4.1 displays signals that were ranked as Category 1 or 2, and also lists which of these signals were flagged as potentially cross-reactive when compared to the saponin array conducted on *P. falciparum*-infected erythrocytes in Chapter 3 (Figure 3.2). The saponin cross-reactivity array was completed on *P. falciparum* and consequently may not be a highly accurate representation of the cross-reactivity to *P. knowlesi* proteins due to the evolutionary distance between these two *Plasmodium* species. Nevertheless, as signalling proteins are generally highly conserved, we still used it here as an indicator of cross-reactivity. Table 4.1 lists two Category 1 signals from this dataset; both flagged as potentially cross-reactive, and of the 11 signals ranked as Category 2 four were not flagged as cross-reactive.

The two Category 1 signals are the Estrogen-receptor alpha (ER-alpha) phosphorylated at Ser104 and the Retinoblastoma-associated protein (Rb) phosphorylated at Ser795. ER-alpha is phosphorylated at Ser104 by ERK1/2 and is associated with increased activity of the ER-alpha receptor [330]. The *P. knowlesi* dataset did not indicate a clear increase in the levels of ERK1/2 phosphorylation (Table 4.2), which could indicate that these kinases were active earlier during infection and that the phosphorylation seen on ER-alpha is the residual of this earlier activity (we have seen in the preceding chapter that there appears to be a negative feedback loop that shuts down the MAPK pathway in late stages of *P. falciparum* infection). Presently, only ERK1/2 are known to phosphorylate ER-Alpha at the Ser104 site. There is, however, elevated phosphorylation of ERK1/2 in uninfected reticulocytes (Table 4.2.2), compared to uninfected erythrocytes. Consequently, *P. knowlesi* infection of reticulocytes may not require further ERK1/2 phosphorylation to enable activity for ER-Alpha phosphorylation. Further discussion of the differences in phosphorylation and protein levels between reticulocytes and erythrocytes will be covered in the following section (4.2.2).

The function of Rb phosphorylation at Ser795 is not well understood; Rb controls progression through the G1-phase of the cell cycle [331]. The array contained a number of antibodies against the phosphorylated forms of Rb, which all indicate a reduction in phosphorylation during infection (Appendix 4). Rb has a role in hematopoietic homeostasis and erythropoiesis by regulating the proliferation of erythroblasts and enucleation of erythroblasts [332]. However, there is no reported function later in reticulocytes or erythrocytes. Since the ER-alpha and Rb signals have been flagged as potentially cross-reactive, it is not possible to conclude on the involvement of these host cell proteins at this stage.

Of the six signals that displayed a fold change of 2 or higher or below 0.5 (Figure 4.1c), only one of these signals ranked at least a Category 2 signal (excluding Rb due to potential cross-reactivity). This signal was Fibroblast growth factor receptor substrate 2 (FRS2) phosphorylated at Tyr348. FRS2 is an adapter molecule, which facilitates signal transduction from a number of RTKs to downstream pathways such as the MAPK and PI3K/AKT pathway. FRS2 phosphorylation on Tyr348 is associated with grb2 binding, a key component of subsequent MAPK activation [333]. FRS2 was also prominent in the dataset for *B. bovis* (section 4.3) and will be covered in greater detail in the following section.

Protein	Phospho Site (human)	Category	Cross-reactive signal	Fold change
BTK	Y223+Y225	2	no	1.8
FRS2	Y348	2	no	2.1
JUN	S73	2	no	1.1
SRPK1	S222	2	no	0.72
ER-alpha	S104	1	yes	1.3
Rb	S795	1	yes	0.49
EphA3	Y779	2	yes	1.3
GTF2F1	S385+T389	2	yes	1.6
LCK	S158	2	yes	1.2
PRKACB	S339	2	yes	0.81
PKCg	T674	2	yes	1.2
Ron	Y1238	2	yes	1.2
RSK1	T359	2	yes	0.73

Table 4.1 – Most prominent changes in host signalling protein phosphorylation during *P. knowlesi* infection of reticulocytes.

The signals listed here were all ranked as Category 1 or 2 error, changes in fold change are coloured so that increases are marked in yellow, decreases are marked in blue. Category 1 signals are highlighted in green; both antibodies showed cross-reactivity against *P. falciparum* proteins, as shown in Chapter 3.2.

		P. knowlesi infected Reticuclytes	Reticulcytres vs erythrocytes (uninfected)	
Protein	**Phospho site (Human)**	**Fold change**	**Fold change**	**Cross-reactive signal**
ERK1	T202	1.07	0.56	yes
	T207	0.57	1.40	yes
	Y204	1.16	0.60	no
	Y204	0.92	1.88	yes
	Pan-specific	0.98	0.93	no
	Pan-specific	0.93	1.18	no
ERK2	T185+Y187	0.72	1.35	no
	Pan-specific	0.75	1.47	no

Table 4.2 – Fold change data for ERK1/2 for *P. knowlesi* dataset and comparison between reticulocytes and erythrocytes (uninfected).

Changes in fold change are coloured so that increases are marked in yellow; decreases are marked in blue. Signals listed here are not low-intensity signals. Highlighted in red are the signals, which showed cross-reactivity to *P. falciparum* proteins (Chapter 3.2). The reticulocyte vs erythrocyte data will be discussed in full in Section 4.2.2.

One of the limitations of this reticulocyte study was the difficulty in generating enough material to conduct a microarray analysis. The consequence of this was the low level of parasitised cells in the infected sample (10% parasitemia). Because of this, 90% of the cells present in this sample were uninfected. However, they were exposed to infected cells for over 22 hours. During this time, these cells may have been affected by the metabolic waste and exported proteins released from the parasitised cells in the culture. *P. falciparum* is known to export several parasite kinases into the host cell and the surrounding media, which may affect uninfected bystander cells [334, 335]. If exported elements from infected cells can affect bystander cells, we could also expect there to be an effect on the signalling pathways in the uninfected host cells. Given these bystander cells were present in the infected sample of the *P. knowlesi* array, many of the changes in host phosphorylation levels may have been the result of these uninfected cells. Bystander cells were also present in the *P. falciparum* dataset for the ring stage array, as only 33% of that sample was infected, while they were absent in both the trophozoite and schizont *P. falciparum* arrays, which contained purified parasitized cells. Additionally, the array completed on *B. bovis* was likewise performed on a sample with 50% parasitemia (section 4.3). Following the discussion of the *B. bovis* dataset in section 4.3, we discuss this potential bystander effect across erythroid infecting Apicomplexan parasites.

Human reticulocytes are significantly more metabolically active than mature erythrocytes and are known to continue mRNA translation for up to a week following release from the bone marrow [336]. During this time frame, substantial production of proteins occurs, although a large percentage of these are the hemoglobin α and β subunits. Studies of the mRNA transcripts present in reticulocytes indicate that there are hundreds of transcripts for non-hemoglobin related proteins [178]. In the top 100 most abundant transcripts are mRNAs that encode for the protein kinase MEK3; however, whether reticulocytes translate all of the available mRNA is unknown [178]. Compared to mature erythrocytes, continued mRNA translation and the initial presence of mitochondria make reticulocytes more active cells; therefore it is highly likely many more signalling pathways are active in these cells prior to infection [178, 337].

Our study of *P. knowlesi* was conducted using reticulocytes to enable the comparison of host cell signalling between erythrocytes and reticulocytes. In Table 4.2, we observed that although ERK1/2 was not more phosphorylated in infected (versus non-infected) reticulocytes, it was already more phosphorylated than was observed in mature erythrocytes. This suggests that although we did not detect increased ERK1/2 phosphorylation during infection, these kinases may have a basal level of activation in reticulocytes, in such a way that the parasite does not need to activate this pathway early during infection (as was observed for *P. falciparum* [Figure 3.6]) We, therefore, hypothesised that reticulocytes would have elevated levels of phosphorylation across many signalling proteins and that this phosphorylation may play an important role for *Plasmodium spp.* that exclusively invade host reticulocytes. The following section will compare four biological replicates of uninfected erythrocytes to the single sample of uninfected reticulocyte data obtained throughout this study. The purpose of this comparison is to highlight differences in host cell phosphorylation in reticulocytes and to determine if there are any clear changes in the overall abundance of any signalling proteins we could detect using the array system.

4.2.2 Comparison of host signalling between reticulocytes and mature erythrocytes

The previously described differences between uninfected erythrocytes and those infected with ring, trophozoite, schizont and the sexual stages of *P. falciparum*, provided four biological replicates of uninfected erythrocytes signals, originating each from different blood donors. Additionally, the array completed on reticulocytes infected with *P. knowlesi* provided one biological replicate of uninfected reticulocytes signals. The mean of the four erythrocyte samples for each antibody signal was determined and compared against the reticulocyte signal. Unlike the previous datasets, we are now comparing reticulocytes to their subsequent developmental form, erythrocytes. As reticulocytes are known to translate mRNA, the abundance of signalling elements may change during this development. Therefore, the signals from the pan-specific antibodies, which are antibodies that recognise proteins regardless of their phosphorylation status, were included throughout this comparison. The complete dataset was sorted to separate the pan-specific and phosphorylation-specific signals to allow easier interpretation of changes in protein abundance and presented as a heatmap (Figure 4.2). Each pixel represents the fold change of a single antibody on the array. Notably, there is an even distribution of blue and yellow pixels indicating a variety of different protein abundances and phosphorylation statuses in reticulocytes when compared to erythrocytes. The blue pixels in the pan-specific signal heatmap suggest that reticulocytes are indeed translating mRNA of signalling proteins during development. Interestingly, the yellow pixels indicate that several signalling proteins are less abundant in reticulocytes than in erythrocytes, suggesting these proteins are degraded.

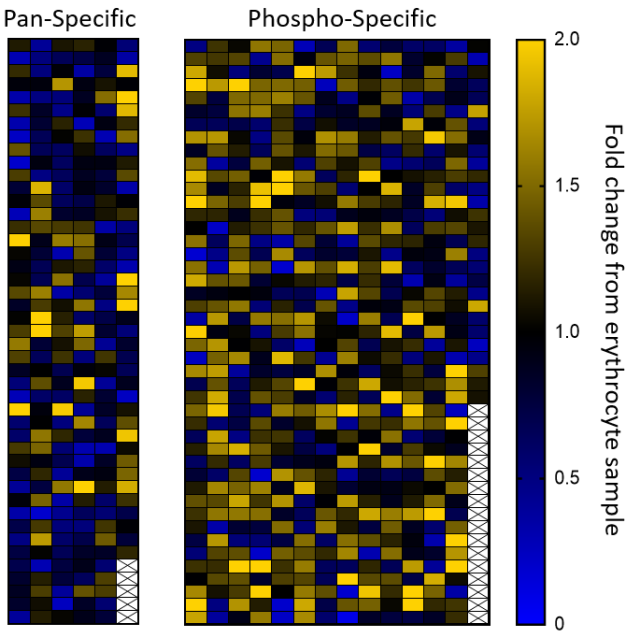

Figure 4.2 – **Heatmap of antibody microarray data representing the changes in reticulocyte signalling protein abundance and phosphorylation compared to erythrocytes**.

Data compares the uninfected human erythrocytes signal mean (n=4) against uninfected human reticulocytes signals (n=1). Each square represents one antibody signal on the array. The colour represents the change in abundance compared to the erythrocyte mean. Blue squares indicate that the abundance of a specific kinase/phosphorylated kinase has decreased (fold change < 1), yellow indicates an increased (fold change > 1). All increases in fold change above a fold change of 2 appear the brightest yellow.

To further refine the signals for this dataset, we removed signals that had low intensities, similar to the datasets previously discussed. (See Chapter 3.2 for details and Appendix 6 for these signals). Cross-reactivity was not applicable for this dataset, as no parasites were present during sample preparation of uninfected host cells. The removal of low-intensity signals reduced the dataset to 227 pan-specific and 518 phosphorylation-specific signals. To visualise the distribution of the signals and to determine the effect of removing these low-intensity signals, we displayed the dataset as a dot plot (Figure 4.3a). Notably, low-intensity signal removal increased the median fold changes for both the pan-specific and phosphorylation-specific signals (0.88 → 0.93, Pan-specific, 1.13 → 1.20 phosphorylation-specific). A Mann-Whitney statistical test indicated there was no significant change for the pan-specific signals (p=0.0878); however, it did suggest the phosphorylation-specific signals were significantly changed (p=0.0148). Both Figure 4.2 and 4.3 indicated that there was quite a number of signals with fold change values above 2 and below 0.5, reflective of what was observed for the *P. falciparum* datasets discussed in Chapter 3. We quantified the number of signals that met this criterion and summarised this information with similar analysis performed on the *P.*

falciparum, and *P. knowlesi* datasets, specifically comparing phosphorylation-specific signals (Figure 4.3b). The signals from the *P. falciparum* datasets with fold changes above 2 or below 0.5 made up 12-16% of the phosphorylation-specific signals, while they made up only 2% of the *P. knowlesi* dataset. Interestingly, the comparison between uninfected erythrocytes and reticulocytes indicated that 17% of the phosphorylation-specific signals also met this criterion. This suggests that the differences in phosphorylation between reticulocytes and erythrocytes are similar to the level of perturbation in host cell signalling seen during erythrocyte infection with *P. falciparum*. The following sections will compare these signals to determine if there are indeed similarities in the phosphorylation of signalling elements between uninfected reticulocytes and erythrocytes infected with *P. falciparum*. Additionally, the large number of phosphorylation changes seen during reticulocyte development may in part explain why so few large fold change values were observed for the *P. knowlesi* dataset.

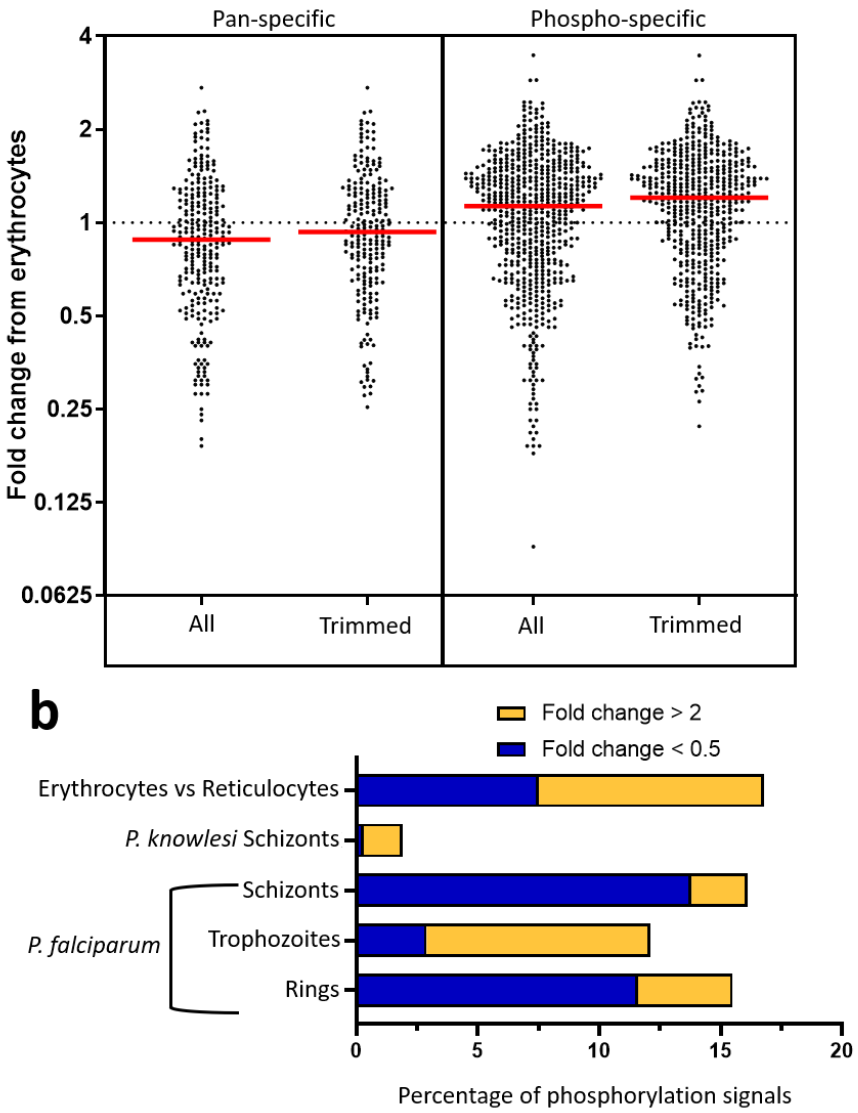

Figure 4.3 – Fold change in uninfected reticulocyte datasets compared to the signals of uninfected erythrocytes and comparison of the largest phosphorylation changes across the arrays complete.

a) Dot plot of the erythrocyte and reticulocyte signal comparison before and after removal of low-intensity signals. Pan-specific (left) signals before (all) and after removal of low-intensity signals (trimmed). Phospho-specific (right) signals before (all) and after removal of low-intensity signals (trimmed). The median fold change is represented in red. Median values are as follows: Pan-specific, all = 0.88, trimmed = 0.93 p = 0.0878 Mann-Whitney statistical test. Phosphorylation-specific, all=1.13, trimmed = 1.20, p = 0.0148 Mann-Whitney statistical test). Y-axis represented in a Log2 scale. **b)** Comparison of phosphorylation-specific signals that were above a fold change of 2 or below 0.5 compared to their respective controls. *P. falciparum* asexual stage arrays included here for comparison. Values represented as a percentage of the total signals after low-intensity, and cross-reactive signals were removed (removal of cross-reactive signals was not applied to the uninfected erythrocyte to uninfected reticulocyte comparison).

4.2.3 Differences in host cell signalling between reticulocytes and erythrocytes

From the remaining 227 pan-specific and 518 phosphorylation-specific signals, we sought to determine which of these signals were significantly different between the reticulocyte and erythrocyte samples. We determined the standard deviation for each antibody signal for the four erythrocyte biological replicates and searched the reticulocyte dataset to flag which signals were outside two standard deviations of the erythrocyte mean signal for each antibody ($p<0.05$). This process flagged 38 pan-specific and 128 phosphorylation-specific signals equating to 17% and 25% of total signals respectively. We further refined these lists by removing any signal with an error value above 25% for the erythrocyte mean and the technical duplicate error value above 25% for reticulocyte signals, which reduced the pan-specific signals to 22 and phosphorylation-specific signals to 85 (Table 4.3). Due to the number of signals listed in Table 4.3, we will not discuss each signal listed; however, we will focus on a few of the more noteworthy differences.

Protein	Phospho Site (Human)	Fold change
AAK1	S637	1.78
ABL1	Y257	1.52
ABL1	Y412	0.62
ACK1	Y284	2.01
AKT1	T308	1.78
AKT3	Pan-specific	1.29
ALK	Y1092	1.59
ANKRD3	S438	2.00
ASK1	Pan-specific	2.27
ATM	S1981	1.68
ATM	Y2969	1.62
ATR	S435+S436	1.56
Aurora B	Pan-specific	1.58
Aurora B	S227	1.95
Aurora C	Pan-specific	1.31
BARK1	Y356	1.60
BCR	Y177	1.70
BCR	Y644	1.78
BLK	Y188	1.25
BMPR2	S375	1.28
B-Raf	S729	2.89
BRD2	S37	1.96
CaMK2a	T286	1.61
CDC7	T376	1.58
COT	S334	1.73
Crystallin aB	Pan-specific	1.86
Crystallin aB	Pan-specific	0.49
CSF1R	Pan-specific	1.61
DDR1	Y796+Y797	1.65
DDR2	Y736	1.78
DDR2	Y740	1.65
eEF1A1	Y141	1.40
EFNB2	Y316	0.51

Protein	Phospho Site (Human)	Fold change
EGFR	Pan-specific	2.10
EGFR	Pan-specific	1.61
EGFR	Y1069	1.33
EGFR	Y1172	1.39
EGFR	Y869	1.54
eIF2a	Pan-specific	2.08
EML4	Y226	2.06
ERK1	Y204	1.88
ERK3	Pan-specific	1.27
ERK3	S189	1.64
ERK4	Pan-specific	1.74
ESYT1	Y822	1.99
FGFR1	Y653+Y654	1.82
FGFR3	Y647+Y648	1.96
FLT3	Y842	1.81
FRK	Y387	1.56
G6PD	Y401	1.57
GIT1	Y545	2.32
GSK3a	T19+S21	2.45
Histone H2B	S14	0.49
Histone H3	S28	0.41
Histone H3	T3	0.47
HSP27	S78	0.68
HSP90a/b	Pan-specific	0.59
HSP90AB1	Pan-specific	0.64
JAK2	Y570	1.32
JAK3	Y980+Y981	2.26
KHS1	S174	1.71
KIT	S821+Y823	1.86
KSR1	S404	1.74
LATS1	S909	1.39
LCK	Y192	1.59
LCK	Y263+Y264	1.58
LMR2	S1450	1.77
LOK	S191	2.14
LTK	Y672	1.75
MAPKAPK2	Y225+T226	2.20

Protein	Phospho Site (Human)	Fold change
MARK1	T215	1.64
MET	Y1234+Y1235	1.54
MET	Y1234+Y1235+S1236	1.71
MKK7	Pan-specific	1.75
MLK3	Pan-specific	1.49
MOK	T159+Y161	1.94
mTOR	Pan-specific	1.64
NUAK1	T211	2.06
p38b MAPK	T180+Y182	1.80
p38g MAPK	Pan-specific	1.39
p70 S6KB	S423	1.41
PAK1	T423	1.50
PBK	Y74	2.26
PCTAIRE2	S180	1.45
PDK1	S241	1.49
PDLIM5	Y251	1.50
PKCd	T507	1.60
PKM2	Y390	1.70
PTEN	S380+T382+S385	0.61
Rac1/cdc42	Pan-specific	0.55
RIPK2	S176	2.04
Ron	Pan-specific	1.89
ROS	Pan-specific	1.88
RSK1	S221	1.61
RSK1	S363	1.84
RSK1	T359	1.75
RSK1	T573	1.56
Sgk223	Y413	1.84
Shc1	Y349	1.92
SMG1	T3550	0.78
TIE2	Y992	1.80
TNK1	Y277	2.10
TSSK3	T168	1.80
VEGFR1	Y1048	1.74
VEGFR3	Pan-specific	1.43
WNK1	S382	2.05
YES	Y222+Y223	1.39

Table 4.3 – The most reliable and significant differences between reticulocyte and erythrocyte host cell signalling.

Signals represented here are the fold change from the reticulocyte signal (n=1) compared to the mean erythrocyte signal (n=4). Each listed signal is outside two standard deviations of the erythrocyte mean. The mean erythrocyte signal error and the technical duplicate error for the reticulocyte signal is less than 25% for each fold change listed. Fold change values are coloured so that increases marked in yellow, decreases are marked in blue.

The epidermal growth factor receptor (EGFR) appears five times in Table 4.3 and indicates that EGFR is more abundant and more phosphorylated in reticulocytes compared to erythrocytes. EGFR belongs to a large family of transmembrane receptors that play important roles in cellular proliferation, motility and differentiation in nucleated cells [338]. EGFR is a RTK with demonstrated activity in the early stages of hematopoiesis [339]. Like other RTKs, EGFR is usually activated through the binding of a specific ligand (this includes the epidermal growth factor [EGF] and the transforming growth factor-alpha [TGF-α]) to the extracellular domain, resulting in trans-autoactivation [338]. However, EGFR has been reported to have ligand-independent functions, in which the receptor activates the transcription factor IRF3 [340]. Additional ligand-independent roles of EGFR have been identified, although these interactions are coupled with mutant EGFR, which is present in several forms of cancer [340, 341]. The higher abundance of EGFR in reticulocytes, together with its increased phosphorylation, indicate a potential role for this RTK in erythrocyte maturation.

Table 4.3 also lists several different RTKs, including Discoidin domain-containing receptor 1 and 2 (DDR1/2), fibroblast growth factor receptor 1 and 3 (FGFR1/3), Mast/stem cell growth factor receptor (KIT), vascular EGFR 1 and 3 (VEGFR1/3) and MET, all of which appear to have higher levels of phosphorylation in reticulocytes. Of these kinases, KIT and MET have roles in hematopoiesis, with KIT also being involved in acute erythroid expansion during anemia recovery [175, 339, 342]. None of the listed RTKs have a reported function in reticulocytes or erythrocytes and therefore may be remnants from erythroblast signalling prior to enucleation. This would suggest that many of these kinases are degraded during the process of formation of mature erythrocytes. Consequently, we would also expect to see a higher abundance of these RTKs in reticulocytes compared to erythrocytes, and indeed we do for EGFR, KIT and VEGFR. However, this is not the case for FGFR and MET as their abundance remains relatively consistent (MET is slightly more abundant in erythrocytes). These findings suggest that RTKs may have yet to be determined roles in reticulocyte development. The observation that *P. knowlesi* has a lower impact on signalling in reticulocytes than *P. falciparum* has on erythrocytes might reflect that since many pathways are still active in reticulocytes than in erythrocyte, the parasite does not need to activate those pathways that are needed for successful infection. This raises interesting questions regarding the requirement for reticulocyte of *P. knowlesi* and *P. vivax*: it is tempting to propose the hypothesis that these species cannot infect erythrocytes at least in part because (unlike *P. falciparum*) they are unable to activate pathways that are inactive in erythrocytes but still active in reticulocytes

As was mentioned in the introduction to this section, MEK3 is highly expressed in the bone marrow, with a role in hematopoiesis regulation [343]. MEK3 transcripts were shown to be abundant in reticulocytes. However, it was unknown whether these transcripts were translated into protein [178]. If MEK3 is translated during reticulocyte development, we would expect to see a higher abundance of MEK3 in erythrocytes, assuming the protein is not quickly degraded in these cells. MEK3 was not listed in Table 4.3 as the MEK3 specific signals were not noted as significantly different from the erythrocyte mean. We compiled the MEK3 specific signals (Table 4.4) to assess if MEK3 is translated from mRNA during reticulocyte development. Three different pan-specific signals for MEK3 are listed in Table 4.4 and have fold change values of 1.25, 1.53 and 0.87 with an average of 1.22, indicating slightly higher levels of MEK3 in reticulocytes. The overall small increase in MEK3 abundance indicates that it is unlikely that translation of the kinase occurs during reticulocyte development. Note, the levels of MEK3 phosphorylation also remain consistent for both cells, illustrating no observed function in these samples. Alternatively, it is possible that MEK3 is indeed translated during reticulocyte development and is slowly degraded during the life span of erythrocytes. It is well established that erythrocytes have an average life span of 115 days, which means our sample of erythrocytes would contain cells of various ages post maturation, potentially dampening the signals observed on the array [183]. Therefore, MEK3 may be more abundant at the initial transition from reticulocyte to mature erythrocyte, before degradation during erythrocytes lifespan.

Protein	Phospho Site (Human)	Fold change
MEK3	S218	1.13
	Y230	1.39
	Pan-specific	1.25
	Pan-specific	1.53
	Pan-specific	0.87

Table 4.4 – MEK3 specific signals for the comparison of reticulocytes and erythrocytes.
Only the signals specific to MEK3 are listed here. These signals were not flagged as low-intensity signals. Fold change values are coloured so that increases marked in yellow, decreases are marked in blue.

From the listed signals of Table 4.3, B-Raf phosphorylated at Ser729 showed the largest difference between the two host cells, with a fold change of 2.89 from erythrocytes recorded. B-Raf was previously discussed in Chapter 3 with high levels of phosphorylation observed during asexual development of *P. falciparum*. Phosphorylation of B-RAF at S729 is the result of AMP-activated protein kinase (AMPK) activity under energy stress conditions, which promotes association with the scaffolding protein 14-3-3 and C-Raf, enabling downstream MAPK signalling [272]. Table 4.5 lists the differences in erythrocyte and reticulocyte signals for the MAPK pathway involving B-Raf and indicates the differences in the protein abundance and the level of phosphorylation for members of this pathway. The abundance of B-Raf also seems to be higher in reticulocytes, matching what was observed for erythrocytes infected with *P. falciparum* (Figure 3.5 and Table 4.5). Interestingly the C-Raf, ERK1 and ERK2 signals from Table 4.5 appear to have an almost identical pattern of phosphorylation and protein abundance to erythrocytes infected with *P. falciparum* at the ring stage of development (Figure 3.5). While the signals for B-Raf more closely resemble erythrocyte infection with *P. falciparum* trophozoites and schizonts, due to the small change in phosphorylation seen on Ser446+Ser447 (Figure 3.5).

As discussed in Section 4.1, *P. knowlesi* infection did not result in increased phosphorylation of B-Raf during infection of reticulocytes. As Table 4.3 suggests, this could be because B-Raf is already phosphorylated and active in reticulocytes, therefore no further increase in phosphorylation results from *P. knowlesi* infection. In Chapter 3.2, we tested the effect of the B-Raf inhibitor SB-590885 on the asexual development of *P. falciparum* and *P. knowlesi* in human erythrocytes. This study revealed that both parasites are susceptible to B-Raf inhibition, with nanomolar IC50s recorded (Figure 3.6a). This indicates that although we do not have information on B-Raf phosphorylation status in erythrocytes infection with *P. knowlesi*, it is highly likely that B-Raf is phosphorylated based on the *P. falciparum* data and B-Raf inhibition study (Figure 3.5 and 3.6a). Taken together, the phosphorylation of B-Raf may have wider implications for other species of *Plasmodium*, as B-Raf/MAPK pathway activity may be critical for the development of these parasites in blood cells. *P. falciparum* can activate B-Raf in erythrocytes, and though not directly shown in this study, we propose that *P. knowlesi* also activates this pathway in these cells. As our data suggest, B-Raf is not further phosphorylated in *P. knowlesi* infection of reticulocytes; therefore, parasites such as *P. vivax*, which exclusively infect reticulocytes may be relying on host B-Raf signalling for development in these cells. Further exploration of B-Raf activity, especially in the context of *P. vivax* infection could help

understand why these parasites are not able to also develop successfully in erythrocytes. Furthermore, chemical activation of B-Raf is possible, therefore it would be interesting to see if this enabled *P. vivax* to develop within erythrocytes.

		Erythrocyte mean	Reticuclyte	
Protein	**Phospho Site (Human)**	**%Error**	**Fold change**	**%Error**
B-Raf	S446+S447	13	1.16	3
	S729	25	2.89*	2
	Pan-specific	30	2.13*	24
C-Raf	S296	10	1.50	9
	Pan-specific	30	1.25	7
	Pan-specific	49	1.43	16
MEK1	S298	10	1.00	6
	T292	4	1.01	9
	T386	4	1.08	4
	T386	9	1.17	7
	Pan-specific	24	1.02	10
	Pan-specific	24	1.16	2
MEK1/2	S218+S222	18	0.66	9
MEK2	T394	11	0.87	3
	T394	24	0.85	3
	Pan-specific	21	0.93	5
ERK1	T202	16	0.56	16
	T207	16	1.40	31
	Y204	9	0.60	17
	Y204	14	1.88*	1
	Pan-specific	12	0.93	6
	Pan-specific	9	1.18	12
ERK2	T185+Y187	14	1.35	1
	Pan-specific	7	1.47	14

* Signals outside of 2x standard deviation of erythrocyte mean

Table 4.5 – Traditional MAPK pathway elements, highlighting the differences between reticulocytes and erythrocytes.

All listed signals were not low-intensity signals, denoted by * are reticulocyte signals which were outside two standard deviations of the erythrocyte mean. Fold change values are coloured so that increases marked in yellow, decreases are marked in blue.

In the previous section, we outlined the similarities between B-Raf signalling in reticulocytes and *P. falciparum* infection of erythrocytes. To further this understanding, we compared the filtered datasets completed on *P. falciparum* and the comparison between erythrocytes and reticulocytes. Note this comparison used the four uninfected erythrocyte replicates for the *P. falciparum* datasets (unlike Chapter 3 which used only the three replicates present in the manuscript), to enable a direct comparison to the reticulocyte analysis complete in this chapter. This identified 73 phosphorylation-specific signals, displaying similarity to at least one of the five *P. falciparum* developmental stages tested, this table can be viewed in Appendix 5. Many of the kinases mentioned throughout this section were listed here, including B-Raf, DDR1/2, EGFR, FGFR3, KIT and VEGFR, together indicating roles for RTKs across *P. falciparum* development. The activation of RTKs, though usually through extracellular ligand binding, may be activated during *P. falciparum* infection through parasite directed remodelling of the host erythrocyte.

Of the 73 signals listed in Appendix 5, three were for the ribosomal S6 kinase 1 (RSK1) at the phosphorylation sites Ser363, Thr359 and S221. Ser363 and Thr359 are phosphorylated by ERK1/2 activity and are part of the sequence of phosphorylation that enables RSK1 activation [344]. For complete activation, RSK1 also requires phosphorylation by PDK1 at Ser221 [345]. All three of these phosphorylation sites were increased in erythrocytes infected with *P. falciparum* trophozoites. As previously discussed, ERK1/2 is phosphorylated on several residues in erythrocytes infected with *P. falciparum* ring-stage parasites, as were the upstream components of the MAPK pathway (Figure 3.5a). Additionally, though not a significant signal, PDK1 was more phosphorylated in erythrocytes infected with *P. falciparum* trophozoites, compared to uninfected erythrocytes (Supplementary Figure 1). Together this suggests that the MAPK pathway is activated during *P. falciparum* ring stage development before PDK1 activation (trophozoite stage) and the Ser221 phosphorylation, necessary for complete RSK1 activity. These same series of activations all appear to be more heavily phosphorylated in reticulocytes compared to erythrocytes (Table 4.5), suggesting that the same RSK1 pathway may be active. If this pathway is activated during *P. falciparum* development, it could indicate that the parasite is manipulating host cell signalling to make the infected erythrocyte more like a reticulocyte. Activated RSK1 has a multitude of downstream substrates, including transcription factors, cell cycle progression/proliferation, protein synthesis, cell survival and migration [346]. In the context of reticulocytes and erythrocytes, the function of RSK1 is unknown; however, upstream components of the MAPK pathway have been demonstrated to

protect erythrocytes from eryptosis (erythrocyte apoptosis) [347]. The MAPK pathway and its substrate RSK1 may therefore be activated during *P. falciparum* erythrocyte infection to keep the host cell alive during parasite development. Consequently, the ability to stimulate MAPK and RSK1 activity in erythrocytes could be one of the crucial steps for successful parasite development within erythrocytes.

4.3 Host cell signalling during *B. bovis* infection of bovine erythrocytes

Babesia bovis is a tick-borne intracellular parasite, which causes a large disease burden in cows and represents a significant threat to the global cattle industry. *B. bovis,* like *Plasmodium,* infects and replicates within erythrocytes of its mammalian bovine host and requires an intermediate arthropod vector for completion of its lifecycle. However, *B. bovis* erythrocytic development is highly divergent from that of *Plasmodium,* producing far fewer daughter cells and taking only hours for completion [111]. Despite this short development window, we hypothesised that interactions between the bovine host cell signalling and the parasite occur. No such interactions had been documented to date. An initial concern with using the antibody microarray for the study of bovine signalling elements was that the antibody set is specific for human signalling proteins. However, most of the regulatory phosphorylation sites on kinases are highly conserved throughout eukaryotes, as demonstrated by the application of this same array technique on the exploration of *Wolbachia* infection of mosquito cells [249]. Therefore, we suspected that given cows are more closely related to humans than mosquitos are, we would be able to detect the bovine signalling proteins with this approach.

There are also two further considerations for this study; (1) Although the continuous culture of *B. bovis* in host bovine erythrocytes is possible, there is no reliable way to synchronise the parasites, and (2) there is no published protocol to purify *B. bovis*-infected erythrocytes from uninfected cells. In *P. falciparum,* the capacity for magnetic purification is based on the built-up of hemozoin, a magnetic by-product during host cell hemoglobin digestion [348]. *Babesia* does also similarly digest host cell hemoglobin; however, there is no hemozoin generated [349]. Consequently, magnetic purification was not possible here. It has been proposed that *Babesia* more completely digests the host hemoglobin, eliminating the need to create and store hemozoin by-product during development [349]. Due to the aforementioned considerations, the array completed here compared a mixed culture of uninfected bovine erythrocytes and erythrocytes infected with unsynchronised *B. bovis* (50% parasitemia). This could have potentially dampened the signals derived from the parasitised cells, similarly to what was observed and discussed in the *P. knowlesi* section of this chapter (Chapter 4.1). Additionally, the unsynchronised *B. bovis* sample used could result in weaker phosphorylation levels of host signalling proteins, as some signalling events may occur only at specific stages of *B. bovis* development.

The sample of *B. bovis* was developed in collaboration with Professor Brian Cooke and his team from Monash University, Melbourne, Australia. His team generated the sample described above, and we lysed the cells, processed the lysate on the array and analysed the data. Similarly to human erythrocytes, bovine erythrocytes are enucleated and therefore do not undergo protein expression upon maturation. Therefore we focused on the phosphorylation-specific signals achieved using the antibody microarray. However, the pan-specific signals are available, along with the complete dataset in Appendix 4. To view the changes in phosphorylation of host signalling proteins during *B. bovis* infection, we generated a heatmap, where each pixel represents a single antibody on the array (Figure 4.4a). There were notably very few signals with fold change values greater than 2 recorded; these signals are listed in Figure 4.4b. This could be explained by the parasitemia and lack of synchronisation in the infected sample. Additionally, this could also be due to issues with antibody recognition of bovine proteins. Despite the low number of large fold changes recorded, Figure 4.4a does still illustrate that a number of dynamic phosphorylation changes occur during *B. bovis* infection of bovine erythrocytes.

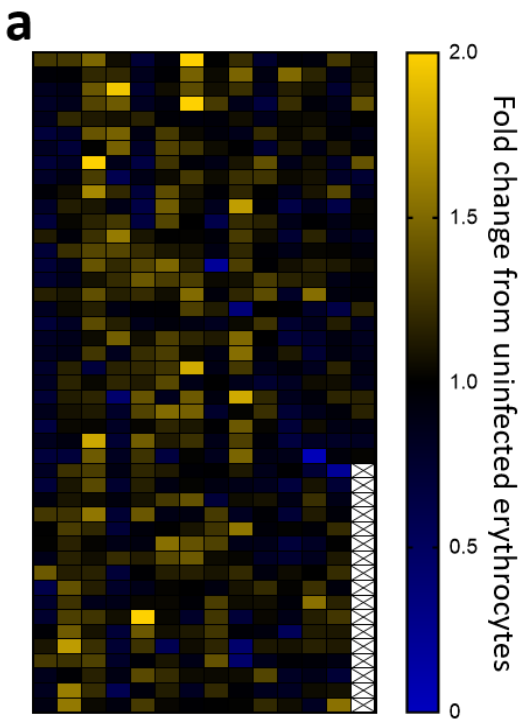

b

Protein	Phospho Site (Human)	Fold change
FRS2	Y348	27.3
CDK2	T160	2.5
IRS1	Y612	2.2
JAK1	Y1034	2.2

Figure 4.4 – Heatmap of antibody microarray data representing the changes in bovine erythrocyte phosphorylation during infection with *B. bovis*, and largest changes.

a) The infected sample included mixed development stages of *B. bovis* with a parasitemia of 50%. Each square represents the fold change in signal for one antibody on the array. The colour represents the change in abundance compared to the uninfected reticulocyte control. Blue squares indicate that the abundance of a specific phosphorylated kinase has decreased, yellow indicates an increase. All signals above a fold change of 2 are coloured as brightest yellow. **b)** Table of the signals represented in a, which had fold changes greater than 2 from the uninfected bovine erythrocyte control. Signals listed here are for the fibroblast growth factor receptor substrate 2 (FRS2) at Tyr348, cyclin-dependent protein kinase 2 (CDK2) at Thr160, the insulin receptor substrate 1 (IRS1) at Tyr612 and Janus kinase 1 (JAK1) at Tyr1034.

The signals presented in Figure 4.4 demonstrate that the microarray approach was able to detect bovine signalling proteins, with a number of differences in phosphorylation during infection recorded. Moving forward, we applied the low-intensity signal cut off to the *B. bovis* dataset, analogous to the *P. falciparum* datasets covered in the previous chapter and the *P. knowlesi* section of the current chapter (For full description see Chapter 3.2). Briefly, signals that displayed low intensity in both the control and parasite-infected samples were removed from further analysis; these signals are still available in Appendix 4. Due to time constraints and unlike for the studies on *Plasmodium*, we did not complete an array using saponin to determine which antibodies could be cross-reactive with *B. bovis* proteins. Given the above limitation, we

applied the *P. falciparum* cross-reactivity determination to the *B. bovis* dataset. However, instead of removing the signals identified, they were flagged and remained throughout the analysis (see Chapter 3.2 for a description of cross-reactivity determination). This provided an additional level of information, despite the possibility of inaccuracy due to species differences. In future experiments, saponin lysis could also be used for *B. bovis* infected erythrocytes to determine the cross-reactivity of antibodies more accurately.

Removal of low-intensity signals reduced the 613 phosphorylation-specific signals to 525. This equated to the removal of 88 signals and was in line with the average 98 low-intensity signals removed from the *Plasmodium* datasets. The datasets before and after signal removal were represented as a dot plot to visualise the effect this had on the signal distribution. Figure 4.5a displays the datasets before signal removal (left) compared to the signals after removal (right). Each dot represents one phosphorylation-specific signal on the array, in red is the median of the datasets. Completion of a Mann Whitney-U statistical test indicated that the signals removed did not significantly alter the data distribution (p=0.7909). Unlike the *P. knowlesi* dataset (Figure 4.2), there are outlier signals present in the *B. bovis* dataset, which displayed substantial differences in fold change during infection (Figure 4.5a). To further determine the perturbation of host cell signalling during *B. bovis* infection, we quantified the number of signals with fold changes above 2 and below 0.5 for the phosphorylation-specific signals (Figure 4.5b). Figure 4.5b lists these values as a percentage of the phosphorylation-specific signals (after removing the low-intensity signals). For *B. bovis,* only 0.8% of signals were above a fold change of 2, and 1.1% were below 0.5. Interestingly this is similar to the *P. knowlesi* dataset, which also compared a non-enriched population of parasites, yet so did the *P. falciparum* ring stage array. Unlike the *B. bovis* dataset, the *P. falciparum* ring stage data contained 15% of signals that met the above criteria. Moreover, the *B. bovis* dataset had a higher level of parasitemia than both the *P. knowlesi* and *P. falciparum* ring stage samples, illustrating that parasitemia of this sample is unlikely to have caused this discrepancy observed in Figure 4.5b. The difference observed could illustrate that unlike *Plasmodium spp., B. bovis* does not cause as many large changes to host cell signalling phosphorylation during infection (see Discussion).

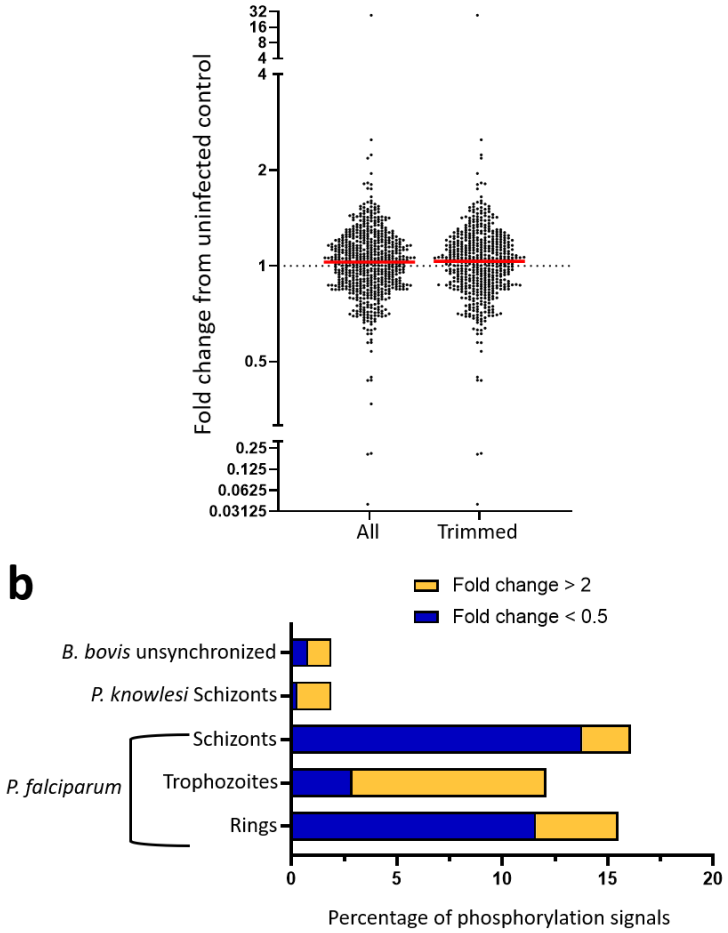

Figure 4.5 – Fold change in bovine erythrocyte signalling protein phosphorylation during infection with *B. bovis* and comparison of the largest phosphorylation changes across arrays complete.

a) Dot plot of the Phospho-specific signals before signal removal (left), and after signal removal (right). The median fold change is represented in red (1.028 and 1.033, respectively) (p = 0.7909, Mann-Whitney statistical test). Y-axis represented in a Log2 scale; note axis is split into three sections to give a clear distribution of signals. **b)** Comparison of phosphorylation-specific signals that were above a fold change of 2 or below 0.5 compared to their respective controls. *Plasmodium* asexual stage arrays and *P. knowlesi* array included here for comparison. Values represented as a percentage of the total signals after low-intensity, and cross-reactive signals were removed (removal of cross-reactive signals was not applied to the *B. bovis* dataset).

4.3.1 The most reliable host phosphorylation changes during *B. bovis* erythrocytic infection

To further assess the 525 viable signals, we took into consideration the total error for each signal compared to the %CFC during infection. This system was applied to the *P. knowlesi* dataset (section 4.2) for more details on this system see Section 4.2.1. In brief, the most reliable signals are ranked as Category 1 (total signal error<10% of the %CFC during infection), with Category 2 signals as the next most reliable (total signal error <25% of the %CFC during infection). We compiled the identified Category 1 and 2 signals for the *B. bovis* dataset into Table 4.6. Three signals achieved a rank of Category 1; these were FRS2 (Tyr348), CDK1/2 (Tyr15) and CDK9 (Ser347). Both Category 1 CDK signals were flagged as cross-reactive to *P. falciparum*, therefore may also be cross-reactive in this dataset. Additionally, CDK1/2 appears four times in Table 4.6 (highlighted pink). Both CDK1 and 2 are important triggers for the transition from interphase to mitosis [350]. Additionally, CDK2/4 play a role in cell cycle regulation of erythroblasts, which is linked to erythrocyte size; however, to date, there has been no reported function of CDKs in mature erythrocytes [351]. Sequence alignment (not shown) of human CDK1/2 with the *B. bovis* equivalents indicated 46% identity to *B. bovis* CDK1 and 62% identity for *B. bovis* CDK2. The reported functions of CDKs in human cells and the level of conservation with *B. bovis* CDKs make it unlikely that bovine CDKs are activated here. Instead, it is more likely that we have detected the CDKs encoded by *B. bovis*. Therefore, these antibodies could be re-purposed in the future to study the function of *B. bovis* CDKs, due to their cross-reactivity.

Protein	Phospho Site (Human)	Fold change	Category	Cross-reactive signal
FRS2	Y348	27.3	1	no
CDK1/2	Y15	1.4	1	yes
CDK9	S347	1.4	1	yes
CDK2	T160	2.5	2	no
DNAPK	Y883	2.0	2	no
CDK5	Y15	1.6	2	yes
CDK1	T161	1.6	2	no
EGFR	Y1172	1.6	2	yes
OSR1	T185	1.5	2	no
Huntingtin	S421	1.5	2	no
CDK1/2	T14+Y15	1.5	2	yes
ITK	Y512	1.5	2	no
CLK1	S337+T338	1.4	2	no
DOK3	Y398	1.4	2	no
MSK1	S212	1.4	2	no
PIK3R1	Y580	1.4	2	no
GSK3a	S278+Y279	1.3	2	no
PKCa	T497	1.2	2	no
PDLIM5	Y251	1.2	2	no
WASP	Y291	0.84	2	yes
MKK3	Y230	0.70	2	no
ACTB	Y53	0.69	2	yes
AMPKa1	T183+S184	0.68	2	yes
ALK	Y1096	0.66	2	yes

Table 4.6 – Largest changes in host signalling protein phosphorylation during *B. bovis* infection of bovine erythrocytes.

The signals listed here represent the fold change from the uninfected bovine erythrocyte control, yellow indicates an increase during infection, blue a decrease. All signals listed here ranked as Category 1 (highlighted in green) and 2, see above text for the determinate for each category ranking. Cross-reactivity column states if the antibody showed reactivity to *P. falciparum* proteins. Highlighted in pink are CDK1/2 as they appeared multiple in this table.

4.3.1.1 The phosphorylation of fibroblast growth factor receptor substrate 2 (FRS2) during infection with erythroid lineage infecting Apicomplexan parasites

Phosphorylation of FRS2 at Tyr348 was a prominent signal in the *P. knowlesi* dataset (Table 4.1) with a fold change of 2.1, indicating higher levels of phosphorylation in *P. knowlesi* infected reticulocytes and for *B. bovis* dataset (Table 4.6) with a fold change of 27.3, indicating a higher level of phosphorylation in *B. bovis* infected bovine erythrocytes. FRS2 Tyr348 is also more phosphorylated in reticulocytes compared to erythrocytes, suggesting the molecule may be active in these cells before infection (Appendix 2). FRS2 is a scaffold adapter protein which localises to the inner plasma membrane of cells [352]. The localisation at the membrane enables FRS2 to bind specifically to a set of RTKs through a phosphotyrosine binding domain (PTB) and to amplify their signals [353]. FRS2 binds to the following RTKs; FGFR, the neurotrophin receptor (Trk), RET, EGFR, and ALK [354-358]. Interestingly, FRS2 can bind to FGFR before the receptor is activated, while binding to Trk, RET, EGFR and ALK are all dependent on receptor activation before recruitment [354-358]. Once docked, phosphorylation of FRS2 occurs following activation of the bound RTK, which results in six unique tyrosine phosphorylations, the first four of which are Tyr196, Tyr306, Tyr349 (Tyr348 on the array) and Tyr392 [333]. The receptor-bound protein 2 (Grb2), another adapter molecule, recognises and binds FRS2 at these four tyrosine phosphorylation sites. Grb2 is constitutively bound to Son of sevenless (SOS), Casitas B-lineage lymphoma (Cbl) and GRB2-associated protein 1 (Gab1) and therefore the FRS2-Grb2 complex has multiple downstream signalling functions (Figure 4.6) [353]. FRS2-Grb2-SOS complex results in signalling through Ras, into the MAPK pathway. FRS2-Grb2-Gab1 recruits and enables signalling into the PI3K-Akt pathway, and FRS2-Grb2-Cbl signals for FRS2 and the bound RTK for ubiquitination and degradation [353]. The remaining two tyrosine phosphorylation sites on FRS2, Tyr436, and Tyr471, recruit the SH2 containing protein tyrosine phosphatase (Shp2) [333, 359]. The FRS2-Shp2 complex results in Shp2 phosphorylation and subsequent activation of Ras and the MAPK pathway [333, 360]. Activation of the MAPK pathway and ERK activation causes phosphorylation of FRS2 at multiple threonine residues inhibiting the adapters signalling in an inhibitory feedback loop [353, 361]. A schematic representation of the interactors of FRS2 and their downstream functions are represented in Figure 4.6.

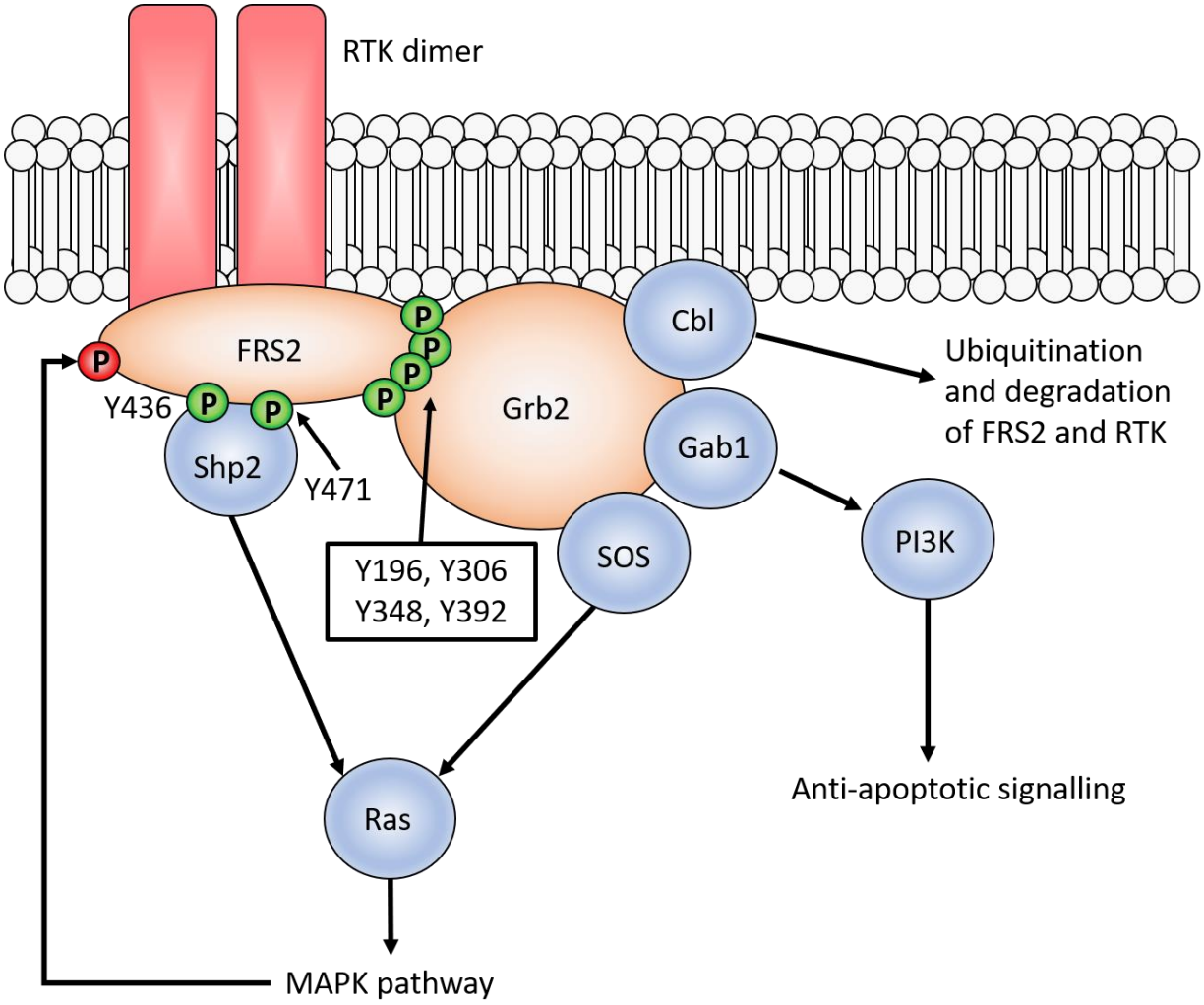

Figure 4.6 – Schematic representation of the signalling molecules involved with FRS2.

Red illustrates a receptor tyrosine kinase (RTK) dimer, in orange is FRS2 as well as Grb2 as they are both adapter molecules. In the blue circles are signalling molecules downstream of the RTK dimer/adapter complex. Phosphorylation sites of FRS2 are listed with the known tyrosine phosphorylation sites denoted. Green 'P's' indicates that the tyrosine phosphorylation site results in activation, while the red 'P' indicates inhibition of FRS2 by phosphorylation with ERK.

The Kinexus antibody array used in these studies only contained a single antibody to FRS2, which was specific to Tyr348 phosphorylation. The summary of these phosphorylation changes across the erythroid-infecting Apicomplexan parasites examined in this thesis is presented in Table 4.7. Notably, there is a large increase in FRS2 Tyr348 phosphorylation in *P. falciparum*-infected erythrocytes at the trophozoite stage of development (fold change = 2.5) and during male gametocyte infection (fold change = 1.9), *P. knowlesi* infected reticulocytes at the schizont stage of development (fold change = 2.07) and the largest change in *B. bovis* infected bovine erythrocytes (fold change = 27.32). In the *P. falciparum* ring, schizont, and female samples, FRS2 phosphorylation was reduced (Fold change = 0.35, 0.06 and 0.64 respectively). However, there was a high level of error associated with the uninfected erythrocyte signal mean, as well as the *P. falciparum* female gametocyte signal. This makes interpretation of these signals more difficult as the error could account for the fold change observed. Despite the error on the uninfected erythrocyte mean, both the trophozoite and reticulocyte signals for FRS2 Tyr348 were identified as significant changes.

For the *B. bovis* and *P. knowlesi* datasets, FRS2 phosphorylation at Tyr348 was one of a shortlist of signals that had fold changes above 2 during infection of their respective host cells (Table 4.1 and 4.4). One of the commonalities between these two samples was that both used non-enriched parasites in their comparisons (*P. knowlesi* 10% parasitemia, *B. bovis* 50% parasitemia). However, the similarity in FRS2 phosphorylation was not shared by the *P. falciparum* ring stage data (33% parasitaemia), which was also a non-enriched population of parasites, although this could be a consequence of the high error associated with these signals (uninfected erythrocyte mean error 428% and ring stage error 81%, Table 4.7). As a consequence of the high error values for the *P. falciparum* ring stage data, we focused on the *B. bovis* and *P. knowlesi* FRS2 signal. Interestingly the phosphorylation of FRS2 in these samples could be the result of the uninfected co-cultured cells, rather than the parasitised cells, and therefore may represent an effect of being exposed to the metabolic waste or secreted elements of these parasites. Apart from the inclusion of bystander cells in the samples analysed, there was no other obvious connection between these two parasites. These co-cultured, parasite exposed cells will be referred to as bystander cells in the following discussion. We also attempted to determine what the function of FRS2 was in these cells; however, due to the numerous downstream effects that FRS2 has on signalling (Figure 4.6), we were unable to identify a conserved signalling pathway present in both datasets.

		Erythrocyte mean	Comparison	
Parasite/cell	**Development stage**	**% error**	**Fold change**	**% error**
P. falciparum	**Ring**	428	0.35	81
	Trophozoite		2.50 *	17.2
	Schizont		0.06	13
	Female		0.64	1532
	Male		1.90	22
Reticulocyte	**-**		2.45 *	17

		Reticulocyte	Comparison	
Parasite	**Development stage**	**% error**	**Fold change**	**% error**
P. knowlesi	**Schizont**	17	2.07	1

		Bovine erythrocyte	Comparison	
Parasite	**Development stage**	**% error**	**Fold change**	**% error**
B. bovis	**unsynchronised**	117	27.32	18

* Signals outside of 2x standard deviation of erythrocyte mean

Table 4.7 – Summary table for the fold change values of FRS2 Y348 during infection with the Apicomplexan parasites tested in this thesis that infect erythroid lineage cells.

Values are represented in fold change from the respective uninfected control. All listed signals were not low-intensity signals or flagged as cross-reactive. Denoted by * are signals which were outside two standard deviations of the erythrocyte mean (not applicable to the *P. knowlesi* or *B. bovis* datasets). Fold change values are coloured so that increases are marked in yellow; decreases are marked in blue.

Data validation of FRS2 phosphorylation during erythrocyte infection with *P. falciparum* and *B. bovis*

The consistency in FRS2 phosphorylation across multiple Apicomplexan parasites, and the possibility that we had detected a bystander signalling pathway prompted us to further validate FRS2 phosphorylation during infection with *B. bovis*. Additionally, we also sought to determine if FRS2 was phosphorylated in *P. falciparum* infection, as the error associated with the FRS2 Tyr348 signal in Table 4.7 made it difficult to interpret its phosphorylation status. We hypothesised that FRS2 phosphorylation was the result of the bystander cells in the infected culture. The array data presented in Table 4.7 was exclusively for FRS2 Tyr348 phosphorylation. Unfortunately, this antibody was discontinued by the manufacturer, and therefore unavailable. No other commercial antibody specific for FRS2 Tyr348 phosphorylation exists to the best of our knowledge. Due to the extensive time and monetary investment into generating a phosphorylation-specific Tyr348 antibody, we chose to instead look for FRS2 activity by determining the phosphorylation status of Tyr196, as antibodies to this phosphosite are commercially available. Phosphorylation of Tyr196 and Tyr348 leads to the binding of Grb2; therefore, we believed it to be a good substitute for investigating Tyr348 phosphorylation. However, no published data indicates that these two sites are always phosphorylated together, nor is there data suggesting differential phosphorylation. We aimed to test our hypothesis by immunoblotting, with the expectation that if we were indeed seeing a bystander effect then uninfected erythrocytes cultured in the spent media of infected cells, would have higher levels of phosphorylation on FRS2 at Tyr196.

The Kinexus arrays used in this study did not include a pan-specific antibody for FRS2; therefore, we did not know if levels of FRS2 protein changed during infection. To begin validation of FRS2 phosphorylation, we first determined if we could detect human and bovine FRS2 in erythrocytes by Immunoblotting (Figure 4.7). FRS2 has a mass of 57kDa and is reported to migrate through SDS-PAGE with an apparent MW of 80kDa [362]. A distinct band of approximately 75kDa was observed in the uninfected and *P. falciparum*-infected human erythrocytes. However, there was no band detected in the uninfected bovine erythrocyte sample tested. Due to time limitations, a sample of *B. bovis* infected erythrocytes was not available for analysis. Sequence alignment between human and bovine FRS2 indicates approximately 98% sequence identity. However, the bovine sequence for FRS2 is unreviewed and based on protein prediction.

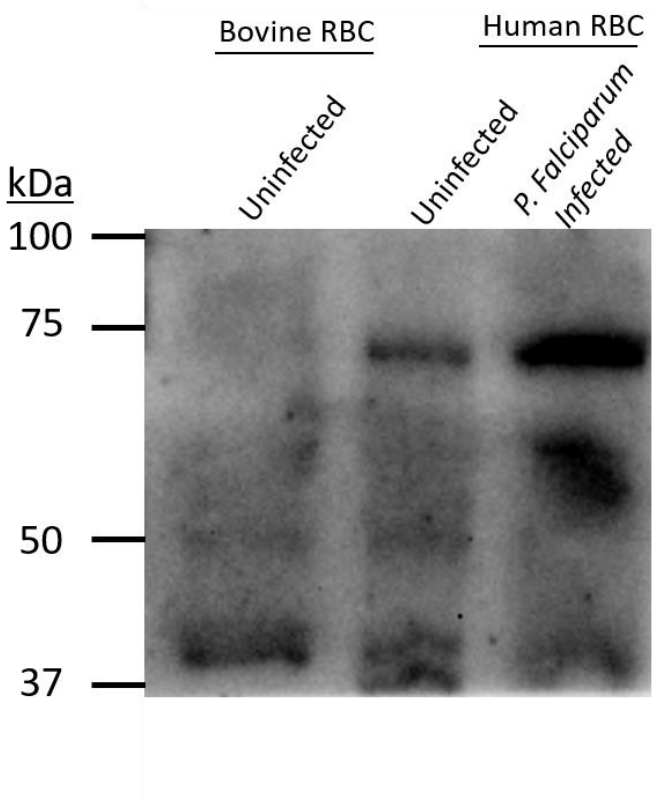

Figure 4.7 – Western blot Identification of FRS2 in uninfected and *P. falciparum*-infected human erythrocytes.

Lanes from left to right: uninfected bovine RBCs, contains a total lysate of uninfected bovine erythrocytes. Uninfected human erythrocytes (total lysate). Human erythrocytes infected with *P. falciparum* (total lysate). Blot incubated with a pan-specific monoclonal FRS2 antibody, incubated as per Table 2.1. Band detected at approximately 75kDa is the expected size of FRS2 (seen in both human samples).

Despite the inability to detect bovine FRS2 using a pan-specific antibody (Figure 4.7), we moved forward and probed with an FRS2 Tyr196 phosphorylation-specific antibody, as phosphorylation sites are often the most conserved regions of proteins [363]. We hypothesised, based on the results of the arrays, that FRS2 phosphorylation occurs in bystander cells. To test this, we extracted the used media from a *B. bovis* infected culture (48 hours of growth in said media) and applied multiple rounds of high-speed centrifugation to remove all cells from the media. This media was placed onto fresh uninfected bovine erythrocytes for 24 hours before cell lysis and extract analysis via Immunoblotting. Additionally, the human erythrocyte samples from Figure 4.7 and a lysate of synovial sarcoma cells (Aska-SS) [364] were run alongside the bovine samples to help identification of FRS2 (Figure 4.8). The expected 75kDa band of FRS2 seen in Figure 4.7 (red arrow) was only detected in the Aska-SS lane (Figure 4.8). Due to limited antibody quantity at the time we were unable to continue optimisation of this Western blot further. Therefore, the Tyr196 could still be phosphorylated in bovine

erythrocytes, despite our inability to detect it here. The *P. falciparum* sample used in this experiment contained purified trophozoites, which demonstrated a fold change of 2.5 in FRS2 phosphorylation at Tyr348 (Table 4.7) that was not detected here (Blue arrow). This could be due to the limited optimisation of this Western blot. Alternatively, the error values detected on the array for *P. falciparum* were high (Table 4.7); therefore, FRS2 may not be phosphorylated during infection of *P. falciparum* trophozoites. In the bovine samples, only one band was detected, which was at approximately 50kDa (Green Arrow). FRS3, a structurally similar protein to FRS2, has been found to migrate in SDS-PAGE gels at approximately 50-60kDa [365]. FRS3 also contains multiple tyrosine phosphorylation sites, used for Grb2 docking [353], and the sites are very similar in FRS2 (EEQVHT**Y**VNTTG) and FRS3 (DESHTYVNTPA) (phosphorylation site in bold; identical residues underlined). Therefore, we may have detected bovine FRS3 in the bovine sample here. Interestingly this 50kDa band is more prominent in the cells incubated with spent media; therefore, if it is indeed FRS3, this could indicate bystander specific phosphorylation. In future studies, a pan-specific FRS3 antibody should be sourced/generated to confirm the identity of the 50kDa band seen in Figure 4.8. If successful, longer incubations using spent media on bovine erythrocytes should be considered to determine if the phosphorylation of FRS3 is linked to the duration of exposure. Additionally, FRS2 was detected in human erythrocytes, and therefore should be considered for further validation. Also, an experiment using spent *P. falciparum* media on uninfected human erythrocytes would prove valuable in the assessment of the bystander effect proposed in this Chapter. Furthermore, generating an FRS2 Tyr348 phosphorylation-specific antibody would be highly valuable for the validation of the signals seen across the Kinexus arrays on *Plasmodium* and *B. bovis,* and would complement the results for FRS2 Tyr196 phosphorylation presented here.

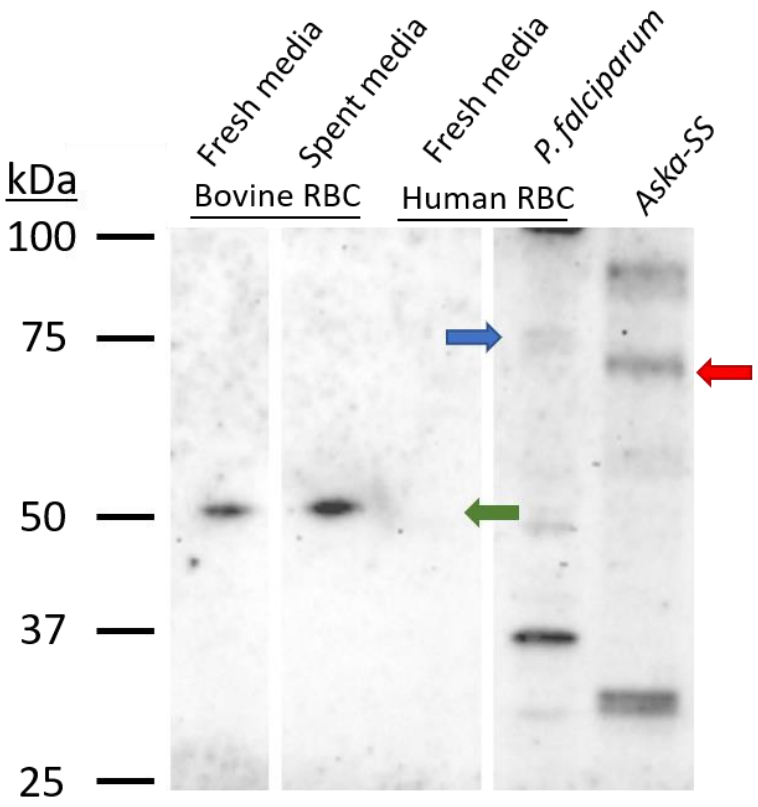

Figure 4.8 – Western blot attempt using FRS2 phosphorylation specific antibody (Tyr196) on uninfected bovine erythrocytes and uninfected human erythrocytes and erythrocytes infected with *P. falciparum*.
All panels originate from the same Western blot membrane, detected together. Lanes from left to right are as follows: (1) uninfected bovine erythrocytes cultured for 24 with fresh media. (2) Uninfected bovine erythrocytes culture for 24 hours in *B. bovis* spent media. (3) Uninfected human erythrocytes, no bands detected; however, the same sample was used in Figure 4.7 lane two indicating that there is indeed sample in this lane. (4) human erythrocytes infected with P. falciparum trophozoites. (5) Synovial sarcoma cells. An FRS2, Tyr196 phosphorylation-specific polyclonal antibody was used. Correct band detected in (5). Potentially FRS3 detected in (1) and (2). Red arrow – expected FRS2 size. Blue arrow – possible FRS2 approximately 75kDa in lane 4. Green arrow – possible FRS3 detection.

4.4 Host cell signalling during *Toxoplasma gondii* tachyzoite development

The previous sections of this chapter looked more broadly at Apicomplexan parasites, which infect host erythroid cells. Many different Apicomplexan parasites infect various host cell types; most are very restrictive in their host cell type, while others, such as *T. gondii* are less so. *T. gondii* can infect virtually all nucleated cells of warm-blooded animals. One of the well-known ways *T. gondii* manipulates host cell signalling is through its secreted ROP proteins. One example of this is ROP16, which translocates into the host cell nucleus and interferes with host cell STAT3/6 signalling [235, 236]. *T. gondii* has also been shown to interrupt IFN-γ driven activation of JAK/STAT1 phosphorylation [238]. To comprehensively investigate host cell signalling in this context, we completed an array which compared *T. gondii* infected human foreskin fibroblasts with an uninfected fibroblast control. A high level of parasitemia was achieved by exposing host cells to *T. gondii* tachyzoites at a multiplicity of infection (MOI) of 5:1 for six hours. Cells were then lysed and analysed via antibody-microarray. The *T. gondii* sample analysed here was produced in collaboration with Dr Giel Van Dooren and his team at ANU, Canberra, Australia. I travelled to Canberra to process the samples for the microarray, and later analyse the dataset created.

This is the first study in this thesis that includes a nucleated host cell; therefore, transcription and translation during infection can enable fluctuation in host signalling protein abundance. The pan-specific signals from this array were included throughout this section as they may represent the host cells response to infection or *T. gondii* manipulation of host protein expression. To visualise the overall changes in protein expression and phosphorylation, we represented the microarray results as a heatmap (Figure 4.9). Notably, there are a large number of increases and decreases in fold change for both protein expression and phosphorylation during *T. gondii* infection. This may be due to the more dynamic capacity for nucleated cells to respond during infection.

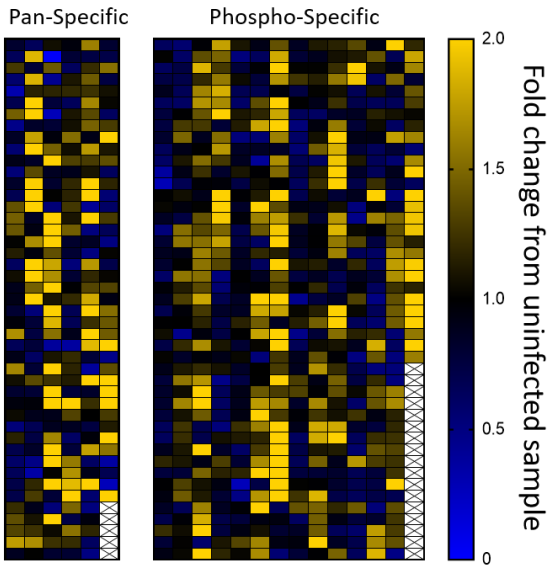

Figure 4.9 – **Heatmap of antibody microarray data representing the changes in human foreskin fibroblast protein expression and phosphorylation during infection with *T. gondii.***

Pan-specific signals (left), phosphorylation-specific signals (right), each square represents the fold change in signal for one antibody on the array. The colour represents the change in abundance compared to the uninfected control. Blue squares indicate that the abundance of a specific kinase or phosphorylated kinase has decreased, yellow indicates an increase. All signals above a fold change of 2 are coloured as brightest yellow.

Similar to the other datasets presented in this thesis, low-intensity signals were removed from the *T. gondii* dataset as they were deemed unreliable (See chapter 3.2 for more details). This resulted in the removal of 47 pan-specific signals and 132 phosphorylation-specific signals. Note, unlike the studies on *Plasmodium*, due to time limitations; we did not complete an array to determine which antibodies could be cross-reactive with *T. gondii* proteins. Given the above limitation, we applied the *P. falciparum* cross-reactivity determination to the *T. gondii* dataset, as was done for *B. bovis* dataset. However, instead of removing the signals identified, they were flagged and remained throughout the analysis (see Chapter 3.2 for a description of cross-reactivity determination). This provided an additional level of information, despite the possibility of inaccuracy. The pan- and phosphorylation-specific signals which passed low-intensity signal filtering are represented as a dot plot to visualise the distribution of the *T. gondii* dataset (Figure 4.10a). In both the pan and phosphorylation-specific signal sets, the largest outlier signals were removed due to low signal intensity. Also, the low-intensity signals did not significantly change the distribution of the pan-specific ($p=0.2158$) or phosphorylation-specific ($p=0.3467$) signals (Mann-Whitney U statistical test). Overall the distribution of the pan-specific signals is slightly skewed above a fold change of 1, while the phosphorylation-specific signals were more evenly distributed around 1, suggesting increased host protein expression,

while more dynamic phosphorylation changes. Comparisons of the signals with fold changes above 2 or below 0.5 indicate that *T. gondii* infection resulted in substantially higher levels of host signalling protein phosphorylation (Figure 4.10b). In the context of the other arrays conducted in this study, the *T. gondii* data is unique as there were few signals with fold changes below 0.5, and yet many signals above a fold change of 2. This indicates that a large number of host signalling proteins are heavily phosphorylated during infection, suggesting major changes to the host signalling network.

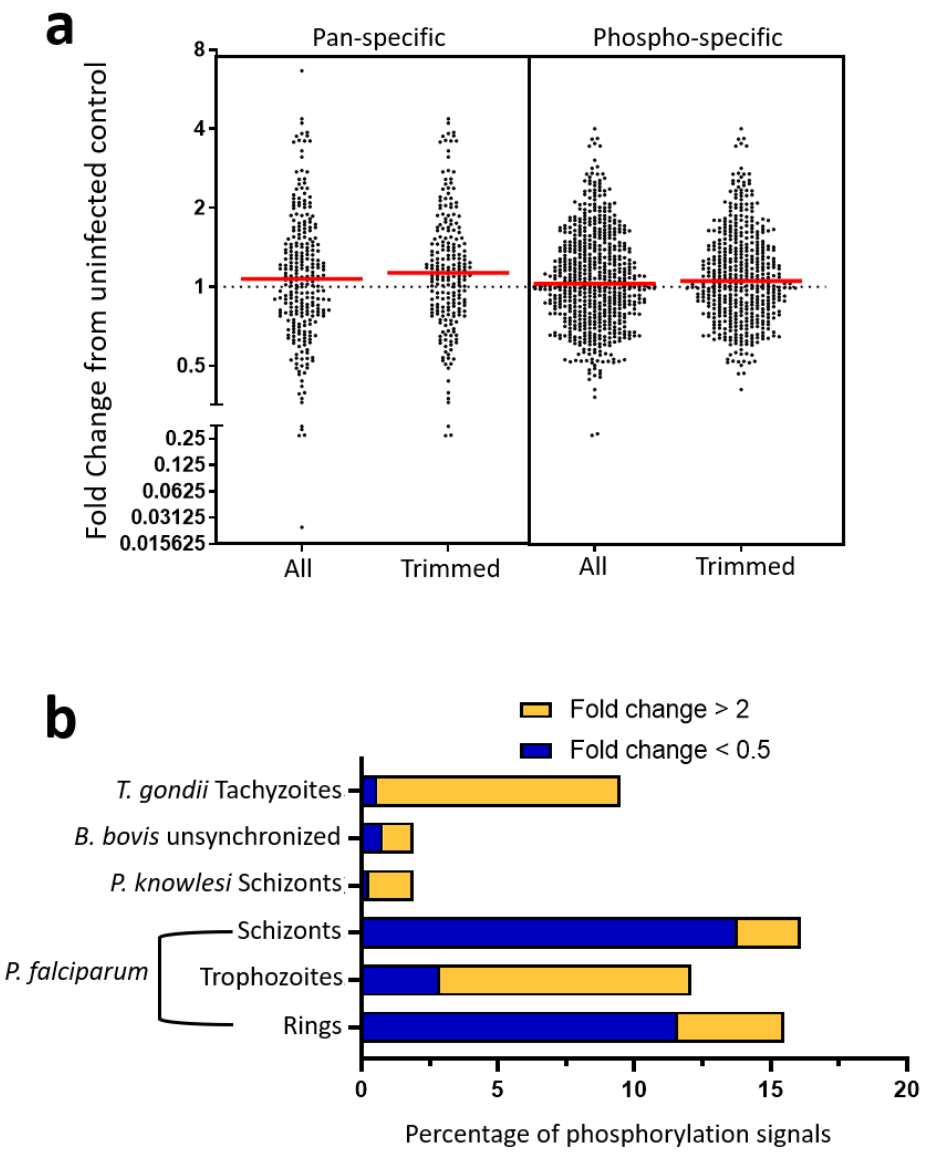

Figure 4.10 – Fold changes in fibroblast signalling protein abundance and phosphorylation during infection with *T. gondii* and comparison of the largest phosphorylation changes across arrays complete.

a) Dot plot of the Pan-specific and Phospho-specific signals before low-intensity signal removal (left), and after signal removal (right). The median fold change is represented in red for the Pan-specific signals (1.071 and 1.131, respectively, p = 0.2158, Mann-Whitney statistical test) and the phosphorylation-specific signals (1.027 and 1.053, respectively, p=0.3467, Mann-Whitney statistical test). Y-axis represented in a Log2 scale; note axis is split into two sections to give a clear distribution of signals. **b)** Comparison of phosphorylation-specific signals during *T. gondii* infection that were above a fold change of 2 or below 0.5. *Plasmodium* asexual stage, *P. knowlesi* and *B. bovis* arrays included here for comparison. Values represented as a percentage of the total signals after low-intensity, and cross-reactive signals were removed (removal of cross-reactive signals was not applied to the *B. bovis or T. gondii* datasets).

4.4.1 The most reliable host signalling expression and phosphorylation changes during *T. gondii* infection

To determine which of the remaining signals were the best leads moving forward, we further took into consideration the total error associated with each signal (see Section 4.2.1 for full description). The results of this analysis produced a number of Category 1 signals (total error <10% of the %CFC), which were compiled into Table 4.8; note the same inclusion of the cross-reactivity column as seen in the *B. bovis* analysis (for more details on this inclusion see Section 4.3.1). All of the signals, including those flagged as cross-reactive and those with low-intensity, are available in Appendix 4. Several of the phosphorylation-specific signals ranked as Category 1 during *T. gondii* infection. The largest changes were observed for the lysine deficient protein kinase 1 (WNK1) at Thr60 and the liver kinase B1 (LKB1) at Ser31 (fold change of 3.7) (Table 4.8). For the pan-specific signals, the lymphocyte-specific protein tyrosine kinase (LCK) had the largest fold change (4.4); however, this signal was flagged as cross-reactive to *P. falciparum* proteins and therefore may be cross-reactive to *T. gondii* proteins. Sequence alignment of the human LCK protein against the proteome of *P. falciparum* and *T. gondii* produce one notable alignment for each parasite. For *P. falciparum*, this was a TKL protein kinase (sequence ID: KNC37210.1) which contained 25% identity to the 272 amino acids at the carboxyl-terminal. For *T. gondii* this was a CAM kinase SNF1/AMK1 family *T. gondii* kinase (sequence ID: PUA87269.1) which contained 26% sequence identity to the 253 amino acids at the carboxyl-terminal. Unfortunately, we do not have access to the Pan-specific LCK antibody epitope information to confirm it was raised against this region of LCK; however, the mentioned parasite proteins are likely cross-reacting with this antibody. Table 4.8 also lists two independent pan-specific antibodies against the vascular endothelial growth factor receptor 2 (VEGFR2), also known as KDR, that indicated fold changes above 2.5.

Phosphorylation-specific

Protein	Phospho Site (Human)	Fold change	Cross-reactive signal
WNK1	T60	3.7	no
LKB1	S31	3.7	no
PDLIM5	Y251	2.5	no
DDR2	Y736	2.5	no
PKCq	S695	2.4	no
SMC1	S957	2.2	no
HSP90AB1	Y484	2.1	no
YES	Y222+Y223	2.0	no
VIM	Y117	1.9	no
PIK3R1	Y580	1.9	no
KHS1	S174	1.8	no
CDK12	S383+S385	1.7	yes
JUN	S73	1.5	no
MKK3	Y230	1.3	no
ErbB3	Y1307	1.2	no
eIF4B	S422	0.51	yes

Pan-specific

Protein	Phospho Site (Human)	Fold change	Cross-reactive signal
LCK	Pan-specific	4.4	Yes
IKKa	Pan-specific	3.7	no
JNK1	Pan-specific	3.6	no
HSP90a/b	Pan-specific	3.3	yes
VEGFR2	Pan-specific	3.1	no
VEGFR2	Pan-specific	2.5	no
AKT2	Pan-specific	1.5	yes

Table 4.8 – Largest and most reliable changes in host cell signalling during *T. gondii* infected human foreskin fibroblasts.

The signals listed here are all ranked as Category 1 with the phosphorylation-specific signals (left), and the pan-specific signals (right) presented separately. Highlighted in green is VEGFR2 as it appears twice in the same table. Cross-reactivity column determines if the antibody showed cross-reactivity to the *P. falciparum* proteins specifically. Fold change values are coloured so that increases marked in yellow, decreases are marked in blue.

4.4.2 VEGFR2, the PAK4 to cofilin pathway, and their roles in actin reorganisation during infection with *T. gondii*

VEGFR2 is a receptor tyrosine kinase, whose natural ligand is the vascular endothelial growth factor (VEGF). Ligand binding and activation of VEGFR2 occurs through trans-autophosphorylation, which promotes angiogenesis and vascular permeability [366]. VEGFR2 is primarily expressed in the vascular system, although there are reports of lower expression in many other cell types, including fibroblasts [367, 368]. Increased expression of VEGFR2 occurs during hypoxic conditions, and during angiogenesis, however, its roles during infection are not well understood [367]. In infection with other intracellular pathogens such as the human cytomegalovirus (HCMV) and *Leishmania major*, host VEGFR2 expression increases [369-371]. In *L. major* infection, increased VEGFR2 expression is thought to be a key factor in the inflammatory pathology seen in leishmaniasis [371].

VEGFR2 is understood to be phosphorylated at the following tyrosine phosphorylation sites 1054, 1059, 951, 1175 and 1214, and utilises molecules such as Grb2, Gab1 and Shp2 to provide a large diversity of downstream signalling [372]. The listed phosphorylation sites have the following functions. Tyr1054 and Tyr1059 are known auto-phosphorylation sites critical for VEGFR2 kinase activity [373]. Tyr951 is a binding site for VEGF receptor-associated protein (VRAP) and is involved in endothelial cell migration and angiogenesis [374]. Tyr1175 recruits PLCγ and results in ERK1/2 activation and proliferation [375], Tyr1175 can also activate the PI3K/AKT pathway, for pro-survival signalling [376]. Lastly, Tyr1214 is involved in actin remodelling through CDC42 and p38 MAPK activation [377]. The Kinexus array contained antibodies specific for Tyr1059, Tyr1054 and Tyr1214, of which only Tyr1214 passed the low-intensity signal threshold (Appendix 4). Tyr1214 produced a fold change of 3.4 (Category 2) during *T. gondii* infection and indicates that p38 MAPK and actin-associated signalling is likely to be increased. The p38 MAPK signals on the array were for the most part below the low-intensity threshold, which makes interpretation difficult. However, there was an increase in p38β pan-specific signal during infection, with an average fold change 2 (See Appendix 4). The infected fibroblast sample used in this experiment contained *T. gondii* parasites between 0 – 6 hours post-invasion. Consequently, many of the host signalling pathways may not yet have been activated and therefore, it would be interesting to see if p38 MAPK phosphorylation occurred later during parasite development. The inhibitor Sunitinib, which targets VEGFR2 was explored in a larger RTK inhibition study with *T. gondii* [369]. Sunitinib was demonstrated to be ineffective at killing intracellular *T. gondii* [369].

Consequently, the increased expression of VEGFR2 observed in Table 4.8 could indicate a host-mediated response to infection or pathway redundancy exists with another pathway.

As VEGFR2 Tyr1214 phosphorylation appeared to increase during *T. gondii* infection, other actin-associated signalling pathways were explored and enabled the identification of the PAK4/cofilin pathway. During *T. gondii* infection PAK4 phosphorylation of Ser474, a well-known auto-phosphorylation site, was increased. PAK4 is one of six PAK isoforms in humans, which serve unique, and in some instances overlapping functions. One of the overlapping functions between PAK1 and PAK4 is the phosphorylation of LIM domain kinase 1 (LIMK1) at Thr508 [378-380]. Phosphorylation at Thr508 activates LIMK1, which in turn, phosphorylated cofilin1/2 on Ser3 [381]. Cofilin is an actin-binding protein, responsible for depolymerising of actin filaments. LIMK1 phosphorylation of cofilin results in the inactivation of cofilin, which in turn stabilises the actin cytoskeleton (Figure 4.11) [382]. The *T. gondii* dataset indicated that each of the phosphorylations mentioned above was increased during infection; PAK4 Ser474 (fold change = 2.8), LIMK1 Thr508 (fold change = 2.1) and Cofilin1/2 Ser3 (fold change = 1.2 and 1.7 respectively) (Figure 4.11). However, each of these signals was ranked as either Category 3 or 4, indicating that error could account for a significant proportion of this change. This is not the first reported manipulation of cofilin phosphorylation during infection. The measles virus and HIV both phosphorylated cofilin on Ser3 to aid in viral replication [383, 384]. More broadly, manipulation of the host cells cytoskeleton is quite common and aids intracellular pathogens in a number of ways, including; host cell invasion [385, 386], for structural support of the pathogen [387] and to create an isolated niche for replication [388]. Notably, Cofilin was also more phosphorylated across the *P. falciparum* developmental stages covered in Chapter 3; however, cross-reactivity made interpretation difficult (Supplementary Figure 1). During the invasion process, *T. gondii* secrets a cofilin-like molecule, toxofilin, which induces host actin depolymerisation and facilitates parasite invasion [389]. Interestingly, no obvious role of toxofilin beyond invasion has been reported [390]. In our study, *T. gondii* was at 0 - 6 hours post-invasion, and therefore, some of the host cells may have very recently been infected, where toxofilin is actively breaking down host actin filaments. Therefore, phosphorylation of host cofilin may represent a host cell response in an attempt to reduce the de-polymerisation of actin.

Protein	Phospho Site (Human)	Fold change	Category	Cross-reactive signal
PAK4	S474	2.8	3	no
LIMK1	T508	2.1	3	no
	Pan-specific	0.79	4	yes
Cofilin 1	S3	1.2	4	yes
	Pan-specific	0.84	4	yes
Cofilin 2	S3	1.7	3	yes

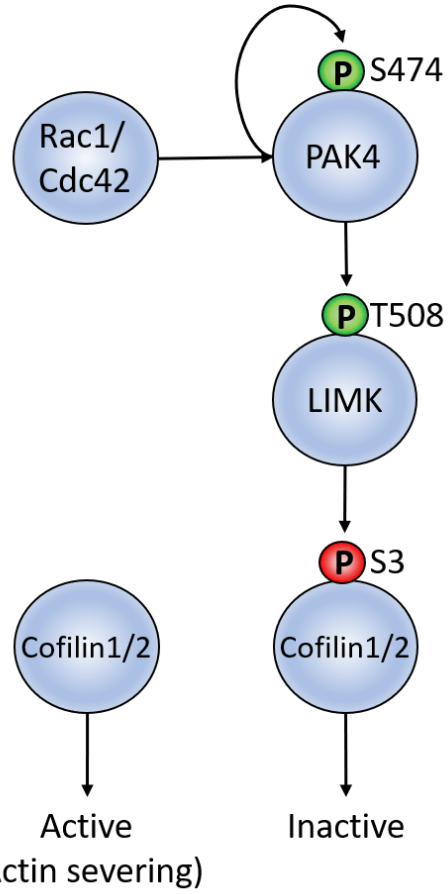

Figure 4.11 – PAK4/Cofilin signals and potential activation pathway during *T. gondii* infection.

A table containing the signals from the antibody microarray, indicating the fold change, Category rank and potential cross-reactivity (using a comparison to *P. falciparum*) (left). Fold change values are coloured so that increases marked in yellow, decreases are marked in blue. (Right) Potential signalling pathway activated during *T. gondii* infection, which involves PAK4, LIMK1 and cofilin1/2. Green 'P's' indicates phosphorylation sites associated with activation; Red 'P's' indicates an inhibitory phosphorylation site.

4.4.3 The expression and phosphorylation of JAK-STAT pathway during *T. gondii* infection

The JAK-STAT pathway, as previously discussed in Chapter 1 and 4.1, is involved in *T. gondii* infection. The ROP16 protein of *T. gondii* can directly phosphorylate STAT3/6, resulting in the activation of the host kinases [391, 392]. The initial studies conducted on STAT3/6 activation noted no JAK involvement in this activation; however, interactions of ROP16 and JAK were not explored in these studies [391, 392]. In a later study, chemical inhibition of JAK1-3 was shown to stop STAT3 activation, illustrating the possible involvement of JAKs in STAT activation during infection [236]. The current body of knowledge indicates that STAT3/6, and potentially JAK1-3 may be phosphorylated during infection with *T. gondii* [236, 391, 392]. We, therefore, looked to see if the JAK-STAT pathway was activated in the sample analysed on our antibody microarray. The antibody microarray contains antibodies against JAK1-3 as well as STAT1-5; unfortunately, no STAT6 antibodies are present on this array. STAT1-5 expression and phosphorylation appear to have slightly decreased during infection (See Appendix 4). However, JAK1-3 showed a clear increase across most signals present on the array (Table 4.9). Additionally, the phosphorylation site (Tyr1034) on JAK1, increased by a fold change of approximately two across multiple other arrays completed. These other arrays were; *P. falciparum* rings, *P. knowlesi* schizonts and *B. bovis*, the three arrays completed on non-enriched parasite samples (see Supplementary Figure 1 and Appendix 4 for these signals). Tyr1034 resides in the activation loop of JAK1 and is phosphorylated by tyrosine kinase activity [393, 394]. To understand why we did not detect the expected STAT3 phosphorylation in our *T. gondii* array sample, we looked back into the previous studies to determine the experimental differences that could explain this discrepancy. The most likely reason for our inability to detect STAT3 activation is due to the cell type we used. In the previous studies, macrophages were the cells of choice, while we used foreskin fibroblasts in our study [391, 392]. Due to the immune functionality of macrophages, STAT activation by *T. gondii* may be specific to the survivability in these cells.

	Phospho Site (Human)	Fold change	Category	Cross-reactive Signal
JAK1	Y1034	1.71	4	no
	Pan-specific	2.17	4	no
JAK2	Y570	1.79	4	no
	Y1007+Y1008	0.96	4	yes
	Pan-specific	1.10	4	no
	Pan-specific	2.57	3	no
	Pan-specific	1.87	4	no
JAK3	Y980+Y981	2.15	2	no
	Pan-specific	1.53	4	yes
	Pan-specific	1.10	4	yes

Table 4.9 – The JAK1-3 pan- and phosphorylation-specific signals detected on the antibody microarray. All signals listed were above the low-intensity threshold. Cross-reactivity refers to the *P. falciparum* cross-reactivity array and may not necessarily indicate cross-reactivity to *T. gondii* proteins here. Note none of these signals are ranked as Category 1. Fold change values are coloured so that increases marked in yellow, decreases are marked in blue.

4.4.5 The microtubule-associated protein Tau and its phosphorylation during intracellular Apicomplexan infection

After completion of the analysis of the *T. gondii* dataset, we sought to determine if there were any consistencies in host cell signalling across all of the Apicomplexan datasets we generated, yet no clear pathways stood out immediately. Interestingly, one protein did appear to have overall phosphorylation similarities across the datasets. This protein was the microtubule-associated protein Tau. Tau associates with microtubules and promotes their assembly and stabilisation [395]. Tau has been demonstrated to bind to microtubules more efficiently when it is less phosphorylated [396]. Therefore, the dephosphorylation of tau can be associated with increased microtubule stability and indeed, other intracellular pathogens such as *Chlamydia trachomatis* and many viruses have been demonstrated to stabilise microtubules during infection [397, 398]. There is a large number of reported protein kinases, which can phosphorylate tau, at one or more of the 85 known phosphorylation sites [399]. Likewise, dephosphorylation of tau occurs through the activity of a number of protein phosphatases [400]. Tau is highly expressed in neurons; however, lower expression has been detected in other cell types, including erythrocytes and fibroblasts [401-403].

The microarray signals for tau across the array datasets were compiled into a single table (Table 4.10). Notably, all datasets, except *P. falciparum* trophozoites and schizonts, show an overall decrease in tau phosphorylation. The array did not contain a pan-specific signal for tau, so we are unable to determine if the overall decrease in phosphorylation is the result of tau protein degradation during infection. However, the increase in tau phosphorylation in *P. falciparum* trophozoites and schizonts supports the notion that tau is unlikely to be heavily degraded during *P. falciparum* development. To date, there is no direct link between tau phosphorylation/dephosphorylation during intracellular infection. Although, there are numerous reports of intracellular pathogens manipulating and utilising host cell microtubules for invasion, intracellular localisation and vesicle transport [397, 404, 405]. Taken together this suggests that host cell microtubules may also be important for the intracellular development of Apicomplexan parasites and that host tau may be central to this interaction.

	P. falciparum					*P. knowlesi*	*B. bovis*	*T.gondii*
Phospho Site (Human)	**Ring**	**Trophozoite**	**Schizont**	**Female**	**Male**	**Schizont**	**Unsychornised**	**Trophozoite**
S516	0.33	0.98	1.07	0.59	0.45	0.71	0.89	0.55
S713	0.36	0.82	0.78	0.37	0.44	0.57	0.80	0.63
S713	0.40	1.11	1.05	0.51	0.25	0.67	0.94	0.52
S721	0.54	1.70	1.38	0.42	0.56	0.64	0.21	0.53
S739	0.82	1.23	1.25	0.51	0.41	0.75	0.72	0.52
T522	0.36	1.06	0.63	0.70	0.69	0.86	0.89	1.61

Table 4.10 – Antibody microarray signals for the microtubule-associated protein Tau for all arrays completed in this thesis.

All values are represented in fold change from the respective uninfected control. Fold change values are coloured so that increases marked in yellow, decreases are marked in blue. Note no signal was flagged as low-intensity or cross-reactive to *P. falciparum.*

4.5 Summary and concluding remarks

This chapter sought to address the second aim of this thesis, which was '*to apply the antibody microarray approach from Aim 1 to other Apicomplexan parasites. Namely, Plasmodium knowlesi, Babesia bovis and Toxoplasma gondii.'* Through the utilisation of the antibody approach outlined in Chapter 3, we were able to determine that the Apicomplexan parasites, *P. knowlesi*, *B. bovis* and *T. gondii* all dynamically and quite uniquely affect the phosphorylation of host cell signalling proteins. After signal removal and the flagging of potential cross-reactivity signals, each dataset was presented as a shortlist of the best lead signals for further validation. For the *P. knowlesi* dataset, this was quite a limited listed, likely due to the low level of parasitemia in the analysed sample. However, using reticulocytes in this array enabled us to directly analyse the differences in phosphorylation and expression of signalling molecules between uninfected erythrocytes and reticulocytes. B-Raf, which was covered extensively in Chapter 3, also appeared to be highly phosphorylated on Ser729 in reticulocytes and showed higher protein levels. The array comparing bovine erythrocytes during infection with *B. bovis* illustrated that the Kinexus antibody microarrays work effectively in detecting bovine signalling proteins. The largest fold change detected in the *B. bovis* dataset was against FRS2 on Tyr348. Interestingly, this same phosphorylation site also appeared on the *P. falciparum* trophozoite stage array and the *P. knowlesi* schizont stage array. There were no obvious commonality between these three parasite samples; however, the *P. knowlesi* and *B. bovis* samples each compared an unenriched population of parasites with an uninfected control. Therefore, these samples contained differing amounts of bystander cells and could suggest that FRS2 may be activated in these exposed cells. Finally, we completed one further array on the Apicomplexan parasite *T. gondii*. Of the parasite in this chapter, *T. gondii* had the largest dynamic changes in host signalling phosphorylation, and it also had diverse changes in signalling protein expression. From this dataset, the activation of JAK1-3, previously reported, could be verified. This chapter illustrated that infection with Apicomplexan parasites could be analysed by using antibody signalling arrays. Through these microarrays, we have been able to successfully identify numerous host signalling proteins which represent promising leads for future validation studies.

Chapter 5 – General discussion and future directions

5.1 General considerations

5.1.1 Difficulties associated with the mapping of signalling pathways

This thesis has covered many different host cell signalling proteins and the functions of their specific phosphorylation sites. However, this analysis and pathway determination is all achieved manually and therefore has levels of bias towards signalling elements, which are better represented in the literature. Additionally, manually searching each protein is a slow process, which is further impeded by the inconsistencies in the literature in regards to phosphorylation site position, function and even the name of the associated kinase or the types of cells used to generate protein extracts. In some instances, a kinase has undergone several changes of name in the past 20 years, which makes tracking the relevant literature all the more difficult. Also, the phosphorylation sites are not always consistent in the literature as some studies have looked at the mouse equivalent protein. Often these studies do not state they are working with the mouse equivalent, which makes understanding the roles of different phosphorylation sites difficult to interpret for those who are not heavily engaged in research of the protein in question. Uniprot does somewhat alleviate this problem as it lists the mouse and human sites separately, however, Uniprot does not effectively list the interacting partners for each protein's phosphorylation sites. In an ideal setting, curation of a larger phosphorylation and signalling network would remove a lot of the conflicting and confusing statements that are made throughout the literature. Though large protein interaction pathways exist, most do not directly annotate phosphorylation sites. The networks that do are often purpose-built for a particular disease, and consequently, do not provide a good representation of homeostatic conditions. If a database was developed with a clear emphasis on phosphorylation interactions, computer modelling of the entire array results could be achieved and may unveil many signalling molecules and pathways, which are more subtly activated during infection.

5.1.2 Study limitations

Throughout this study, we have utilised antibody microarrays as our initial experiment for the determination of changes in host signalling protein phosphorylation during infection. These arrays contain technical duplicates of each antibody present and therefore enabled us to use the percentage error between these values to determine signal quality. However, each of these arrays, as they were performed on a specific stage of parasite infection, only represents a single biological replicate. Further replicates were not conducted in this study, as they were cost-prohibitive; instead, we chose to validate the most promising hits separately by Western blot analysis and by using small molecule inhibitors. This was overall quite a successful strategy for the proteins we chose to validate, although this is not ideal for the analysis of the dataset as a whole. In the future, validation experiments should consider repeating the microarray experiments to ensure they are consistent, which would enable larger claims on the overall phosphorylation status of host proteins during Apicomplexan infection to be made.

5.2 Salient findings from this study

Four unique Apicomplexan parasites, *P. falciparum*, *P. knowlesi*, *B. bovis* and *T. gondii,* have been discussed throughout this study. Each of these parasites presents a different threat to global health, and together, these four are a major health burden worldwide. Large advances in the control and prevention of malaria infection have allowed huge strides towards malaria eradication, yet resistance to the frontline treatment, ACT in the form of delayed parasite clearance has spread from the Thai-Cambodian border into neighbouring countries [13, 14, 18, 19]. This is reminiscent of chloroquine, sulphadoxine/pyrimethamine and mefloquine resistance before each spread globally, suggesting that global dissemination of artemisinin resistance is not a question of "how" but rather "when" [21, 33-35]. Clearly, new anti-malarial treatments are required for the successful eradication of malaria, although targeting a parasite-encoded target as treatment carries the immediate potential for novel resistance development. We need novel treatments for malaria, which are likely to remain resistance-free for a greater span, allowing disease eradication. Host-directed therapy (HDT) is a field of research which is gaining traction and suggests that targeting the host, instead of the pathogen, could be the solution for long term efficacy of drugs, as it deprives the parasite of the most direct avenues of mutagenesis, and therefore easy resistance development [162].

Babesia spp. are less understood Apicomplexan parasites, comparative to *Plasmodium*; however, *Babesia* has been a problematic pathogen for the global cattle industry for some time and is more recently becoming a more prevalent infection of humans [98]. *T. gondii* has been highly prevalent in humans for some time, with the previously unknown chronic effects of infection now being linked to several psychiatric conditions [75, 76, 84-89]. Vaccination at present has not proven to be efficacious or effective long term for Apicomplexan infection, although, there has been some success with *B. bovis* [104]. Treatment of *Babesia* and *Toxoplasma* both rely on inhibiting parasite-encoded targets and consequently will likely become ineffective similar to the compounds used to treat *Plasmodium* infection. Additionally, chronic infection of *T. gondii* is completely untreatable, due to parasite dormancy.

How these parasites function on a cellular level is quite well understood, with a substantial body of knowledge available; however, very few studies have delved into how the infected cell responds to infection or unveiled how the host cell's signalling pathways are modulated. We chose to address this critical gap in the current literature by utilising an antibody microarray developed by the company Kinexus. The aims of this study were 1) To generate a comprehensive phospho-signalling derived map of host erythrocyte signalling during the development of the malaria parasite *Plasmodium falciparum*, using antibody microarrays. 2) To apply the antibody microarray approach to other Apicomplexan parasites, namely, *P. knowlesi*, *B. bovis* and *T. gondii*. The goal of this study was to identify how phosphorylation of host cells changes throughout infection with Apicomplexan parasites and to identify lead host kinases as targets for further exploration and possibly as targets for anti-parasitic interventions.

5.2.1 *P. falciparum* study (Aim 1)

Chapter 3 addressed the first of our aims stated above and used nine antibody microarrays. eight of these arrays compared a co-cultured uninfected erythrocyte control to five different developmental stages of the parasite, namely ring, trophozoite, schizont, stage IV female gametocytes and stage IV male gametocytes. The final array compared a fractionated mixed population of trophozoites and schizonts using saponin. Saponin results in the destabilisation of the erythrocyte membrane, releasing the cytoplasmic components of the host cell (saponin supernatant) [260]. The remaining material contains most of the erythrocyte membrane and all the parasite material (saponin pellet). The saponin supernatant and saponin pellet were compared on this final array and used to identify antibodies which were cross-reactive with the

parasite directly. We wanted to be sure we identified all potentially cross-reactive signals on the array, so instead of loading based on cell number at a 1:1 saponin supernatant to saponin pellet ratio, we instead loaded the array as 1:20. Using the results of this final array, we identified 224 potentially cross-reactive signals. On a side note, many of the signals flagged as cross-reactive were against the phosphorylated forms of histones and other highly conserved phosphorylated proteins [406]. Therefore, these commercially available antibodies, though not used for this study, may have a role in studying highly conserved parasite proteins.

Phosphorylation of host signalling molecules changes dynamically during infection with *P. falciparum*

Completion of the nine microarrays mentioned in 5.2.1 produced five very unique different datasets. The unique nature of each dataset is illustrated in the following Figures; Chapter 3 Figure 3.3 and 3.8 in heatmaps and dot plots. In the asexual stages of development, the ring stage of development, indicating that there were more reductions in phosphorylation than increases (Figure 3.3c). By the trophozoite stage of development, the dataset indicated a clear increase in many phosphorylation sites. By the final time point (schizonts), there was an overall reduction in the phosphorylation status of most host signalling proteins (Figure 3.3). The reduction in overall protein phosphorylation in schizont-infected erythrocytes is consistent with the results of a previous study that was restricted to purified membranes [228]. Taken together, this illustrates that the asexual development of *P. falciparum* causes a multitude of changes in host erythrocyte signalling, which appears to be very specific to the developmental stage of the harboured parasite. The same is also true for the arrays completed on stage IV male and female gametocytes, which indicated that the sex of the harboured parasite affects the phosphorylation status of many host proteins, suggesting alternative host pathway activation (Figure 3.8). Contextually these findings illustrate that erythrocyte signalling is heavily modulated during *P. falciparum* infection and that the host molecules identified in this study may represent attempts by the erythrocyte to initiate eryptosis or could represent parasite manipulation of host cell signalling.

The host kinases B-Raf and c-Met are activated during *P. falciparum* asexual development

The complete datasets for each of the *P. falciparum* arrays were further shortlisted to identify the most reliable and interesting changes in host cell phosphorylation during infection. This was achieved by removing the signals identified as cross-reactive (discussed above) and those with low intensities, before determining which of the remaining signals were significantly different from the uninfected erythrocyte mean (n=4). This identified numerous changes (Supplementary Figure 4); however, the kinases c-Met and B-Raf stood out. We compiled the signals for c-Met from the asexual and sexual datasets, which indicated a very specific trophozoite stage increase in the phosphorylation sites present on the array (Figure 3.5 and 3.6). c-MET is a receptor tyrosine kinase and is involved in proliferation, motility and cell cycle progression, which it achieves through activation of the PI3K and MAPK pathways [207]. We validated the activation of c-Met by Western blot, using an antibody specific to two well-known phosphorylation sites associated with kinase activation (Tyr1234+Tyr1235)[284]. Our Western blot results verified that c-Met is indeed phosphorylated during trophozoite development (Figure 3.6c).

Another kinase, B-Raf was also notable, as it maintained elevated levels of phosphorylation at the site Ser729 across all three of the asexual time points (Figure 3.5a). B-Raf belongs to the MAP3K family of kinases were it is activated the GTPase Ras, which can occur by RTK activity [265]. Notably, many of the downstream MAPK components also showed increased phosphorylation at specific stages of asexual parasite development. This is the first report of c-Met and B-Raf activation during *P. falciparum* blood-stage development and indicates that there may be many more kinases activated during infection, all of which may represent strong candidates for anti-malarial HDT.

Inhibitors which target host B-Raf or c-Met have parasiticidal effects on asexual *P. falciparum*

The phosphorylation and activation of B-Raf and c-Met was discussed in the previous section. These kinases are key candidates for anti-cancer therapeutics, as their signalling is often dysregulated in cancer cells [207, 407]. The large body of research into targeting these kinases for the development of cancer therapeutics has produced multiple highly specific compounds, which are at various stages of clinical development. Given the availability of these compounds, we tested their effects on asexual *P. falciparum in vitro* culture and identified sub-micromolar IC_{50}s (Figure 3.7b). In addition, we tested these compounds on *P. knowlesi* and achieved

similar IC_{50} values (Figure 3.7c). Given the potency of the compounds Crizotinib (c-Met inhibitor), PHA-665752 (c-Met inhibitor) and SB-590885 (B-Raf inhibitor), we performed a time-dependent growth assay with *P. falciparum*. This experiment illustrated that these compounds began actively killing parasites from 24 hours post-invasion onwards (figure 3.7d). However, we cannot discount the possibility that these inhibitors have off-target effects. Yet, the activation of their target kinases does overlay well with the time of parasiticidal effects (Figures 3.5 and 3.6). Furthermore, we demonstrated that PHA-665752 could reduce the *P. berghei* burden in an *in vivo* mouse model (Figure 3.7e). Together this illustrates that PHA-665752 and potentially other c-MET inhibitors could affect multiple species of *Plasmodium* during erythrocyte development. Therefore, further research into these inhibitors is warranted as they may represent a starting point for novel drug development targeting the host for the treatment of malaria. Additionally, as compounds such as Crizotinib are already FDA approved, the cost and time to market for use as an antimalarial are substantially reduced compared to a novel compound.

Activation of p38a MAPK and other lead signals on the stage IV gametocyte arrays

The array conducted on stage IV female gametocytes indicated higher phosphorylation on the activation loop of p38a MAPK (Tyr180+Tyr182) during infection (Table 3.4). Further analysis of the potential upstream activators identified that the following signalling pathway was likely, based on the array dataset; MKK4 → p38a MAPK (Table 3.5). The function of p38a MAPK in erythrocytes is unknown; however, in nucleated cells, the kinase has many roles ranging from actin reorganisation through to cell proliferation [408]. In addition, there were many lead molecules identified during the analysis of these arrays, including PKCd and p70 S6K. The listed signalling proteins are currently undergoing validation by Professor Alex Maier and his team at ANU. If validation is successful, these host signalling proteins will be the first host signalling elements identified to be active during *P. falciparum* gametocytogenesis.

5.2.2 Wider Apicomplexan study (Aim 2)

The second aim of this study was addressed in Chapter 4, using three antibody microarrays. Each of these arrays was performed on a different Apicomplexan parasite that was obtainable in sufficient quantities for microarray analysis. These parasites were *P. knowlesi* (schizonts), *B. bovis* (mixed population) and *T. gondii* (tachyzoites). In the following sections, the key findings and conclusions of these studies will be addressed.

Antibody microarrays that target phosphorylation can effectively be used to study the effects of Apicomplexan infection on host cell signalling cells

The three microarrays completed on the parasites mentioned above all created unique datasets (Appendix 4). This was somewhat surprising, as we expected there to be more consistency in the phosphorylation of host cell signalling proteins, during infection. Analysis of each dataset further verified that there were very few commonalities between all of the Apicomplexan parasites used in this study. However, the minimal number of commonalities identified could be a consequence of the different host cells used for each array. To overcome this issue in the future, infection of the same host cell type by two different Apicomplexan parasites should be explored. Using the parasites in this study, this could be achieved as *P. knowlesi* can also infect human erythrocytes, like *P. falciparum*.

The array completed on *B. bovis* relied on the antibodies from the array, designed to recognise human proteins, to identify the highly conserved signalling proteins in bovine erythrocytes. This was successful, with a number of large changes in signalling protein phosphorylation recorded (Figure 4.4 and Table 4.6) and illustrated that these arrays could be applied successfully to non-human cells infected with Apicomplexan parasites, in fact, a recent study used Kinexus' antibody microarrays on mosquito cells infected with Wolbachia and identified increased insulin receptor phosphorylation [249].

Phosphorylation of host cell FRS2 is shared by infection with multiple Apicomplexan parasites, a potential bystander cell effect

Three of the arrays completed in this study compared non-enriched populations of the parasitised cells, due to an inability to purify the infected cells from those that were uninfected. These uninfected cells are referred to in this study as bystander cells, as they had been exposed to parasitised cells in their surroundings. The following arrays contained bystander cells in the infected sample; *P. falciparum* ring stage, *P. knowlesi* and *B. bovis*. This diluted the signals of the infected cells and can be observed in the associated datasets. (Supplementary Figure 1 and

Appendix 4). Notably, the B. bovis and P. knowlesi datasets contained overall smaller changes in the phosphorylation of host cell signalling proteins during infection. In future experiments, it would be ideal if higher levels of parasitemia could be achieved as this may unveil many more subtle changes in host cell signalling. Interestingly, both the B. bovis and P. knowlesi datasets commonly list phosphorylation of host FRS2 at Tyr348 (Table 4.7). FRS2 is an adapter molecule that facilitates signal amplification form several RTKs into downstream pathways, including MAPK and PI3K-Akt [353]. We attempted to validate by immunoblot if this was indeed a bystander effect using both *P. falciparum* and *B. bovis*; however, we were unable to detect FRS2 in the bovine samples (Figure 4.7 and 4.8). The bovine samples used in Figure 4.8 are cells cultured with fresh or spent media. Spent media refers to media taken from a culture of *B. bovis* infected bovine cells and therefore included any metabolites, kinases and other factors secreted or released during *B. bovis* erythrocyte development. In Figure 4.8 there was a band detected at approximately 50kDa, which could be phosphorylated bovine FRS3, due to high sequence homology. This still requires confirmation with an FRS3 pan-antibody; however, if a pan-FRS3 antibody can detect the 50kDA band, it is highly likely to be bovine FRS3. This 50kDa band was more phosphorylated in the cultured in spent media and therefore could illustrate a bystander effect.

FRS2 (approximately 75kDa) could be detected in human erythrocytes using a pan-specific antibody (Figure 4.7). Unfortunately, the phosphorylation site Tyr348 on FRS2 could not be probed for in this follow-up study as the commercially available antibody on the array had been discontinued. We were able to source an antibody specific to phosphorylation of FRS2 Tyr196, which serves a similar function to Ty348 [333]; however, we were unable to detect the 75kDa signal in the erythrocyte samples. Generating an antibody specific to FRS2 phosphorylated at Tyr348 would be ideal, and could then be used in Western blot validation of the signals we observed for *P. falciparum* trophozoites, *P. knowlesi* and *B. bovis*.

Activation of host cell JAK1 during *T. gondii* infection confirmed by microarray analysis

Compared to the *P. knowlesi* and *B. bovis* datasets, the *T. gondii* dataset contained substantially more Category 1 lead signals warranting future validation. One of the better-studied host signalling pathways manipulated during *T. gondii* infection is the JAK-STAT pathway. The ROP16 protein of *T. gondii* can directly phosphorylate STAT3/6, resulting in the activation of the host kinases [391, 392]. In a later study, inhibition of JAK1-3 was shown to inhibit STAT3 activation, indicating the possible involvement of JAKs in STAT activation during infection [236]. The hijacking of STAT3 signalling by *T. gondii* is thought to aid the parasite in the

down-regulation of host pro-inflammatory effects, while STAT6 activation may subvert host cell apoptosis [238, 392]. We further investigated this pathway in our microarray data to ascertain if we could confirm the activation of the JAK-STAT pathway. The array completed on human foreskin fibroblasts infected with *T. gondii* did not indicate increased phosphorylation or expression of STAT1-5; note STAT6 was not present on the array (Appendix 4). However, STAT activation has only been reported in the intracellular infection of host macrophages, and therefore may not be required during infection of non-immune cells [238, 392]. Increased JAK1-3 expression and phosphorylation was detected for almost all antibodies present on the array, confirming the activation of these kinases during *T. gondii* infection (Table 4.9). This suggests that during *T. gondii* infection, host cell phosphorylation and expression is specific to the host cell type infected. Future studies on the host cell signalling of bradyzoites, the chronic and dormant form of *T. gondii*, may help further this work, and illustrate host protein targets, which could be exploited in anti-parasitic treatments.

Differential phosphorylation of host B-Raf in reticulocytes and mature erythrocytes may be pivotal in the successful development of *Plasmodium* in erythrocytes.

Through the completion of arrays on erythrocytes infected with *P. falciparum* and reticulocytes infected with *P. knowlesi*, we had a number of uninfected erythrocytes and an uninfected reticulocyte dataset. Using this uninfected data, we were able to directly compare how host cell signalling differs between reticulocytes and mature erythrocytes. This comparison contained four biological replicates of uninfected erythrocytes and used the mean signal value to compare to the one biological replicate of uninfected reticulocytes we had. Surprisingly, there were a large number of differences, some of which suggests higher levels of phosphorylation in mature erythrocytes (Figure 4.2). We determined which of these signals were significantly different from uninfected erythrocytes, full dataset available in Appendix 6. One of the signals, which stood out in this analysis, was B-Raf Ser729. This was quite an interesting discovery, as we have previously discussed, B-Raf Ser729 is more phosphorylated across *P. falciparum* erythrocytic asexual and sexual development (Figure 3.4 and Table 3.4). Additionally, inhibition of B-Raf with the compound SB-590885 killed *P. falciparum* during asexual development (Figure 3.7). We checked the phosphorylation of B-Raf in our *P. knowlesi* dataset and noted a slight reduction in the Ser729 phosphosite (fold change = 0.73, Appendix 4), suggesting no further phosphorylation during *P. knowlesi* reticulocyte infection. Furthermore, we established that the compound SB-590885 had a sub-micromolar IC_{50} value for *P. knowlesi* asexual growth (Figure 3.7c). From these findings, we postulate that the phosphorylation of B-

Raf might be required for successful erythrocytic development and, due to the already phosphorylated state in reticulocytes, the infecting parasite is not required to phosphorylate the kinase for survival. To further validate this, studies or an array on *P. knowlesi* during infection of erythrocytes would be required. If our hypothesis proves true, this finding may have greater implications and could be potentially exploited for *in vitro* culturing of *P. vivax*, which will only grow successfully in reticulocytes.

Potentially conserved function of host microtubule-associated protein Tau during intracellular Apicomplexan infection

Comparative analysis across the four Apicomplexan parasites investigated in this study illustrated that there were very few overall commonalities between host cell signalling phosphorylation. This suggested that each parasite has evolved unique interactions within its selective host cell type. Of the host proteins targeted on the array, the microtubule-associated protein Tau did show overall consistency across the Apicomplexan parasites investigated here. Tau associates with microtubules and promotes their assembly and stabilisation [395]. Across the arrays completed, Tau phosphorylation was reduced on several sites, indicating that the protein was overall less phosphorylated during Apicomplexan intracellular infection. Tau has been demonstrated to bind to microtubules more efficiently when it is less phosphorylated [396]. Therefore, the dephosphorylation of tau can be associated with increased microtubule stability. The bacterium *Chlamydia trachomatis*, as well as many viruses, have been demonstrated to stabilise microtubules during infection [397, 398]; however, no direct link between tau phosphorylation/dephosphorylation during infection by any intracellular eukaryotic pathogens have been reported. Together this suggests, that like other intracellular pathogens, Apicomplexan parasites may actively stabilise microtubules, which could be facilitated through host Tau, providing a convenient vesicle transport system for the parasites.

5.2.3 Overall conclusions of research findings

This study has identified that during infection with the Apicomplexan parasites, *P. falciparum*, *P. knowlesi*, *B. bovis* and *T. gondii*, the host cells signalling is altered. In some instances, phosphorylation of host signalling proteins is quite dramatic (*P. falciparum* trophozoites and schizonts and *T. gondii*) while other infections have a subtler effect on signalling (*B. bovis* and *P. knowlesi*). Overall this study has illustrated that although these parasites all infect host cells for survival, there are very few host cell signalling similarities which are shared during infection. Additionally, we identified and validated the phosphorylation of host c-MET and B-Raf during *P. falciparum* asexual development. We also identified that compounds targeting these kinases have parasiticidal effects for *P. falciparum* and *P. knowlesi*. The c-MET inhibitor PHA-665752 was further shown to reduce the parasite burden *in vivo* for *P. berghei* infection. This illustrates that targeting host kinases for HDT could be achieved for anti-malarial interventions. Furthermore, inhibition of c-Met, B-Raf or another identified kinase in this study would significantly reduce the parasite's capacity to overcome the compound through target-directed mutagenesis and therefore, may be key in developing an effective novel anti-malarial or antiparasitic compound in the future.

Appendix

Appendix 1-6 - Due to the size of these tables the Appendix material has been placed on dropbox;

https://www.dropbox.com/sh/0zklb3n5teh63wr/AAC-tEaydkWGvY98MTVvdfcLa?dl=0

References

1. Weedall, G.D. and N. Hall, *Sexual reproduction and genetic exchange in parasitic protists.* Parasitology, 2015. **142 Suppl 1**: p. S120-7.
2. Blader, I.J. and J.P. Saeij, *Communication between Toxoplasma gondii and its host: impact on parasite growth, development, immune evasion, and virulence.* APMIS, 2009. **117**(5-6): p. 458-76.
3. Kaushansky, A., et al., *Malaria parasite liver stages render host hepatocytes susceptible to mitochondria-initiated apoptosis.* Cell Death Dis, 2013. **4**: p. e762.
4. Sicard, A., et al., *Activation of a PAK-MEK signalling pathway in malaria parasite-infected erythrocytes.* Cell Microbiol, 2011. **13**(6): p. 836-45.
5. Hall, B.S., et al., *Modulation of protein kinase C activity in Plasmodium falciparum-infected erythrocytes.* Blood, 1997. **89**(5): p. 1770-8.
6. Pantaleo, A., et al., *Syk inhibitors interfere with erythrocyte membrane modification during P falciparum growth and suppress parasite egress.* Blood, 2017. **130**(8): p. 1031-1040.
7. Carvalho, T.G., et al., *The ins and outs of phosphosignalling in Plasmodium: Parasite regulation and host cell manipulation.* Mol Biochem Parasitol, 2016. **208**(1): p. 2-15.
8. World-Health-Organisation. *World Malaria Report 2018*. 2018; Available from: https://www.who.int/malaria/publications/world-malaria-report-2018/report/en/.
9. William, T., et al., *Increasing incidence of Plasmodium knowlesi malaria following control of P. falciparum and P. vivax Malaria in Sabah, Malaysia.* PLoS Negl Trop Dis, 2013. **7**(1): p. e2026.
10. Cox-Singh, J., *Zoonotic malaria: Plasmodium knowlesi, an emerging pathogen.* Curr Opin Infect Dis, 2012. **25**(5): p. 530-6.
11. Barber, B.E., et al., *Epidemiology of Plasmodium knowlesi malaria in north-east Sabah, Malaysia: family clusters and wide age distribution.* Malar J, 2012. **11**: p. 401.
12. World-Health-Organisation. *World Malaria Report 2016*. 2016; Available from: https://www.who.int/malaria/publications/world-malaria-report-2016/report/en/.
13. Otten, M., et al., *Initial evidence of reduction of malaria cases and deaths in Rwanda and Ethiopia due to rapid scale-up of malaria prevention and treatment.* Malar J, 2009. **8**: p. 14.
14. Aregawi, M.W., et al., *Reductions in malaria and anaemia case and death burden at hospitals following scale-up of malaria control in Zanzibar, 1999-2008.* Malar J, 2011. **10**: p. 46.
15. (WHO), W.H.O. *World malaria report*. 2017.
16. Gallup, J.L. and J.D. Sachs, *The economic burden of malaria.* Am J Trop Med Hyg, 2001. **64**(1-2 Suppl): p. 85-96.
17. Sicuri, E., et al., *The economic costs of malaria in children in three sub-Saharan countries: Ghana, Tanzania and Kenya.* Malar J, 2013. **12**: p. 307.
18. Kheang, S.T., et al., *Prevalence of K13 mutation and Day-3 positive parasitaemia in artemisinin-resistant malaria endemic area of Cambodia: a cross-sectional study.* Malar J, 2017. **16**(1): p. 372.
19. Imwong, M., et al., *The spread of artemisinin-resistant Plasmodium falciparum in the Greater Mekong subregion: a molecular epidemiology observational study.* Lancet Infect Dis, 2017. **17**(5): p. 491-497.
20. Tanwar, J., et al., *Multidrug resistance: an emerging crisis.* Interdiscip Perspect Infect Dis, 2014. **2014**: p. 541340.
21. Wongsrichanalai, C. and C.H. Sibley, *Fighting drug-resistant Plasmodium falciparum: the challenge of artemisinin resistance.* Clin Microbiol Infect, 2013. **19**(10): p. 908-16.
22. Achan, J., et al., *Quinine, an old anti-malarial drug in a modern world: role in the treatment of malaria.* Malar J, 2011. **10**: p. 144.
23. Bateman, D.N. and E.H. Dyson, *Quinine toxicity.* Adverse Drug React Acute Poisoning Rev, 1986. **5**(4): p. 215-33.
24. Wellems, T.E. and C.V. Plowe, *Chloroquine-resistant malaria.* J Infect Dis, 2001. **184**(6): p. 770-776.
25. World-Health-Organisation. *World Malaria Report 2008*. 2008; Available from: https://www.who.int/malaria/publications/atoz/9789241563697/en/.
26. Nosten, F. and N.J. White, *Artemisinin-based combination treatment of falciparum malaria.* Am J Trop Med Hyg, 2007. **77**(6 Suppl): p. 181-92.
27. de Vries, P.J. and T.K. Dien, *Clinical pharmacology and therapeutic potential of artemisinin and its derivatives in the treatment of malaria.* Drugs, 1996. **52**(6): p. 818-36.
28. Dondorp, A.M., et al., *Artemisinin resistance in Plasmodium falciparum malaria.* N Engl J Med, 2009. **361**(5): p. 455-67.
29. Noedl, H., et al., *Evidence of artemisinin-resistant malaria in western Cambodia.* N Engl J Med, 2008. **359**(24): p. 2619-20.

30. Ouji, M., et al., *Plasmodium falciparum resistance to artemisinin-based combination therapies: A sword of Damocles in the path toward malaria elimination.* Parasite, 2018. **25**: p. 24.
31. Adams, J., R. Kelso, and L. Cooley, *The kelch repeat superfamily of proteins: propellers of cell function.* Trends Cell Biol, 2000. **10**(1): p. 17-24.
32. Ariey, F., et al., *A molecular marker of artemisinin-resistant Plasmodium falciparum malaria.* Nature, 2014. **505**(7481): p. 50-5.
33. Payne, D., *Spread of chloroquine resistance in Plasmodium falciparum.* Parasitol Today, 1987. **3**(8): p. 241-6.
34. Roper, C., et al., *Intercontinental spread of pyrimethamine-resistant malaria.* Science, 2004. **305**(5687): p. 1124.
35. Price, R.N., et al., *Mefloquine resistance in Plasmodium falciparum and increased pfmdr1 gene copy number.* Lancet, 2004. **364**(9432): p. 438-447.
36. Witkowski, B., et al., *Reduced artemisinin susceptibility of Plasmodium falciparum ring stages in western Cambodia.* Antimicrob Agents Chemother, 2013. **57**(2): p. 914-23.
37. Witkowski, B., et al., *Increased tolerance to artemisinin in Plasmodium falciparum is mediated by a quiescence mechanism.* Antimicrob Agents Chemother, 2010. **54**(5): p. 1872-7.
38. Thanh, N.V., et al., *Rapid decline in the susceptibility of Plasmodium falciparum to dihydroartemisinin-piperaquine in the south of Vietnam.* Malar J, 2017. **16**(1): p. 27.
39. Das, S., et al., *Evidence of Artemisinin-Resistant Plasmodium falciparum Malaria in Eastern India.* N Engl J Med, 2018. **379**(20): p. 1962-1964.
40. Huang, F., et al., *A Single Mutation in K13 Predominates in Southern China and Is Associated With Delayed Clearance of Plasmodium falciparum Following Artemisinin Treatment.* J Infect Dis, 2015. **212**(10): p. 1629-35.
41. Mohon, A.N., et al., *Mutations in Plasmodium falciparum K13 propeller gene from Bangladesh (2009-2013).* Malar J, 2014. **13**: p. 431.
42. Malaria, G.E.N.P.f.C.P., *Genomic epidemiology of artemisinin resistant malaria.* Elife, 2016. **5**.
43. Fairhurst, R.M. and A.M. Dondorp, *Artemisinin-Resistant Plasmodium falciparum Malaria.* Microbiol Spectr, 2016. **4**(3).
44. Rts, S.C.T.P., *Efficacy and safety of RTS,S/AS01 malaria vaccine with or without a booster dose in infants and children in Africa: final results of a phase 3, individually randomised, controlled trial.* Lancet, 2015. **386**(9988): p. 31-45.
45. Olotu, A., et al., *Seven-Year Efficacy of RTS,S/AS01 Malaria Vaccine among Young African Children.* N Engl J Med, 2016. **374**(26): p. 2519-29.
46. N'Guessan, R., et al., *Reduced efficacy of insecticide-treated nets and indoor residual spraying for malaria control in pyrethroid resistance area, Benin.* Emerg Infect Dis, 2007. **13**(2): p. 199-206.
47. Ordinioha, B., *The use and misuse of mass distributed free insecticide-treated bed nets in a semi-urban community in Rivers State, Nigeria.* Ann Afr Med, 2012. **11**(3): p. 163-8.
48. Alout, H., et al., *Consequences of insecticide resistance on malaria transmission.* PLoS Pathog, 2017. **13**(9): p. e1006499.
49. Ashley, E.A. and A.P. Phyo, *Drugs in Development for Malaria.* Drugs, 2018. **78**(9): p. 861-879.
50. Tavares, J., et al., *Role of host cell traversal by the malaria sporozoite during liver infection.* J Exp Med, 2013. **210**(5): p. 905-15.
51. Vaughan, A.M., et al., *Complete Plasmodium falciparum liver-stage development in liver-chimeric mice.* J Clin Invest, 2012. **122**(10): p. 3618-28.
52. Sturm, A., et al., *Manipulation of host hepatocytes by the malaria parasite for delivery into liver sinusoids.* Sci, 2006. **313**(5791): p. 1287-1290.
53. Bartoloni, A. and L. Zammarchi, *Clinical Aspects of Uncomplicated and Severe Malaria.* Mediterr J Hematol Infect Dis, 2012. **4**(1).
54. Gilson, P.R. and B.S. Crabb, *Morphology and kinetics of the three distinct phases of red blood cell invasion by Plasmodium falciparum merozoites.* Int J Parasitol, 2009. **39**(1): p. 91-6.
55. Cowman, A.F. and B.S. Crabb, *Invasion of Red Blood Cells by Malaria Parasites.* Cell. **124**(4): p. 755-766.
56. Terkuile, F., et al., *Plasmodium falciparum: In Vitro Studies of the Pharmacodynamic Properties of Drugs Used for the Treatment of Severe Malaria.* Experimental Parasitology, 1993. **76**(1): p. 85-95.
57. Barcia, J.J., *The Giemsa stain: its history and applications.* Int J Surg Pathol, 2007. **15**(3): p. 292-6.
58. Wallqvist, A., et al., *Metabolic host responses to malarial infection during the intraerythrocytic developmental cycle.* BMC Syst Biol, 2016. **10**(1): p. 58.
59. Lazarus, M.D., T.G. Schneider, and T.F. Taraschi, *A new model for hemoglobin ingestion and transport by the human malaria parasite Plasmodium falciparum.* J Cell Sci, 2008. **121**(11): p. 1937-49.

60. Martiney, J.A., A. Cerami, and A.F. Slater, *Inhibition of hemozoin formation in Plasmodium falciparum trophozoite extracts by heme analogs: possible implication in the resistance to malaria conferred by the beta-thalassemia trait.* Mol Med, 1996. **2**(2): p. 236-46.
61. Bannister, L.H., et al., *A Brief illustrated guide to the ultrastructure of Plasmodium falciparum asexual blood stages.* Parasitol, 2000. **16**(10): p. 427-433.
62. Bozdech, Z., et al., *Expression profiling of the schizont and trophozoite stages of Plasmodium falciparum with a long-oligonucleotide microarray.* Genome Biol, 2003. **4**(2): p. R9.
63. Gruring, C., et al., *Human red blood cell-adapted Plasmodium knowlesi parasites: a new model system for malaria research.* Cell Microbiol, 2014. **16**(5): p. 612-20.
64. Gerald, N., B. Mahajan, and S. Kumar, *Mitosis in the Human malaria parasite Plasmodium falciparum.* Eukaryot Cell, 2011. **10**(4): p. 474-82.
65. Antinori, S., et al., *Biology of human malaria plasmodia including Plasmodium knowlesi.* Mediterr J Hematol Infect Dis, 2012. **4**(1): p. e2012013.
66. Baker, D.A., *Malaria gametocytogenesis.* Mol Biochem Parasitol, 2010. **172**(2): p. 57-65.
67. Hogh, B., et al., *The differing impact of chloroquine and pyrimethamine/sulfadoxine upon the infectivity of malaria species to the mosquito vector.* Am J Trop Med Hyg, 1998. **58**(2): p. 176-82.
68. Liu, Z., J. Miao, and L. Cui, *Gametocytogenesis in malaria parasite: commitment, development and regulation.* Future Microbiol, 2011. **6**(11): p. 1351-69.
69. Filarsky, M., et al., *GDV1 induces sexual commitment of malaria parasites by antagonizing HP1-dependent gene silencing.* Science, 2018. **359**(6381): p. 1259-1263.
70. Smalley, M.E. and J. Brown, *Plasmodium falciparum gametocytogenesis stimulated by lymphocytes and serum from infected Gambian children.* Trans R Soc Trop Med Hyg, 1981. **75**(2): p. 316-7.
71. Talman, A.M., et al., *Gametocytogenesis: the puberty of Plasmodium falciparum.* Malar J, 2004. **3**: p. 24.
72. Ikadai, H., et al., *Transposon mutagenesis identifies genes essential for Plasmodium falciparum gametocytogenesis.* Proc Natl Acad Sci U S A, 2013. **110**(18): p. E1676-84.
73. Saliba, K.S. and M. Jacobs-Lorena, *Production of Plasmodium falciparum gametocytes in vitro.* Methods Mol Biol, 2013. **923**: p. 17-25.
74. Aly, A.S.I., A.M. Vaughan, and S.H.I. Kappe, *Malaria Parasite Development in the Mosquito and Infection of the Mammalian Host.* Annu Rev Microbiol, 2009. **63**: p. 195-221.
75. Pappas, G., N. Roussos, and M.E. Falagas, *Toxoplasmosis snapshots: global status of Toxoplasma gondii seroprevalence and implications for pregnancy and congenital toxoplasmosis.* Int J Parasitol, 2009. **39**(12): p. 1385-94.
76. Montoya, J.G. and O. Liesenfeld, *Toxoplasmosis.* Lancet, 2004. **363**(9425): p. 1965-76.
77. Howe, D.K. and L.D. Sibley, *Toxoplasma gondii comprises three clonal lineages: correlation of parasite genotype with human disease.* J Infect Dis, 1995. **172**(6): p. 1561-6.
78. Hamilton, C.M., et al., *Predominance of atypical genotypes of Toxoplasma gondii in free-roaming chickens in St. Kitts, West Indies.* Parasit Vectors, 2017. **10**(1): p. 104.
79. Su, C., et al., *Recent expansion of Toxoplasma through enhanced oral transmission.* Science, 2003. **299**(5605): p. 414-6.
80. Alday, P.H. and J.S. Doggett, *Drugs in development for toxoplasmosis: advances, challenges, and current status.* Drug Des Devel Ther, 2017. **11**: p. 273-293.
81. Xiao, J. and R.H. Yolken, *Strain hypothesis of Toxoplasma gondii infection on the outcome of human diseases.* Acta Physiol (Oxf), 2015. **213**(4): p. 828-45.
82. Khan, A., et al., *Genotyping of Toxoplasma gondii strains from immunocompromised patients reveals high prevalence of type I strains.* J Clin Microbiol, 2005. **43**(12): p. 5881-7.
83. Jones, J.L., M.E. Parise, and A.E. Fiore, *Neglected parasitic infections in the United States: toxoplasmosis.* Am J Trop Med Hyg, 2014. **90**(5): p. 794-9.
84. Torrey, E.F., et al., *Antibodies to Toxoplasma gondii in patients with schizophrenia: a meta-analysis.* Schizophr Bull, 2007. **33**(3): p. 729-36.
85. Pearce, B.D., D. Kruszon-Moran, and J.L. Jones, *The relationship between Toxoplasma gondii infection and mood disorders in the third National Health and Nutrition Survey.* Biol Psychiatry, 2012. **72**(4): p. 290-5.
86. Arling, T.A., et al., *Toxoplasma gondii antibody titers and history of suicide attempts in patients with recurrent mood disorders.* J Nerv Ment Dis, 2009. **197**(12): p. 905-8.
87. Gajewski, P.D., et al., *Toxoplasma gondii impairs memory in infected seniors.* Brain Behav Immun, 2014. **36**: p. 193-9.
88. Kamerkar, S. and P.H. Davis, *Toxoplasma on the brain: understanding host-pathogen interactions in chronic CNS infection.* J Parasitol Res, 2012. **2012**: p. 589295.

89. Fekadu, A., T. Shibre, and A.J. Cleare, *Toxoplasmosis as a cause for behaviour disorders--overview of evidence and mechanisms.* Folia Parasitol (Praha), 2010. **57**(2): p. 105-13.
90. Torgerson, P.R. and P. Mastroiacovo, *The global burden of congenital toxoplasmosis: a systematic review.* Bull World Health Organ, 2013. **91**(7): p. 501-8.
91. Robert-Gangneux, F. and M.L. Darde, *Epidemiology of and diagnostic strategies for toxoplasmosis.* Clin Microbiol Rev, 2012. **25**(2): p. 264-96.
92. Walker, M. and J.R. Zunt, *Parasitic central nervous system infections in immunocompromised hosts.* Clin Infect Dis, 2005. **40**(7): p. 1005-15.
93. Hu, K., et al., *Daughter cell assembly in the protozoan parasite Toxoplasma gondii.* Mol Biol Cell, 2002. **13**(2): p. 593-606.
94. Luder, C.G.K. and T. Rahman, *Impact of the host on Toxoplasma stage differentiation.* Microb Cell, 2017. **4**(7): p. 203-211.
95. Black, M.W. and J.C. Boothroyd, *Lytic cycle of Toxoplasma gondii.* Microbiol Mol Biol Rev, 2000. **64**(3): p. 607-23.
96. Furtado, J.M., et al., *Toxoplasmosis: a global threat.* J Glob Infect Dis, 2011. **3**(3): p. 281-4.
97. Vannier, E., B.E. Gewurz, and P.J. Krause, *Human babesiosis.* Infect Dis Clin North Am, 2008. **22**(3): p. 469-88, viii-ix.
98. Hersh, M.H., et al., *Reservoir competence of wildlife host species for Babesia microti.* Emerg Infect Dis, 2012. **18**(12): p. 1951-7.
99. Brayton, K.A., et al., *Genome sequence of Babesia bovis and comparative analysis of apicomplexan hemoprotozoa.* PLoS Pathog, 2007. **3**(10): p. 1401-13.
100. Bock, R., et al., *Babesiosis of cattle.* Parasitology, 2004. **129 Suppl**: p. S247-69.
101. Mosqueda, J., et al., *Current advances in detection and treatment of babesiosis.* Curr Med Chem, 2012. **19**(10): p. 1504-18.
102. Rajabi, S., B. Esmaeilnejad, and M. Tavassoli, *A molecular study on Babesia spp. in cattle and ticks in West-Azerbaijan province, Iran.* Vet Res Forum, 2017. **8**(4): p. 299-306.
103. Howell, J.M., et al., *Persistently Infected Calves as Reservoirs for Acquisition and Transovarial Transmission of Babesia bovis by Rhipicephalus (Boophilus) microplus.* Journal of Clinical Microbiology, 2007. **45**(10): p. 3155-3159.
104. De Vos, A.J. and R.E. Bock, *Vaccination against bovine babesiosis.* Ann N Y Acad Sci, 2000. **916**: p. 540-5.
105. de Waal, D.T. and M.P. Combrink, *Live vaccines against bovine babesiosis.* Vet Parasitol, 2006. **138**(1-2): p. 88-96.
106. Homer, M.J., et al., *Babesiosis.* Clin Microbiol Rev, 2000. **13**(3): p. 451-69.
107. Rudzinska, M.A., *Ultrastructure of intraerythrocytic Babesia microti with emphasis on the feeding mechanism.* J Protozool, 1976. **23**(2): p. 224-33.
108. Hajdusek, O., et al., *Interaction of the tick immune system with transmitted pathogens.* Front Cell Infect Microbiol, 2013. **3**: p. 26.
109. Mehlhorn, H. and E. Shein, *The piroplasms: life cycle and sexual stages.* Adv Parasitol, 1984. **23**: p. 37-103.
110. Heekin, A.M., et al., *The ovarian transcriptome of the cattle tick, Rhipicephalus (Boophilus) microplus, feeding upon a bovine host infected with Babesia bovis.* Parasit Vectors, 2013. **6**: p. 276.
111. Chauvin, A., et al., *Babesia and its hosts: adaptation to long-lasting interactions as a way to achieve efficient transmission.* Vet Res, 2009. **40**(2): p. 37.
112. Cohen, P., *The origins of protein phosphorylation.* Nat Cell Bio, 2002. **4**: p. E127+.
113. Kannan, N., et al., *Structural and functional diversity of the microbial kinome.* PLoS Biol, 2007. **5**(3): p. e17.
114. Walsh, C.T., S. Garneau-Tsodikova, and G.J. Gatto, Jr., *Protein posttranslational modifications: the chemistry of proteome diversifications.* Angew Chem Int Ed Engl, 2005. **44**(45): p. 7342-72.
115. Fabbro, D., S.W. Cowan-Jacob, and H. Moebitz, *Ten things you should know about protein kinases: IUPHAR Review 14.* Br J Pharmacol, 2015. **172**(11): p. 2675-700.
116. Endicott, J.A., M.E. Noble, and L.N. Johnson, *The structural basis for control of eukaryotic protein kinases.* Annu Rev Biochem, 2012. **81**: p. 587-613.
117. Taylor, S.S. and A.P. Kornev, *Protein kinases: evolution of dynamic regulatory proteins.* Trends Biochem Sci, 2011. **36**(2): p. 65-77.
118. Cargnello, M. and P.P. Roux, *Activation and function of the MAPKs and their substrates, the MAPK-activated protein kinases.* Microbiol Mol Biol Rev, 2011. **75**(1): p. 50-83.
119. Nishi, H., K. Hashimoto, and A.R. Panchenko, *Phosphorylation in protein-protein binding: effect on stability and function.* Structure, 2011. **19**(12): p. 1807-15.

120. Arthur, J.S.C. and S.C. Ley, *Mitogen-activated protein kinases in innate immunity.* Nat Rev Immunol, 2013. **13**(9): p. 679-692.
121. Pearson, G., et al., *Mitogen-activated protein (MAP) kinase pathways: regulation and physiological functions.* Endo Rev, 2001. **22**(2): p. 153-183.
122. Dhillon, A.S., et al., *MAP kinase signalling pathways in cancer.* Oncogene, 2007. **26**: p. 3279.
123. Zehorai, E., et al., *The subcellular localization of MEK and ERK--a novel nuclear translocation signal (NTS) paves a way to the nucleus.* Mol Cell Endocrinol, 2010. **314**(2): p. 213-20.
124. Andreadi, C., et al., *Regulation of MEK/ERK pathway output by subcellular localization of B-Raf.* Biochem Soc Trans, 2012. **40**(1): p. 67-72.
125. Morice, C., et al., *Raf-1 and B-Raf proteins have similar regional distributions but differential subcellular localization in adult rat brain.* Eur J Neurosci, 1999. **11**(6): p. 1995-2006.
126. Abd Elmageed, Z.Y., et al., *Prognostic Role of BRAF(V600E) Cellular Localization in Melanoma.* J Am Coll Surg, 2018. **226**(4): p. 526-537.
127. Vlastaridis, P., et al., *Estimating the total number of phosphoproteins and phosphorylation sites in eukaryotic proteomes.* Gigascience, 2017. **6**(2): p. 1-11.
128. Ardito, F., et al., *The crucial role of protein phosphorylation in cell signalling and its use as targeted therapy (Review).* Int J Mol Med, 2017. **40**(2): p. 271-280.
129. Pruitt, K.D., et al., *NCBI Reference Sequences (RefSeq): current status, new features and genome annotation policy.* Nucleic Acids Res, 2012. **40**(Database issue): p. D130-5.
130. Raggiaschi, R., S. Gotta, and G.C. Terstappen, *Phosphoproteome analysis.* Biosci Rep, 2005. **25**(1-2): p. 33-44.
131. Ubersax, J.A. and J.E. Ferrell, Jr., *Mechanisms of specificity in protein phosphorylation.* Nat Rev Mol Cell Biol, 2007. **8**(7): p. 530-41.
132. Manning, G., et al., *The protein kinase complement of the human genome.* Science, 2002. **298**(5600): p. 1912-34.
133. LaRonde-LeBlanc, N. and A. Wlodawer, *The RIO kinases: an atypical protein kinase family required for ribosome biogenesis and cell cycle progression.* Biochim Biophys Acta, 2005. **1754**(1-2): p. 14-24.
134. Talevich, E., A. Mirza, and N. Kannan, *Structural and evolutionary divergence of eukaryotic protein kinases in Apicomplexa*. BMC Evol Biol, 2011. **11**: p. 321.
135. Miranda-Saavedra, D., et al., *The kinomes of apicomplexan parasites.* Microbes Infect, 2012. **14**(10): p. 796-810.
136. Miranda-Saavedra, D. and G.J. Barton, *Classification and functional annotation of eukaryotic protein kinases.* Proteins, 2007. **68**(4): p. 893-914.
137. Lourido, S. and S.N. Moreno, *The calcium signalling toolkit of the Apicomplexan parasites Toxoplasma gondii and Plasmodium spp.* Cell Calcium, 2015. **57**(3): p. 186-93.
138. Peixoto, L., et al., *Integrative genomic approaches highlight a family of parasite-specific kinases that regulate host responses.* Cell Host Microbe, 2010. **8**(2): p. 208-18.
139. Fox, B.A., et al., *The Toxoplasma gondii Rhoptry Kinome Is Essential for Chronic Infection.* MBio, 2016. **7**(3).
140. Ward, P., et al., *Protein kinases of the human malaria parasite Plasmodium falciparum: the kinome of a divergent eukaryote.* BMC Genomics, 2004. **5**(1): p. 79.
141. Anamika, N. Srinivasan, and A. Krupa, *A genomic perspective of protein kinases in Plasmodium falciparum.* Proteins, 2005. **58**(1): p. 180-9.
142. Schneider, A.G. and O. Mercereau-Puijalon, *A new Apicomplexa-specific protein kinase family : multiple members in Plasmodium falciparum, all with an export signature.* BMC Genomics, 2005. **6**: p. 30.
143. Ward, P., et al., *Protein kinases of the human malaria parasite Plasmodium falciparum: the kinome of a divergent eukaryote.* BMC Genomics, 2004. **5**: p. 79.
144. Nunes, M.C., et al., *A novel protein kinase family in Plasmodium falciparum is differentially transcribed and secreted to various cellular compartments of the host cell.* Mol Microbiol, 2007. **63**(2): p. 391-403.
145. Nunes, M.C., et al., *Plasmodium falciparum FIKK kinase members target distinct components of the erythrocyte membrane.* PLoS One, 2010. **5**(7): p. e11747.
146. Kats, L.M., et al., *An exported kinase (FIKK4.2) that mediates virulence-associated changes in Plasmodium falciparum-infected red blood cells.* Int J Parasitol, 2014. **44**(5): p. 319-28.
147. Solyakov, L., et al., *Global kinomic and phospho-proteomic analyses of the human malaria parasite Plasmodium falciparum.* Nat Commun, 2011. **2**: p. 565.
148. Dorin, D., et al., *PfPK7, an atypical MEK-related protein kinase, reflects the absence of classical three-component MAPK pathways in the human malaria parasite Plasmodium falciparum.* Mol Microbiol, 2005. **55**(1): p. 184-96.
149. Murungi, E.K. and H.M. Kariithi, *Genome-Wide Identification and Evolutionary Analysis of Sarcocystis neurona Protein Kinases.* Pathogens, 2017. **6**(1).

150. Hidaka, H., et al., *Isoquinolinesulfonamides, novel and potent inhibitors of cyclic nucleotide dependent protein kinase and protein kinase C.* Biochemistry, 1984. **23**(21): p. 5036-41.
151. Cohen, P., *Protein kinases--the major drug targets of the twenty-first century?* Nat Rev Drug Discov, 2002. **1**(4): p. 309-15.
152. Davies, S.P., et al., *Specificity and mechanism of action of some commonly used protein kinase inhibitors.* Biochem J, 2000. **351**(Pt 1): p. 95-105.
153. Roskoski, R., Jr., *Properties of FDA-approved small molecule protein kinase inhibitors.* Pharmacol Res, 2019. **144**: p. 19-50.
154. Zhou, C., et al., *Laser mimicking mosquito bites for skin delivery of malaria sporozoite vaccines.* J Control Release, 2015. **204**: p. 30-7.
155. Downward, J., *Targeting RAS signalling pathways in cancer therapy.* Nat Rev Cancer, 2003. **3**(1): p. 11-22.
156. Gysin, S., et al., *Therapeutic Strategies for Targeting Ras Proteins.* Genes Cancer, 2011. **2**(3): p. 359-72.
157. Flaherty, K.T., et al., *Improved survival with MEK inhibition in BRAF-mutated melanoma.* N Engl J Med, 2012. **367**(2): p. 107-14.
158. Rotella, D.P., *Recent results in protein kinase inhibition for tropical diseases.* Bioorg Med Chem Lett, 2012. **22**(22): p. 6788-93.
159. Lucet, I.S., et al., *Plasmodium kinases as targets for new-generation antimalarials.* Future Med Chem, 2013. **4**(18): p. 2295-310.
160. Gurnett, A.M., et al., *Purification and molecular characterization of cGMP-dependent protein kinase from Apicomplexan parasites. A novel chemotherapeutic target.* J Biol Chem, 2002. **277**(18): p. 15913-22.
161. Ojo, K.K., et al., *Toxoplasma gondii calcium-dependent protein kinase 1 is a target for selective kinase inhibitors.* Nat Struct Mol Biol, 2010. **17**(5): p. 602-7.
162. Schor, S. and S. Einav, *Combating Intracellular Pathogens with Repurposed Host-Targeted Drugs.* ACS Infect Dis, 2018. **4**(2): p. 88-92.
163. Deitsch, K.W., *Self-targeting blocks malaria parasite invasion.* J Exp Med, 2015. **212**(8): p. 1143.
164. Zenonos, Z.A., et al., *Basigin is a druggable target for host-oriented antimalarial interventions.* J Exp Med, 2015. **212**(8): p. 1145-51.
165. Ingley, E., *Integrating novel signalling pathways involved in erythropoiesis.* IUBMB Life, 2012. **64**(5): p. 402-10.
166. Schnoder, T.M., et al., *Epo-induced erythroid maturation is dependent on Plcgamma1 signalling.* Cell Death Differ, 2015. **22**(6): p. 974-85.
167. Chin, H., et al., *Lyn physically associates with the erythropoietin receptor and may play a role in activation of the Stat5 pathway.* Blood, 1998. **91**(10): p. 3734-45.
168. Carroll, M.P., et al., *Erythropoietin induces Raf-1 activation and Raf-1 is required for erythropoietin-mediated proliferation.* J Biol Chem, 1991. **266**(23): p. 14964-9.
169. Polak, R. and M. Buitenhuis, *The PI3K/PKB signalling module as key regulator of hematopoiesis: implications for therapeutic strategies in leukemia.* Blood, 2012. **119**(4): p. 911-23.
170. Remy, I., I.A. Wilson, and S.W. Michnick, *Erythropoietin receptor activation by a ligand-induced conformation change.* Science, 1999. **283**(5404): p. 990-3.
171. Kling, P.J., et al., *Insulin-like growth factor-I stimulates erythropoiesis when administered enterally.* Growth Factors, 2006. **24**(3): p. 218-23.
172. Ratajczak, J., et al., *The role of insulin (INS) and insulin-like growth factor-I (IGF-I) in regulating human erythropoiesis. Studies in vitro under serum-free conditions--comparison to other cytokines and growth factors.* Leukemia, 1998. **12**(3): p. 371-81.
173. Nocka, K., et al., *Expression of c-kit gene products in known cellular targets of W mutations in normal and W mutant mice--evidence for an impaired c-kit kinase in mutant mice.* Genes Dev, 1989. **3**(6): p. 816-26.
174. Munugalavadla, V. and R. Kapur, *Role of c-Kit and erythropoietin receptor in erythropoiesis.* Crit Rev Oncol Hematol, 2005. **54**(1): p. 63-75.
175. Broudy, V.C., et al., *Interaction of stem cell factor and its receptor c-kit mediates lodgment and acute expansion of hematopoietic cells in the murine spleen.* Blood, 1996. **88**(1): p. 75-81.
176. Heynen, M.J. and R.L. Verwilghen, *A quantitative ultrastructural study of normal rat erythroblasts and reticulocytes.* Cell Tissue Res, 1982. **224**(2): p. 397-408.
177. Setchenska, M.S., S.A. Bonanou-Tzedaki, and H.R. Arnstein, *Characteristic enzymatic changes during rabbit bone marrow erythroid cell development.* Biomed Biochim Acta, 1990. **49**(2-3): p. S59-63.
178. Goh, S.H., et al., *The human reticulocyte transcriptome.* Physiol Genomics, 2007. **30**(2): p. 172-8.

179. Son, Y., et al., *Mitogen-Activated Protein Kinases and Reactive Oxygen Species: How Can ROS Activate MAPK Pathways?* J Signal Transduct, 2011. **2011**: p. 792639.
180. Olson, J.M. and A.R. Hallahan, *p38 MAP kinase: a convergence point in cancer therapy.* Trends Mol Med, 2004. **10**(3): p. 125-9.
181. Chu, T.T.T., et al., *Quantitative mass spectrometry of human reticulocytes reveal proteome-wide modifications during maturation.* Br J Haematol, 2018. **180**(1): p. 118-133.
182. Fonslow, B.R., et al., *Improvements in proteomic metrics of low abundance proteins through proteome equalization using ProteoMiner prior to MudPIT.* J Proteome Res, 2011. **10**(8): p. 3690-700.
183. Franco, R.S., *Measurement of red cell lifespan and aging.* Transfus Med Hemother, 2012. **39**(5): p. 302-7.
184. D'Alessandro, A., P.G. Righetti, and L. Zolla, *The red blood cell proteome and interactome: an update.* J Proteome Res, 2010. **9**(1): p. 144-63.
185. Kostova, E.B., et al., *Identification of signalling cascades involved in red blood cell shrinkage and vesiculation.* Biosci Rep, 2015. **35**(2).
186. Carafoli, E. and J. Krebs, *Why Calcium? How Calcium Became the Best Communicator.* J Biol Chem, 2016. **291**(40): p. 20849-20857.
187. Bogdanova, A., et al., *Calcium in red blood cells-a perilous balance.* Int J Mol Sci, 2013. **14**(5): p. 9848-72.
188. Makhro, A., et al., *N-methyl-D-aspartate receptors in human erythroid precursor cells and in circulating red blood cells contribute to the intracellular calcium regulation.* Am J Physiol Cell Physiol, 2013. **305**(11): p. C1123-38.
189. Romero, P.J. and E.A. Romero, *The role of calcium metabolism in human red blood cell ageing: a proposal.* Blood Cells Mol Dis, 1999. **25**(1): p. 9-19.
190. Nishizuka, Y., *Discovery and prospect of protein kinase C research: epilogue.* J Biochem, 2003. **133**(2): p. 155-8.
191. Klarl, B.A., et al., *Protein kinase C mediates erythrocyte "programmed cell death" following glucose depletion.* Am J Physiol Cell Physiol, 2006. **290**(1): p. C244-53.
192. Gatidis, S., et al., *p38 MAPK activation and function following osmotic shock of erythrocytes.* Cell Physiol Biochem, 2011. **28**(6): p. 1279-86.
193. Mihaylova, M.M. and R.J. Shaw, *The AMPK signalling pathway coordinates cell growth, autophagy and metabolism.* Nat Cell Biol, 2011. **13**(9): p. 1016-23.
194. Wang, S., et al., *AMPKalpha1 deletion shortens erythrocyte life span in mice: role of oxidative stress.* J Biol Chem, 2010. **285**(26): p. 19976-85.
195. Foller, M., et al., *Regulation of erythrocyte survival by AMP-activated protein kinase.* FASEB J, 2009. **23**(4): p. 1072-80.
196. Antonelou, M.H., A.G. Kriebardis, and I.S. Papassideri, *Aging and death signalling in mature red cells: from basic science to transfusion practice.* Blood Transfus, 2010. **8 Suppl 3**: p. s39-47.
197. Ruivo, M.T.G., et al., *Host AMPK Is a Modulator of Plasmodium Liver Infection.* Cell Rep, 2016. **16**(10): p. 2539-2545.
198. Caradonna, K.L., et al., *Host metabolism regulates intracellular growth of Trypanosoma cruzi.* Cell Host Microbe, 2013. **13**(1): p. 108-17.
199. Mankouri, J., et al., *Enhanced hepatitis C virus genome replication and lipid accumulation mediated by inhibition of AMP-activated protein kinase.* Proc Natl Acad Sci U S A, 2010. **107**(25): p. 11549-54.
200. Moser, T.S., D. Schieffer, and S. Cherry, *AMP-activated kinase restricts Rift Valley fever virus infection by inhibiting fatty acid synthesis.* PLoS Pathog, 2012. **8**(4): p. e1002661.
201. Brunton, J., et al., *Feeding uninvited guests: mTOR and AMPK set the table for intracellular pathogens.* PLoS Pathog, 2013. **9**(10): p. e1003552.
202. Walsh, D., et al., *Regulation of the translation initiation factor eIF4F by multiple mechanisms in human cytomegalovirus-infected cells.* J Virol, 2005. **79**(13): p. 8057-64.
203. Moreira, D., et al., *Leishmania infantum modulates host macrophage mitochondrial metabolism by hijacking the SIRT1-AMPK axis.* PLoS Pathog, 2015. **11**(3): p. e1004684.
204. Kumar, S.H. and A. Rangarajan, *Simian virus 40 small T antigen activates AMPK and triggers autophagy to protect cancer cells from nutrient deprivation.* J Virol, 2009. **83**(17): p. 8565-74.
205. Tang, Y., et al., *Enterotoxigenic Escherichia coli infection induces intestinal epithelial cell autophagy.* Vet Microbiol, 2014. **171**(1-2): p. 160-4.
206. Shin, D.M., et al., *Mycobacterial lipoprotein activates autophagy via TLR2/1/CD14 and a functional vitamin D receptor signalling.* Cell Microbiol, 2010. **12**(11): p. 1648-65.
207. Organ, S.L. and M.S. Tsao, *An overview of the c-MET signalling pathway.* Ther Adv Med Oncol, 2011. **3**(1 Suppl): p. S7-S19.

208. Rodrigues, G.A. and M. Park, *Autophosphorylation modulates the kinase activity and oncogenic potential of the Met receptor tyrosine kinase.* Oncogene, 1994. **9**(7): p. 2019-27.
209. Huh, C.G., et al., *Hepatocyte growth factor/c-met signalling pathway is required for efficient liver regeneration and repair.* Proc Natl Acad Sci U S A, 2004. **101**(13): p. 4477-82.
210. Carrolo, M., et al., *Hepatocyte growth factor and its receptor are required for malaria infection.* Nat Med, 2003. **9**(11): p. 1363-9.
211. Leiriao, P., et al., *HGF/MET signalling protects Plasmodium-infected host cells from apoptosis.* Cell Microbiol, 2005. **7**(4): p. 603-9.
212. Churin, Y., et al., *Helicobacter pylori CagA protein targets the c-Met receptor and enhances the motogenic response.* J Cell Biol, 2003. **161**(2): p. 249-55.
213. Shen, Y., et al., *InIB-dependent internalization of Listeria is mediated by the Met receptor tyrosine kinase.* Cell, 2000. **103**(3): p. 501-10.
214. Ozden, M., et al., *Hepatocyte growth factor (HGF) in patients with hepatitis B and meningitis.* J Infect, 2004. **49**(3): p. 229-35.
215. Mota, M.M., et al., *Migration of Plasmodium sporozoites through cells before infection.* Science, 2001. **291**(5501): p. 141-4.
216. Kaushansky, A. and S.H. Kappe, *The crucial role of hepatocyte growth factor receptor during liver-stage infection is not conserved among Plasmodium species.* Nat Med, 2011. **17**(10): p. 1180-1; author reply 1181.
217. Laptenko, O. and C. Prives, *Transcriptional regulation by p53: one protein, many possibilities.* Cell Death Differ, 2006. **13**(6): p. 951-61.
218. Kaushansky, A., et al., *Suppression of host p53 is critical for Plasmodium liver-stage infection.* Cell Rep, 2013. **3**(3): p. 630-7.
219. Kale, J., E.J. Osterlund, and D.W. Andrews, *BCL-2 family proteins: changing partners in the dance towards death.* Cell Death Differ, 2018. **25**(1): p. 65-80.
220. Semblat, J.P. and C. Doerig, *PAK in pathogen-host interactions.* Cell Logist, 2012. **2**(2): p. 126-131.
221. Krachler, A.M., A.R. Woolery, and K. Orth, *Manipulation of kinase signalling by bacterial pathogens.* J Cell Biol, 2011. **195**(7): p. 1083-92.
222. Park, E.R., S.T. Eblen, and A.D. Catling, *MEK1 activation by PAK: a novel mechanism.* Cell Signal, 2007. **19**(7): p. 1488-96.
223. John Von Freyend, S., et al., *Subverting Host Cell P21-Activated Kinase: A Case of Convergent Evolution across Pathogens.* Pathogens, 2017. **6**(2).
224. Millholland, M.G., et al., *A host GPCR signalling network required for the cytolysis of infected cells facilitates release of apicomplexan parasites.* Cell Host Microbe, 2013. **13**(1): p. 15-28.
225. Pakpour, N., et al., *Protein kinase C-dependent signalling controls the midgut epithelial barrier to malaria parasite infection in anopheline mosquitoes.* PLoS One, 2013. **8**(10): p. e76535.
226. Bruce, L.J., et al., *A band 3-based macrocomplex of integral and peripheral proteins in the RBC membrane.* Blood, 2003. **101**(10): p. 4180-8.
227. Zipser, Y. and N.S. Kosower, *Phosphotyrosine phosphatase associated with band 3 protein in the human erythrocyte membrane.* Biochem J, 1996. **314 (Pt 3)**: p. 881-7.
228. Pantaleo, A., et al., *Analysis of changes in tyrosine and serine phosphorylation of red cell membrane proteins induced by P. falciparum growth.* Proteomics, 2010. **10**(19): p. 3469-79.
229. Pantaleo, A., et al., *Oxidized and poorly glycosylated band 3 is selectively phosphorylated by Syk kinase to form large membrane clusters in normal and G6PD-deficient red blood cells.* Biochem J, 2009. **418**(2): p. 359-67.
230. Neves, S.R., P.T. Ram, and R. Iyengar, *G protein pathways.* Science, 2002. **296**(5573): p. 1636-9.
231. Harrison, T., et al., *Erythrocyte G protein-coupled receptor signalling in malarial infection.* Science, 2003. **301**(5640): p. 1734-6.
232. Murphy, S.C., et al., *Erythrocyte G protein as a novel target for malarial chemotherapy.* PLoS Med, 2006. **3**(12): p. e528.
233. Cooke, B.M., N. Mohandas, and R.L. Coppel, *The malaria-infected red blood cell: structural and functional changes.* Adv Parasitol, 2001. **50**: p. 1-86.
234. Butcher, B.A., et al., *IL-10-independent STAT3 activation by Toxoplasma gondii mediates suppression of IL-12 and TNF-alpha in host macrophages.* J Immunol, 2005. **174**(6): p. 3148-52.
235. Saeij, J.P., et al., *Toxoplasma co-opts host gene expression by injection of a polymorphic kinase homologue.* Nature, 2007. **445**(7125): p. 324-7.
236. Butcher, B.A., et al., *Toxoplasma gondii rhoptry kinase ROP16 activates STAT3 and STAT6 resulting in cytokine inhibition and arginase-1-dependent growth control.* PLoS Pathog, 2011. **7**(9): p. e1002236.
237. Portillo, J.C., et al., *Toxoplasma gondii induces FAK-Src-STAT3 signalling during infection of host cells that prevents parasite targeting by autophagy.* PLoS Pathog, 2017. **13**(10): p. e1006671.

238. Leng, J., B.A. Butcher, and E.Y. Denkers, *Dysregulation of macrophage signal transduction by Toxoplasma gondii: past progress and recent advances.* Parasite Immunol, 2009. **31**(12): p. 717-28.
239. Schneider, W.M., M.D. Chevillotte, and C.M. Rice, *Interferon-stimulated genes: a complex web of host defenses.* Annu Rev Immunol, 2014. **32**: p. 513-45.
240. Nandan, D. and N.E. Reiner, *Attenuation of gamma interferon-induced tyrosine phosphorylation in mononuclear phagocytes infected with Leishmania donovani: selective inhibition of signalling through Janus kinases and Stat1.* Infect Immun, 1995. **63**(11): p. 4495-500.
241. Moser, L.A., A.M. Pollard, and L.J. Knoll, *A genome-wide siRNA screen to identify host factors necessary for growth of the parasite Toxoplasma gondii.* PLoS One, 2013. **8**(6): p. e68129.
242. Walliker, D., et al., *Genetic analysis of the human malaria parasite Plasmodium falciparum.* Science, 1987. **236**(4809): p. 1661-6.
243. Lambros, C. and J.P. Vanderberg, *Synchronization of Plasmodium falciparum erythrocytic stages in culture.* J Parasitol, 1979. **65**(3): p. 418-20.
244. Boyle, M.J., et al., *Interactions with heparin-like molecules during erythrocyte invasion by Plasmodium falciparum merozoites.* Blood, 2010. **115**(22): p. 4559-68.
245. Dery, V., et al., *An improved SYBR Green-1-based fluorescence method for the routine monitoring of Plasmodium falciparum resistance to anti-malarial drugs.* Malar J, 2015. **14**: p. 481.
246. Albuquerque, S.S., et al., *Host cell transcriptional profiling during malaria liver stage infection reveals a coordinated and sequential set of biological events.* BMC Genomics, 2009. **10**: p. 270.
247. Chen, Z., et al., *Current applications of antibody microarrays.* Clin Proteomics, 2018. **15**: p. 7.
248. Haab, B.B., *Methods and applications of antibody microarrays in cancer research.* Proteomics, 2003. **3**(11): p. 2116-22.
249. Haqshenas, G., et al., *A Role for the Insulin Receptor in the Suppression of Dengue Virus and Zika Virus in Wolbachia-Infected Mosquito Cells.* Cell Rep, 2019. **26**(3): p. 529-535 e3.
250. Haqshenas, G., et al., *Signalome-wide assessment of host cell response to hepatitis C virus.* Nat Commun, 2017. **8**: p. 15158.
251. Hestvik, A.L., Z. Hmama, and Y. Av-Gay, *Kinome analysis of host response to mycobacterial infection: a novel technique in proteomics.* Infect Immun, 2003. **71**(10): p. 5514-22.
252. Singh, B., et al., *A large focus of naturally acquired Plasmodium knowlesi infections in human beings.* Lancet, 2004. **363**(9414): p. 1017-24.
253. Brasil, P., et al., *Outbreak of human malaria caused by Plasmodium simium in the Atlantic Forest in Rio de Janeiro: a molecular epidemiological investigation.* Lancet Glob Health, 2017. **5**(10): p. e1038-e1046.
254. Haldar, K., S. Bhattacharjee, and I. Safeukui, *Drug resistance in Plasmodium.* Nat Rev Microbiol, 2018. **16**(3): p. 156-170.
255. Bhullar, K.S., et al., *Kinase-targeted cancer therapies: progress, challenges and future directions.* Mol Cancer, 2018. **17**(1): p. 48.
256. Ntumngia, F.B., et al., *The role of the human Duffy antigen receptor for chemokines in malaria susceptibility: current opinions and future treatment prospects.* J Receptor Ligand Channel Res, 2016. **9**: p. 1-11.
257. Brizuela, M., et al., *Treatment of erythrocytes with the 2-cys peroxiredoxin inhibitor, Conoidin A, prevents the growth of Plasmodium falciparum and enhances parasite sensitivity to chloroquine.* PLoS One, 2014. **9**(4): p. e92411.
258. Koncarevic, S., et al., *The malarial parasite Plasmodium falciparum imports the human protein peroxiredoxin 2 for peroxide detoxification.* Proc Natl Acad Sci U S A, 2009. **106**(32): p. 13323-8.
259. Radu, M., et al., *PAK signalling during the development and progression of cancer.* Nat Rev Cancer, 2014. **14**(1): p. 13-25.
260. Elandalloussi, L.M. and P.J. Smith, *Preparation of pure and intact Plasmodium falciparum plasma membrane vesicles and partial characterisation of the plasma membrane ATPase.* Malar J, 2002. **1**: p. 6.
261. Gong, J., M. Park, and S.F. Steinberg, *Cleavage Alters the Molecular Determinants of Protein Kinase C-delta Catalytic Activity.* Mol Cell Biol, 2017. **37**(20).
262. Liu, Y., et al., *Phosphorylation of the protein kinase C-theta activation loop and hydrophobic motif regulates its kinase activity, but only activation loop phosphorylation is critical to in vivo nuclear-factor-kappaB induction.* Biochem J, 2002. **361**(Pt 2): p. 255-65.
263. Wang, X., et al., *Regulation of PKC-theta function by phosphorylation in T cell receptor signalling.* Front Immunol, 2012. **3**: p. 197.
264. Bouyer, G., et al., *Plasmodiumfalciparum infection induces dynamic changes in the erythrocyte phospho-proteome.* Blood Cells Mol Dis, 2016. **58**: p. 35-44.

265. Zhang, B.H. and K.L. Guan, *Activation of B-Raf kinase requires phosphorylation of the conserved residues Thr598 and Ser601.* EMBO J, 2000. **19**(20): p. 5429-39.
266. Chong, H., J. Lee, and K.L. Guan, *Positive and negative regulation of Raf kinase activity and function by phosphorylation.* EMBO J, 2001. **20**(14): p. 3716-27.
267. Leicht, D.T., et al., *Raf kinases: function, regulation and role in human cancer.* Biochim Biophys Acta, 2007. **1773**(8): p. 1196-212.
268. Dorin-Semblat, D., et al., *Functional characterization of both MAP kinases of the human malaria parasite Plasmodium falciparum by reverse genetics.* Mol Microbiol, 2007. **65**(5): p. 1170-80.
269. Brummer, T., et al., *Functional analysis of the regulatory requirements of B-Raf and the B-Raf(V600E) oncoprotein.* Oncogene, 2006. **25**(47): p. 6262-76.
270. Mason, C.S., et al., *Serine and tyrosine phosphorylations cooperate in Raf-1, but not B-Raf activation.* EMBO J, 1999. **18**(8): p. 2137-48.
271. Brummer, T., et al., *Inducible gene deletion reveals different roles for B-Raf and Raf-1 in B-cell antigen receptor signalling.* EMBO J, 2002. **21**(21): p. 5611-22.
272. Varga, A., et al., *RAF1/BRAF dimerization integrates the signal from RAS to ERK and ROKalpha.* Sci Signal, 2017. **10**(469).
273. Hekman, M., et al., *Novel C-Raf phosphorylation sites: serine 296 and 301 participate in Raf regulation.* FEBS Lett, 2005. **579**(2): p. 464-8.
274. Rossomando, A.J., et al., *Mitogen-activated protein kinase kinase 1 (MKK1) is negatively regulated by threonine phosphorylation.* Mol Cell Biol, 1994. **14**(3): p. 1594-602.
275. Brunet, A., G. Pages, and J. Pouyssegur, *Growth factor-stimulated MAP kinase induces rapid retrophosphorylation and inhibition of MAP kinase kinase (MEK1).* FEBS Lett, 1994. **346**(2-3): p. 299-303.
276. Xu, B., et al., *The N-terminal ERK-binding site of MEK1 is required for efficient feedback phosphorylation by ERK2 in vitro and ERK activation in vivo.* J Biol Chem, 1999. **274**(48): p. 34029-35.
277. Roskoski, R., Jr., *MEK1/2 dual-specificity protein kinases: structure and regulation.* Biochem Biophys Res Commun, 2012. **417**(1): p. 5-10.
278. Bromberg-White, J.L., N.J. Andersen, and N.S. Duesbery, *MEK genomics in development and disease.* Brief Funct Genomics, 2012. **11**(4): p. 300-10.
279. Payne, D.M., et al., *Identification of the regulatory phosphorylation sites in pp42/mitogen-activated protein kinase (MAP kinase).* EMBO J, 1991. **10**(4): p. 885-92.
280. Goetz, E.M., et al., *ERK mutations confer resistance to mitogen-activated protein kinase pathway inhibitors.* Cancer Res, 2014. **74**(23): p. 7079-89.
281. Lai, S. and S. Pelech, *Regulatory roles of conserved phosphorylation sites in the activation T-loop of the MAP kinase ERK1.* Mol Biol Cell, 2016. **27**(6): p. 1040-50.
282. Zarnegar, R. and G.K. Michalopoulos, *The many faces of hepatocyte growth factor: from hepatopoiesis to hematopoiesis.* J Cell Biol, 1995. **129**(5): p. 1177-80.
283. Teofili, L., et al., *Expression of the c-met proto-oncogene and its ligand, hepatocyte growth factor, in Hodgkin disease.* Blood, 2001. **97**(4): p. 1063-9.
284. Emaduddin, M., et al., *Cell growth, global phosphotyrosine elevation, and c-Met phosphorylation through Src family kinases in colorectal cancer cells.* Proc Natl Acad Sci U S A, 2008. **105**(7): p. 2358-62.
285. Peschard, P., et al., *Mutation of the c-Cbl TKB domain binding site on the Met receptor tyrosine kinase converts it into a transforming protein.* Mol Cell, 2001. **8**(5): p. 995-1004.
286. Jeffers, M., et al., *Degradation of the Met tyrosine kinase receptor by the ubiquitin-proteasome pathway.* Mol Cell Biol, 1997. **17**(2): p. 799-808.
287. Neelam, S., et al., *Functional 20S proteasomes in mature human red blood cells.* Exp Biol Med (Maywood), 2011. **236**(5): p. 580-91.
288. Abella, J.V., et al., *Met/Hepatocyte growth factor receptor ubiquitination suppresses transformation and is required for Hrs phosphorylation.* Mol Cell Biol, 2005. **25**(21): p. 9632-45.
289. Trusolino, L., A. Bertotti, and P.M. Comoglio, *MET signalling: principles and functions in development, organ regeneration and cancer.* Nat Rev Mol Cell Biol, 2010. **11**(12): p. 834-48.
290. King, A.J., et al., *Demonstration of a genetic therapeutic index for tumors expressing oncogenic BRAF by the kinase inhibitor SB-590885.* Cancer Res, 2006. **66**(23): p. 11100-5.
291. Zhi, J., et al., *Effects of PHA-665752 and vemurafenib combination treatment on in vitro and murine xenograft growth of human colorectal cancer cells with BRAF(V600E) mutations.* Oncol Lett, 2018. **15**(3): p. 3904-3910.
292. Trager, W. and J.B. Jensen, *Human malaria parasites in continuous culture.* Science, 1976. **193**(4254): p. 673-5.

293. Lyth, O., et al., *Cellular dissection of malaria parasite invasion of human erythrocytes using viable Plasmodium knowlesi merozoites.* Sci Rep, 2018. **8**(1): p. 10165.
294. Dankwa, S., et al., *Ancient human sialic acid variant restricts an emerging zoonotic malaria parasite.* Nat Commun, 2016. **7**: p. 11187.
295. Hill, D.L., E.M. Eriksson, and L. Schofield, *High yield purification of Plasmodium falciparum merozoites for use in opsonizing antibody assays.* J Vis Exp, 2014(89).
296. Ribaut, C., et al., *Concentration and purification by magnetic separation of the erythrocytic stages of all human Plasmodium species.* Malar J, 2008. **7**: p. 45.
297. Johnson, J.D., et al., *Assessment and continued validation of the malaria SYBR green I-based fluorescence assay for use in malaria drug screening.* Antimicrob Agents Chemother, 2007. **51**(6): p. 1926-33.
298. Wilson, D.W., B.S. Crabb, and J.G. Beeson, *Development of fluorescent Plasmodium falciparum for in vitro growth inhibition assays.* Malar J, 2010. **9**: p. 152.
299. Nguyen, N., et al., *Broad activity of diphenyleneiodonium analogues against Mycobacterium tuberculosis, malaria parasites and bacterial pathogens.* Eur J Med Chem, 2018. **148**: p. 507-518.
300. Wilson, D.W., et al., *Defining the timing of action of antimalarial drugs against Plasmodium falciparum.* Antimicrob Agents Chemother, 2013. **57**(3): p. 1455-67.
301. Lin, J.W., et al., *Screening inhibitors of P. berghei blood stages using bioluminescent reporter parasites.* Methods Mol Biol, 2013. **923**: p. 507-22.
302. Franke-Fayard, B., et al., *A Plasmodium berghei reference line that constitutively expresses GFP at a high level throughout the complete life cycle.* Mol Biochem Parasitol, 2004. **137**(1): p. 23-33.
303. Yeoh, L.M., et al., *Comparative transcriptomics of female and male gametocytes in Plasmodium berghei and the evolution of sex in alveolates.* BMC Genomics, 2017. **18**(1): p. 734.
304. Delves, M.J., et al., *Male and female Plasmodium falciparum mature gametocytes show different responses to antimalarial drugs.* Antimicrob Agents Chemother, 2013. **57**(7): p. 3268-74.
305. Miao, J., et al., *Sex-Specific Biology of the Human Malaria Parasite Revealed from the Proteomes of Mature Male and Female Gametocytes.* Mol Cell Proteomics, 2017. **16**(4): p. 537-551.
306. Bousema, T. and C. Drakeley, *Epidemiology and infectivity of Plasmodium falciparum and Plasmodium vivax gametocytes in relation to malaria control and elimination.* Clin Microbiol Rev, 2011. **24**(2): p. 377-410.
307. Fu, Z., et al., *Intestinal cell kinase, a MAP kinase-related kinase, regulates proliferation and G1 cell cycle progression of intestinal epithelial cells.* Am J Physiol Gastrointest Liver Physiol, 2009. **297**(4): p. G632-40.
308. Paige Taylor, S., et al., *An inactivating mutation in intestinal cell kinase, ICK, impairs hedgehog signalling and causes short rib-polydactyly syndrome.* Hum Mol Genet, 2016. **25**(18): p. 3998-4011.
309. Fu, Z., et al., *Activation of a nuclear Cdc2-related kinase within a mitogen-activated protein kinase-like TDY motif by autophosphorylation and cyclin-dependent protein kinase-activating kinase.* Mol Cell Biol, 2005. **25**(14): p. 6047-64.
310. Macdonald, J.I. and F.A. Dick, *Posttranslational modifications of the retinoblastoma tumor suppressor protein as determinants of function.* Genes Cancer, 2012. **3**(11-12): p. 619-33.
311. Nair, J.S., et al., *Aurora B kinase regulates the postmitotic endoreduplication checkpoint via phosphorylation of the retinoblastoma protein at serine 780.* Mol Biol Cell, 2009. **20**(8): p. 2218-28.
312. Yeste-Velasco, M., et al., *The p38(MAPK) signalling pathway regulates neuronal apoptosis through the phosphorylation of the retinoblastoma protein.* Neurochem Int, 2009. **54**(2): p. 99-105.
313. Vogel, W.F., R. Abdulhussein, and C.E. Ford, *Sensing extracellular matrix: an update on discoidin domain receptor function.* Cell Signal, 2006. **18**(8): p. 1108-16.
314. Yang, K., et al., *Tyrosine 740 phosphorylation of discoidin domain receptor 2 by Src stimulates intramolecular autophosphorylation and Shc signalling complex formation.* J Biol Chem, 2005. **280**(47): p. 39058-66.
315. Chen, H.R., et al., *DDR1 promotes E-cadherin stability via inhibition of integrin-beta1-Src activation-mediated E-cadherin endocytosis.* Sci Rep, 2016. **6**: p. 36336.
316. Leitinger, B., *Discoidin domain receptor functions in physiological and pathological conditions.* Int Rev Cell Mol Biol, 2014. **310**: p. 39-87.
317. Guo, A., et al., *Signalling networks assembled by oncogenic EGFR and c-Met.* Proc Natl Acad Sci U S A, 2008. **105**(2): p. 692-7.
318. Turner, C.E., *Paxillin and focal adhesion signalling.* Nat Cell Biol, 2000. **2**(12): p. E231-6.
319. Bellis, S.L., J.T. Miller, and C.E. Turner, *Characterization of tyrosine phosphorylation of paxillin in vitro by focal adhesion kinase.* J Biol Chem, 1995. **270**(29): p. 17437-41.

320. Doza, Y.N., et al., *Activation of the MAP kinase homologue RK requires the phosphorylation of Thr-180 and Tyr-182 and both residues are phosphorylated in chemically stressed KB cells.* FEBS Lett, 1995. **364**(2): p. 223-8.
321. Enslen, H., J. Raingeaud, and R.J. Davis, *Selective activation of p38 mitogen-activated protein (MAP) kinase isoforms by the MAP kinase kinases MKK3 and MKK6.* J Biol Chem, 1998. **273**(3): p. 1741-8.
322. Wang, P.N., et al., *Downregulation of phosphorylated MKK4 is associated with a poor prognosis in colorectal cancer patients.* Oncotarget, 2017. **8**(21): p. 34352-34361.
323. Kinexus, *MKK3-pS218*. 2019.
324. Cuenda, A. and S. Rousseau, *p38 MAP-kinases pathway regulation, function and role in human diseases.* Biochim Biophys Acta, 2007. **1773**(8): p. 1358-75.
325. Barber, B.E., et al., *World Malaria Report: time to acknowledge Plasmodium knowlesi malaria.* Malar J, 2017. **16**(1): p. 135.
326. Daneshvar, C., et al., *Clinical and laboratory features of human Plasmodium knowlesi infection.* Clin Infect Dis, 2009. **49**(6): p. 852-60.
327. Moon, R.W., et al., *Adaptation of the genetically tractable malaria pathogen Plasmodium knowlesi to continuous culture in human erythrocytes.* Proc Natl Acad Sci U S A, 2013. **110**(2): p. 531-6.
328. Amir, A., et al., *Invasion characteristics of a Plasmodium knowlesi line newly isolated from a human.* Sci Rep, 2016. **6**: p. 24623.
329. Priya, P.P. and R.S. A, *Role of absolute reticulocyte count in evaluation of pancytopenia-a hospital based study.* J Clin Diagn Res, 2014. **8**(8): p. FC01-3.
330. Thomas, R.S., et al., *Phosphorylation at serines 104 and 106 by Erk1/2 MAPK is important for estrogen receptor-alpha activity.* J Mol Endocrinol, 2008. **40**(4): p. 173-84.
331. Sherr, C.J., *Cancer cell cycles.* Science, 1996. **274**(5293): p. 1672-7.
332. Spike, B.T. and K.F. Macleod, *The Rb tumor suppressor in stress responses and hematopoietic homeostasis.* Cell Cycle, 2005. **4**(1): p. 42-5.
333. Hadari, Y.R., et al., *Binding of Shp2 tyrosine phosphatase to FRS2 is essential for fibroblast growth factor-induced PC12 cell differentiation.* Mol Cell Biol, 1998. **18**(7): p. 3966-73.
334. Dorin-Semblat, D., et al., *Malaria Parasite-Infected Erythrocytes Secrete PfCK1, the Plasmodium Homologue of the Pleiotropic Protein Kinase Casein Kinase 1.* PLoS One, 2015. **10**(12): p. e0139591.
335. Paul, A., et al., *Studying the rigidity of red blood cells induced by Plasmodium falciparum infection.* Sci Rep, 2019. **9**(1): p. 6336.
336. Lee, E., et al., *The RNA in reticulocytes is not just debris: it is necessary for the final stages of erythrocyte formation.* Blood Cells Mol Dis, 2014. **53**(1-2): p. 1-10.
337. Zhang, J. and P.A. Ney, *Reticulocyte mitophagy: monitoring mitochondrial clearance in a mammalian model.* Autophagy, 2010. **6**(3): p. 405-8.
338. Yewale, C., et al., *Epidermal growth factor receptor targeting in cancer: a review of trends and strategies.* Biomaterials, 2013. **34**(34): p. 8690-707.
339. Ryan, M.A., et al., *Pharmacological inhibition of EGFR signalling enhances G-CSF-induced hematopoietic stem cell mobilization.* Nat Med, 2010. **16**(10): p. 1141-6.
340. Guo, G., et al., *Ligand-Independent EGFR Signalling.* Cancer Res, 2015. **75**(17): p. 3436-41.
341. Stommel, J.M., et al., *Coactivation of receptor tyrosine kinases affects the response of tumor cells to targeted therapies.* Science, 2007. **318**(5848): p. 287-90.
342. Jalili, A., et al., *The HGF/c-Met axis synergizes with G-CSF in the mobilization of hematopoietic stem/progenitor cells.* Stem Cells Dev, 2010. **19**(8): p. 1143-51.
343. Geest, C.R. and P.J. Coffer, *MAPK signalling pathways in the regulation of hematopoiesis.* J Leukoc Biol, 2009. **86**(2): p. 237-50.
344. Frodin, M. and S. Gammeltoft, *Role and regulation of 90 kDa ribosomal S6 kinase (RSK) in signal transduction.* Mol Cell Endocrinol, 1999. **151**(1-2): p. 65-77.
345. Richards, S.A., et al., *Ribosomal S6 kinase 1 (RSK1) activation requires signals dependent on and independent of the MAP kinase ERK.* Curr Biol, 1999. **9**(15): p. 810-20.
346. Romeo, Y., X. Zhang, and P.P. Roux, *Regulation and function of the RSK family of protein kinases.* Biochem J, 2012. **441**(2): p. 553-69.
347. Lupescu, A., et al., *Enhanced erythrocyte membrane exposure of phosphatidylserine following sorafenib treatment: an in vivo and in vitro study.* Cell Physiol Biochem, 2012. **30**(4): p. 876-88.
348. Paul, F., et al., *Separation of malaria-infected erythrocytes from whole blood: use of a selective high-gradient magnetic separation technique.* Lancet, 1981. **2**(8237): p. 70-1.
349. Rudzinska, M.A., W. Trager, and R.S. Bray, *Pinocytotic uptake and the digestion of hemoglobin in malaria parasites.* J Protozool, 1965. **12**(4): p. 563-76.
350. Pines, J. and T. Hunter, *Human cyclins A and B1 are differentially located in the cell and undergo cell cycle-dependent nuclear transport.* J Cell Biol, 1991. **115**(1): p. 1-17.

351. Jayapal, S.R., et al., *Hematopoiesis specific loss of Cdk2 and Cdk4 results in increased erythrocyte size and delayed platelet recovery following stress.* Haematologica, 2015. **100**(4): p. 431-8.
352. Schlessinger, J., *Cell signalling by receptor tyrosine kinases.* Cell, 2000. **103**(2): p. 211-25.
353. Gotoh, N., *Regulation of growth factor signalling by FRS2 family docking/scaffold adaptor proteins.* Cancer Sci, 2008. **99**(7): p. 1319-25.
354. Ong, S.H., et al., *FRS2 proteins recruit intracellular signalling pathways by binding to diverse targets on fibroblast growth factor and nerve growth factor receptors.* Mol Cell Biol, 2000. **20**(3): p. 979-89.
355. Kurokawa, K., et al., *Identification of SNT/FRS2 docking site on RET receptor tyrosine kinase and its role for signal transduction.* Oncogene, 2001. **20**(16): p. 1929-38.
356. Degoutin, J., M. Vigny, and J.Y. Gouzi, *ALK activation induces Shc and FRS2 recruitment: Signalling and phenotypic outcomes in PC12 cells differentiation.* FEBS Lett, 2007. **581**(4): p. 727-34.
357. Zeng, L., et al., *Structural insights into FRS2alpha PTB domain recognition by neurotrophin receptor TrkB.* Proteins, 2014. **82**(7): p. 1534-41.
358. Wu, Y., Z. Chen, and A. Ullrich, *EGFR and FGFR signalling through FRS2 is subject to negative feedback control by ERK1/2.* Biol Chem, 2003. **384**(8): p. 1215-26.
359. Gotoh, N., et al., *Tyrosine phosphorylation sites on FRS2alpha responsible for Shp2 recruitment are critical for induction of lens and retina.* Proc Natl Acad Sci U S A, 2004. **101**(49): p. 17144-9.
360. Mohi, M.G. and B.G. Neel, *The role of Shp2 (PTPN11) in cancer.* Curr Opin Genet Dev, 2007. **17**(1): p. 23-30.
361. Lax, I., et al., *The docking protein FRS2alpha controls a MAP kinase-mediated negative feedback mechanism for signalling by FGF receptors.* Mol Cell, 2002. **10**(4): p. 709-19.
362. Xu, B., L. Yang, and B.T. Hinton, *The Role of fibroblast growth factor receptor substrate 2 (FRS2) in the regulation of two activity levels of the components of the extracellular signal-regulated kinase (ERK) pathway in the mouse epididymis.* Biol Reprod, 2013. **89**(2): p. 48.
363. Landry, C.R., E.D. Levy, and S.W. Michnick, *Weak functional constraints on phosphoproteomes.* Trends Genet, 2009. **25**(5): p. 193-7.
364. Naka, N., et al., *Synovial sarcoma is a stem cell malignancy.* Stem Cells, 2010. **28**(7): p. 1119-31.
365. Novus-Biologicals. *FRS3 antibody and expected size in Western blot analysis* 2019 [cited 2019 27.05]; Available from: https://www.novusbio.com/products/frs3-antibody_nbp1-52962.
366. Ferrara, N., H.P. Gerber, and J. LeCouter, *The biology of VEGF and its receptors.* Nat Med, 2003. **9**(6): p. 669-76.
367. Olsson, A.K., et al., *VEGF receptor signalling - in control of vascular function.* Nat Rev Mol Cell Biol, 2006. **7**(5): p. 359-71.
368. Imoukhuede, P.I. and A.S. Popel, *Expression of VEGF receptors on endothelial cells in mouse skeletal muscle.* PLoS One, 2012. **7**(9): p. e44791.
369. Yang, Z., H.J. Ahn, and H.W. Nam, *Gefitinib inhibits the growth of Toxoplasma gondii in HeLa cells.* Korean J Parasitol, 2014. **52**(4): p. 439-41.
370. Reinhardt, B., et al., *Upregulation of functionally active vascular endothelial growth factor by human cytomegalovirus.* J Gen Virol, 2005. **86**(Pt 1): p. 23-30.
371. Weinkopff, T., et al., *Leishmania major Infection-Induced VEGF-A/VEGFR-2 Signalling Promotes Lymphangiogenesis That Controls Disease.* J Immunol, 2016. **197**(5): p. 1823-31.
372. Tan, W.H., A.S. Popel, and F. Mac Gabhann, *Computational Model of Gab1/2-Dependent VEGFR2 Pathway to Akt Activation.* PLoS One, 2013. **8**(6): p. e67438.
373. Dougher, M. and B.I. Terman, *Autophosphorylation of KDR in the kinase domain is required for maximal VEGF-stimulated kinase activity and receptor internalization.* Oncogene, 1999. **18**(8): p. 1619-27.
374. Matsumoto, T., et al., *VEGF receptor-2 Y951 signalling and a role for the adapter molecule TSAd in tumor angiogenesis.* EMBO J, 2005. **24**(13): p. 2342-53.
375. Takahashi, T., et al., *A single autophosphorylation site on KDR/Flk-1 is essential for VEGF-A-dependent activation of PLC-gamma and DNA synthesis in vascular endothelial cells.* EMBO J, 2001. **20**(11): p. 2768-78.
376. Dayanir, V., et al., *Identification of tyrosine residues in vascular endothelial growth factor receptor-2/FLK-1 involved in activation of phosphatidylinositol 3-kinase and cell proliferation.* J Biol Chem, 2001. **276**(21): p. 17686-92.
377. Lamalice, L., et al., *Phosphorylation of tyrosine 1214 on VEGFR2 is required for VEGF-induced activation of Cdc42 upstream of SAPK2/p38.* Oncogene, 2004. **23**(2): p. 434-45.
378. Dan, C., et al., *Cytoskeletal changes regulated by the PAK4 serine/threonine kinase are mediated by LIM kinase 1 and cofilin.* J Biol Chem, 2001. **276**(34): p. 32115-21.
379. Jang, I., et al., *Pak1/LIMK1/Cofilin Pathway Contributes to Tumor Migration and Invasion in Human Non-Small Cell Lung Carcinomas and Cell Lines.* Korean J Physiol Pharmacol, 2012. **16**(3): p. 159-65.

380. Edwards, D.C., et al., *Activation of LIM-kinase by Pak1 couples Rac/Cdc42 GTPase signalling to actin cytoskeletal dynamics.* Nat Cell Biol, 1999. **1**(5): p. 253-9.
381. Romarowski, A., et al., *PKA-dependent phosphorylation of LIMK1 and Cofilin is essential for mouse sperm acrosomal exocytosis.* Dev Biol, 2015. **405**(2): p. 237-49.
382. Bamburg, J.R. and O.P. Wiggan, *ADF/cofilin and actin dynamics in disease.* Trends Cell Biol, 2002. **12**(12): p. 598-605.
383. Koga, R., et al., *Actin-Modulating Protein Cofilin Is Involved in the Formation of Measles Virus Ribonucleoprotein Complex at the Perinuclear Region.* J Virol, 2015. **89**(20): p. 10524-31.
384. Vorster, P.J., et al., *LIM kinase 1 modulates cortical actin and CXCR4 cycling and is activated by HIV-1 to initiate viral infection.* J Biol Chem, 2011. **286**(14): p. 12554-64.
385. Colonne, P.M., C.G. Winchell, and D.E. Voth, *Hijacking Host Cell Highways: Manipulation of the Host Actin Cytoskeleton by Obligate Intracellular Bacterial Pathogens.* Front Cell Infect Microbiol, 2016. **6**: p. 107.
386. Gonzalez, V., et al., *Host cell entry by apicomplexa parasites requires actin polymerization in the host cell.* Cell Host Microbe, 2009. **5**(3): p. 259-72.
387. Kumar, Y. and R.H. Valdivia, *Reorganization of the host cytoskeleton by the intracellular pathogen Chlamydia trachomatis.* Commun Integr Biol, 2008. **1**(2): p. 175-7.
388. Elliott, D.A. and D.P. Clark, *Cryptosporidium parvum induces host cell actin accumulation at the host-parasite interface.* Infect Immun, 2000. **68**(4): p. 2315-22.
389. Delorme-Walker, V., et al., *Toxofilin upregulates the host cortical actin cytoskeleton dynamics, facilitating Toxoplasma invasion.* J Cell Sci, 2012. **125**(Pt 18): p. 4333-42.
390. Lodoen, M.B., C. Gerke, and J.C. Boothroyd, *A highly sensitive FRET-based approach reveals secretion of the actin-binding protein toxofilin during Toxoplasma gondii infection.* Cell Microbiol, 2010. **12**(1): p. 55-66.
391. Yamamoto, M., et al., *A single polymorphic amino acid on Toxoplasma gondii kinase ROP16 determines the direct and strain-specific activation of Stat3.* J Exp Med, 2009. **206**(12): p. 2747-60.
392. Ong, Y.C., M.L. Reese, and J.C. Boothroyd, *Toxoplasma rhoptry protein 16 (ROP16) subverts host function by direct tyrosine phosphorylation of STAT6.* J Biol Chem, 2010. **285**(37): p. 28731-40.
393. Babon, J.J., et al., *The molecular regulation of Janus kinase (JAK) activation.* Biochem J, 2014. **462**(1): p. 1-13.
394. Gordon, G.M., et al., *Transforming JAK1 mutations exhibit differential signalling, FERM domain requirements and growth responses to interferon-gamma.* Biochem J, 2010. **432**(2): p. 255-65.
395. Mietelska-Porowska, A., et al., *Tau protein modifications and interactions: their role in function and dysfunction.* Int J Mol Sci, 2014. **15**(3): p. 4671-713.
396. Lindwall, G. and R.D. Cole, *Phosphorylation affects the ability of tau protein to promote microtubule assembly.* J Biol Chem, 1984. **259**(8): p. 5301-5.
397. Naghavi, M.H. and D. Walsh, *Microtubule Regulation and Function during Virus Infection.* J Virol, 2017. **91**(16).
398. Al-Zeer, M.A., et al., *Chlamydia trachomatis remodels stable microtubules to coordinate Golgi stack recruitment to the chlamydial inclusion surface.* Mol Microbiol, 2014. **94**(6): p. 1285-97.
399. Stoothoff, W.H. and G.V. Johnson, *Tau phosphorylation: physiological and pathological consequences.* Biochim Biophys Acta, 2005. **1739**(2-3): p. 280-97.
400. Liu, F., et al., *Contributions of protein phosphatases PP1, PP2A, PP2B and PP5 to the regulation of tau phosphorylation.* Eur J Neurosci, 2005. **22**(8): p. 1942-50.
401. Shahani, N. and R. Brandt, *Functions and malfunctions of the tau proteins.* Cell Mol Life Sci, 2002. **59**(10): p. 1668-80.
402. Murphy, D.B. and K.T. Wallis, *Erythrocyte microtubule assembly in vitro. Determination of the effects of erythrocyte tau, tubulin isoforms, and tubulin oligomers on erythrocyte tubulin assembly, and comparison with brain microtubule assembly.* J Biol Chem, 1985. **260**(22): p. 12293-301.
403. Ingelson, M., E. Vanmechelen, and L. Lannfelt, *Microtubule-associated protein tau in human fibroblasts with the Swedish Alzheimer mutation.* Neurosci Lett, 1996. **220**(1): p. 9-12.
404. Radhakrishnan, G.K. and G.A. Splitter, *Modulation of host microtubule dynamics by pathogenic bacteria.* Biomol Concepts, 2012. **3**(6): p. 571-580.
405. Sweeney, K.R., et al., *Host cell invasion by Toxoplasma gondii is temporally regulated by the host microtubule cytoskeleton.* Eukaryot Cell, 2010. **9**(11): p. 1680-9.
406. Frades, I., S. Resjo, and E. Andreasson, *Comparison of phosphorylation patterns across eukaryotes by discriminative N-gram analysis.* BMC Bioinformatics, 2015. **16**: p. 239.
407. Ascierto, P.A., et al., *The role of BRAF V600 mutation in melanoma.* J Transl Med, 2012. **10**: p. 85.
408. Cuadrado, A. and A.R. Nebreda, *Mechanisms and functions of p38 MAPK signalling.* Biochem J, 2010. **429**(3): p. 403-17.